

2 0 0 8 - 0 9



E L E T T R A   H I G H L I G H T S   >   0 8 - 0 9

2 0 0 8 - 0 9






**ELETTRA HIGHLIGHTS 2008-2009**  
**EDITORIAL COMMITTEE**

- > Alessandro Baraldi
- > Simone Di Mitri
- > Tevfik Onur Mentès
- > Silvia Onesti
- > Laura Bibi Palatini
- > Adriana Pertosi
- > Marco Zangrando

*Graphic Design:*  
Studio Link ([www.studio-link.it](http://www.studio-link.it))  
Graphart s.r.l.

*Print:*  
Graphart s.r.l.

---



**T**he Elettra Highlights publication for 2008-2009 well illustrates the coincidence of achievements, challenges and opportunities emerging as the many upgrade projects of our facility are being implemented while user operation continues. The most important project completed was the new booster injector, inaugurated by the President of the Republic of Italy, Giorgio Napolitano, on March 28, 2008, which has brought on a major decrease in injection time and overall improvements in the reliability of the storage ring. Challenges include the major excavations performed nearby for the construction of FERMI@Elettra.


Elettra continues to be very successful in attracting new users. The total number of proposals received in 2008 (812) has seen a notable increase in comparison to the previous years (606 in 2007 and 636 in 2006). This even though users were notified that the available beamtime would be limited in the first trimester of 2008 due to the installation of the booster full-energy injector.

The ensuing Elettra and booster machine physics activities concentrated on the top-up tests, in other words, on the system that will be capable of selectively filling with electrons the single electron bunches circulating in Elettra, thus maintaining the current constant without interrupting the operation of the beamlines. The possibility of top-up operation of Elettra was conclusively demonstrated at both 2.4 and 2.0 GeV, and top-up operation for users is scheduled to begin by the end of 2009.

Following up on the indications of the Scientific Advisory Council and of the Elettra user community, we initiated a program to strengthen services and research in structural biology, in cooperation with other research institutions. A major upgrade of the XRD1 beamline is nearing completion, with the installation of a new robot and related management software developed at Elettra, which will take care of extracting the biological samples from the liquid nitrogen container, place it on the beamline and align it in order to begin measurements. This system, coupled with GRID technologies also developed at Elettra, will allow external users to carry out protein diffraction measurements through remote control. A new high-performance X-ray detector is scheduled to be installed in the Fall of 2009. The optical design of the second protein diffraction beamline has been completed and procurement of the optical components has begun.

A new state-of-the-art facility for the expression, purification and crystallization of proteins was designed and built on the Elettra site in close cooperation with SISSA and staffed with newly hired senior researchers who will be the core of the strengthening plan of the structural biology program at Elettra. The new facility will be inaugurated in conjunction with the 2009 Elettra Users' Meeting, that will take place on December 14-18.

In 2008, both the construction and civil engineering works related to the FERMI@Elettra Free Electron Laser (FEL) project have taken off, as well as the acquisition of technical components for the FEL. A new industrial spin-off company of Sincrotrone Trieste, Kyma S.r.l. was established for the construction and commercialization of undulators and magnetic measurements equipment. Kyma delivered the laser heater undulator and the first linear and elliptical polarization undulators for FERMI on time and under budget in 2009.



Through a collaboration with the MAX-lab Laboratory in Lund (Sweden), which started in the framework of the actual construction of the European Consortium EuroFEL (formerly, IRUVX), tests of the FERMI photoinjector were performed in Lund while the civil construction was being completed in Trieste. The successfully tested photoinjector was installed in its final location in the Spring of 2009, and at 6:44 p.m. on August 19, 2009, the first electron beam was extracted from the copper photocathode and accelerated to about 5 MeV in the linac tunnel of FERMI@Elettra. This was a step of capital importance in the commissioning of the new fourth-generation light source, but there is still a very large amount of work ahead of us.

Progress is starting on the next phase of installation of the linac systems. With much experience gained from the recent installation of the photocathode gun system, injector linac, and laser heater regions, we expect even smoother progress assembling this unique seeded FEL source. FERMI@Elettra is scheduled to produce gigawatt pulses at wavelength tunable down to 10 nm by the end of 2010 and down to 3-4 nm by the end of 2011. Initially, three beamlines will be devoted to a variety of time-dependent imaging, diffraction, inelastic and elastic scattering, and spectroscopy experimental programs, that currently see the involvement of over 30 partner institutions worldwide.

The new strategic directions opening up are exemplified by the thematic workshops that took place as part of the XVI Elettra Users' Meeting, covering the topics: "Time-resolved Studies with Synchrotron and FEL Radiation" and "Emerging Applications of Synchrotron Radiation in the Life Sciences". The workshops served the important purpose of engaging a broader user community, and our partner institutions had a prominent role in the above events, addressing emerging applications of synchrotron radiation in two burgeoning and highly strategic fields.

We take this opportunity to thank our employees, our Partners and external Users for their enthusiasm and dedication over the years. We trust that with their help we will be able to meet the major challenge of fully exploiting an upgraded Elettra light source while developing the new FERMI@Elettra FEL source.

**Alfonso Franciosi**  
*Chief Executive Officer*  
*Sincrotrone Trieste S.C.p.A.*

# TABLE OF CONTENTS

## RESEARCH HIGHLIGHTS

<b>Chemical and Materials Science</b>	10
> Nano-patterning of Ag surfaces by electron-assisted oxidation	12
> Selective production of reactive and non reactive oxygen atoms on Pd(001) by rotationally aligned O <sub>2</sub> molecules	14
> A silver bullet to combat wound infection?	16
> Unravelling the internal structure of complex nanocrystals: spectroscopy beyond microscopy	18
> Structural and chemical effects of plasma treatment on close-packed colloidal nanoparticle layers	20
> An in-situ SXTM, XAS and XRF investigation of the electrochemical corrosion of metal-based bipolar plate materials used in fuel cells	22
<b>Organic Films and Self-Assembly</b>	24
> <b>Shedding light on transport properties</b> , <i>an interview with Philip Hofmann</i>	25
> Direct measurement of electrical conductance through a self-assembled molecular layer	28
> Zn-tetraphenyl-porphyrin and C <sup>70</sup> : donor-acceptor couples to mimic the photosynthesis for solar cell devices	30
> Self-assembly of L-methionine nanogratings on the Ag(111) and Cu(111) surface	32
> The electronic structure and adsorption geometry of histidine on Cu(110)	34
> Electron resist behavior of Pd hexadecanethiolate examined using x-ray photoelectron spectroscopy with nanometric lateral resolution	36
> Periodic mesoporous organosilica in confined environments	38
<b>Carbon-based Nanostructures</b>	40
> Reversible phase transformation and doubly charged anions at the surface of simple cubic RbC <sub>60</sub>	42
> The formation of graphite and carbon nanotubes from thermal decomposition of silicon carbide	44
> Imaging and spectroscopy of multiwalled carbon nanotubes during oxidation: defects and oxygen bonding	46
> NEXAFS evidence of the electron “CH···π” bridges in films of noncovalently functionalized SWNTs	48

<b>Magnetic and Electronic Properties</b>	<b>50</b>
> <b>Magnets of Lilliput</b> , <i>an interview with Olivier Fruchart</i>	51
> How many bits can fit in a single magnetic dot? XMCD-PEEM evidences the switching of Néel caps inside Bloch domain walls	54
> Evidence for a magnetic proximity effect up to room temperature at Fe/(Ga,Mn)As interfaces	56
> In a correlated metal, quasiparticles are not superficial at all	58
> Evidence for strong itinerant fluctuations in the normal state of CeFeAsO <sub>0.89</sub> F <sub>0.11</sub> iron-oxypnictides	60
> Pressure and alloying effects on the metal to insulator-transition in NiS <sub>2-x</sub> Se <sub>x</sub> studied by infrared spectroscopy	62
<b>Atomic and Molecular Physics</b>	<b>64</b>
> Excitation of <sup>1</sup> S and <sup>3</sup> S metastable helium atoms to doubly excited states	66
> A mystery solved? Photoelectron spectroscopic and quantum chemical studies of the ion states of CeCp <sub>3</sub> <sup>+</sup>	68
> Dissociative double photoionization of CO <sub>2</sub> molecules in the 34-50 eV energy range	70
<b>Free Electron Laser and other coherent light sources</b>	<b>72</b>
> <b>Recent upgrades of Elettra and perspectives for FERMI@Elettra</b> , <i>an interview with Emanuel Karantzoulis and Stephen Milton</i>	73
> Self-induced harmonic generation in a storage-ring Free Electron Laser	76
> Experiments for characterizing the harmonic emission in a Free Electron Laser	78
> Generation of ultra-short photon pulses using electron storage rings: a new bright source of coherent VUV light	80
> Impact of an initial energy chirp and an initial energy curvature on a seeded Free Electron Laser	82
> Physics and simulation challenges of FERMI@Elettra	84
> Damping of the tunneling mechanism in high-order harmonic generation processes induced by fs visible laser pulses	86
<b>Life Sciences</b>	<b>88</b>
> <b>Structural biology at Elettra: recent advances and new perspectives</b> , <i>an interview with Dorian Lamba</i>	89
> Radiation-driven reactivation of human carbonic anhydrase: a movie of binding and processing of the CO <sub>2</sub> at the atomic level	92
> Crystal structure of Mycobacterium tuberculosis YefM antitoxin reveals that it is not an intrinsically unstructured protein	94
> Insights into the molecular basis of transcriptional activation in archaea: structural analysis of BidR from Sulfolobus solfataricus	96

- > FTIR microspectroscopy characterization of Synbeads, a porous support for solid phase peptide synthesis 98
- > Nucleation and growth of deoxyguanosine 5'-monophosphate quadruplexes in dilute solution studied by SAXS 100
- > Tautomerism in DNA/RNA bases: an experimental and theoretical core level spectroscopic study 102
- > Leading neurons with carbon nanotubes 104

### **Theory@Elettra** 106

- > Surface core level shift: highly sensitive probe to oxygen-induced reconstruction 108
- > Optimal representation of the polarization propagator for large-scale GW calculations 110
- > Bonding at the organic/metal interface: adenine on Cu(110) 112
- > Insight into the initial stages of oxidation on graphitic surfaces from photoemission spectroscopy and density functional theory calculations 114

### **Instrumentation Developments** 116

- > Free jet micromixer to study fast chemical and biological reactions by small angle x-ray scattering 118
- > Recent upgrades of the BaDEIPh beamline 120
- > Transient grating spectroscopy to investigate nanoscale dynamics 122
- > Synchrotron radiation meets laser ablation: photoionization mass spectrometry of clusters in a laser plume 124

## **FACTS & FIGURES**

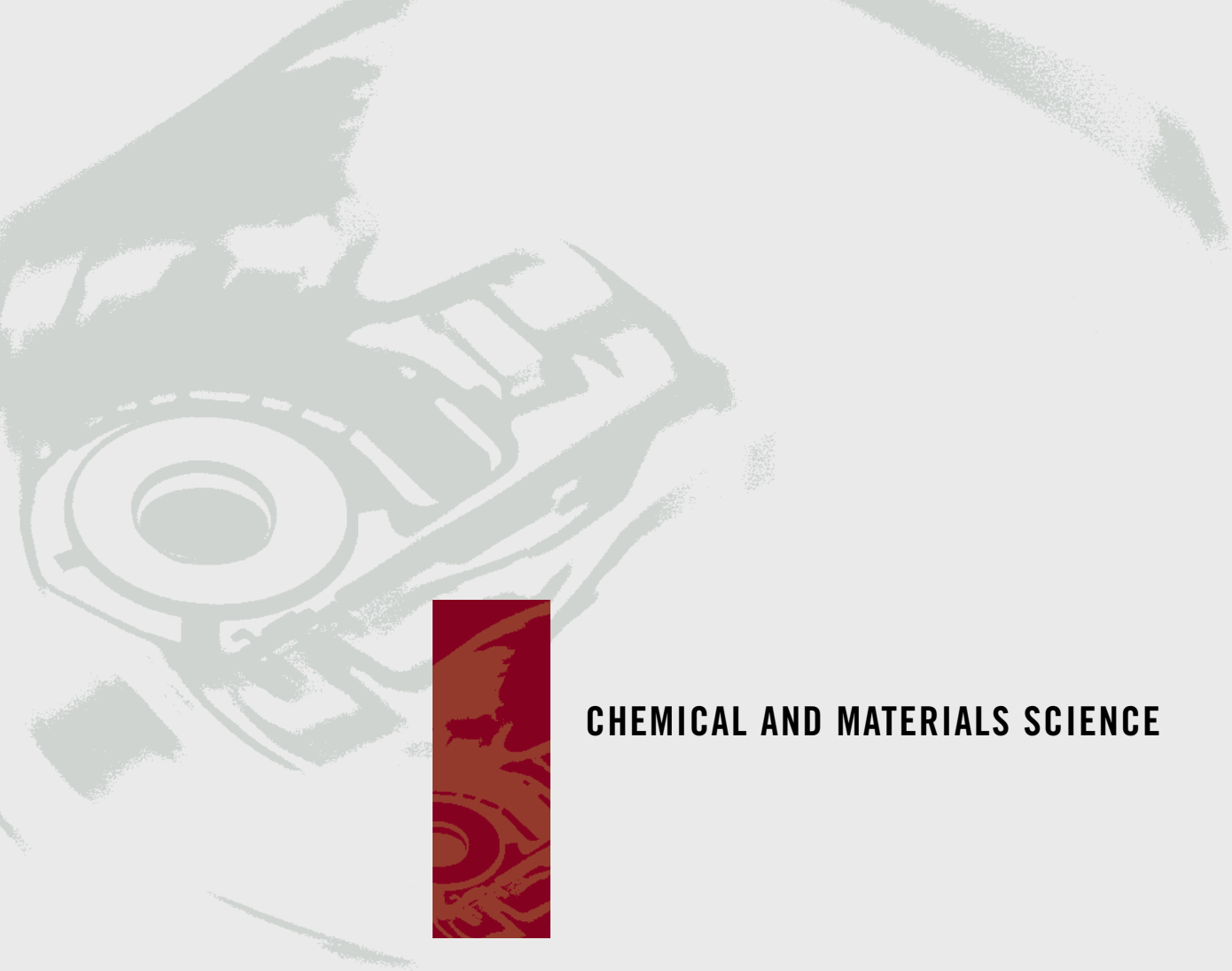
- > The company 128
- > Staff 130
- > Training and education 131
- > Beamlines and users 132
- > Financial figures 135
- > Projects / Sponsored research 136
- > Technology transfer at Elettra 138

## **EVENTS**

- > Visits 144
- > Workshops, conferences, meetings and schools 147
- > Other events 150
- > A look at the past... and one to the future 155







**CHEMICAL AND MATERIALS SCIENCE**





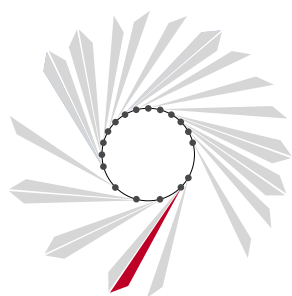
# NANO-PATTERNING OF Ag SURFACES BY ELECTRON-ASSISTED OXIDATION

S. Günther<sup>1</sup>, R. Reichelt<sup>1</sup>, J. Wintterlin<sup>1</sup>, A. Barinov<sup>2</sup>, T. O. Menteş<sup>2</sup>, M. Á. Niño<sup>2</sup>, A. Locatelli<sup>2</sup>

<sup>1</sup>Department Chemie, LMU München, Munich, Germany

<sup>2</sup>Sincrotrone Trieste S.C.p.A., Trieste, Italy

E-mail: [sebastian.guenther@cup.uni-muenchen.de](mailto:sebastian.guenther@cup.uni-muenchen.de)



NANOSPECTROSCOPY

Nanofabrication and surface patterning are key processes in the semiconductor industry. As standard patterning techniques mainly lithography methods are used, where patterns are written onto a resist which resides on the substrate to be processed. To pattern the resist photons, electrons or ions are used by applying scanning or projection geometries. These are complex, expensive processes, and currently several non-classical patterning techniques are explored that are capable of structuring substrates at high lateral resolution and low cost. Examples are nanoimprint or soft lithography, where molds or stamps are used to transfer a pattern onto a resist or to directly print materials onto a substrate.

In this study we have developed a method to pattern Ag(111) by a local oxidation reaction that is induced by irradiation with low energy electrons [1]. This structuring technique has the advantage of neither requiring a resist, nor any subsequent resist development, etching or metallization processes, as the structures are directly grown on the surface. The idea of the technique, which uses NO<sub>2</sub> as oxidizing gas, is based on the fact that NO<sub>2</sub> alone, with the exposures reached in usual UHV experiments, does not oxidize Ag(111). NO<sub>2</sub> adsorbs dissociatively leading to NO<sub>ad</sub> + O<sub>ad</sub>. At temperature below 500 K both species, NO<sub>ad</sub> and O<sub>ad</sub>, remain adsorbed [2], and NO<sub>ad</sub> forms a kind of protective layer that prevents oxidation of the Ag surface. At T > 500 K NO<sub>ad</sub> desorbs and O<sub>ad</sub> remains on the surface [3]. However, the O<sub>ad</sub> does not accumulate to concentrations required for silver oxide, because Ag<sub>2</sub>O is not thermodynamically stable at these temperatures. Hence, in both cases the silver surface remains metallic, i.e. covered by an adsorbate layer, but not oxidized.

However, if NO<sub>2</sub> was adsorbed at room temperature and NO<sub>ad</sub> was, at the same time, removed non-thermally, oxygen could be further accumulated. Figure 1 shows that this is achieved by irradiating the surface with an electron beam that causes electron stimulated desorption of NO<sub>ad</sub>. In the upper row of Figure 1 LEED (Low Energy Electron Diffraction) patterns of the Ag(111) surface are displayed, which were recorded during NO<sub>2</sub> dosing at 300 K and simultaneously irradiating with 40 eV electrons. Starting from a clean Ag(111) surface with its (1x1) LEED pattern, a sharp (4x4) pattern was observed after adsorption of 1 Langmuir of NO<sub>2</sub>. This pattern corresponds to the known O(4x4) surface structure formed by adsorbed oxygen atoms on the reconstructed Ag(111) surface. The formation of this O<sub>ad</sub> phase is already a sign that under the irradiating electron beam only oxygen remains on the surface. Further NO<sub>2</sub> adsorption resulted in the complete loss of the LEED pattern, indicating that an amorphous layer had formed. When the surface was imaged after the adsorption experiment with MEM (mirror electron microscopy) or LEEM (low energy electron microscopy) dark spots were resolved, with sizes determined by the diameters of the electron beam (2 μm and 8 μm) used for NO<sub>ad</sub> desorption. The edge profile extracted from the image of the 2 μm spot shows a ~100 nm sharp border. Area selective photoelectron spectroscopy on the non-irradiated (A) and on the irradiated (B) part of the sample revealed the chemical composition of the spot. The O 1s, Ag 3d and valence band spectra displayed in the lower row of Figure 1 show that on the irradiated spot Ag<sub>2</sub>O was formed, whereas the non-irradiated surface remained metallic. Ag<sub>2</sub>O was evidenced by the correct intensity ratio of the O 1s and Ag 3d peaks, the binding energy

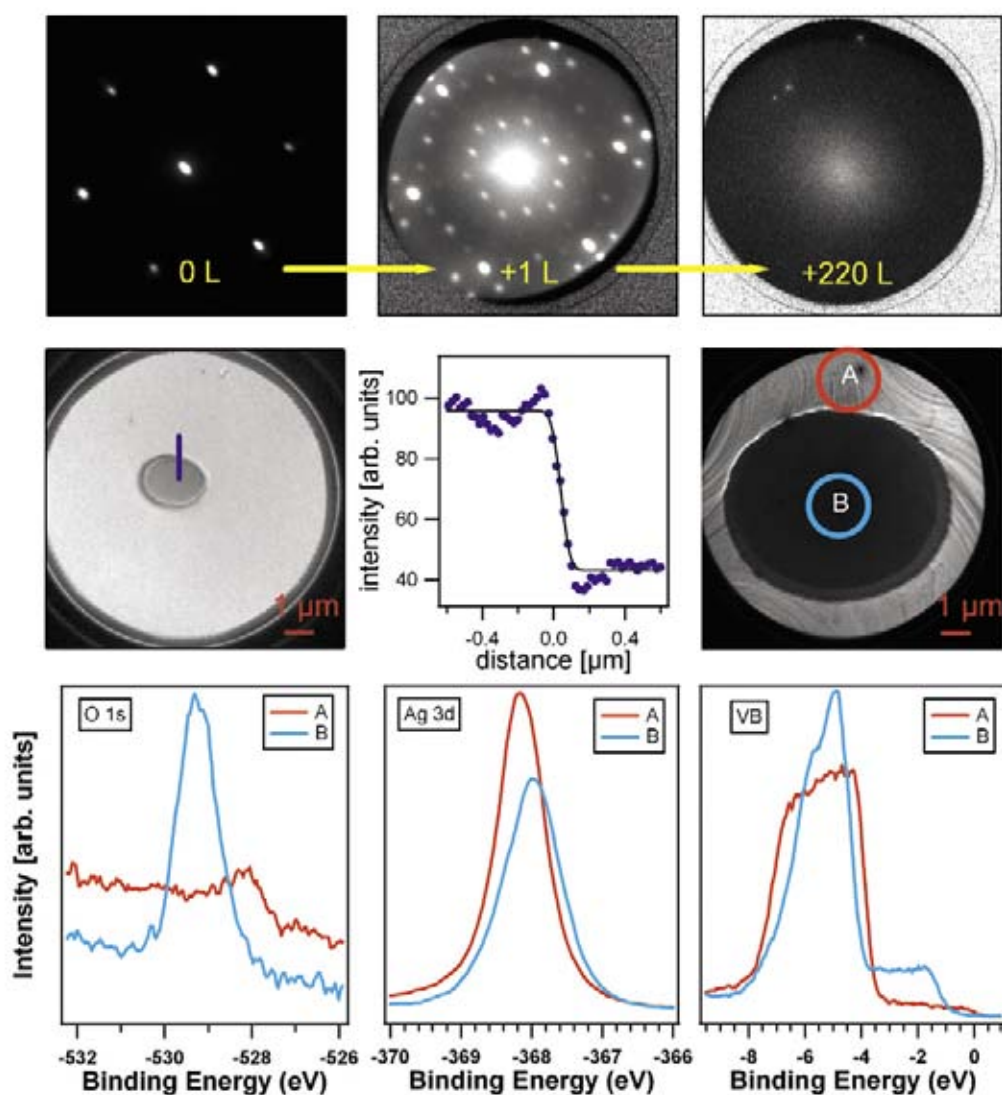


**Figure 1.** Upper row: Evolution of the LEED pattern during  $\text{NO}_2$  dosing at 300 K under an irradiating beam of 40 eV electrons ( $\sim 2 \text{ pA}/\mu\text{m}^2$ ). Center row: MEM images ( $E = 1.5$  and  $2.1 \text{ eV}$ ) of spots created by  $\text{NO}_2$  dosing under a beam with  $2 \mu\text{m}$  ( $360 \text{ L NO}_2$ ,  $30 \text{ eV}$ ,  $0.4 \text{ pA}/\mu\text{m}^2$ ) and  $8 \mu\text{m}$  diameter ( $70 \text{ L NO}_2$ ,  $40 \text{ eV}$ ,  $2 \text{ pA}/\mu\text{m}^2$ ), respectively. An about  $100 \text{ nm}$  sharp edge profile could be extracted from the image of the  $2 \mu\text{m}$  sized spot. Lower row: Area selective photoelectron spectroscopy at positions (A) and (B) shows that the grown spot consists of  $\text{Ag}_2\text{O}$ , whereas the non-irradiated part of the  $\text{Ag}(111)$  remains metallic.

position of both peaks and finally the shape of the valence band, with a narrower Ag 4d band compared to the metallic surface, the O 2p-induced emission between 2 and 3 eV, and the absence of a Fermi edge [4]. The metallic properties of non-irradiated  $\text{Ag}(111)$  is attributed to the fact that here the remaining  $\text{NO}_{\text{ad}}$  prevented the surface from further oxygen uptake.

The new patterning method allows us to write laterally confined oxide structures with the help of a focused electron beam without any photoresist, lifting-off or etching techniques. Moreover, the process consists of only one step and it does not require any pre- or post-patterning treatment.

## References

- [1] S. Günther, R. Reichelt, J. Winterlin, A. Barinov, T.O. Menteş, M.Á. Niño, A. Locatelli, *Appl. Phys. Lett.* **93**, 233117 (2008).
- [2] G. Polzonetti, P. Alnot and C. R. Brundle, *Surf. Sci.* **238**, 226 (1990).
- [3] S. Bare *et al.*, *Surf. Sci.* **342**, 185 (1995).
- [4] L.H. Tjeng *et al.*, *Phys. Rev. B* **41**, 3190 (1990).

# SELECTIVE PRODUCTION OF REACTIVE AND NON REACTIVE OXYGEN ATOMS ON Pd(001) BY ROTATIONALLY ALIGNED O<sub>2</sub> MOLECULES

L. Vattuone<sup>1</sup>, A. Gerbi<sup>1</sup>, D. Cappelletti<sup>2</sup>, F. Pirani<sup>3</sup>, R. Gunnella<sup>4</sup>, L. Savio<sup>1</sup>, M. Rocca<sup>1</sup>

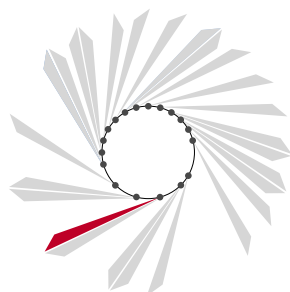
<sup>1</sup>Physics Department and CNISM-CNR, University of Genova, Genova, Italy

<sup>2</sup>Department of Civil and Environmental Engineering, University of Perugia, Perugia, Italy

<sup>3</sup>Chemistry Department, University of Perugia, Perugia, Italy

<sup>4</sup>Physics Department, University of Camerino, Camerino, Italy

E-mail: vattuone@fisica.unige.it



SUPERESCA

Understanding gas surface reactions at the atomic level provides the deepest possible insight into the basic physical and chemical processes governing gas-surface interaction. It is therefore pivotal for further knowledge based improvements of the efficiency and/or the selectivity of catalytic reactions. Under industrial operating conditions (high pressure and temperature) several species are co-adsorbed on the active surface in equilibrium with the gas phase and it is generally not easy to find out which parameters (chemical nature, abundance, geometrical factors, etc.) are the most important for promoting the desired process. A control of both translational energy and internal degrees of freedom of the incoming molecules and of the structure of the catalyst surface could, in principle, lead to a total selectivity for one process/product with respect to another with important practical consequences such as saving expensive reactants and avoiding pollution. Therefore, preparation of molecules in defined quantum states has been a major goal in experimental physical-chemistry. While the role of the molecular vibrations has been directly demonstrated experimentally, relatively less attention has been devoted so far to the role of the rotational states, i.e. to the modulus of the quantized angular momentum vector and to its spatial orientation.

In the present study we exploited the final velocity dependence of the molecular alignment, generated by collisions in supersonic expansions [1]. This allows to prepare supersonic molecular beams (SMB) of hyperthermal (0.40 eV), rotationally cold O<sub>2</sub> with a dominant concentration of helicopters (rotating parallel to the surface) or of cartwheels

(rotating perpendicularly to the surface). The former are dominant in the slow speed tail (ST) of the velocity distribution of the SMB while the latter prevail in the high speed tail (FT). FT and ST are filtered from the SMB by a two disks mechanical velocity selector, suited for surface science experiments thanks to its high transmittance.

A pronounced stereodynamical effect is observed for O<sub>2</sub>/Pd(100), in spite of the direct and dissociative adsorption mechanism. We investigated the X-ray Photoelectron Diffraction pattern (XPD) of the O 2s level of oxygen atoms deposited by exposing the bare surface to the same amount of O<sub>2</sub> produced either with ST or with FT. The XPD experiments have been performed at the SuperESCA beamline of Elettra by inserting our velocity selector into the available SMB. Using the degree of alignment of ST and FT we have deconvoluted the measured XPD pattern with respect to O atoms resulting from the dissociation of helicopters (HE) and cartwheels (CW) (see Figure 1).

O atoms generated by HE and CW parent O<sub>2</sub> occupy different sites, which we identify with the fourfold hollow for HE and with the octahedral interstitial for CW, demonstrating that rotational alignment controls the final site occupied by the reaction products.

CO oxidation experiments, performed in Genoa, confirm the formation of two O moieties, out of which only the one produced by parent HE O<sub>2</sub> is reactive. As shown in Figure 2, the amount of CO<sub>2</sub> produced when dosing ST on a surface pre-covered with a small amount of CO (0.04 ML) is much larger than that obtained when dosing FT, despite the very similar adsorption probability.

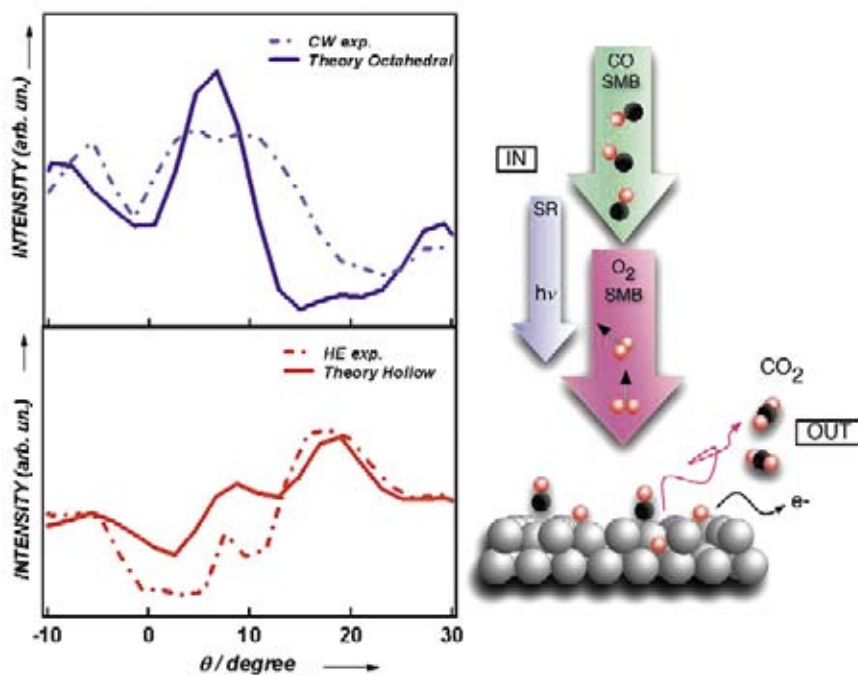


**Figure 1.** Photoemitted intensity from the O 2s level versus the electron emission angle  $\theta$ , for 150 eV photons impinging along the [110] azimuth. Upper panel: CW (dash-dotted) compared with the theoretical fit for O in octahedral interstitials (continuous line); lower panel: HE (dash-dotted) compared with the theoretical fit for O in the fourfold hollow site (continuous line).

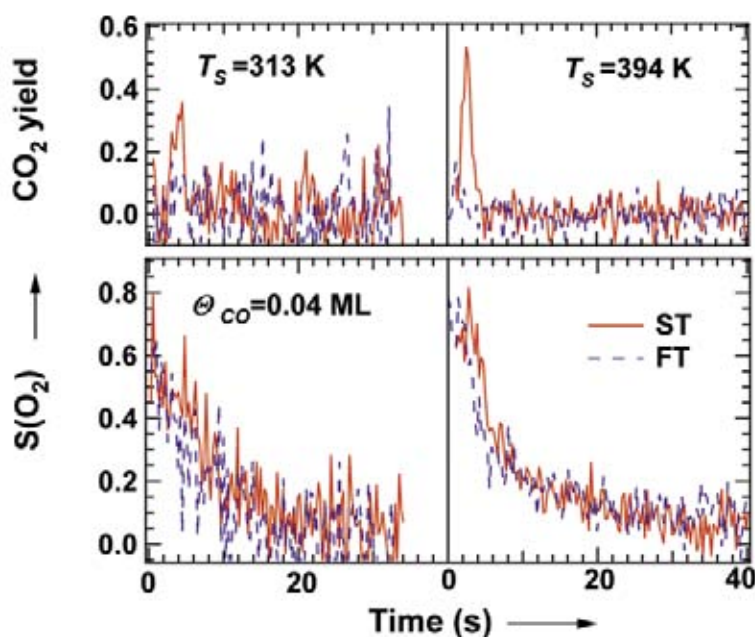


**Figure 2.**  $\text{CO}_2$  yield (upper panels) and sticking probability  $S(\text{O}_2)$  (lower panels) for ST and FT impinging on Pd(001) pre-dosed with 0.04 ML CO at two different surface temperatures.

A significant amount of  $\text{CO}_2$  is produced only when dosing with ST; the higher reaction rate at 394 K is expected since the reaction occurs via the Langmuir-Hinshelwood mechanism, involving co-adsorbed O adatoms at fourfold hollow sites and CO ad molecules. FT produces, on the contrary, unreactive O atoms, in accord with their subsurface location. Note that the residual reactivity observed for FT at 394 K is compatible with the HE fraction in that tail.

In conclusion, we have shown by XPD and supersonic molecular beam techniques that the dissociation of hyperthermal, rotationally

cold,  $\text{O}_2$  on Pd(001) is controlled by its rotational alignment. This experiment opens the way to exploit collisional alignment to selectively populate defined surface and subsurface sites, thus allowing to enhance the selectivity of a reaction towards the desired product.

#### References

- [1] V. Aquilanti, D. Ascenzi, D. Cappelletti, F. Pirani, *Nature* **371**, 399 (1994).
- [2] L. Vattuone, A. Gerbi, D. Cappelletti, F. Pirani, R. Gunnella, L. Savio, M. Rocca, *Angew. Chem Int. Ed.* **48**, 4845 (2009).

# A SILVER BULLET TO COMBAT WOUND INFECTION?

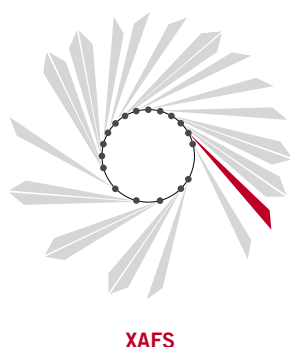
J.J. Buckley<sup>1</sup>, Pratibha L. Gai<sup>1</sup>, A.F. Lee<sup>1,2</sup>, L. Olivi<sup>3</sup>, K. Wilson<sup>1,2</sup>

<sup>1</sup>Department of Chemistry, University of York, York, UK

<sup>2</sup>School of Chemistry, Cardiff University, Cardiff, UK

<sup>3</sup>Sincrotrone Trieste S.C.p.A., Trieste, Italy

E-mail: LeeAF@cardiff.ac.uk



Silver metal has been used as a medium for commerce and decorative jewellery for millennia, but also has a long history of health applications [1]. The first documented use of silver in water purification dates back to ancient Greece, where silver coins were added to water vessels to prevent bacterial growth, while the Phoenicians used silver jars to preserve wine and vinegar during long military and exploratory campaigns. The first scientific papers detailing silver's medicinal benefits for the treatment of eye infections were published in the 1880s, wherein dilute silver nitrate solutions helped alleviate blindness in infants. Topical silver treatments were subsequently extended to burns in 1964 [2], with silver sulfadiazine (SSD) introduced to reduce wound infections in 1968, an important treatment that remains in use today [3]. Nowadays, silver coated medical devices are employed to prevent biofilm formation, and even NASA space shuttles utilise silver based purification systems for guarding against pathogens.

The successful implementation of silver therapies depends heavily on the choice of silver presentation. Although silver metal is itself antimicrobial, its low solubility renders it ineffective for the rapid treatment of infected wounds. Silver nitrate is a potent antiseptic agent, but toxic to human tissues at high concentrations, stains markedly in light and its clinical use requires significant dressing time and nursing cost. We therefore set out to design next-generation wound dressings incorporating highly soluble, non-toxic forms of active silver.

In order to achieve this goal, we utilised a mesoporous form of alumina, which would hopefully act as a chemically inert support matrix to stabilise nanoparticulate silver in a solid powder format. High-resolution elec-

tron microscopy revealed that treatment of the alumina matrix with low concentrations of silver nitrate precursor (~0.1-6 wt% Ag) induced its crystallisation into high surface area  $\gamma$ -Al<sub>2</sub>O<sub>3</sub> nanoneedles (Figure 1). High-resolution transmission electron microscopy (Figure 1 inset) showed these nanoneedles were in turn decorated with silver-containing cubic single crystals around 3-5 nm diameter [4]. The XAFS beamline at Elettra was employed to shed light on the nature of these finely divided silver clusters, crucial to regulating their antibacterial performance. While conventional low area alumina supports favour large, slow dissolving metallic and silver oxide particles, which only exhibit moderate bactericidal activity, Ag K-edge XANES and EXAFS show that  $\gamma$ -Al<sub>2</sub>O<sub>3</sub> nanoneedles promote Ag<sub>2</sub>CO<sub>3</sub> clusters (Figure 2). X-ray photoelectron spectroscopy confirmed the presence of surface carbonate, and not the more common oxide or metal phases common in many commercial wound dressings. These silver carbonate nanoparticles dissolve rapidly in simulated wound fluid, and were therefore screened for antibacterial action against *Staphylococcus aureus* NCTC 10788 and *Pseudomonas aeruginosa* NCIMB 8626, respective Gram positive and -negative bacteria found on the skin and in chronic wounds such as burns. The results were striking: ultra-low concentrations of our Ag<sub>2</sub>CO<sub>3</sub> nanoparticles outperformed the standard Ag<sub>2</sub>O and AgO benchmarks, and even SSD commercial wound treatments, killing over 99.9% of bacteria for over a week.

The link between silver nanoparticle composition and size revealed by XAS measurements offers a simple means to tune the release rate of dissolved silver and thus their final antimicrobial application. These new



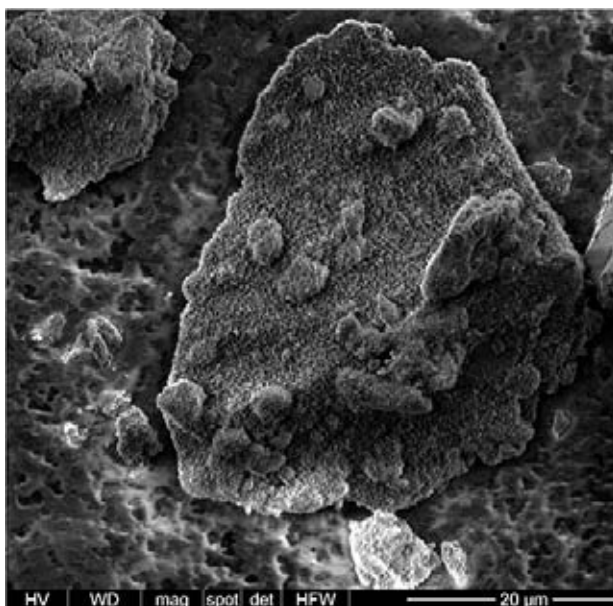


**Figure 1.** Scanning electron micrograph of 0.15 wt% Ag treated / mesoporous  $\text{Al}_2\text{O}_3$ . Inset shows alumina nanoneedles and a high resolution transmission electron micrograph of a  $\text{Ag}_2\text{CO}_3$  nanoparticle.

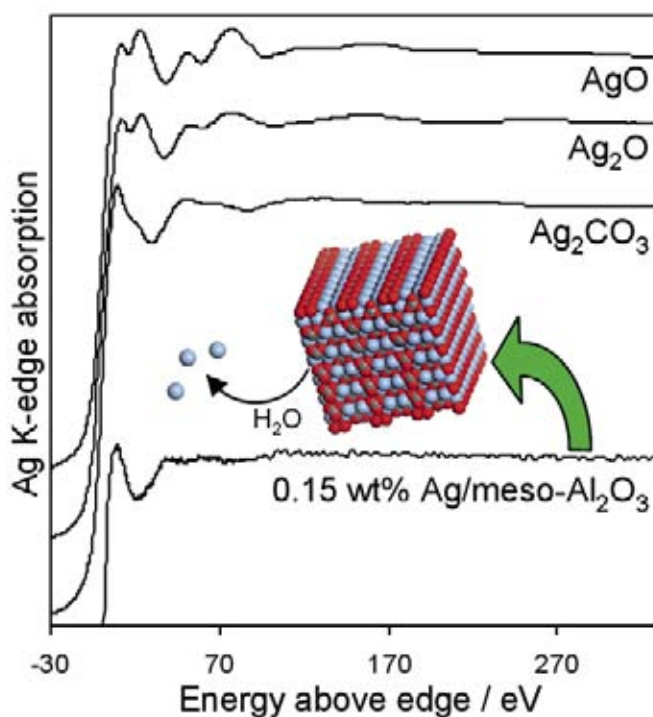


**Figure 2.** Ag K-edge XANES spectra of  $\text{Ag}_2\text{CO}_3$  nanoparticles dispersed on alumina nanoneedles which provide a reservoir of fast dissolving  $\text{Ag}^+$  ions with potent antibacterial action.

alumina-silver carbonate composites are stable to air and light, and unlike silver nitrate dressings, can be safely handled without staining. Future research will explore the development of cheaper, simpler presentation formats and optimizing the matrix and nanoparticle morphology.

#### References

- [1] J. Gibbard, *J. Am. Public Health* **27**, 122 (1937).
- [2] C.A. Moyer, L. Brentono, D.L. Gravens, H.W. Margrat, W.W. Monafu, *Arch. Surg.* **90**, 812 (1965).
- [3] C.L. Fox, B.W. Rappole, W. Stanford, *Surg. Gynecol. Obstet.* **14**, 168 (1969).
- [4] J.J. Buckley, P.L. Gai, A.F. Lee, L. Olivi, K. Wilson, *Chem. Comm.* 4013 (2008).

# UNRAVELLING THE INTERNAL STRUCTURE OF COMPLEX NANOCRYSTALS: SPECTROSCOPY BEYOND MICROSCOPY

P.K. Santra<sup>1</sup>, R. Viswanatha<sup>1</sup>, S.M. Daniels<sup>2</sup>, N.L. Pickett<sup>3</sup>, J.M. Smith<sup>4</sup>, P.O'Brien<sup>2</sup>, D.D. Sarma<sup>1,5</sup>

<sup>1</sup>*Solid State and Structural Chemistry Unit, Indian Institute of Science, Bangalore, India*

<sup>2</sup>*Department of Chemistry, University of Manchester, Manchester, United Kingdom*

<sup>3</sup>*Nanco Technologies Ltd., Manchester, United Kingdom*

<sup>4</sup>*Department of Materials, University of Oxford, Oxford, United Kingdom*

<sup>5</sup>*Centre for Advanced Materials, Indian Association of Cultivation of Science, Kolkata, India*

E-mail: [sarma@sscu.iisc.ernet.in](mailto:sarma@sscu.iisc.ernet.in)



VUV

In recent times, semiconductor nanoparticles with enormous diversity of the internal structure, such as core-shell structures, have attracted substantial interest due to their immense potential applications in different fields such as light emitting diodes and displays, optoelectronics, bio-sensing, bio-labeling etc. Over a period of time, syntheses of different semiconductor nanoparticles have improved systematically in terms of the tunability and quantum efficiency of photoluminescence, which is central to many of the applications mentioned above. A new variant of complex internal structure for such nanoparticles is the so-called quantum dot-quantum well (QDQW). QDQW structure is synthesized with a core of higher band gap material followed by two shells, the first of a low band gap material and an outer layer of the same high band gap material as that of the core. These types of heterostructured nanoparticles are specifically interesting, as these allow independent control of the band gap and the overall nanoparticle size. Such heterostructured nanoparticles, QDQW as well as core-shell ones, are implicitly assumed to have a sharp and pure interface between the constituent layers. However, the chemical processes used for synthesizing such heterostructured nanoparticles do not preclude the possibility of intermixing/alloying between different layers. Unfortunately, various forms of microscopy, such as transmission electron microscopy (TEM), can only determine the overall size and shape of such nanoparticles, but not the internal structure, due to a lack of substantial contrast between different elements; this problem is further complicated in presence of any inter-diffusion of different elements across the interfaces.

In this context, we recall the high surface sensitivity of X-ray photoelectron spectroscopy (XPS), in the order of 0.5 nm, arising from an extremely short escape depth of the photoelectron. Moreover, a change in the photon energy enables one to change the escape depth controllably. XPS can determine the average composition from the intensity ratios of the core level spectra of different components. Thus, the intensity ratios of different core level spectra provide a certain weighted average value for the composition relevant for the thickness of the sample being probed at that photon energy. By increasing the photon energy moderately, one then averages the composition over a slightly larger thickness. Therefore, the change in the average composition with changing photon energy contains compositional information of the extra thickness of the sample that is added in the averaging of the composition with the higher photon energy. Thus, it becomes possible to extract the composition layer-by-layer of any complex material by systematically changing the photon energy. In essence, in place of a lateral resolution afforded by any microscopic technique, the vertical resolution using the depth sensitivity and composition sensitivity, both unique to XPS, can be used to unravel the compositional structure in such detail that is unique to this technique. It is obvious that the determination of the internal structure of the nanocrystal is made possible by a happy coincidence of the typical mean escape depth of electrons in XPS being in the same order as the size of these nanocrystals.

Using extensive photon-energy dependent XPS experiments on ZnS-CdSe-ZnS nanoparticles with QDQW structures at VUV beamline of Elettra, we recently determined *unique-*

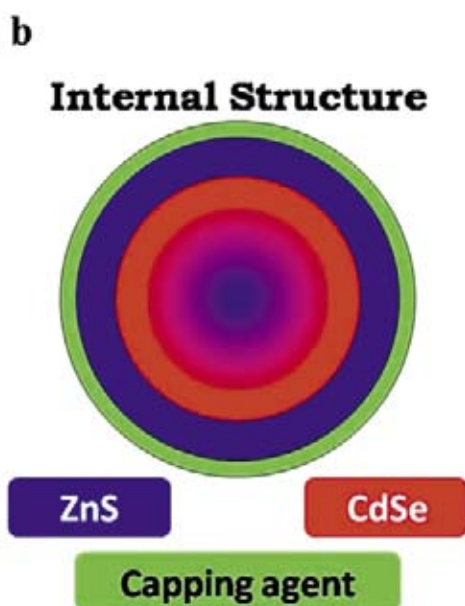
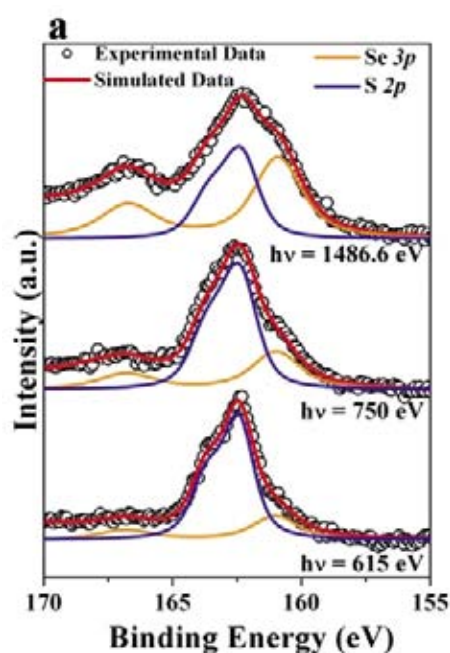


**Figure 1.** (a) High resolution X-ray photoemission spectra of S 2p and Se 3p core levels collected at different photon energies. The experimental data are shown by the black dots and the total fit is by the thick red line which is the sum of two independent component functions of S 2p (blue) and Se 3p (saffron). b. Schematic model of the heterostructured nanoparticle, which has three main layers. A gradient non homogenous alloy has formed at the core followed by a thick shell of CdSe and thinner shell of ZnS.

ly and *unambiguously* the internal heterostructure of such a complex nanoparticle for the first time [1]. The credibility of the analysis was further extended by requiring that the overall chemical composition and the total size obtained from the XPS analysis be consistent with those obtained from inductively coupled plasma assisted Atomic Emission Spectroscopy and TEM, respectively. We have shown the XPS signals of S 2p and Se 3p collected at different photon energies in Figure 1(a). Evidently, the relative intensity of the Se 3p signal increases rapidly compared to S 2p with an increasing photon energy. This rapid increase arises from a higher abundance of Se

towards the core of the sample. A detailed analysis of the intensity ratio provides a clear understanding of the radial compositional variation within the sample. Our analysis shows that such materials do not have the idealized and generally assumed sharp interface; instead the sample forms a graded alloy structure with significant and positive impact on its optical properties. Detailed information of internal structures of these samples is available in Ref. [1].

#### References

- [1] P. K. Santra, R. Viswanatha, S. M. Daniels, N. Pikett, J. Smith, P. O'Brien and D. D. Sarma, *J. Am. Chem. Soc.* **131**, 470 (2009).

# STRUCTURAL AND CHEMICAL EFFECTS OF PLASMA TREATMENT ON CLOSE-PACKED COLLOIDAL NANOPARTICLE LAYERS

J.I. Flege<sup>1</sup>, B. Gehl<sup>2</sup>, V. Aleksandrovic<sup>3</sup>, Th. Schmidt<sup>1</sup>, A. Frömsdorf<sup>3</sup>, A. Pretorius<sup>1</sup>, S. Bernstorff<sup>4</sup>, A. Rosenauer<sup>1</sup>, H. Weller<sup>3</sup>, J. Falta<sup>1</sup>, M. Bäumer<sup>2</sup>

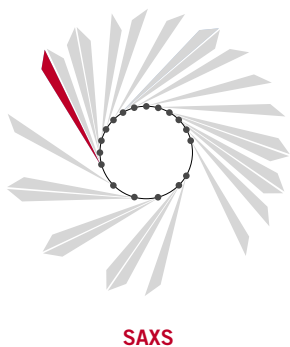
<sup>1</sup>Institute of Solid State Physics, University of Bremen, Bremen, Germany

<sup>2</sup>Institute of Applied and Physical Chemistry, University of Bremen, Bremen, Germany

<sup>3</sup>Institute of Physical Chemistry, University of Hamburg, Hamburg, Germany

<sup>4</sup>Sincrotrone Trieste S.C.p.A., Trieste, Italy

E-mail: flege@ifp.uni-bremen.de



Bimetallic nanoparticles (NPs) comprise a class of materials with unique electronic, chemical and magnetic properties that suggest their use in a wide range of applications, e. g. in heterogeneous catalysis, as chemical sensors or for magnetic data storage. A facile, easily scalable way of producing NPs is offered by wet-chemical synthesis, which quite generally results in their controlled formation with a Gaussian-like size distribution exhibiting a width of less than 10% if performed in an optimized fashion. Frequently, the as-prepared particles are surrounded by a shell of organic molecules, which act as stabilizers and passivate their surfaces to prevent their participation in unwanted chemical reactions. Another beneficial role of the ligand shell is their mediation of self-assembly processes when the NPs are deposited onto flat substrates in ordered arrays employing, e. g., spin-coating, dip-coating, or comparable methods, thereby paving the road to an efficient production of nanostructured materials with superior characteristics from collective effects. However, once the NP films are realized, the organic molecules may interfere with potential applications by modifying their surface chemistry. This is the main reason why several schemes of removing the ligand shell are being developed, the main criterion for suitability being its non-destructive removal with respect to both NP composition and ordering. Here, we present a study that targets selective etching of the organic shell of CoPt<sub>3</sub> NPs suspended on oxidic substrates (SiO<sub>2</sub> and Al<sub>2</sub>O<sub>3</sub>) by exposure to various plasmas and the effects caused on both structure and chemical properties of the NP film [1,2]. Among other techniques, grazing-

incidence small-angle x-ray scattering (GISAXS) is employed for a precise quantitative structural characterization of the sample morphology.

The GISAXS pattern displayed in Figure 1(a) demonstrates the high *average* degree of lateral ordering of NPs in the film by virtue of the pronounced correlation peaks in the horizontal direction, the strongest one being found at an in-plane scattering vector of about 0.64 nm<sup>-1</sup>, from which inter-particle distances of (10.18±0.15) nm can be deduced. In the out-of-plane direction, the ideally rod-like correlation features, which represent the two-dimensional flat film morphology, are modulated in intensity due to the interplay with the form factor corresponding to the spherical shape of the NPs, in very good agreement with theoretical simulations (not shown here). Furthermore, from the width of the first correlation peak, a characteristic length scale for the ordering, the so-called correlation length, can be calculated, which amounts to approximately (90±3) nm, indicating a relatively high degree of correlation within the film.

In order to remove the ligand shell, hydrogen, oxygen, and nitrogen gases were used as active media in an ultra-high-vacuum compatible, home-built radio-frequency plasma source [3]. In-situ x-ray photoelectron spectroscopy (XPS) readily shows that all organic compounds may be removed in this fashion, but especially nitrogen induces severe agglomeration and sintering of the particles, as qualitatively demonstrated by scanning electron microscopy (not shown) [1]. Interestingly, oxygen proves to be the only gas that leads to a complete loss of the ligand shell. However,

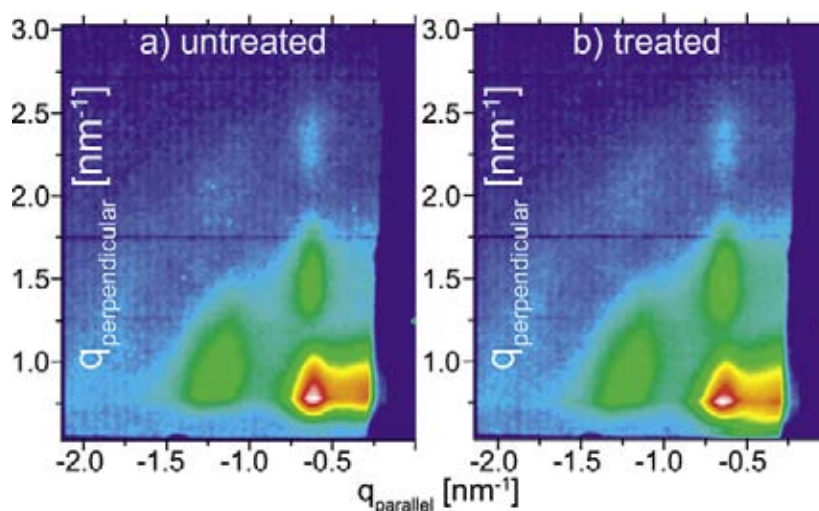


**Figure 1.** 2D GISAXS data for (a) as-prepared and (b) O-H plasma-treated CoPt<sub>3</sub> nanoparticles on SiO<sub>2</sub> (from [2]).

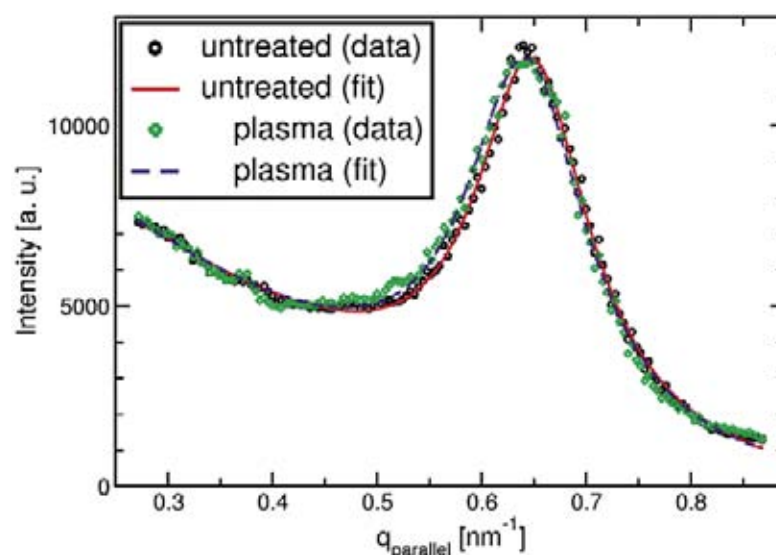


**Figure 2.** In-plane line profiles and Lorentzian fit through first-order correlation peaks in Figures 1(a) and (b) demonstrating subtle differences in the film morphology due to the O-H plasma treatment (from [2]).

XPS reveals substantial oxidation of the NPs, and of the Co component in particular. Fortunately, this circumstance can be remedied by applying hydrogen plasma for a reasonably short time, which reduces the particles into their original metallic state [1]. The GISAXS pattern for this treatment is displayed in Figure 1(b), which qualitatively does not show any significant change as compared to Figure 1(a), indicating the general success of the ligand removal procedure. A closer analysis of the scattering data even suggests a slight contraction of the inter-particle spacing on the order of 1-2%, in accordance with a removal of the organic ligand shell. However, as the order in the film remains virtually unchanged (highlighted by a correlation length of about

(92±4) nm), agglomeration of the particles was effectively suppressed even for close-packed layers.

#### References

- [1] B. Gehl, A. Frömsdorf, V. Aleksandrovic, Th. Schmidt, A. Pretorius, J. I. Flege, S. Bernstorff, A. Rosenauer, J. Falta, H. Weller, M. Bäumer, *Adv. Funct. Mater.* **18**, 2398 (2008).
- [2] B. Gehl, J. I. Flege, V. Aleksandrovic, Th. Schmidt, A. Kornowski, S. Bernstorff, J. Falta, H. Weller, M. Bäumer, *J. Vac. Sci. Technol. A* **26**, 908 (2008).
- [3] B. Gehl, U. Leist, V. Aleksandrovic, P. Nikkut, V. Zielasek, H. Weller, K. Al-Shamery, M. Bäumer, *Rev. Sci. Instrum.* **77**, 083902 (2006).

# AN IN-SITU SXTM, XAS AND XRF INVESTIGATION OF THE ELECTROCHEMICAL CORROSION OF METAL-BASED BIPOLAR PLATE MATERIALS USED IN FUEL CELLS

B. Bozzini<sup>1</sup>, L. D'Urzo<sup>1</sup>, A. Gianoncelli<sup>2</sup>, B. Kaulich<sup>2</sup>, M. Prasciolu<sup>3</sup>, I. Sgura<sup>4</sup>, M. Kiskinova<sup>2</sup>

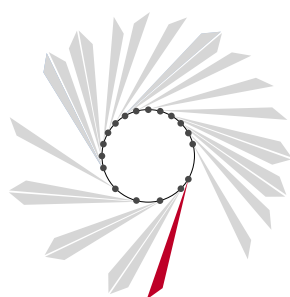
<sup>1</sup>Brindisi Fuel Cell Durability Laboratory, University of Salento, Brindisi, Italy

<sup>2</sup>Sincrotrone Trieste S.C.p.A., Trieste, Italy

<sup>3</sup>Laboratorio Nazionale TASC INFM-CNR, Trieste, Italy

<sup>4</sup>Department of Mathematics, University of Salento, Lecce, Italy

E-mail: burkhard.kaulich@elettra.trieste.it



TWINMIC

The two most critical barriers to widespread commercial application of Polymer-Electrolyte Membrane Fuel-Cells (PEMFC) are: (i) excessive weight and (ii) limited durability. 80% of the weight and 45% of the cost are currently due to the use of graphite bipolar plates (BP) [1]. Thinner, lighter and cheaper BPs can be fabricated with stainless-steel grades, but their poorly known corrosion stability under PEMFC operating conditions requires a notable amount of research. Chemical degradation of membranes is a major cause of PEMFC failure, related to increase of ohmic drop and fuel crossover. In all-graphite PEMFCs the typical cause of chemical degradation is radical attack ( $\bullet\text{OH}$ ,  $\bullet\text{OOH}$ ). With BPs, a new degradation pathway appears, related to the fact that the proton groups of the Nafion side chains may be exchanged with metal ions from the corroding BPs. In particular, it has been proved that the presence of trace amounts of  $\text{Fe}^{2+}$  enhances radical attack of Nafion, no information is available about  $\text{Ni}^{2+}$ .

Following recent success of in-situ characterization of complex systems in electrochemical environments with sub-micrometer lateral resolution using soft X-ray transmission microscopy (SXTM) [2-4], here we demonstrate the expanded potential for such studies adding to X-ray imaging and X-ray absorption spectroscopy (XAS) also X-ray fluorescence-spectroscopy (XRF). The accurate location of corrosion products released by the metal electrodes within the hydrated Nafion film has been provided by correlation of morphological features in the X-ray images, typical of the relevant electrochemistry, with the XRF maps. The evolved chemical states of the species, resulting from the corrosion process and fixation in Nafion, can be identified by micro-spot XAS. This correlative approach is opening new opportunities for exploring fundamental aspects of Nafion contamination, by corrosion products. A critical step for the success of the experiments is the design and fabrication of the electrochemical cell (Figure 1). It consists of

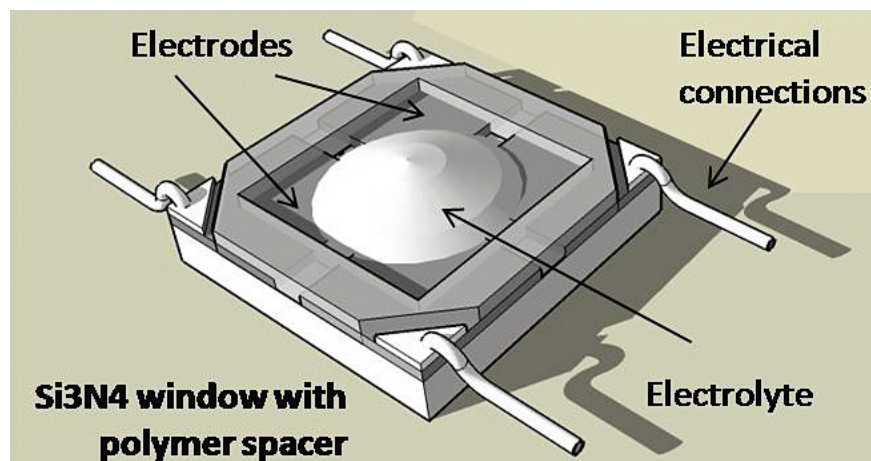


**Figure 1.** Scheme of the electrochemical liquid cell developed in this investigation.

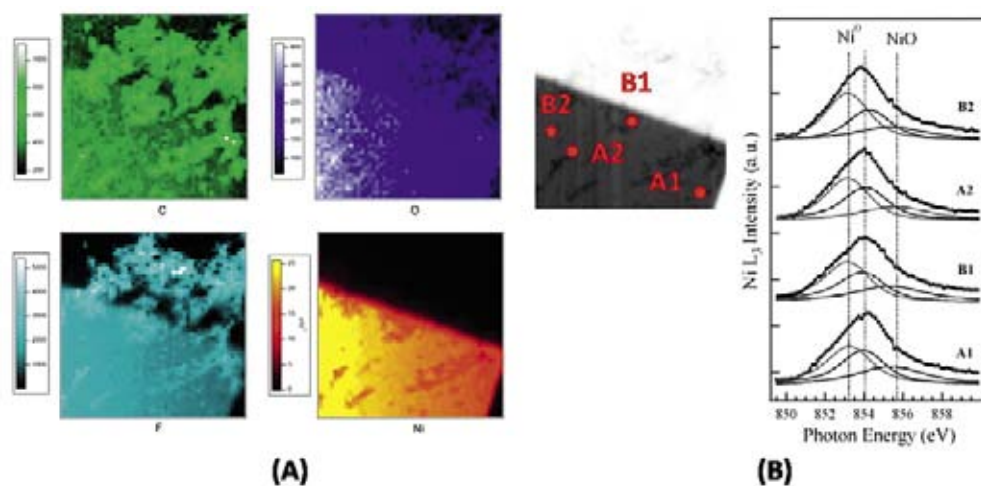


**Figure 2.** (A)  $80 \times 80 \mu\text{m}^2$  XRF maps recorded on a corner of the Ni electrode and the surrounding Nafion electrolyte region (photon energy 1014 eV). The sample was raster scanned  $50 \times 50$  pixels with 11s/pixel acquisition time. (B) Ni  $L_3$  XAS spectra at the positions indicated in the corresponding STM image taken at Ni  $L_3$  edge.

a  $\text{Si}_3\text{N}_4$  window with deposited two square, 40 nm thick Au counter- and quasi-reference electrodes and two 75 nm thick Fe or Ni working electrodes. Lateral electrolyte containment is ensured by a 500 nm thick resist layer, deposited on top of the assembly. The X-ray beam hits normally the cell: the transmitted X-rays and the emitted XRF signal are simultaneously monitored, using CCD and Si detectors, respectively.

The X-ray absorption and XRF images (Figure 2) show a corner of a Ni electrode after galvanic corrosion in the presence of Nafion. We did not highlight any morphology changes of the Ni electrode, where contrast variations in the X-ray maps are related to the Nafion islands. The perfect correlation between C and F lateral distribution in the XRF maps allows to locate the Nafion flakes. No Ni can be found outside of the electrode, whereas O seems to be shared by both the Ni and Nafion areas and is coherent with the distribution of the oxygen containing material. The chemical state of the Ni electrode was assessed on the basis of the Ni  $L_3$  spectra measured inside the electrode. The deconvolution of the spectra was made considering the reported spectra corresponding to the  $\text{Ni}^0$  (single component at  $\sim 853.1$  eV) and NiO

(two components at  $\sim 854$  and  $855.8$  eV). The spectra show some degree of lateral inhomogeneity in the thickness of the NiO passivating layer. The portion of the Ni electrode covered with a Nafion layer (point C2) seems slightly less oxidised. The absence of Ni species outside the electrode confirms the passivation ability of Ni in the relevant environment, at variance with the corrosion mode of the Fe electrode that we revealed under identical conditions.

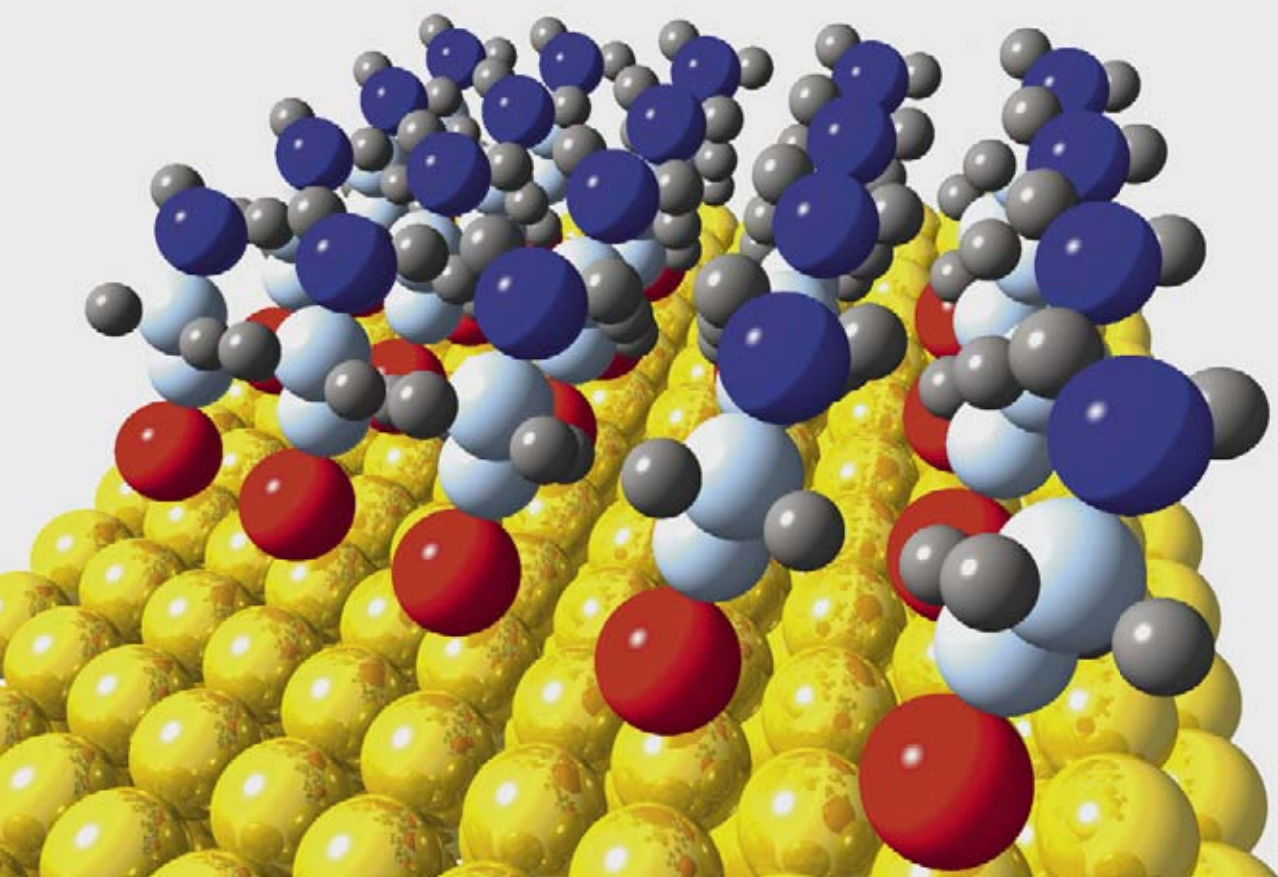
In-situ investigation of an electrochemical system employing simultaneously soft X-ray microscopy and space resolved X-ray spectroscopies has potential impact in the acquisition of fundamental information relevant to fuel-cell technology, but also potentially to all fields of electrochemical materials science and bio-electrochemistry.

### References

- [1] Ch. Y. Chung *et al.*, *J. Power Sources* **176**, 276 (2008).
- [2] D. Guay *et al.*, *Anal. Chem.* **77**, 3479 (2005).
- [3] B. Bozzini *et al.*, *Electrochem. Comm.* **10**, 1680 (2008).
- [4] B. Bozzini *et al.*, *J. Phys. Chem. C* **113**, 9783 (2009).



## ORGANIC FILMS AND SELF-ASSEMBLY





# SHEDDING LIGHT ON TRANSPORT PROPERTIES

## A link between electrical conductivity and structure of surfaces and nano-materials

*An interview with Philip Hofmann*

We have caught up with Philip Hoffman to ask a few questions related to his recent work on conductance measurements. Here you will find a transcript of his views on various issues ranging from molecular electronics to the fundamental role played by synchrotron radiation for understanding the properties of these complex systems. More information can be found in his highlighted article at page 28.

Philip Hofmann studied physics at the Free University, Berlin and did his PhD research at the Fritz-Haber-Institute of the Max Planck Society, also in Berlin. He stayed at the Oak Ridge National Laboratory, USA as a Feodor Lynen Fellow of the Alexander von Humboldt Foundation. In 1998, he moved to the University of Aarhus, Denmark, where he is associated with the Synchrotron Radiation Source and the Interdisciplinary Nanoscience Center (iNANO). His research is primarily focused on the electronic structure of solids and their surfaces.



**Your recent research deals with the conductance measurement through a layer of molecules on a surface. Can you tell us a little about the background of this and why the scientific community is nowadays so interested in measuring it?**

We are currently reaching the physical size limits for building electronic component on computer chips. While we got used to having a new and more powerful generation of computers every few years or so, this is no longer possible because one just cannot make the components any smaller. People have thought of many possible approaches to solve this problem and following the well-established path of better lithography for smaller structures just does not seem to be an option any more.

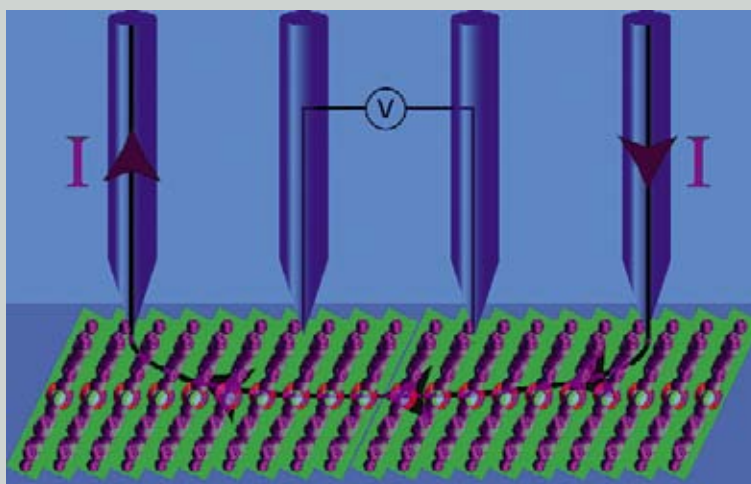
One revolutionary idea to solve the problem is called “molecular electronics” and on the face of it sounds extremely bold: the reasoning goes that if we can find the right mixture of very special molecules and put them on a surface, they could find each other to build a complex and functional structure. For example, they could form a network of structures working as transistors and the whole network then acts as a self-assembled memory chip or microprocessor.

... but this sounds extremely far-fetched....

Indeed, but maybe less than you would think. In fact, researchers have made tremendous progress in building rather fancy molecular networks on surface and there are many clever ideas about how this can be improved even more. Single-stranded DNA fragments, for example, have the build-in ability to recognize each other such that a mixture of them can spontaneously self-assemble into some pre-programmed structures. A group at my University has, for example, created a mix of DNA which spontaneously forms tiny dolphins on a surface, the emblem of the University of Aarhus.

The downside of all this, and this is where our work comes into play, is that while it is possible to create complicated structures, almost nothing is known about the electrical conductivity of the structures but this is, in the end of the day, the most crucial feature in molecular electronics. To put it quite frankly: forming the nicest structures of molecules does us very little good if we do not know anything about their conductive properties. This is why we have started our research project featured here: we wanted to measure the electrical conductivity of a film of molecules on a surface along the direction of the film. The system we have chosen for this is admittedly extremely simple, a long way from anything meaningful in practice, but it is important as a proof of principle.

**Illustration 1.**  
Schematic representation of the multi-probe experimental set-up used for determining the conductance of CoPC molecules.



### What is then so special about these new measurements?

The most important point is to realize that the measurement itself is far from easy: most self-assembled molecular layers people have studied so far are placed on the surfaces of copper or gold crystals, i.e. on very good conductors. While this favours the formation of the networks, it also renders the structures useless for any electronic application. Roughly spoken, the metal underneath the molecules conducts so well that no reasonable fraction of current is ever going through the molecules. Consequently, a useful molecular film has to be placed on a semiconductor or an insulator. But even then, it is difficult to pass a current through the molecules. One possibility to do this is to use contacts which are placed at a very small distance from each other. Then, the current does not penetrate very deeply into the substrate and one can measure the contribution of the molecules.

In order to achieve this, we have used a very special sensor fabricated by Capres in Copenhagen. On this sensor the distance between the contacts can be as small as 500 nm and this enabled us to measure the current through the molecules.

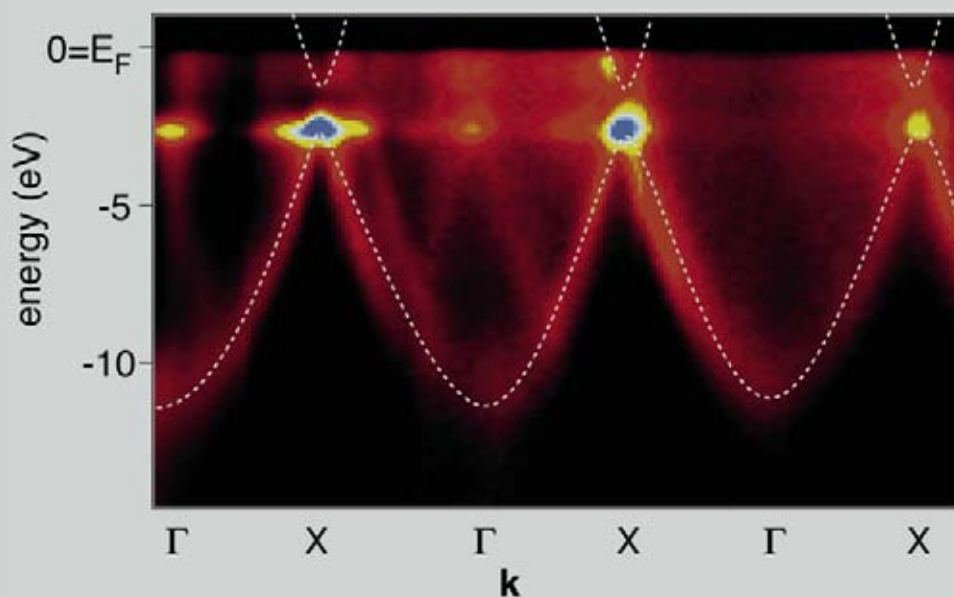


**Illustration 2.**  
An example of band structure determined at the SuperESCA beamline by angle-resolved photoemission. Front cover of "Solid State Physics" Philip Hofmann, Wiley WCH Verlag GmbH&Co. KGaA (2008).

### What role does the use of Elettra's synchrotron radiation play in the understanding the properties of these complex systems?

The conductance measurements are done with the sensors just mentioned and do, of course, not require any synchrotron radiation. It turned out, however, that the physics of the molecular conductance is quite complex. When one layer of molecules is put on the surface, these lie flat down and just touch each other at the edges. Such a layer conducts very poorly. However, when more molecules are put on the surface, they start to stand up and form a stack of touching molecules. Only then does the layer start to conduct. In order to understand all this, one has to know the orientation of the molecules on the surface and here the synchrotron radiation comes into play. Sources like Elettra give brilliant x-rays for which the energy can be tuned over a wide range. The technique called Near Edge X-Ray Absorption Fine Structure has enabled us to know how the molecules are oriented for different coverages and this turned out to be essential for understanding their conductance.

On a more general note, the link between conductance measurements and the structural and spectroscopic techniques offered at a synchrotron is a very important one: Angle-resolved photoemission spectroscopy, for instance, gives us very detailed insight in the electronic properties of solids in general and at the highest occupied states in particular. The electrons in these highest occupied states, which form the so-called Fermi surface, are the ones which conduct electricity through a sample. Photoemission spectroscopy has given us many examples of the surface of a material or a nano-structure having more of such electrons than the inner bulk material but it is very difficult to find out if this also leads to higher conductance. Here the nano-scale conductance sensors can really make a difference because we will be able to learn as much about the conductance of surfaces and nano-materials as we already know for big chunks of bulk material.

### In which direction will future experiments move?

We are now in a position to measure the conductance through molecular structures and to related this to the structure and electronic structure. I believe that this research is the basis for a more systematic search for molecular structures and concepts which can be employed in molecular electronics. This type of research is going to be an interplay of many techniques. One is the actual measurement of the conductance but equally important are the determination of molecular structures and electronic structures, and both are going to be investigated mainly using synchrotron radiation.

# DIRECT MEASUREMENT OF ELECTRICAL CONDUCTANCE THROUGH A SELF-ASSEMBLED MOLECULAR LAYER

F. Song<sup>1,2,3,4</sup>, J.W. Wells<sup>1,2,4</sup>, K. Handrup<sup>1,2</sup>, Z.S. Li<sup>5</sup>, S.N. Bao<sup>3</sup>, K. Schulte<sup>6</sup>, M. Ahola-Tuomi<sup>7</sup>, L.C. Mayor<sup>6</sup>, J.C. Swarbrick<sup>6</sup>, E.W. Perkins<sup>1,2,6</sup>, L. Gammelgaard<sup>8</sup>, Ph. Hofmann<sup>1,2</sup>

<sup>1</sup>Institute for Storage Ring Facilities, University of Aarhus, Aarhus, Denmark

<sup>2</sup>Interdisciplinary Nanoscience Center, University of Aarhus, Aarhus, Denmark

<sup>3</sup>Department of Physics, Zhejiang University, Hangzhou, China

<sup>4</sup>Norwegian University of Science and Technology, Trondheim, Norway

<sup>5</sup>Institute for Storage Ring Facilities, University of Aarhus, Aarhus, Denmark

<sup>6</sup>School of Physics and Astronomy, University of Nottingham, Nottingham, United Kingdom

<sup>7</sup>Department of Physics and Astronomy, University of Turku, Turku, Finland

<sup>8</sup>Capres A/S, Lyngby, Denmark

E-mail: justin.wells@ntnu.no



BACH

The self-assembly of conductive structures on surfaces is a promising approach for the development of nanoscale electronic devices (see, for example Ref. [1]). A variety of strategies have been employed in order to achieve this, but direct measurement of the electrical transport between molecules has remained largely unexplored. Extended electronic states (an important pre-requisite for good conductivity) have been revealed for a variety of molecules on metal surfaces, but this is of little practical use since any real device requires a substrate which is less conductive than the self-assembled film. Semiconducting substrates appear to be the best approach for device applications, however this presents some challenges since self-assembly processes of molecules on semiconductor surfaces are less understood, and since such surfaces are often more reactive than noble metal surfaces, and hence have the likelihood of damaging the adsorbed molecules.

In this work [2], we have endeavoured to address some of these challenges. First, we use a silicon substrate since this allows easier integration with existing silicon-based technologies. In order to pacify the otherwise reactive (111) surface, we adsorb a monolayer of silver to form the semi-metallic  $\text{Ag}(\sqrt{3}\times\sqrt{3})$  reconstruction, referred to hereafter as Ag/Si (the conductivity of this surface has been characterised by ourselves in earlier work [3]). Onto this surface, we adsorb carefully controlled amounts of the organic molecule Cobalt phthalocyanine (CoPC) (see Figure 1(a)), which is known to be semiconducting in its solid bulk phase.

A prerequisite to understanding the conductivity of a film is understanding the film itself. Whilst Ag/Si has been extensively studied, the growth of CoPC on this surface has not been reported previously. Using NEXAFS at the BACH beamline of Elettra, we have studied the growth of CoPC on Ag/Si for a wide range of film thicknesses. From this, we have been able to conclude that these planar molecules lie almost flat on the surface for sub-monolayer coverages (see Figure 1(e)), and stack at  $\sim 64^\circ$  to the surface normal for thicker films, similar to the bulk  $\alpha$  geometry (see Figure 1(d)). Furthermore, using synchrotron photoemission techniques (in Elettra as well as MAXlab in Sweden and Astrid in Denmark) we can probe the physics and chemistry of the interface. From these studies, we can conclude that the CoPC molecules are weakly interacting with the underlying Ag/Si; there is evidence of charge transfer between the  $\text{Co}^{2+}$  ion and the substrate, but no strong bonding.

In addition to these synchrotron studies, we have developed a multi-probe instrument which enables us to make 4-point conductance measurements over a range of length scales down to a few hundred nanometers (see Figure 1(b) and Ref. [4] for details). This multi-point probe is almost unique and allows us to directly measure the conductivity of the molecular layer (Figure 1(c)), rather than trying to infer the conductivity from photoemission measurements.

Using this multi-probe instrument we found that for sub-monolayer coverages of CoPC the molecules form an incomplete layer and are

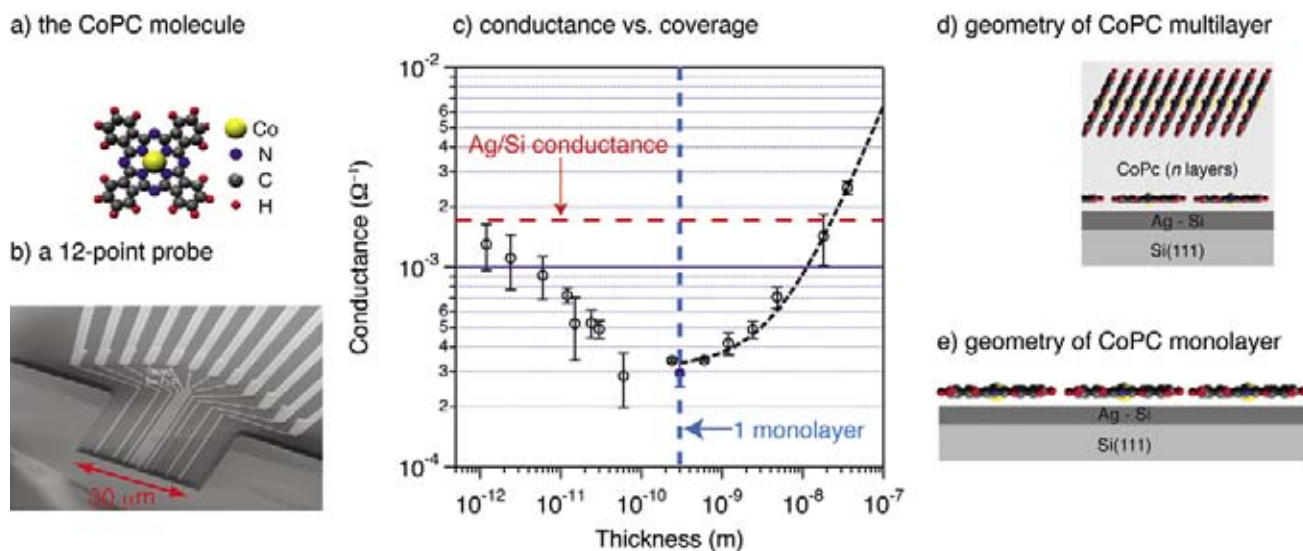


**Figure 1.** (a) The structure of the CoPC molecule; (b) a picture of the multi-contact probe used. The measurements reported here are performed using the innermost 4 contacts which have a separation of 500 nm. (c) Measured conductance of the Ag/Si/CoPC structure as a function of CoPC film thickness. The conductance of the clean Ag/Si surface is indicated by the dashed red line. The dashed blue line indicates the film thickness corresponding to 1 monolayer. (d) and (e) show the geometric structure of the self-assembled CoPC multilayer and monolayer respectively, as calculated from the NEXAFS measurements performed at Elettra (see Ref. [2] for details).

unable to conduct over any macroscopic distance. However, a reduction in the conductivity of the underlying Ag/Si surface is observed, and this is attributed to the observed charge transfer from the surface to the adsorbed CoPC molecules.

For monolayer and multilayer coverages, the CoPC molecules self assemble to form a conducting film. The conductivity was found to be similar to that of the electron-doped bulk value reported previously.

Further details of this work can be found in our recent publication [2] and in the supporting online material.

In conclusion, we have used a variety of techniques to study the self-assembly of the con-

ducting organic molecule CoPC on the silver passivated silicon (111) surface. We have been able to directly measure the conductivity of the self-assembled layer and to describe the observed behaviour using complementary studies of the geometric and electronic structure.

#### References

- [1] J.V. Barth *et al.*, *Nature* **437**, 671 (2005).
- [2] F. Song *et al.*, *Nature Nanotechnology* **4**, 373 (2009).
- [3] J.W. Wells *et al.*, *J. Phys. Condens. Matter* **19**, 176008 (2007).
- [4] L. Gammelgaard *et al.*, *Appl. Phys. Lett.* **93**, 093104 (2008).

# ZN-TETRAPHENYL-PORPHYRIN AND C<sub>70</sub>: DONOR-ACCEPTOR COUPLES TO MIMIC THE PHOTOSYNTHESIS FOR SOLAR CELL DEVICES

P. Vilmercati<sup>1,2</sup>, C. Castellarin-Cudia<sup>1</sup>, R. Gebauer<sup>3,4</sup>, P. Ghosh<sup>3</sup>, S. Lizzit<sup>1</sup>, L. Petaccia<sup>1</sup>, C. Cepek<sup>5</sup>, R. Larciprete<sup>1,6</sup>, A. Verdini<sup>5</sup>, L. Floreano<sup>5</sup>, A. Morgante<sup>5</sup>, A. Goldoni<sup>1</sup>

<sup>1</sup>Sincrotrone Trieste S.C.p.A., Trieste, Italy

<sup>2</sup>Physics Department, University of Trieste, Trieste, Italy

<sup>3</sup>International Center for Theoretical Physics, Trieste, Italy

<sup>4</sup>INFM-Democritos, Trieste, Italy

<sup>5</sup>Laboratorio Nazionale TASC INFM-CNR, Trieste, Italy

<sup>6</sup>CNR - Istituto dei Sistemi Complessi, Roma, Italy

E-mail: andrea.goldoni@elettra.trieste.it



**SUPERESCA and ALOISA**

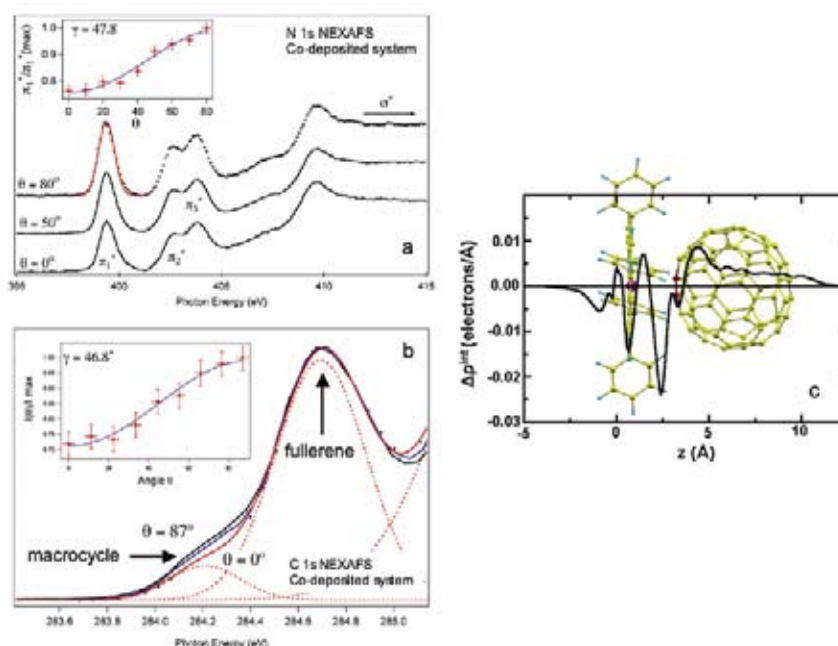
**Figure 1.**

(a) NEXAFS spectrum at the N1s threshold as a function of angle between the linear light polarization and the substrate. It gives the average orientation of the ZnTPP macrocycle plane with respect to the substrate surface by fitting the data reported in the inset. (b) The same as above at the C1s threshold. In the inset are reported the data relative to the first structure (macrocycle). The fullerene peak does not show dichroism. (c) DFT calculations showing the obtained relative molecular orientations and the charge bond reorganization in the ground state.

The modern society has a general trend toward renewable energy sources. Solar energy is certainly the most interesting one and the ability to create high-efficiency solar cells is a key strategy to meet the growing world energy needs. However, to become competitive in term of price/watt, compared to the oil or gas sources, the cost of the solar cell should be reduced by a factor of 5. A possible way is to use organic material instead of silicon to form the devices, since organic materials can absorb sunlight with high efficiency. The first step in the process of light conversion into electricity can be schematically described as the absorption of a photon with the formation of an excited bound electron-hole pair (exciton) and the exciton diffusion to a region where it can dis-

sociate, i.e. a donor-acceptor reaction center where the excited electron is transferred from the donor to the acceptor [1].

In nature a quite similar mechanism happens in photosynthetic materials [2]. Chlorophyll (Mg-based porphyrin) and carotenes are used as donors, while quinones are used as acceptors. With the advent of fullerenes a new three-dimensional electron acceptor became available with remarkable properties in both ground and excited states for photovoltaic devices [3]. Therefore, porphyrin and fullerene are promising candidates for the construction of two- and three-dimensional organic-based solar cells. The majority of studies used some molecular linker to connect the fullerene to the porphyrin, but to get more insight into the influence



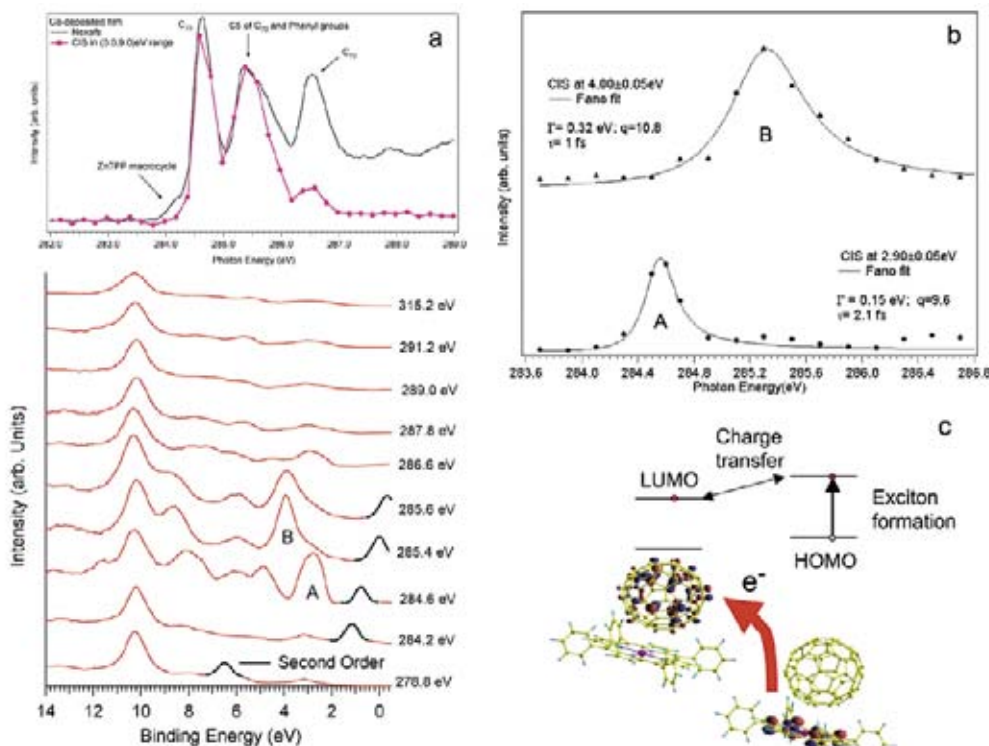


**Figure 2.**

(a) -Bottom panel- A selection of resonant photoemission spectra across the C 1s threshold. The spectra correspond to the maxima in the C 1s NEXAFS spectrum shown above. The peak due to second order radiation has been shown as black line and then subtracted. -Top panel- NEXAFS spectrum at the C 1s threshold compared to the constant initial state (CIS) spectrum obtained by integrating in the range 0–9 eV the valence band at each photon energy. In the  $\pi^*$  region this should be similar to the NEXAFS spectrum unless some resonances are quenched, as in the case of the ZnTPP macrocycle. (b) C 1s spectra of the resonant features A and B and the corresponding fit using a Fano profile. The fit parameters and the resulting hole-lifetime  $\tau$  are also reported. (c) Calculated HOMO and LUMO molecular orbitals of the ZnTPP+C<sub>70</sub> complex and a schematic energy alignment showing the HOMO absorption of light, the photo-excited exciton formation and the transfer of the photo-excited electron to the LUMO with the corresponding exciton dissociation.

of molecular topology on electron transfer, a few porphyrin–fullerene dyads in which the  $\pi$  systems are structurally forced into a face-to-face arrangement were also obtained in solutions or in co-crystals [3].

Here we report on ordered nano-structured multilayers of donor-acceptor pairs obtained by co-deposition of Zn-tetraphenyl-porphyrin (ZnTPP) and C<sub>70</sub> in ultra-high-vacuum by powder sublimation on Si(111) [4]. An important question is how pristine fullerene and porphyrin will organize when co-deposited on surfaces. The occurrence of a preferential orientation was determined using linearly polarized synchrotron radiation by angular dependent Near Edge X-ray Absorption Fine Structure (NEXAFS). Figure 1 shows that co-deposition of C<sub>70</sub> and ZnTPP induces the self-assembly of electron-rich flat aromatic molecules at the curved surface of C<sub>70</sub>, thus enhancing the chromophore interaction and forming a supramolecular multilayer donor-acceptor structure. The porphyrins have an average preferential angle of  $47.3 \pm 2.5^\circ$  and the fullerenes stay with the long axis at the magic angle of  $35.3^\circ$  with respect to the substrate surface. These measurements were complemented by density-functional (DFT) calculations for an isolated pair of ZnTPP+C<sub>70</sub>. The fullerene have a “side on” orientation with respect to the porphyrin macrocycle. The angle between the long axis of C<sub>70</sub> and the macrocycle plane is  $\sim 10^\circ$  in agreement with the experiment. To have charges transported at the electrodes, the first point for a solar cell is the exciton charge transfer timescale that should be faster than the typical timescale of other electron de-

excitation mechanisms (ms–500 fs). This problem was investigated using resonant photoemission (ResPES). This technique is equivalent to a pump-and-probe experiment, where one electron is *pumped* from a core level to an empty bond state, and the decay channels of the core hole are studied. The balance between the resonant and the non-resonant decay channel is a fingerprint of the fast excited charge delocalization. The core-hole lifetime gives an upper limit for this timescale.

As demonstrated by photoemission experiments and DFT calculations the ground-state electronic spectra almost reflect a simple summation of ZnTPP and C<sub>70</sub> components. As expected the calculated HOMO and LUMO states are localized on the porphyrin and on the fullerene, respectively, as shown in Figure 2(c). On the other hand, our ResPES studies (Figure 2(a,b)) indicate the existence of charge-transfer interactions in the excited states. The resulting face-to-face geometry of the dyads allows efficient photoinduced electron transfer from the ZnTPP macrocycle to the C<sub>70</sub> moiety in order to produce the charge-separated state in a time faster than 1–2 fs. This is an extremely fast charge transfer time, making the co-deposited porphyrin–fullerene multilayer a promising system for organic solar cells.

## References

- [1] J.-M Nunzi, *C. R. Physique* **3**, 523 (2002).
- [2] Y. Sakata and H. Imahori, *Adv. Mater.* **9**, 537 (1997).
- [3] D. Sun *et al.*, *PNAS U.S.A.* **99**, 5088 (2002).
- [4] P. Vilmercati *et al.*, *J. Am. Chem. Soc.* **131**, 644 (2009).

# SELF-ASSEMBLY OF L-METHIONINE NANOGRATINGS ON THE Ag(111) AND Cu(111) SURFACE

A. Schiffrin<sup>1,2</sup>, J. Reichert<sup>3,4</sup>, Y. Pennec<sup>3</sup>, W. Auwärter<sup>3,4</sup>, A. Weber-Bargioni<sup>3</sup>, M. Marshall<sup>4</sup>, M. Dell'Angela<sup>5</sup>, D. Cvetko<sup>7</sup>, G. Bavdek<sup>7</sup>, A. Cossaro<sup>5</sup>, A. Morgante<sup>5,6</sup>, J. V. Barth<sup>3,4</sup>

<sup>1</sup>Department of Chemistry, The University of British Columbia, Vancouver, Canada

<sup>2</sup>Max-Planck-Institut für Quantenoptik, Garching, Germany

<sup>3</sup>Department of Physics & Astronomy, The University of British Columbia, Vancouver, Canada

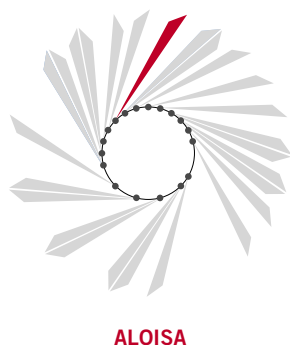
<sup>4</sup>Physik Department, Technische Universität München, Garching, Germany

<sup>5</sup>Laboratorio Nazionale TASC INFN-CNR, Trieste, Italy

<sup>6</sup>Physics Department, University of Trieste, Trieste, Italy

<sup>7</sup>Physics Department, University of Ljubljana, Ljubljana, Slovenia

E-mail: morgante@tasc.infn.it

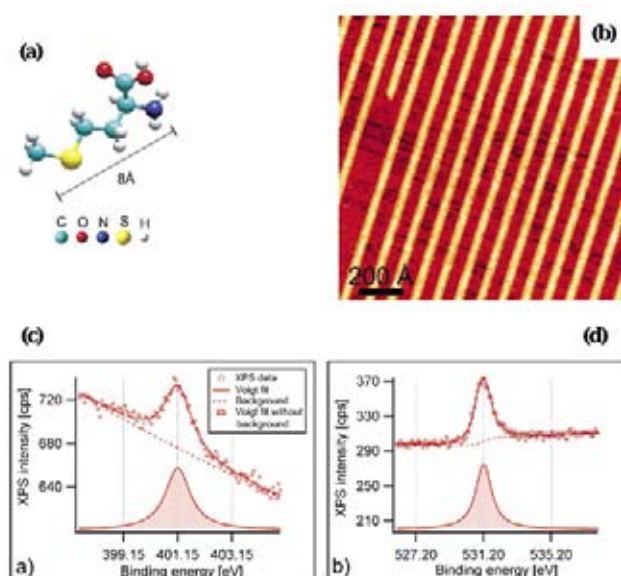


The study of the adsorption of amino acids on surfaces and the translation of their chiral properties in two dimensions are the key to rationalize processes such as molecular recognition and chiral selectivity in biological systems [1]. Moreover this understanding can lead to the evaluation of their self-assembly capabilities for potential noncovalent synthesis of functional two-dimensional nanostructures and can be useful for the prospective design of biocompatible materials [2]. In general, the formation of stable two-dimensional supramolecular self-assemblies at thermodynamic equilibrium is governed by the lateral interactions between the adsorbed molecular entities, but also by the nature of the chemical and structural characteristics of the underlying support. Strong substrate-molecule interac-

tions influence the diffusion properties of the adsorbed species, induce intramolecular conformational changes and even catalytically alter the chemical state of the molecules, having dramatic consequences on the supramolecular self-assembly configuration. We have performed a combined Low-Temperature Scanning Tunnelling Microscopy (LT-STM), He Atom Scattering (HAS) and X-ray Photoelectron Spectroscopy (XPS) study on the self-assembly of the chiral amino acid L-methionine on Ag(111) and Cu(111) in ultra high vacuum conditions [3,4]. L-methionine (Figure 1(a)), in particular, presents three functional groups that can potentially govern molecule-molecule or molecule-substrate interactions: the amino (-NH<sub>2</sub>), the carboxyl (-COOH) and the thioether (-S-) group.

**Figure 1.**

(a) Structure model of L-methionine in its neutral gas phase state with color-coded atoms. (b) STM topographic data show the L-methionine molecules self-assembling on Ag(111) into extended 1D arrangements following the close packed <110> orientations of the substrate. (c) N 1s and (d) O 1s XPS spectra with singular peaks at 401.15 eV and 531.2 eV respectively, corresponding to zwitterionic molecules.





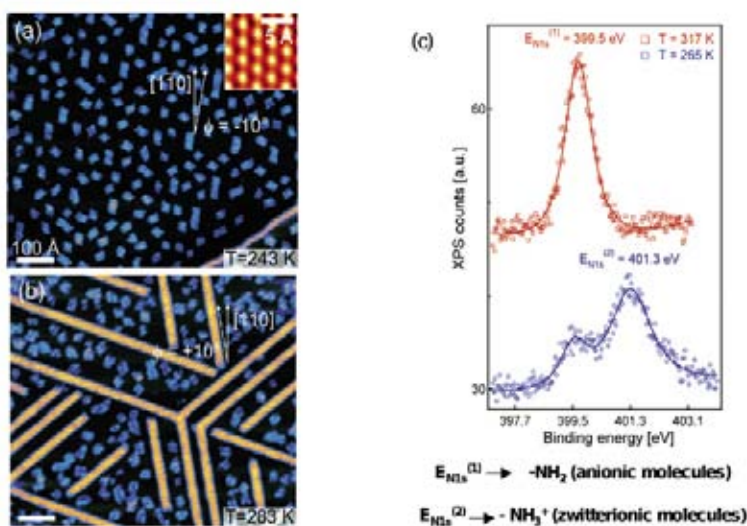


**Figure 2.** Homochiral L-methionine biomolecular self-assembly on Cu(111). (a) L-methionine strings following deposition on Cu(111) at T=243 K. Inset: atomic resolution of the Cu(111) substrate. (b) Deposition at T=283 K: extended 1D chains emerge. Scale bars: 100 Å (c) N 1s XPS spectra of the assemblies formed at T=265 K (blue trace) and T=317 K (red trace) comprising respectively mostly zwitterionic molecules and anionic molecules.

On Ag(111) L-methionine self-assembles in extended one-dimensional (1D) nanostructures running parallel to the close packed crystallographic orientations of the underlying atomic lattice. These commensurate chains arrange mesoscopically into regular biomolecular gratings whose periodicity can be controlled by tuning the molecular coverage (Figure 1(b)). Molecular resolution STM data and XPS measurements (Figure 1(c) and (d)) [3] revealed that the formation of the molecular chains is driven by the hydrogen bonding of L-methionine molecules in the zwitterionic state ( $\text{CH}_3\text{SCH}_2\text{CH}_2\text{CH}(\text{NH}_3^+)(\text{COO}^-)$ ).

On Cu(111) the molecular ordering is strongly influenced by the higher reactivity and the smaller lattice constant of the substrate with respect to Ag(111). STM and HAS measurements [4] indicated that at low temperature (<273 K), irregular molecular strings evolve for submonolayer coverages (Figure 2(a)), whereas the saturated monolayer exhibits partial ordering arising from the influence of the substrate symmetry, with linear structures growing with a  $-10^\circ$  (clockwise) tilt with respect to the  $\langle 110 \rangle$  crystalline orientations. On the other hand, following deposition on the substrate held at temperatures above 283 K, a regular 1D phase arises oriented with an angle of  $+10^\circ$  with respect to the  $\langle 110 \rangle$  axes coexisting with patches of disordered low temperature phase (Figure 2(b)). Molecular resolution STM measurements of the ordered 1D arrangement indicate dimerization and a second-order commensurability with the atomic lattice of the substrate along the chain direction. O 1s and N 1s (Figure 2(c)) XPS measurements revealed that the high temperature ordered phase comprises the molecules in their anionic state, with a deprotonated carboxylic group ( $-\text{COO}^-$ ) and a neutral amino group ( $-\text{NH}_2$ ). In contrast, the

low temperature disordered phase reflects an heterogeneous zwitterionic and anionic self-assembly, where the anionic state is associated with metal-ligand binding of the amino acid molecular with the more reactive, less coordinated copper atoms at step-edges. XPS and HAS measurements have shown that the supramolecular assembly formed at low temperature can be transformed into the high temperature phase by heating, which means that the self-assembly is triggered by a thermally activated chemical transformation which is mediated by the reactivity of the underlying Cu(111) substrate and which switches the adsorbed molecular units chiral organization. The chemical reactivity of the Cu(111) substrate, in fact, induces a thermally activated deprotonation of the amino acid amonium group, which drives a morphological chiral switching process within the biomolecular ensemble and reveals an entirely new supramolecular configuration. The underlying crystal, through its structural and chemical properties, plays therefore a key role in the equilibrium outcome of the self-assembly process.

## References

- [1] A. Kühnle, T.R. Linderoth, B. Hammer, F. Besenbacher, *Nature* **415**, 891 (2002).
- [2] J.V. Barth, G. Costantini, K. Kern, *Nature* **437**, 671 (2005).
- [3] A. Schiffrin, A. Riemann, W. Auwärter, Y. Pennec, A. Weber-Bargioni, D. Cvetko, A. Cossaro, A. Morgante, J.V. Barth, *Proc. Natl. Acad. Sci.* **104**, 5279 (2007).
- [4] A. Schiffrin, J. Reichert, Y. Pennec, W. Auwärter, A. Weber-Bargioni, M. Marschall, M. Dell'Angela, D. Cvetko, G. Bavdek, A. Cossaro, A. Morgante, J.V. Barth, *J. Phys. Chem. C* **113**, 12101 (2009).

# THE ELECTRONIC STRUCTURE AND ADSORPTION GEOMETRY OF HISTIDINE ON Cu(110)

V. Feyer<sup>1</sup>, O. Plekan<sup>1</sup>, T. Skála<sup>1</sup>, V. Cháb<sup>2</sup>, V. Matolín<sup>3</sup>, K.C. Prince<sup>1</sup>

<sup>1</sup>Sincrotrone Trieste S.C.p.A., Trieste, Italy

<sup>2</sup>Institute of Physics, Prague, Czech Republic

<sup>3</sup>Department of Surface and Plasma Science, Charles University, Prague, Czech Republic

E-mail: vitaliy.feyer@elettra.trieste.it

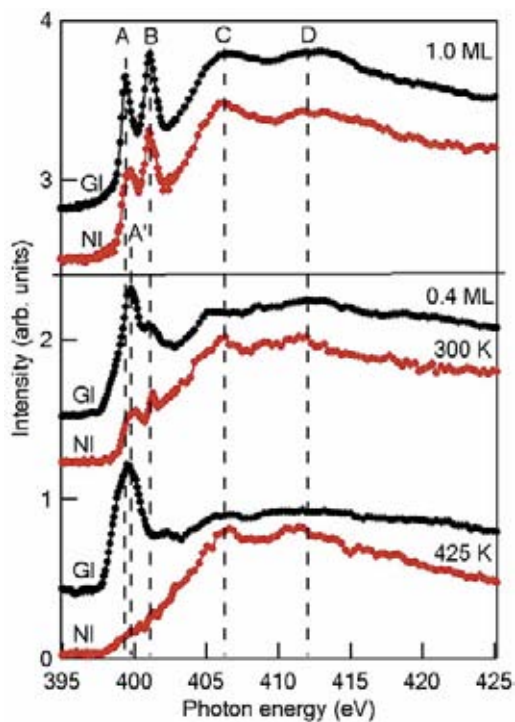


MATERIALS SCIENCE

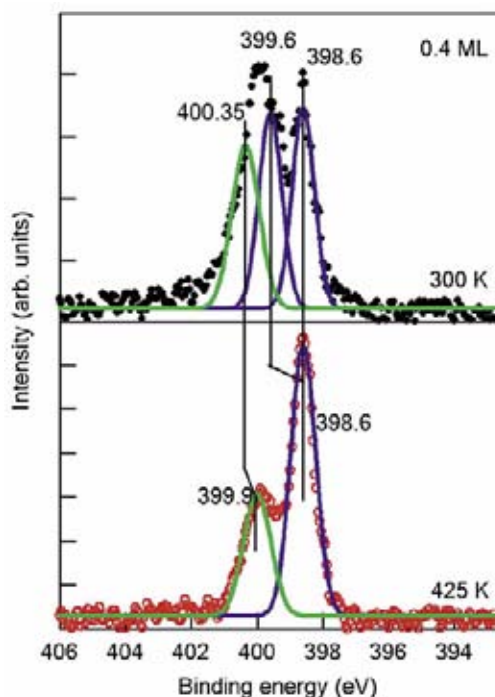
Histidine is an amino acid which consists of amino, imidazole and carboxyl groups. The functional group which distinguishes histidine is the imidazole (IM) ring which has two nitrogen atoms with different properties: one (N3) is bound to hydrogen and donates its lone pair to the aromatic ring and as such is slightly acidic, whereas the other one (N2) donates only one electron pair to the ring so it has a free lone pair and is basic. The nature of the bonding of histidine to copper remained controversial. In one case, the authors [1] proposed a model in which adsorption occurs via two oxygen atoms nearly equidistant from the surface, and via dehydrogenated nitrogen of the imidazole group, which adopts an upright position with respect to the surface, while the amino group (NH<sub>2</sub>) is maintained close to the surface. In a second model NH<sub>2</sub> and COO groups are believed to be involved in the interaction with the Cu(110) surface, with the ring close to the surface [2]. Here we present combined XPS and NEXAFS studies of histidine adsorbed on Cu(110), which provide additional information about the adsorption geometry and electronic structure [3]. The experiments were performed at the Materials Science Beamline. Photoemission spectra were recorded with an angle of incidence of the synchrotron light of 30° with respect to the surface normal and an emission angle of 30°. While the NEXAFS spectra were taken at the N K edge using the nitrogen KVV Auger yield at normal (NI) (90°), grazing (GI) (10°) incidence of the photon beam with respect to the surface.

Figure 1 shows measured N K edge NEXAFS spectra of histidine adsorbed on Cu(110) at a coverage of 1.0 ML and 0.4 ML. Four well separated features marked A, B, C and D are observed. The peak A at 399.5 eV is attributed to the N 1s→π\* transition for the imino nitro-

gen (N2) in the IM ring. The second peak B at 401.2 eV is due to a transition of a ring amino nitrogen (N3) 1s electron to the π\* resonance. The two broad features C and D centered at 406.3 and 412.3 eV are attributed to transitions of 1s electrons of all three nitrogen atoms to σ\* (N-C) shape resonances. In the monolayer spectra there is no strong angular dependence of the π\*/σ\* intensity ratio, indicating that the IM ring in the monolayer regime is randomly oriented. The NEXAFS spectra at lower coverage (~0.4 ML) are different from the monolayer spectra. The spectra do not show the A resonance, but peak A' at 400.0 eV is the dominant peak, which suggests strong interaction via the N2 imino nitrogen atom of the IM ring with the copper surface. The N 1s photoelectron spectrum of histidine after adsorption of 0.4 ML is shown in Figure 2. We assign the higher BE peaks at 400.35 eV to amino N1 nitrogen, the peak at 399.6 eV to N3 nitrogen, and both are not bonded to the copper surface. The third peak at 398.6 eV is due to chemisorbed imino (N2) nitrogen atoms. The NEXAFS spectra change substantially with angle: the π\* (A' and B) resonances are stronger than the σ\* resonances at GI, while at NI the π\*/σ\* intensity ratios reverse. Flashing of the sub-monolayer of histidine to 425 K almost extinguishes the intensity of the π\* resonances at NI, while at GI the B resonance is invisible and one strong broad peak A' is observed. This suggests that after annealing the IM ring is lying more nearly parallel to the surface. The feature due to the ring amino (N3) nitrogen in N 1s photoelectron spectrum, as shown in Figure 2, is moved to lower BE by ~1.0 eV and is located at the same BE as chemisorbed imino nitrogen (N2). This evidence suggests that after annealing the amino nitrogen (N3) has lost H and strongly interacts with the surface. However, also deprotonation



**Figure 1.** N K-edge NEXAFS of histidine adsorbed on Cu(110) surfaces and annealed to the temperature indicated.



**Figure 2.** N 1s photoelectron spectra of histidine adsorbed on Cu(110) surfaces and annealed to the temperature indicated.

can take place and leave charge in the IM ring of histidine, and the two nitrogen atoms in the imidazole anion are indistinguishable.

The O 1s spectra of monolayer and sub-monolayer histidine on a clean surface showed only one component. This indicates that for both a monolayer and low coverage, histidine interacts via the carboxylate group (COO<sup>-</sup>). The two oxygen atoms are in very similar chemical states as no chemical splitting is observed.

The bonding of histidine to Cu(110) can be summarized as follows. At high coverage the IM side chains of the histidine molecules are randomly oriented but lie close to the surface, and the histidine binds to the copper surface via the carboxylate group. At low coverage histidine interacts with the Cu(110) surface

only via the carboxylate group and ring imino (N2) nitrogen atoms with a small tilt angle of the IM ring with respect to the surface. However after annealing to 425 K the N2 nitrogen loses a H atom, and both nitrogen atoms of the IM ring (N2 and N3) and the nitrogen atom of the amino group (N1) bond to the surface covalently. The carboxylate group (COO<sup>-</sup>) forms a strong ionic bond to the Cu(110) surface. This model suggests that histidine bonds to the surface in its HHis<sup>-</sup> ionic form.

#### References

- [1] E. Mateo Marti *et al.*, *J. Phys. Chem. B* **107**, 10785 (2003).
- [2] E. Mateo Marti *et al.*, *Colloids and Surfaces A* **249**, 85 (2004).
- [3] V. Feyer *et al.*, *J. Phys. Chem. B* **112**, 13655 (2008).

# ELECTRON RESIST BEHAVIOR OF Pd HEXADECANETHIOLATE EXAMINED USING X-RAY PHOTOELECTRON SPECTROSCOPY WITH NANOMETRIC LATERAL RESOLUTION

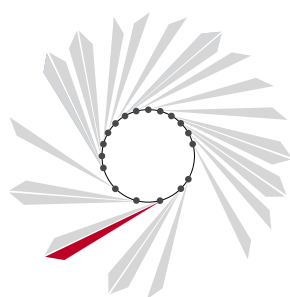
T. Bhuvana<sup>1</sup>, L. Gregoratti<sup>2</sup>, S. Heun<sup>3</sup>, M. Dalmiglio<sup>2</sup>, G.U. Kulkarni<sup>1</sup>

<sup>1</sup>Chemistry and Physics of Materials Unit and DST Unit on Nanoscience, Jawaharlal Nehru Centre for Advanced Scientific Research, Bangalore, India

<sup>2</sup>Sincrotrone Trieste S.C.p.A., Trieste, Italy

<sup>3</sup>NEST, CNR-INFN and Scuola Normale Superiore, Pisa, Italy

E-mail: stefan.heun@sns.it



ESCA MICROSCOPY

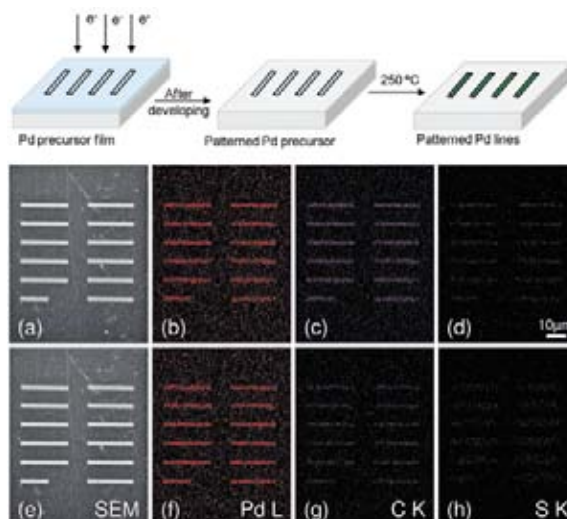
Site-specific fabrication of nanostructures using a minimal number of process steps is still a challenge. This has led to the pursuit for nanomaterial precursors that act as resists in electron beam lithography (EBL): the precursor is coated on a substrate which upon exposure to e-beam undergoes chemical transformation that changes its solubility properties. In addition, following a simple post treatment, it should transform into the desired nanomaterial. Recently, we have demonstrated the use of Pd hexadecanethiolate as a direct write resist for Pd metal patterning [1]. Upon thermolysis, the exposed resist yielded highly metallic patterns with the carbon impurity at record low (<10%). This precursor behaves as negative-tone resists, i.e. the exposed regions have less solubility in chosen solvents than unexposed regions. We have investigated the chemical changes in Pd hexadecanethiolate

under e-beam exposure by employing core-level spectroscopy at the ESCA microscopy beamline [2].

Palladium hexadecanethiolate, Pd(SC<sub>16</sub>H<sub>35</sub>)<sub>2</sub>, was synthesized and dissolved in toluene to obtain a 0.1 mM solution. The solubility of Pd thiolate is clearly a novelty, as it enables further processing. The resist film was made by spin-coating the Pd thiolate solution on Si substrates. EBL was performed at 5 kV with different dosages. The substrate was then developed in toluene for 10 s to dissolve away the unexposed resist. Thermolysis was carried out in air at 250°C for 30 min. Energy dispersive spectroscopy (EDS) was performed before and after the thermolysis. Figure 1 shows an example of the pattern obtained with a dosage of 54 μC·cm<sup>-2</sup>. From the scanning electron microscopy (SEM) image in Figure 1(a) we see that the regions exposed to the e-beam

Figure 1.

Top: Scheme of the Pd precursor film exposed to e-beam, developed in toluene, and after thermolysis. (a) SEM image and (b-d) EDS maps of Pd L, C K, and S K lines of patterned regions exposed to e-beam and developed in toluene. (e-h) Same after thermolysis of the patterned resist.



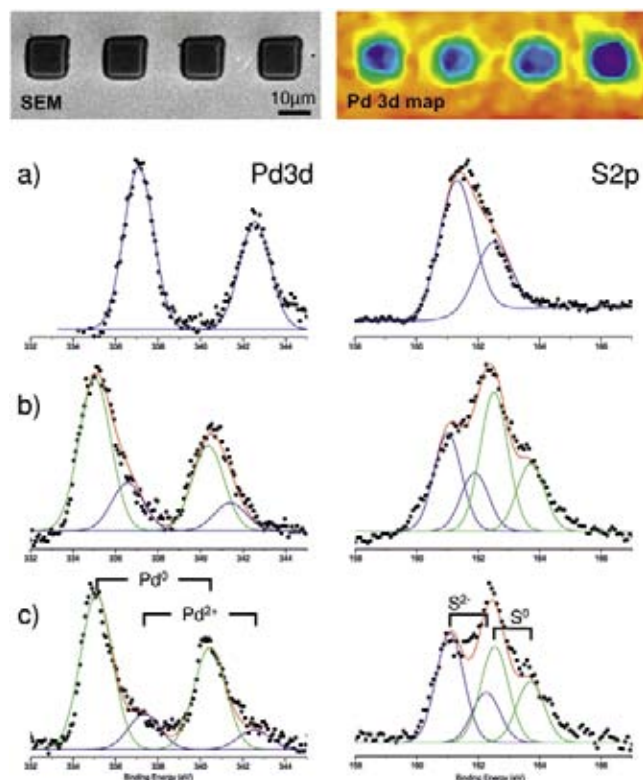


**Figure 2.** Top: SEM and Pd3d ESCA microscopy images of a patterned region. (a) Pd 3d and S 2p core-level spectra of the pristine film. (b) Spectra corresponding to a patterned island subjected to  $2 \mu\text{C}\cdot\text{cm}^{-2}$  dosage. (c) Spectra after in situ thermolysis at  $250^\circ\text{C}$ .

remain on the substrate after developing in toluene, thus indicating the negative-tone resist behavior of the thiolate. The EDS images in Figure 1(b-d) show the presence of Pd, C, and S, respectively, in the designated areas. The Pd/C/S elemental ratios obtained for the patterned regions agrees with the initial composition of the unexposed resist, implying that the e-dosage causes only minimal change in the overall composition. In Figure 1(e-h) we show SEM and EDS images after ex situ thermolysis at  $250^\circ\text{C}$ . The Pd EDS map shows the presence of Pd in the designated regions similar to that in Figure 1(b). However, the C K and S K signals became significantly weaker following thermolysis, suggesting loss of thiol in the patterned regions.

In order to study the chemical changes on Pd thiolate on exposure to e-beam, nano-XPS analysis was carried out (Figure 2). Pd 3d and S 2p core-level spectra recorded on the pristine film (Figure 2(a)) show the presence of Pd<sup>2+</sup> and S<sup>2-</sup> species. Surprisingly, in all spectra taken from patterned regions (Figure 2(b)), the Pd 3d peak indicates the predominant presence of the metallic species Pd<sup>0</sup>. This is the first important finding from the nano-XPS measurements: the e-beam exposure causes significant reduction of Pd<sup>2+</sup> to Pd<sup>0</sup>. Such sensitive variations could not be detected with EDS measurements because of its intrinsic

poor energy resolution. The S 2p spectra show a similar trend as Pd 3d. Here, S<sup>0</sup> is predominant after exposure to the e-beam. The reduction brought about by the e-beam can be further enhanced by thermolysis. Prior to thermolysis, the room temperature spectra of the exposed resist gave a Pd<sup>0</sup>/Pd<sup>2+</sup> ratio of 3.14. Upon heating the substrate to  $250^\circ\text{C}$  for 10 min (Figure 2(c)), the content of metallic species further increased (Pd<sup>0</sup>/Pd<sup>2+</sup> = 4.5). TEM images taken after thermolysis showed the presence of Pd nanoparticles in the size range of 5-15 nm.

In conclusion, we have studied the electron resist behavior of Pd hexadecanethiolate. Electron beam exposure causes defects in the alkyl chain of the thiolate, giving the required solubility contrast during the developing step, thus qualifying the precursor as an e-beam resist. On exposure to the e-beam, the reduction of Pd<sup>2+</sup> to Pd<sup>0</sup> is observed. Thermolysis at  $250^\circ\text{C}$  leads to the formation of Pd nanoparticles, demonstrating the essential feature of a direct write resist for conducting patterns.

## References

- [1] T. Bhuvana and G. U. Kulkarni, *ACS Nano* **2**, 457 (2008).
- [2] T. Bhuvana, L. Gregoratti, S. Heun, M. Dalmiglio, and G.U. Kulkarni, *Langmuir* **25**, 1259 (2009).

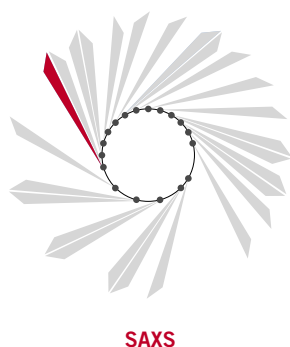
# PERIODIC MESOPOROUS ORGANOSILICA IN CONFINED ENVIRONMENTS

A. Keilbach<sup>1</sup>, M. Döblinger<sup>1</sup>, R. Köhn<sup>1</sup>, H. Amenitsch<sup>2</sup>, T. Bein<sup>1</sup>

<sup>1</sup>Department of Chemistry and Biochemistry and Center for NanoScience (CeNS), University of Munich, Munich, Germany

<sup>2</sup>Institute of Biophysics and Nanosystems Research, Austrian Academy of Sciences, Graz, Austria

E-mail: bein@lmu.de



Mesoporous silicates have been developed by Mobil Oil researchers in 1992 [1]. This kind of materials can be synthesized in the presence of surfactants and is expected to have a large number of possible applications. They offer ordered pore systems and high specific surface areas in combination with tunable pore sizes on the nanometer scale (2 to 15 nm). The hybridization of these materials with functionalities known from organic chemistry led to the development of inorganic-organic hybrid materials [2]. Several routes for the synthesis of such materials have been developed; one route leads to the class of so-called periodic mesoporous organosilica (PMO) materials. They offer an even distribution in combination with a high loading of organic functionality. In this study [3], ethylene-bridged PMO materials have been confined within porous anodic alumina (PAA) membranes, as seen in Figure 1(a). PAA is a porous ceramic offering pores in the range of 15 to 400 nm (depending on the synthesis conditions). The confined environment leads to the formation of new, interesting phases. The solid alumina support makes these composite materials interesting for usage in fields such as separation or nanotemplating.

The synthesis process for the mesostructured composites follows an approach called evaporation-induced self-assembly (EISA). There, the condensation reaction is carried out in the presence of a surfactant acting as structure directing agent (SDA). The ratio of the BTSE (bis(triethoxysilyl)ethane) precursor to the SDA plays a key role regarding the structure to be formed. In this study, hexagonal circular, lamellar, and cubic mesophases were found. The hexagonal circular (Figure 1(c)) and the lamellar phase (Figure 1(e)) can be observed frequently in such composite systems.

Using an ionic surfactant (CTAB) as SDA, the formation of a hexagonal circular mesophase was observed in all cases, independent from the BTSE/SDA ratio. This is remarkable, as earlier experiments carried out with purely inorganic silane precursors (Tetraethoxysilane, TEOS) yielded exclusively the hexagonal columnar mesophase. We attribute this different phase behaviour to the different interactions of the SDA molecules to the changed hydrophobicity of the silica or organosilica pore walls, respectively. Furthermore, with the help of the SAXS beamline at Elettra, the conditions for phase formation could be investigated in detail. For these experiments, a different non-ionic SDA (Brij 56) was used. Besides the formation of the already mentioned hexagonal circular mesophase, the existence of a cubic structure, which has not been reported for such systems before could be proven by SAXS (small angle X-Ray scattering) measurements, displayed in Figure 2(a). The experiments at Elettra helped us to clarify the results obtained from our laboratory X-Ray setup (inset in Figure 2(a)). It allowed us to finally prove that the relatively high angle of incidence of our laboratory machine ( $10^\circ$ ) leads to a change of the characteristic diffraction pattern compared to the ones reported in the literature obtained under GISAXS conditions. Further characterization by transmission electron microscopy, seen in Figure 2(b), confirmed the presence of a cubic phase.

The obtained mesophases were found to be stable against surfactant removal by mild calcination and/or extraction methods, which was shown by solid-state NMR measurements. The accessibility of such synthesized porous AAO/organosilica composites could be successfully demonstrated by nitrogen sorption measurements.

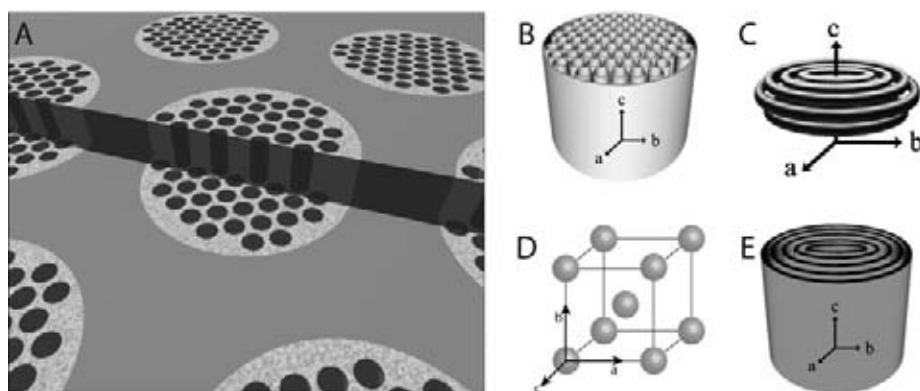


**Figure 1.** (a) Sketch illustrating a cross-section through a PAA/PMO composite membrane. The dark grey areas represent the aluminum oxide, while the light grey parts represent the PMO material. (b) to (e): Schematics of the different mesophases found. (b) hexagonal columnar, (c) hexagonal circular, (d) cubic, and (e) lamellar mesophase.

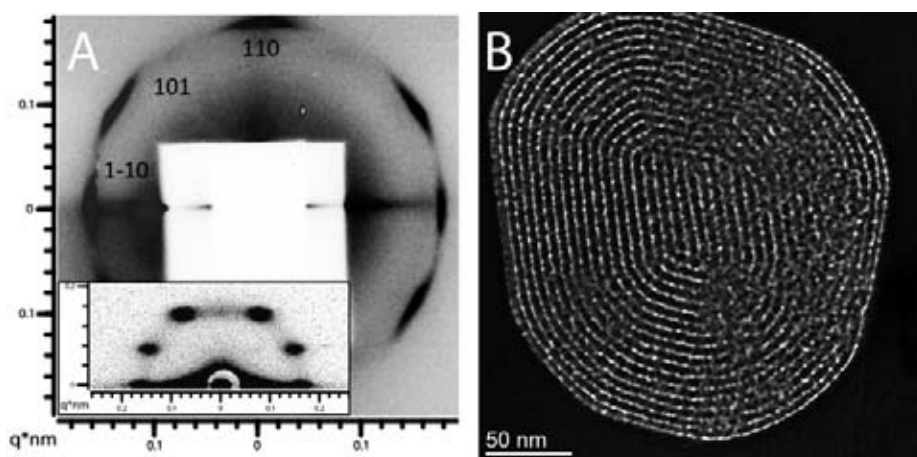


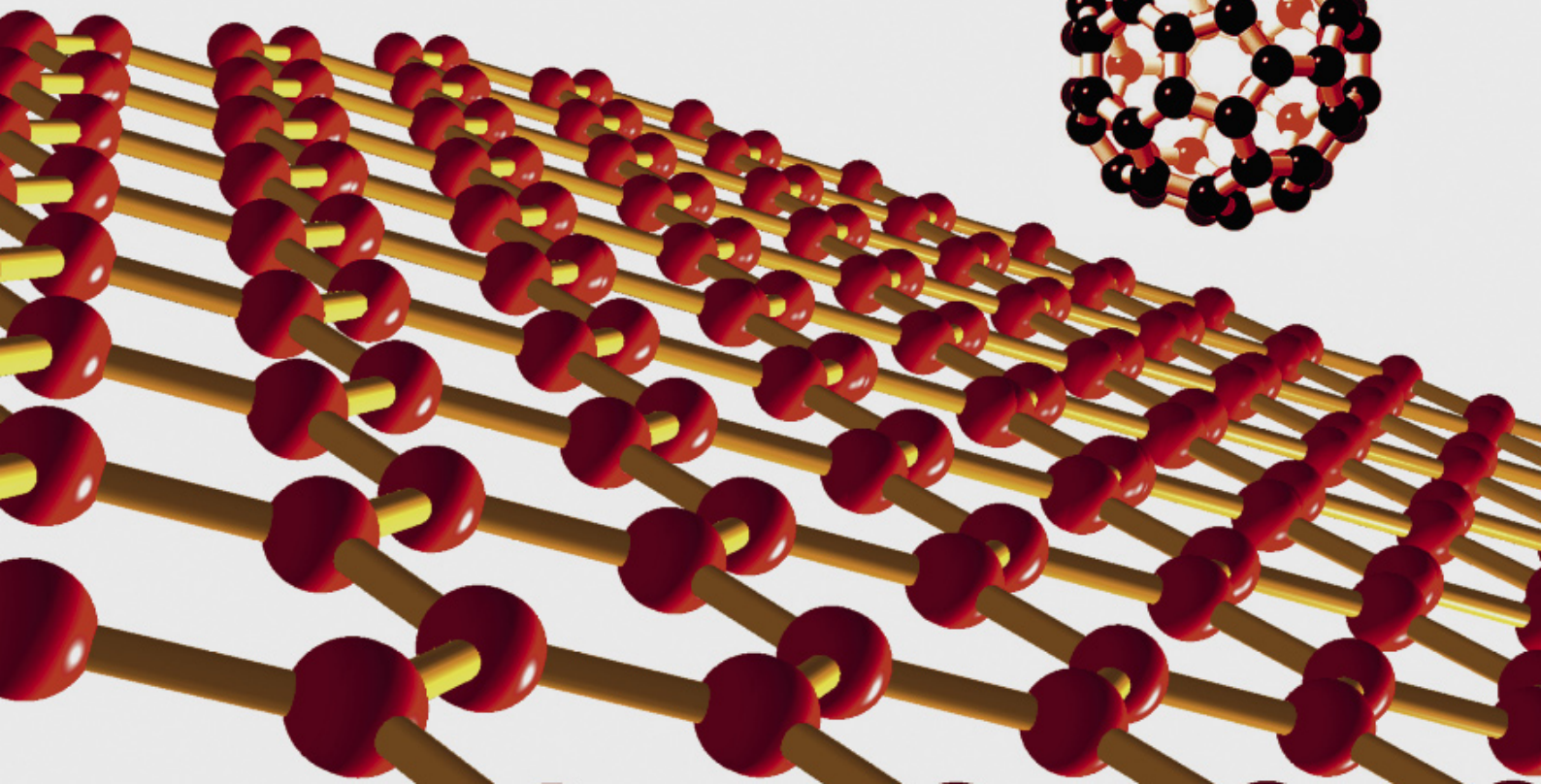
**Figure 2.** (a) 2D SAXS diffractogram acquired at Elettra verifying the presence of a cubic phase in the mesopore system. The inset displays the result from a diffraction experiment obtained by our laboratory equipment. (b) TEM image of the cubic PMO mesophase within its surrounding anodic alumina pore mold.

## References

- [1] J.S. Beck, J.C. Vartuli, W.J. Roth, M.E. Leonowicz, C.T. Kresge, K.D. Schmitt, C.T.W. Chu, D.H. Olson, E.W. Sheppard, S.B. McCullen, J.B. Higgins, J.L. Schlenker, *J. Am. Chem. Soc.* **114**, 10834 (1992).
- [2] F. Hoffmann, M. Cornelius, J. Morell, M. Froeba, *Angew. Chem., Int. Ed.* **45**, 3216 (2006).
- [3] A. Keilbach, M. Döblinger, R. Köhn, H. Amenitsch, T. Bein, *Chem. Eur. J.* **15**, 6645 (2009).



## CARBON-BASED NANOSTRUCTURES







# REVERSIBLE PHASE TRANSFORMATION AND DOUBLY CHARGED ANIONS AT THE SURFACE OF SIMPLE CUBIC $\text{RbC}_{60}$

R. Macovez<sup>1</sup>, A. Goldoni<sup>2</sup>, L. Petaccia<sup>2</sup>, I. Marenne<sup>3</sup>, P.A. Brühwiler<sup>4,5</sup>, P. Rudolf<sup>1</sup>

<sup>1</sup>Zernike Institute for Advanced Materials, University of Groningen, Groningen, The Netherlands

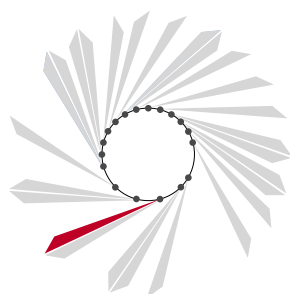
<sup>2</sup>Sincrotrone Trieste S.C.p.A., Trieste, Italy

<sup>3</sup>L.I.S.E., Faculte Universitaire Notre-Dame de la Paix, Namur, Belgium

<sup>4</sup>Department of Physics, Uppsala University, Uppsala, Sweden

<sup>5</sup>Empa, Swiss Federal Laboratories for Materials Testing and Research, St. Gallen, Switzerland

E-mail: goldonia@elettra.trieste.it



SUPERESCA

The study of phase transitions and the balance of energies involved to determine the state properties is the heart of the condensed matter physics. Just to remember some important phase transitions we can consider the ferromagnetic or antiferromagnetic transitions, the ferroelectricity, the change in crystalline symmetry, the superfluidity or superconductivity and the metal-insulator transitions.

Alkali fullerides exhibit a large variety of insulating, metallic, magnetic, and superconducting behaviors as a function of alkali concentration. These ranges of physical properties stem from the proximity of alkali fullerides to a metal-insulator transition governed by the interplay of molecular interactions, the interelectron repulsion and the Jahn-Teller vibronic coupling. Moreover, the lowest stoichiometry  $\text{AC}_{60}$  (where A= K, Rb, Cs) displays also several phases as a function of thermal treatment. Two distinct cubic phases with differing metallic properties are observed: a face-centered cubic (FCC) structure of rapidly spinning molecules, which is thermodynamically stable above 400 K, and a metastable simple cubic (SC) phase, obtained by fast-cooling the FCC phase to 50 K, which differs from the high-temperature structure in that the orientation of the  $\text{C}_{60}$  monomers is fixed with respect to the cubic axes. Upon annealing to 200 K, the SC structure transforms irreversibly into metastable  $(\text{C}_{60})_2^{2-}$  dimers, which can also be obtained by fast cooling the FCC phase to 130-170 K. A weakly conducting phase of polymer chains is thermodynamically stable below 400 K. These phase transitions are bulk properties.

Surface atoms are frustrated because they lose some nearest-neighbours and are interfaced with the vacuum. The presence of a surface may enhance the fluctuations responsible of the bulk phase transitions (for example some melting transitions initiate from the surface) or may behave exactly as the bulk transition, or else may behave in a completely different manner than the bulk case.

Here, we study the simple cubic phase of a  $\text{RbC}_{60}$  thin film and the surface transition between this phase and the dimer phase by means of photoelectron spectroscopy [1]. The measurements were performed at the SuperESCA beamline, using photon energies of 400 eV for core level and 120 eV for valence band spectra.

We have recently shown [2] that a surface charge reconstruction takes place in the FCC and dimer phases of this compound and here we show this surface reconstruction is common also to the simple cubic phase. Figure 1 (a,b) show the C 1s core level and the highest occupied molecular level (HOMO) and HOMO-1 states in the valence band for the FCC phase, respectively. These spectra were fitted with two contributions, one relative to  $\text{C}_{60}^{1-}$  and the second relative to  $\text{C}_{60}$  [2]. Fast cooling down to below 100 K allows the formation of the SC phase. As above, C 1s core level and HOMO and HOMO-1 are shown in Figure 1(c,d). The FCC surface charge reconstruction in  $\text{C}_{60}$  and  $\text{C}_{60}^{1-}$  survives also in this phase and furthermore the  $\text{C}_{60}^{2-}$  is also stabilized in the timescale of photoemission experiments. The formation of doubly charged states must occur at the expense of singly charged species ( $\text{C}_{60}^{1-} + \text{C}_{60}^{1-} \rightarrow \text{C}_{60} + \text{C}_{60}^{2-}$ ), rationalizing the observed intensity redistribution in the spectra.

The  $C_{60}^{2-}$  anions contribute to the spectral intensity at the Fermi level, where a sharp Fermi edge is observed in the frontier levels of the SC phase. Obviously  $C_{60}$  cannot contribute to the density of states at the Fermi level (it is an insulator with a gap of 2.5 eV), therefore only  $C_{60}^{1-}$  and  $C_{60}^{2-}$  are responsible for this intensity. On the other hand,  $C_{60}^{1-}$  is mainly responsible of the bump at 0.4 eV with a faint intensity at the Fermi level as demonstrated by the FCC spectrum reported in Figure 2(a). Therefore, the clear Fermi edge observable at low temperature is due to  $C_{60}^{2-}$ . The energy separation between the components in the C 1s spectrum represents a lower limit for the surface Hubbard U, that is  $\sim 0.5$  eV in the SC phase, hence pointing to a strongly correlated metallic character of the surface in simple cubic  $RbC_{60}$  thin films at low temperature.

Finally, the simple cubic-to-dimer transition, that is irreversible in the bulk, is found to be reversible at the film surface. The sample could be annealed and cooled repeatedly through this transition, which shows its reversible character. This is shown in Figure 2(b), which presents spectra taken while varying the sample temperature between 170 and 50 K twice, and was also verified in other synchrotron runs. Since the inelastic mean free path of electrons in fullerenides is of the order of the intermolecular distance or smaller [3], our data mainly reflect the character of the first and second molecular layer of the film. Our observations thus establish the reversibility of the simple cubic-to-dimer transition at the film surface, in contrast to the bulk case [4]. Remarkably, as the temperature is lowered the covalent strong intermolecular bonds of the dimers are broken, contrary to the bulk case, at the surface.

## References

- [1] R. Macovez, A. Goldoni, L. Petaccia, I. Marenne, P.A. Brühwiler, P. Rudolf, *Phys. Rev. Lett.* **101**, 236403 (2008).
- [2] R. Macovez, P. Rudolf, I. Marenne, L. Kjeldgaard, P.A. Brühwiler, T. Pichler, P. Vilmercati, R. Larciprete, L. Petaccia, G. Bertoni, A. Goldoni, *Phys. Rev. B* **75**, 195424 (2007).
- [3] A. Goldoni, L. Sangaletti, F. Parmigiani, G. Comelli, G. Paolucci, *Phys. Rev. Lett.* **87**, 076401 (2001).
- [4] Q. Zhu, D.E. Cox, J.E. Fischer, *Phys. Rev. B* **51**, 3966 (1995); M. Mehring *et al.*, *Carbon* **38**, 1625 (2000).

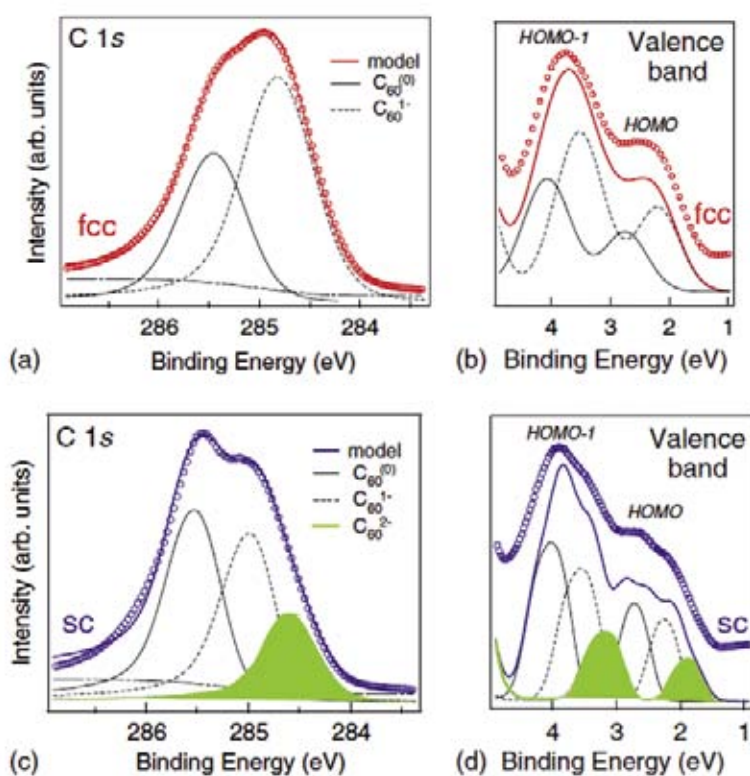


**Figure 1.** C 1s photoemission spectra of the FCC (a) and SC (c) phases, and corresponding valence band photoemission spectra of the HOMO- and HOMO-1-derived region (b),(d). A model in terms of different molecular charge states is shown for all spectra.

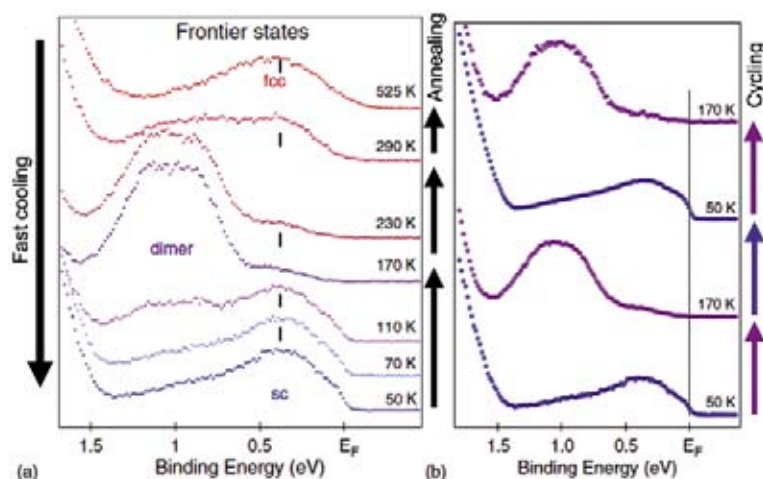


**Figure 2.** (a) Valence band photoemission spectra of  $RbC_{60}$  evidencing the temperature dependence of the states closest to the Fermi level during the quench from the FCC to the SC phase at a rate of 50 K per minute (fast cooling) and then by a slow annealing from the SC to FCC phase. (b) Spectra obtained while cycling the sample temperature between 50 and 170 K (i.e. from the SC to the dimer phase and viceversa).

# THE FORMATION OF GRAPHITE AND CARBON NANOTUBES FROM THERMAL DECOMPOSITION OF SILICON CARBIDE

G. Levita<sup>1</sup>, L. Petaccia<sup>2</sup>, A. Comisso<sup>3</sup>, S. Lizzit<sup>2</sup>, R. Larciprete<sup>2,4</sup>, A. Goldoni<sup>2</sup>, A. De Vita<sup>3</sup>

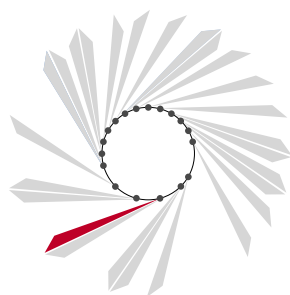
<sup>1</sup>Department of Materials and Natural Resources, University of Trieste, Italy

<sup>2</sup>Sincrotrone Trieste S.C.p.A., Trieste, Italy

<sup>3</sup>Department of Physics, King's College London, London, UK

<sup>4</sup>CNR- Istituto dei Sistemi Complessi, Roma, Italy

E-mail: lizzit@elettra.trieste.it



SUPERESCA

The thermal decomposition of silicon carbide (SiC) has recently attracted considerable attention for its role as precursor of extremely pure graphite and catalyst-free carbon nanotubes (CNTs). SiC is a sequence of Si:C double layers stacked along the (001) direction with two polar surfaces, one terminated with Si atoms, SiC(0001), and the opposite terminated with C atoms, SiC(000 $\bar{1}$ ). Previous experiments revealed that graphite formation is favoured when heating the Si-terminated surface [1,2], while aligned nanotubes are preferentially obtained from the C-terminated one [3]. In this work we followed the formation of CNTs and graphite and propose an atomistic mechanism for both processes.

Photoelectron Spectroscopy (PES) and Near Edge X-ray Absorption Fine Structure (NEXAFS) experiments were performed at the SuperESCA beamline of Elettra. Figure 1 shows the evolution of the C 1s core level spectra of SiC(0001) and (000 $\bar{1}$ ) with annealing temperature until the formation of an ordered graphite film (Figure 1(a)) and CNTs (Figure 1(b)), respectively, as confirmed by the valence band spectra [4] (insets in Figure 1) and the SEM and TEM images of Figures 1(e,f). The main difference between the thermal evolution of the C 1s of the two surfaces is that in SiC(000 $\bar{1}$ ) a graphitic peak immediately appears at 284.6 eV and evolves in the C 1s of the carbon nanotubes, while in SiC(0001) two peaks are present, one broad at about 285.6 eV, due to C atoms forming a disordered layer on the surface, and the second, at 284.8 eV, due to the formation of an ordered graphitic sp<sup>2</sup> network. The peak at the lowest BE due to bulk SiC decays with thermal annealing in SiC(0001), and its small shift to higher BEs indicates a weak interaction with

the graphene overlayers. On the contrary for SiC(000 $\bar{1}$ ) the bulk SiC peak shifts significantly because of band bending at the CNT-SiC interface. In this case a shoulder at ~283.7 eV due to Si-C bonds at the interface also appears.

The orientational order of the final sp<sup>2</sup> networks has been verified by angular dependent NEXAFS measurements (Figures 1(c,d)). The graphite layers are parallel to the surface for SiC(0001), whereas for SiC(000 $\bar{1}$ ) the absorption spectra show the  $\pi^*$  state at each angle. The ( $\pi^*/\sigma^*$ ) peak intensity ratio has a maximum when the polarization vector of the light is perpendicular to the CNT axis, that is at ~70° indicating that the CNTs are almost vertical on the SiC surface, with an angle of ~20° to the substrate normal. This was also confirmed by SEM and TEM images reported in Figure 1(e,f). The CNTs are double-walled with a mean diameter of about 6 nm.

We used the density functional theory (DFT) method based on the Quantum-ESPRESSO plane-wave package to model the graphite and CNTs formation process on the basis of two mechanisms: the removal of Si atoms from the surface upon heating and the position swap of Si and C atoms of the outermost defective bilayer in order to minimize the number of dangling bonds. On the SiC(0001) surface, the decomposition proceeds through formation of horizontal C structures, with an initial degree of disorder due to the co-presence of graphite domains and shorter double C-C bonds, whose presence is confirmed by a broad C 1s peak centred at ~285.6 eV. Such C structures do not form strong bonds with the underlying bilayer which has no C atoms on its upper part, and can be easily detached and undergo rearrangement, which could eventually lead to larger graphitic

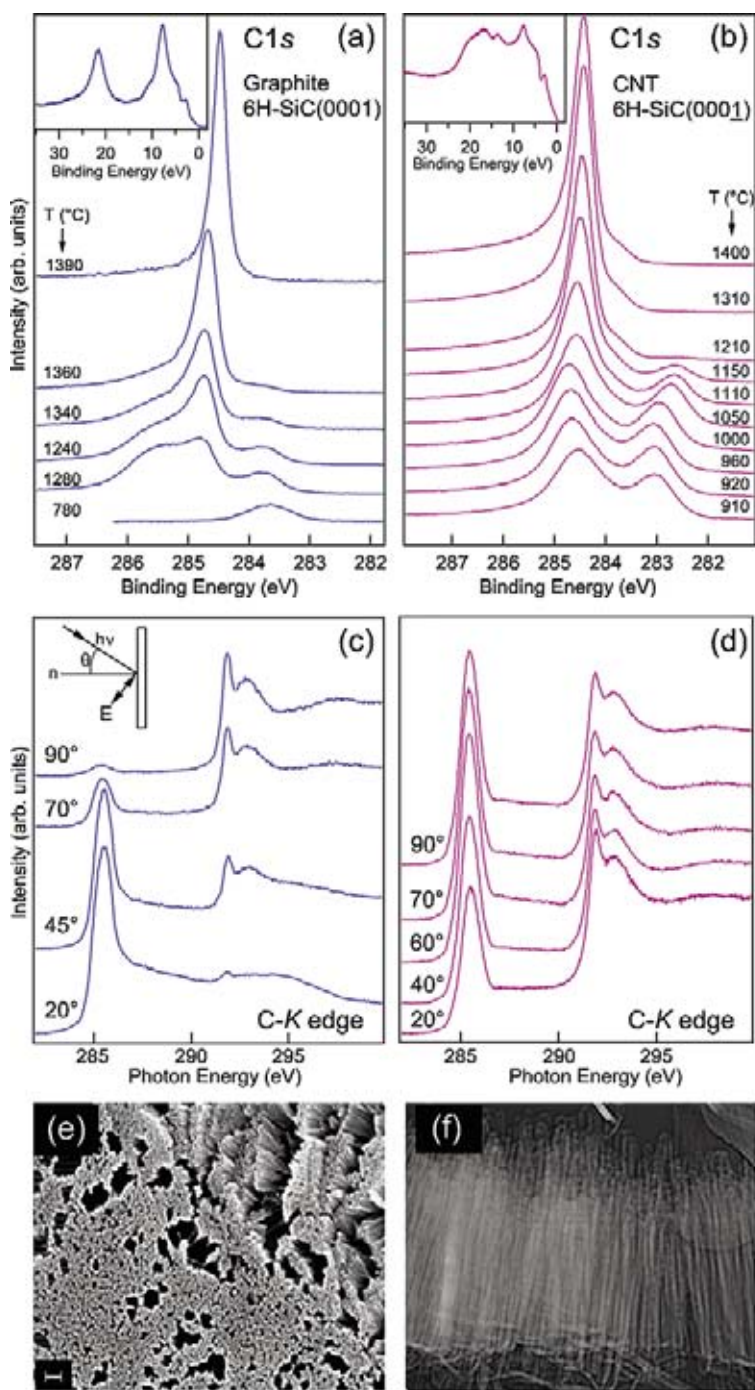


**Figure 1.** C 1s spectra taken on the (a) 6H-SiC(0001) and (b) 6H-SiC(000 $\bar{1}$ ) surfaces annealed at the indicated temperatures. The insets show the valence band spectra measured in normal emission after the annealing at the highest temperature. C-K edge NEXAFS spectra as a function of the angle  $\theta$  taken on the (c) SiC(0001) and (d) SiC(000 $\bar{1}$ ) surfaces after annealing at  $\sim 1400$  K. (e) SEM image (white bar = 100 nm) and (f) 250x170 nm<sup>2</sup> TEM image of the double-walled CNTs grown on SiC(0001).

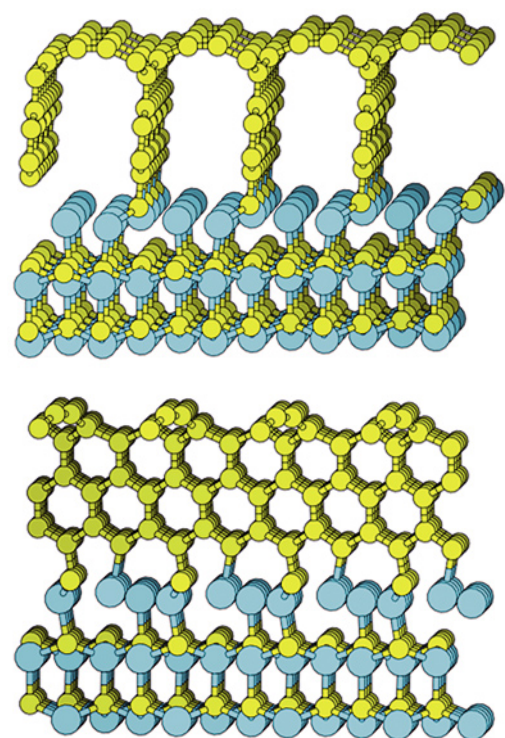


**Figure 2.** One relevant structure representing the thermal decomposition of the SiC(000 $\bar{1}$ ) surface: 3 Si monolayer depletion, leaving an ordered graphite vertical sheet, visualized as the lateral wall of a forming CNT. The bottom picture is a 90° view of the structure represented on the top.

domains. The initial steps of the decomposition of SiC(000 $\bar{1}$ ) are similar to those of the Si-terminated surface. However, in this case C atoms are available for bonding on the upper part of the following subsurface bilayer. These favour the formation of vertical C-C bonds which can easily extend deep through the bilayers during iterated Si removal. The preferential route in this geometry is therefore the creation of vertical graphitic structures, shown in Figure 2, interpreted as likely precursors of lateral nanotube walls with preferential zig-zag termination geometry.

## References

- [1] I. Forbeaux *et al.*, *Phys. Rev. B* **58**, 16396 (1998).
- [2] V. W. Brar *et al.*, *Appl. Phys. Lett.* **91**, 122102 (2007).
- [3] T. Maruyama *et al.*, *Jpn. J. Appl. Phys.* **45**, 7231 (2006).
- [4] L. Petaccia *et al.*, *J. Electron Spectrosc. Relat. Phenom.* **144-147**, 793 (2005).

# IMAGING AND SPECTROSCOPY OF MULTIWALLED CARBON NANOTUBES DURING OXIDATION: DEFECTS AND OXYGEN BONDING

A. Barinov, L. Gregoratti, P. Dudin, S. La Rosa, M. Kiskinova

Sincrotrone Trieste S.C.p.A., Trieste, Italy

E-mail: alexey.barinov@elettra.trieste.it



ESCA MICROSCOPY  
and  
SPECTROMICROSCOPY

The Carbon NanoTubes (CNTs) with their particular tubular structure of honeycomb carbon network are excellent candidates for many potential applications in electronics, composite materials, catalysis etc. Functionalization of CNTs modifies significantly their properties, e.g. converting them from hydrophilic to hydrophobic, in particular changing their chemical activity and selectivity. Processing the CNTs in oxidising environments has already been used for purification, tailoring their length [1] and homogenizing the mixture of metallic/semiconducting CNTs by converting the metallic ones into semiconducting [2]. The atomistic picture of oxidation is complicated involving several consecutive or parallel elementary processes, such as formation of particular O bonds to graphene network and gasification with formation of  $\text{CO}_2$  and CO volatile products. (For atomistic picture of oxidation at the initial stages see the highlight by O. Bariş Malcıoğlu *et al.* on page 114.) Both the presence of defects in the CNT graphene cage and the defects created in the oxidation process play important roles in formation of different oxygen functional groups on the CNT surface and facilitate the gasification.

Using the Scanning PhotoElectron Microscopes at the ESCA Microscopy and Spectromicroscopy beamlines of Elettra, we explored the morphology of a multi-walled CNTs array and obtained spectroscopic information from small areas of individual CNTs. The interpretation of photoemission spectra in terms of relative abundance of various functional groups enabled us to correlate the presence of particular functional groups to the morphological state of the CNT array.

The CNT forest arrays were exposed to atomic oxygen, supplied from a radiofrequency plasma source. We observed strong tempera-

ture dependence of the morphology evolution of the CNT array, as displayed in Figure 1. At room temperature (300 K) only minor changes in the images are visible up to the oxygen doses of  $2 \times 10^{18}$  atoms  $\text{cm}^{-2}$  equivalent to 30 hours (h): maximum exposure time used in our experiments. At 500K the CNTs visibly bend and shorten already at doses of  $\sim 10^{17}$  atoms  $\text{cm}^{-2}$  and undergo almost complete extinction due to gasification after  $8 \times 10^{17}$  atoms  $\text{cm}^{-2}$  dose. At both reaction temperatures the formation of different oxygen functional groups was detected. The O 1s spectra corresponding to different oxidation conditions are shown in Figure 2. In the beginning of the oxidation process three main types of oxygen functional groups are present: epoxy (green), ether (red) and carbonyl (blue). The appearance of a second carbonyl component is attributed to the carbonyl in different configurations in the advanced oxidation stages. As the exposure increases the components related to carbonyl (O atom bonded to a single C atom) prevail. They become unique in the O 1s spectra of the arrays when the significant morphology changes of CNT array are evidenced. Our results correlate the morphology changes of CNTs, a natural consequence of increasing density and size of the vacancy defects, with type and abundance of characteristic oxygen functional groups. Since the ether-bonding configuration can be realized only in a few atom vacancy defects the carbonyl becomes dominant when the multi-atom vacancy defects are formed and prevail [3].

In summary the most important finding is that the type and abundance of the formed oxygenated functional groups is controlled by the presence and size of the vacancy defects in the graphene layers of the CNTs. On one hand this introduces an uncertainty

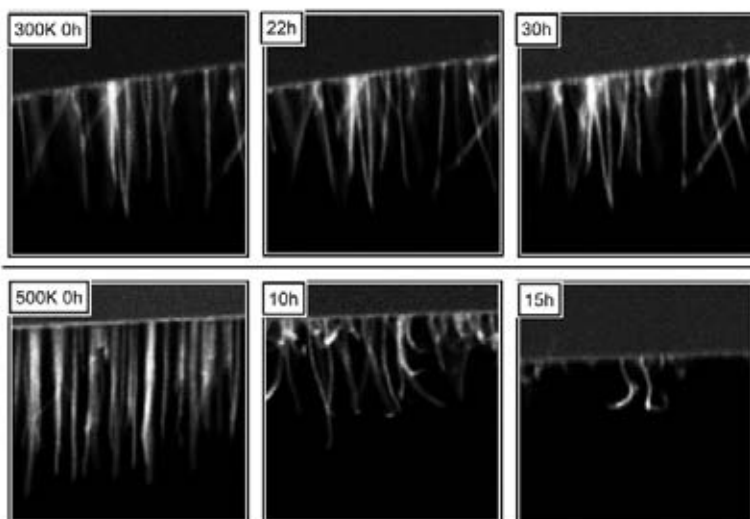


**Figure 1.** The evolution of CNT array morphology at 300K and 500K at various oxygen doses. The oxygen flux  $9 \times 10^{14} \text{ cm}^{-2} \text{ min}^{-1}$ . Image size is  $12.8 \times 12.8 \text{ }\mu\text{m}^2$ .

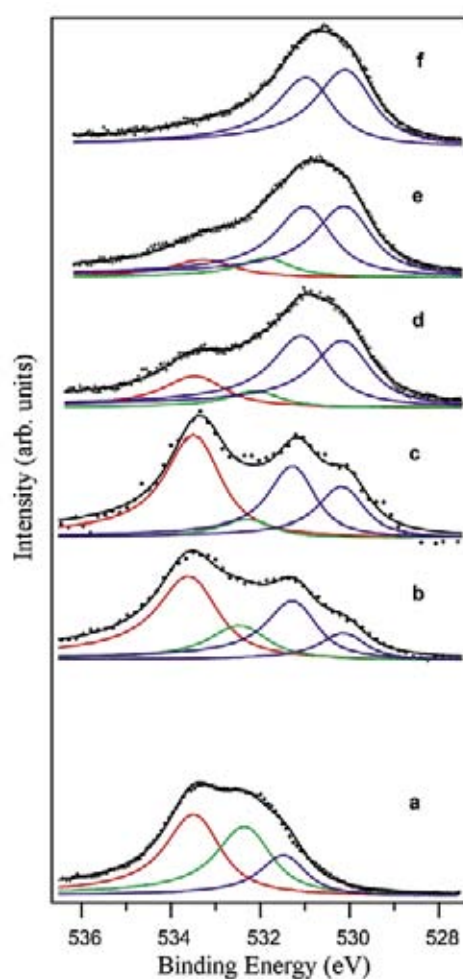


**Figure 2.** O 1s spectra after oxidation at  $20^\circ\text{C}$ : defective HOPG (a)  $4 \times 10^{14}$  and (b)  $1.4 \times 10^{16}$  atoms  $\text{cm}^{-2}$ ; CNTs (c)  $1.4 \times 10^{16}$  and (d)  $5.4 \times 10^{17}$  atoms  $\text{cm}^{-2}$ . O 1s spectra oxidation of CNTs  $200^\circ\text{C}$  (e)  $2.7 \times 10^{17}$  and (f)  $5.4 \times 10^{17}$ . The components related to the O functional groups are drawn in red (ether), epoxy (green) and carbonyl (blue). The picture is reproduction from the work published [3].

when analogous procedures are employed for functionalization of CNTs with undefined density and type of defects, on the other hand it prompts an approach for tailoring the CNTs via controlled introduction of defects, which favor the formation of a preferred functional group.

#### References

- [1] T.W. Ebbesen, P.M. Ajayan, H. Hiura, K. Tanigaki, *Nature* **367**, 519 (1994).
- [2] J.B. Cui, R. Sordan, M. Burghard, K. Kern, *Appl. Phys. Lett.* **81**, 3260 (2002).
- [3] A. Barinov, L. Gregoratti, P. Dudin, S. La Rosa, M. Kiskinova, *Adv. Mat.* **21**, 1916 (2009).

# NEXAFS EVIDENCE OF THE ELECTRON “CH... $\pi$ ” BRIDGES IN FILMS OF NONCOVALENTLY FUNCTIONALIZED SWNTS

N. Kocharova<sup>1</sup>, J. Leiro<sup>2</sup>, T. Skála<sup>3</sup>, F. Šutara<sup>4</sup>, M. Skoda<sup>4</sup>, M. Vondráček<sup>5</sup>

<sup>1</sup>The Laboratory of Materials Chemistry, Chemistry Department, University of Turku, Finland

<sup>2</sup>The Laboratory of Materials Science, Physics Department, University of Turku, Finland

<sup>3</sup>Sincrotrone Trieste S.C.p.A., Trieste, Italy

<sup>4</sup>Department of Surface and Plasma Science, Charles University, Prague, Czech Republic

<sup>5</sup>Institute of Physics, Academy of Sciences of the Czech Republic, Prague, Czech Republic

E-mail: natalia.kocharova@utu.fi



MATERIALS SCIENCE

To fully exploit the unique electron transport properties of Single-Walled Carbon Nanotubes (SWNTs), it is crucial to overcome many processing challenges that are caused by nanotubes insolubility in all solvents, such as SWNT individualization, selective placement and alignment and/or controlled self-assembly in pre-defined structures. We recently obtained water-soluble and thiolated SWNTs by non-covalent nanotube functionalization with the amphiphilic 1-(12-mercaptododecyl)-3-methylimidazolium (MDMetIm) bromide [1]. We also succeeded to get a self-assembled monolayer (SAM) of SWNT-MDMetIm tubes on gold via S-Au bond [1,2]. Noncovalent SWNT functionalization is based on adsorption of the hydrophobic part of amphiphilic molecule on nanotubes via van der Waals,  $\pi$ - $\pi$  and CH... $\pi$  interactions [1]. The understanding of these interactions is crucial for the development of future nanoelectronic devices based on films of functionalized SWNTs. However, such studies are missing and generally very few NEXAFS reports on SWNTs exist so far. In this study, we show that noncovalently functionalized SWNTs exhibit high degree of self-alignment in drop-cast films. We also found that multiple and close CH... $\pi$  interactions serve as “electron bridges” between the organic adsorbate and electron-accepting SWNTs preventing electron scattering and quenching events. This discovery is extremely important for development of new optoelectronic materials based on SWNTs and offers a tremendous overall performance improvement of their films.

We used the Near-Edge X-ray Absorption Fine Structure (NEXAFS) spectroscopy at the Materials Science beamline of ELETTRA for determining the electronic structure, interac-

tions and nanotube alignment within the SAM and drop-cast SWNT-MDMetIm films on gold [2]. The partial electron yield (PEY) signal for all spectra was collected with a  $\sim 0.2$  eV resolution using a carbon Auger line. All the measured carbon K-edge NEXAFS spectra for both the SAM and the drop-cast film (Figure 1) exhibit four main sets of sharp peaks at 284.8 – 286.6 eV, 292 – 294 eV,  $\sim 297$  – 307 eV and 287.1 – 290 eV. The first two sets of peaks are assigned to the  $\pi^*$  and  $\sigma_{CC}^*$  states of free individual SWNTs, respectively, as well as of those having  $\pi$ - $\pi$  interactions with imidazolium ring of MDMetIm; the resonance at 293.4 eV is attributed to  $\sigma_{CC}^*$  state in alkylthiols. The third set of ( $\sigma + \pi$ ) resonances in the 297 – 307 eV range is related to intermolecular  $\pi \rightarrow \pi^*$  and  $\sigma \rightarrow \sigma^*$  transitions associated with molecular adsorption on metal surfaces. Sharp peaks in the 287 – 288.9 eV range are assigned to mixed transitions of core electrons to the lowest Rydberg/valence  $R^*/\sigma_{CH}^*$  series of states in the alkyl chain of MDMetIm, since the high-resolution XPS data on the drop-cast SWNT-MDMetIm film showed an absence of the oxygen-containing groups chemisorbed on nanotubes [2].

Analyzing the intensity behavior of  $\pi^*$  and  $\sigma_{CC}^*$  resonances, we found that in the SAM (Figure 1(a)) the long axis of SWNT-MDMetIm tubes is not entirely parallel to the substrate plane. The high PEY signal of  $\sigma_{CC}^*$  resonance of the MDMetIm alkyl chain at 293.4 eV confirms its lateral orientation to be parallel to the substrate plane evidenced also by PM-IRRAS [2]. In the drop-cast film (Figure 1(b)) SWNTs exhibit self-organization into the well-ordered and aligned structure parallel to the substrate plane and with the preferably A-tube orientation.



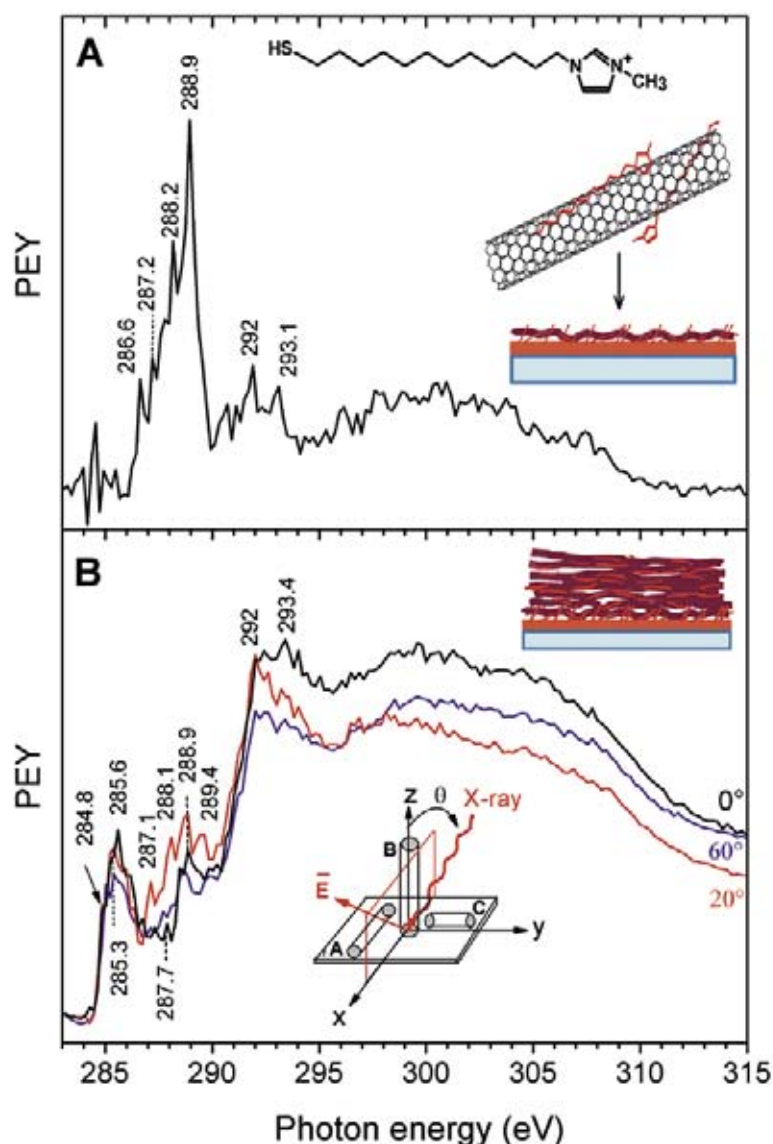


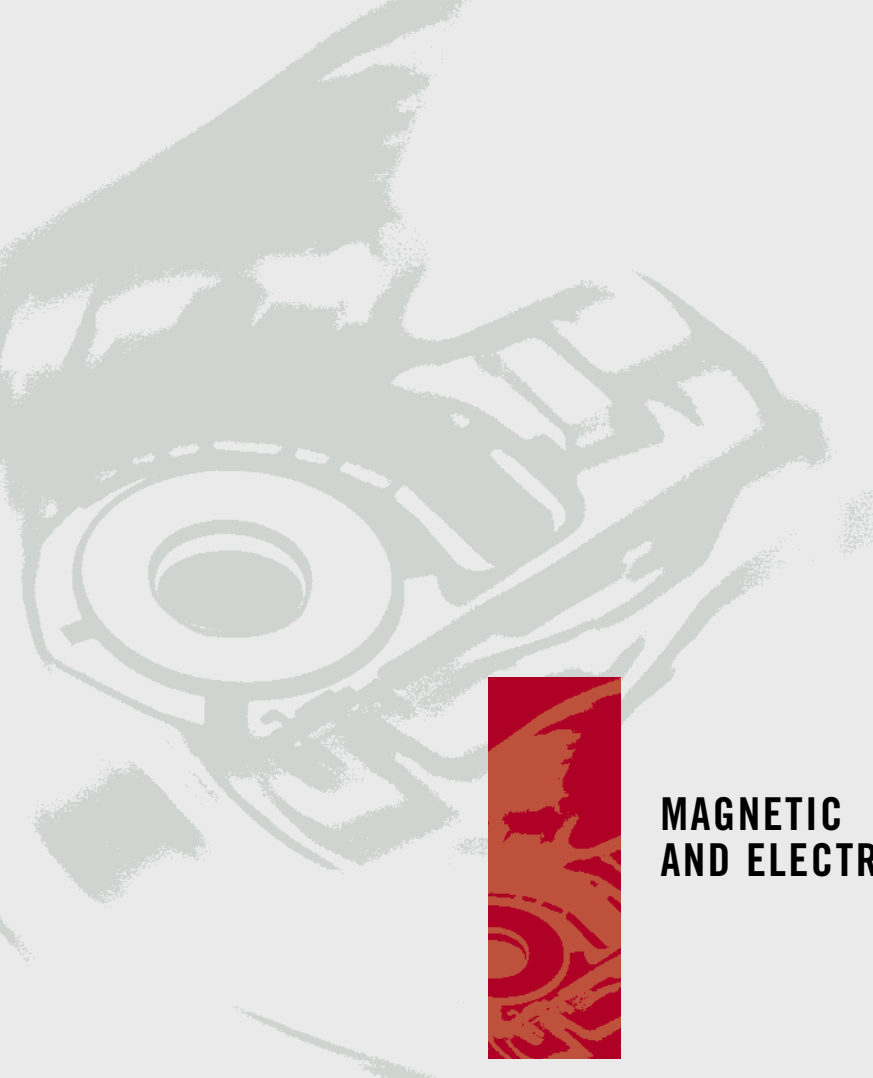
**Figure 1.** The C K-edge NEXAFS spectra for films of thiolated SWNTs on gold prepared from the low-concentrated aqueous solution: (a) the SWNT-MDMetIm SAM film spectrum was taken at normal to the substrate plane ( $\theta = 0^\circ$ ) polarization of incident synchrotron radiation beam. The inset shows chemical structure of the MDMetIm cation and the schematic illustrations of functionalized SWNT and its self-assembly on gold. (b) Angle-dependent spectra for the drop-cast SWNT-MDMetIm film. The inset shows self-alignment of thiolated SWNTs in the film and a scheme for the NEXAFS experiment with nanotubes aligned along  $x$ ,  $y$  and  $z$  axes. Spectra are taken at three angles after rotation of the sample in the plane of incidence. In film schemes, black and red lines represent SWNTs and MDMetIm molecules, respectively.

The analysis of the 287.1 – 290.3 eV range confirmed the existence and revealed a significant role of  $\text{CH}\cdots\pi$  interactions between alkyl chains of the adsorbate and SWNTs. The positions of  $R^*/\sigma^*_{\text{C-H}}$  resonances for our films are very similar to those observed in high-resolution NEXAFS spectra of alkanes and alkylthiols. However, rich vibronic fine structure for  $R^*/\sigma^*_{\text{C-H}}$  states observed for MDMetIm in SWNT-MDMetIm films is very unusual for organic films where electron mobility and lifetime are reduced and resembles that for *gaseous* alkanes, which show a progression of  $1s \rightarrow R^*/\sigma^*_{\text{C-H}}$  transitions with vibronic fine structure [3]. For entirely organic films, the NEXAFS spectra are blue-shifted and broadened [3]. In SWNT-MDMetIm films, the excited electrons in MDMetIm are quickly accepted via the  $\text{CH}\cdots\pi$  “electron bridges” by SWNTs, avoiding scattering and

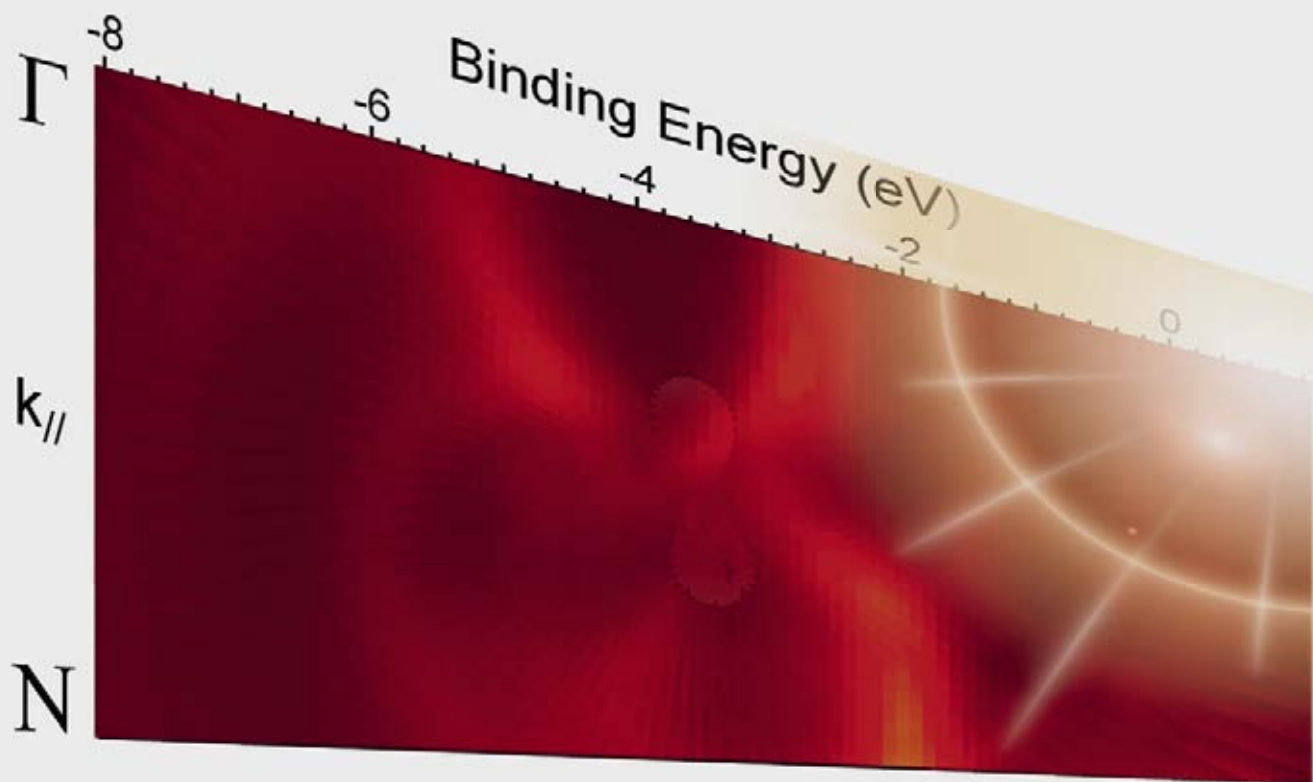
quenching characteristic for organic films. As a result,  $R^*/\sigma^*_{\text{C-H}}$  states take more Rydberg-like character with rich fine structure similar to that of individual molecules. This finding emphasizes the significance of the multiple and close  $\text{CH}\cdots\pi$  interactions for, in particular, enhancement of electronic drift distance (which is a strong function of the electron mobility and lifetime) in photoactive films based on SWNTs.

### References

- [1] N. Kocharova, T. Ääritalo, J. Leiro, J. Kankare, J. Lukkari, *Langmuir* **23**, 3363 (2007).
- [2] N. Kocharova, J. Leiro, J. Lukkari, M. Heimonen, T. Skála, F. Šutara, M. Skoda, M. Vondráček, *Langmuir* **24**, 3235 (2008).
- [3] S.G. Urquart, R. Gilles, *J. Chem. Phys.* **124**, 234704 (2006).



# MAGNETIC AND ELECTRONIC PROPERTIES



# MAGNETS OF LILLIPUT

## Controlling magnetic domains at nanometer scale

*An interview with Olivier Fruchart*

In the following you can find a summary of our discussion with Olivier Fruchart on nanomagnetism. He has given us easy-access to a wide-range of topics ranging from self-organization to the current state of affairs in magnetic technology. More information can be found in his highlighted article at page 54.

Olivier Fruchart completed his university studies in École Normale Supérieure. In 1998 he received his PhD in Laboratoire Louis Néel working with D.Givord and J.-P.Nozières. After a two year stay at the Max-Planck Institut für Mikrostrukturphysik, he returned to Grenoble. Since 1999, he is working in Institut Néel as a permanent scientist. His main research interest is magnetism in low-dimensional structures.



**You belong to a prestigious line of french scientists working on magnetism. I found it interesting that the central quantity (Néel cap) in your highlighted article is termed after a great french scientist, Louis Néel. Do you get a feeling of continuity?**

It always strikes me when I realize how brilliant and visionary our heirs in magnetism were, considering that many of their theories could not be suggested nor checked experimentally, owing to the lack of technology at the time. Consider the case of Néel who issued several seminal papers in the 50's pertaining to modifications of magnetic anisotropy and magnetic domain walls in very thin films and at surfaces, well before these could be reliably fabricated and investigated. The argument developed by Néel, based on simple magnetostatics, was crude however caught the main physics at play, a way of thinking I try to follow in my work. Nowadays powerful computers may solve incredibly complex problems for us (and we heavily depend on these in our group!), however in doing so we may miss the basic physics, and the opportunity to predict new effects. Developing first simple arguments requires that we understand the important parameters in the problem, and thus this should always remain part of the physicist's attitude.

Probably I feel a special link with the spirit of Néel as I am working in Néel Institute, one of the numerous technological and research labs thriving in Grenoble as a consequence of the pioneering settling of Néel here right after WWII.

**Illustration 1.**  
Night-shift  
searching for Néel  
caps with my  
colleague Nicolas  
Rougemaille.



**In your work, you use tricks from thin-film growth to create model magnetic structures. Can you say a few words on these naturally grown patterns?**

For a long time scientists have done their best to grow thin films as smooth as possible, fighting against effects such as dewetting, stress accumulation, dislocations, microstructure etc. Since roughly two decades people are realizing that such effects, initially considered as detrimental, may be tailored to obtain the spontaneous fabrication of nanostructures. In our case we make use of the large lattice mismatch (the difference of atomic size) between the initial surface (tungsten) and the deposited material (iron): in order to fit the latter on the former, nature needs to introduce a large density of dislocations at the interface, nearly one every other 2 nanometers! This induces an incredible cost of energy at the interface between these two materials. As a consequence iron does not wet on tungsten, resulting in nanometer-sized droplets. As the droplets are single-crystalline they display well-defined facets, instead of a spherical shape for isotropic liquids. While we use this trick to deliver model systems for fundamental science, similar approaches are heavily used in semiconductors for providing quantum dots of use for lasing and single-photon emission, for example.

**What is the limit to self organization? Surely you couldn't get the atoms to design Monna Lisa on a surface!**

Well, yes and no. It is true that condensed matter physics, although sometimes appearing complex and in endless progress, is only playing with a few tens of different elements. In that case the types of processes at play during growth are quite simple and limited in number. Thus in the best cases one may induce some degree of local ordering between neighboring dots, using effects such as strain. One makes also use of “self-organization”, where patterns appear spontaneously at surfaces, which can later be used as template for the growth of other materials. Self-organization may happen in physics when two opposite interactions compete (e.g. attractive and repulsive), making a characteristic length scale emerge. However these patterns are often very simple and highly symmetric and repetitive (1D or 2D arrays), and their period is difficult to tune. In chemistry already the number of available molecules is considerably larger than the number of elements, explaining the great current success of chemistry in the fabrication of a wealth of nano-objects: clusters, rods, wires, dumbbells, hedgehogs etc. At a higher level of complexity, life's chemistry playing with huge molecules has a virtually unlimited playground. Living species are the most advanced example of self-organization. In the past years researches managed to program the self-organization of any arbitrary pattern based on sequences of DNA, such as smileys that they used to make the cover of their Letter! Thus the difference with Monna Lisa is just back to the question of its smile... More seriously, the great challenge to address now with self-organization is to put together the know-how of these different fields together, to deliver something useful in terms of order and functionalities.

**In the highlighted article, you and your coworkers show that one can store more information in a simple -and small- magnetic dot. What is the significance of this?**

In the race of data storage for ever higher capacities, if one lets alone disruptive concepts, there are two main strategies for increasing the density of information that one may store over a given area: decrease the size of individual bits (for example, go from CD's to DVDs and Blu-ray), or go to multi-level storage per cell (for example, single-layer to double-layer DVDs). Flash memories have combined both strategies in recent years, explaining their incredible progress. Magnetism (hard disk drives) have only relied on shrinking the size of individual bits, implying a smaller rate of progress. Let us think of a magnetic dot as a spinning toy. One may spin it clockwise or anticlockwise, which makes one bit ('0' or '1'). You may also decide to turn you toys upside down and spin it again, with still clockwise or anticlockwise possibilities. This makes four different ways of spinning, or two bit (upwards clockwise, counterclockwise, downward clockwise or counterclockwise). This is what is being investigated in fundamental labs in magnetic dots with flux-closure (the chirality) around a magnetic 'singularity' (the magnetic vortex, at the center of the dot) which may point up or down (like the spinning toy). In a handwavy argument what we did is just consider a spinning toy with an elongated shape in-the-plane so that it may spin on one end or the other end of the bottom surface. This is a third degree of freedom, or bit in terms of data storage!

**How much can you reduce the dimensions of your magnetic dot before you lose the information coded in the Néel cap?**

We may come again to our heir Louis Néel. He predicted that the Bloch domain wall would become a simpler Néel wall in thin films of thickness below approximately 50 nm. Accurate simulations later refined this to 20 nm. More generally, there exist several characteristic length scales in magnetism, below which magnetic exchange becomes dominant over the other energies relevant in the problem. These length scales are in the range 10-20 nm in most of the magnetic materials. Below these dimensions a magnetic system is always in a so-called macrospin state, i.e. the magnetization is essentially uniform. Then only one bit can be stored, depending on whether the macrospin points up or down. This, by the way, is the current status of hard disk drives, making use of grains of size 10 nm nowadays. As multilevel magnetic bits need much larger lateral dimensions (100 nm or more), if they ever have applications, that will be not to compete with existing technologies, however to bring disruptive advantages such as Random Access Memories, consumption, integration etc.

**I am curious to hear your experience at the synchrotron. You used a special microscopy method (LEEM/XMCD-PEEM): what is the strength of this technique compared to numerous other setups for magnetization measurements?**

Concerning the technique I used, there is not one imaging technique better than all others. Each has its advantages and drawbacks, in terms of ease, interpretation, resolution, versatility for various types of samples etc. The strength of XMCD-PEEM is its relative speed (nearly up to video rate in the best cases), non intrusiveness, capability to image directly magnetization (instead of stray fields for MFM, intrusively), and suitability to both surface science and samples brought from the outside (films, nanostructures from lithography etc.). In case of challenging experiments as ours, the combination of several complementary magnetic imaging techniques such as XMCD-PEEM, MFM, Lorentz is highly recommended.

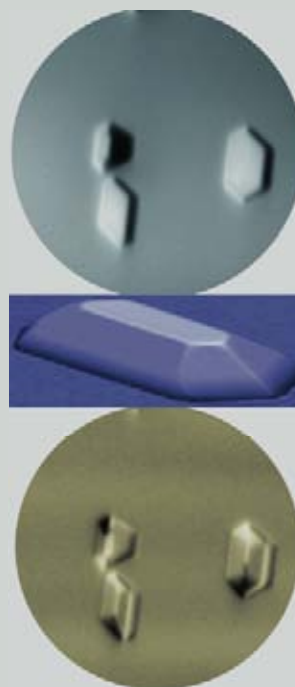


**Illustration 2.**  
An illustrated story on nanomagnetism: self-organized submicron iron dots are grown (top panel), characterized structurally (middle) and shown by XMCD-PEEM to be multi-bit magnetic units (bottom).

# HOW MANY BITS CAN FIT IN A SINGLE MAGNETIC DOT? XMCD-PEEM EVIDENCES THE SWITCHING OF NÉEL CAPS INSIDE BLOCH DOMAIN WALLS

F. Cheynis<sup>1</sup>, A. Masseboeuf<sup>2</sup>, O. Fruchart<sup>1</sup>, N. Rougemaille<sup>1</sup>, J.C. Toussaint<sup>1</sup>, R. Belkhou<sup>3,4</sup>, P. Bayle-Guillemaud<sup>2</sup>, A. Marty<sup>5</sup>

<sup>1</sup>Institut NÉEL, CNRS et Université Joseph Fourier, Grenoble, France

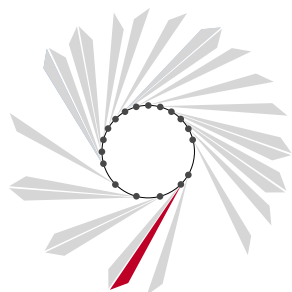
<sup>2</sup>CEA-Grenoble, Grenoble, France

<sup>3</sup>Synchrotron SOLEIL, Gif-sur-Yvette Cedex, France

<sup>4</sup>Sincrotrone Trieste S.C.p.A., Trieste, Italy

<sup>5</sup>CEA-Grenoble, Grenoble, France

E-mail: Olivier.Fruchart@grenoble.cnrs.fr



NANOSPECTROSCOPY

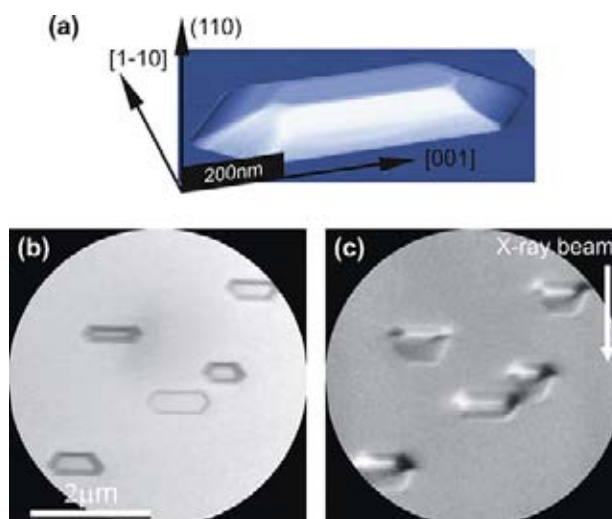
Data storage relies on the handling of two states, called bits. The market of mass storage is currently still dominated by magnetic technology, hard disk drives for the broad public and tapes for massive archiving. In these devices each bit is stored in the form of the direction of magnetization of nanosized magnetic domains. While miniaturization is the conventional way to fuel the continuous increase of device density, disruptive solutions are also sought after. To these pertain in recent years many fundamental studies no longer considering the magnetic domains themselves, but the manipulation of the domain walls (DWs). In magnetic dots of submicrometer dimensions, the magnetization has a tendency to curl along the outer edges of the nanostructure to close its magnetic flux and thereby to reduce its magnetostatic energy. Then both domains and DWs of well-defined geometries arise, whose combined manipula-

tion has been proposed as a multilevel magnetic storage scheme. For example in nanodisks, the chirality of the flux closure and the vertical polarity of the central magnetic vortex provide two bits, which has led to many studies in recent years.

In our study we have been one step further and demonstrated the manipulation of dots with three degrees of freedom. This was achieved considering elongated dots, in which the central vortex is replaced by an elongated DW. Micrometer-sized faceted epitaxial Fe(110) dots self-assembled under ultra-high vacuum and prepared using pulsed laser deposition have been used as model systems (Figure 1(a)) [1]. Beyond its vertical polarity, such a domain wall possesses an extra degree of freedom: at both upper and lower dot surfaces the magnetization of the DW turn in-plane to minimize magnetostatic energy. These areas are called Néel caps (NCs) and are antiparallel to

**Figure 1.**

(a) 3D view of a typical self-assembled epitaxial Fe(110) dot (atomic force microscopy, true aspect ratios). (b) LEEM (topography) and (c) XMCD-PEEM (magnetism) typical view of an ensemble of dots. After magnetization at -130mT all the dots are in the (-,+) state at remanence. The white arrow indicates the direction of the x-rays, thus the component of in-plane surface magnetization imaged.



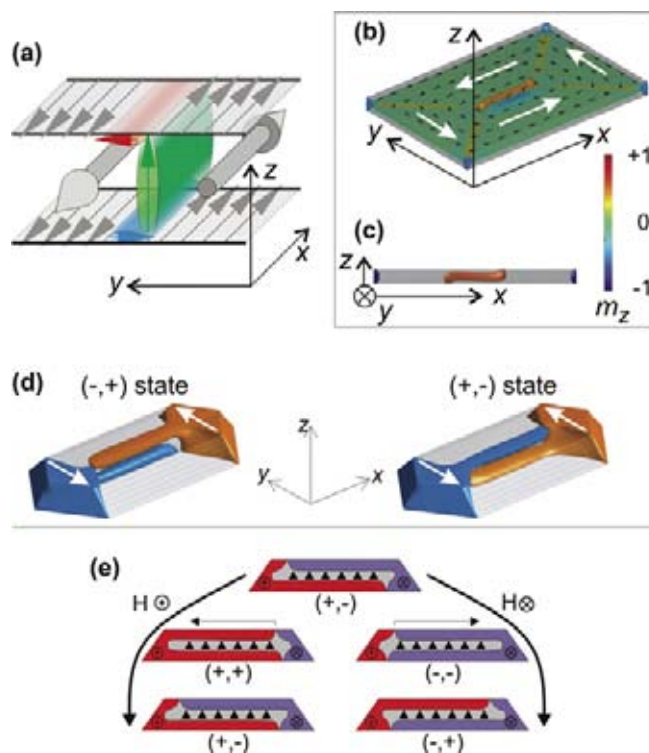


**Figure 2.** (a) Schematic view of a domain wall of Bloch type, terminated by a Néel cap at each surface. The magnetization is opposite in the top and bottom Néel caps, and points along the  $\pm y$  axes. (b–c) 3D and cross section views of a flux-closure state in a rectangular magnetic dot ( $700 \times 500 \times 50 \text{ nm}^3$ ). In (b) only volumes with normalized perpendicular magnetization  $|m_z| > 0.5$  are displayed, which highlights the domain wall. The in-plane curling of magnetization is indicated by white arrows. (d) Simulation in an elongated dot of the  $(-,+)$  and  $(+,-)$  states. Only volumes with  $|m_y| > 0.5$  are displayed, while positive and negative values appear red and blue, respectively. (e) Schematic cross-sectional view of the switching of NCs: the final state is  $(-,+)$  or  $(+,-)$  depending on the sign of the applied field.

each other in the absence of external field as seen in Figure 2(a–c) [2]. The extra degree of freedom is therefore whether the NCs are in a  $(-,+)$  or  $(+,-)$  state (Figure 2(d)). We predicted by simulation that NCs should turn parallel upon application of an external field along the short axis of the dots, while both chirality and DW polarity should remain unchanged. Then upon decreasing the field back to zero, state  $(+,+)$  switches back to  $(+,-)$ , while state  $(-,-)$  switches back to  $(-,+)$ , shown in Figure 2(e). Our experimental confirmation came from the use of the French-Soleil LEEM-PEEM Elmitec instrument currently hosted at the Nanospectroscopy beamline. Exploiting the magnetic sensitivity owing to X-ray Magnetic Circular Dichroism (XMCD), the collection of emitted photoelectrons (PEEM) allows one to build surface magnetization maps with a spatial resolution around 25 nm. NCs are then revealed as a thin stripe of dark or light contrast along the length of the dots, depending on the  $(+,-)$  or  $(-,+)$  state (Figure 2(c)). As magnetic fields are hardly compatible with low-energy electrons the magnetization process was performed off-stage, and observed a posteriori. For each

field several tens of dots were imaged as in Figure 1(b,c). In this way a mean switching field of 100 mT was found, in close agreement with simulations [3]. In addition, the process could be monitored in real time under applied field using Lorentz Microscopy [3]. Beyond potential applications in data storage, this study should mainly excite our physicist curiosity about the extension of the concept of magnetization reversal to the inner structure of DWs, beyond the classical case of extended domains, and trigger new studies in this direction.

## References

- [1] O. Fruchart, M. Eleoui, P.O. Jubert, P. David, V. Santonacci, F. Cheynis, B. Borca, M. Hasegawa, *J. Phys. Condens. Matter* **19**, 053001 (2007).
- [2] R. Hertel, O. Fruchart, S. Cherifi, P. O. Jubert, S. Heun, A. Locatelli, J. Kirschner, *Phys. Rev. B* **72**, 214409 (2005).
- [3] F. Cheynis, A. Masseboeuf, O. Fruchart, N. Rougemaille, J. C. Toussaint, R. Belkhou, P. Bayle-Guillemaud, A. Marty, *Phys. Rev. Lett.* **102**, 107201 (2009).

# EVIDENCE FOR A MAGNETIC PROXIMITY EFFECT UP TO ROOM TEMPERATURE AT Fe/(Ga,Mn)As INTERFACES

F. Maccherozzi<sup>1,2</sup>, M. Sperl<sup>4</sup>, G. Panaccione<sup>3</sup>, J. Minár<sup>5</sup>, S. Polesya<sup>5</sup>, H. Ebert<sup>6</sup>, U. Wurstbauer<sup>4</sup>, M. Hochstrasser<sup>5</sup>, G. Rossi<sup>3,7</sup>, G. Woltersdorf<sup>4</sup>, W. Wegscheider<sup>4</sup>, C. H. Back<sup>4</sup>

<sup>1</sup>Sincrotrone Trieste S.C.p.A., Trieste, Italy

<sup>2</sup>Synchrotron SOLEIL, Saint Aubin, France

<sup>3</sup>Laboratorio Nazionale TASC, INFN-CNR, Trieste, Italy

<sup>4</sup>Institut für Experimentelle Physik, University of Regensburg, Regensburg, Germany

<sup>5</sup>Laboratorium für Festkörperphysik, ETH Hönggerberg, Zürich, Switzerland

<sup>6</sup>Department of Chemistry, Ludwig-Maximilians University, Munich, Germany

<sup>7</sup>Dipartimento di Fisica, Università di Modena e Reggio Emilia, Modena, Italy

E-mail: francesco.maccherozzi@elettra.trieste.it



APE

By doping semiconductors with magnetic impurities it is possible to add them ferromagnetic properties, obtaining the Diluted Magnetic Semiconductors (DMS). The strong interplay between ferromagnetic (FM) and electronic properties of these materials make them good candidates for the realization of spintronic devices, that aim to be based on the spin state of the electrons, instead than on their charge, as is the case for conventional electronic circuits. The (Ga,Mn)As is a prototypical DMS, already used for working spintronic devices, but its low Curie temperature ( $T_c$ ) hamper its use at room temperature.

The study of FM-metal/DMS interfaces recently raised an increasing interest because of the relatively high  $T_c$  of the transition metals thin films, usually well above room temperature, and for the possibility to perform efficient spin injection in the semiconductors at room temperature. The control and the comprehension of the magnetic interactions across such interfaces could suggest new approaches for device realization and electron spin manipulation.

Relying on our knowledge on the structural and magnetic properties of the Fe/GaAs(001) epitaxial films [1], we decided to choose Fe and (Ga,Mn)As for our FM-metal/DMS structures. The measurements show a net magnetization of the Mn induced by the thin Fe layer across the Fe/(Ga,Mn)As interface by proximity effect. The spins of the Mn atoms polarized with this mechanism have antiparallel alignment to that of the Fe [2]. The most relevant point of this finding is that the effect is visible above room temperature: well above the  $T_c$  of the (Ga,Mn)As layer, thus in condi-

tions where it is not expected any magnetic order in the DMS layer. This is the first experimental evidence of a magnetic proximity effect across a FM-metal/DMS interface.

The use of X-Ray absorption with circularly polarized light at the transition metal absorption edges (Magnetic Circular Dichroism) provide information about the electronic and magnetic configuration with elemental selectivity. It is thus an ideal tool to study the relative orientation of the magnetization vector in multilayer structures where different magnetic elements are involved. It also provides both chemical and magnetic information of the probed element.

The left panel of Figure 1 shows the XAS/XMCD spectra of one Fe/(Ga,Mn)As sample across the Mn  $L_{2,3}$ -edges. The sign of the Mn XMCD  $L_3$  peak is negative, indicating the opposite direction of the Mn and Fe magnetization vectors. We recorded elemental selective hysteresis by means of the XMCD signal at the  $L_3$  edges. In Figure 2 it is well visible that the shape of the Fe (red) and Mn (green) hystereses is similar, but opposite in sign. In all the explored magnetic field range (0-200 Oe) the Mn magnetization is proportional to the Fe one. The ratio between the Mn and Fe XMCD, a rough indicator of the magnetic coupling strength, is higher for thicker Fe films and at lower temperature. We did not observe any dependency of the Fe-Mn magnetic coupling with respect to the Mn concentration in the GaAs layer.

A quantitative analysis of the Mn XMCD intensities, based on the surface sensitivity of the total electron yields detection, indicates a



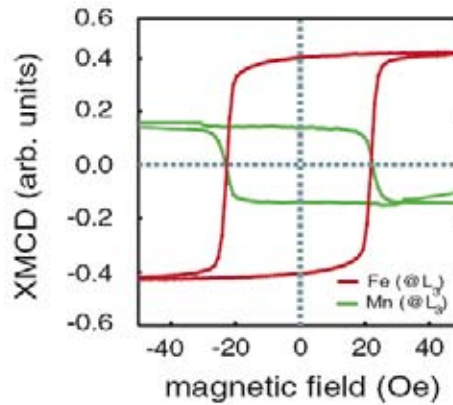
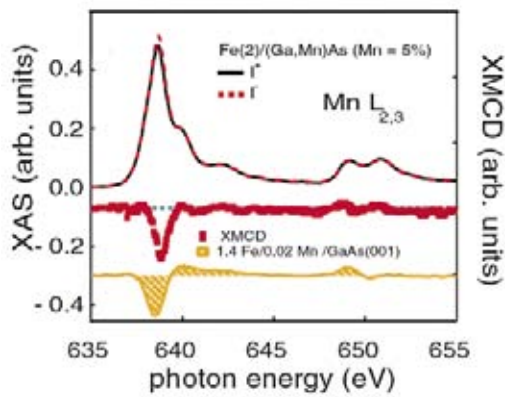


**Figure 1.** Room temperature XAS (black/red lines) and XMCD (red squares) spectra of a Mn/(Ga,Mn)As sample at the Fe  $L_{2,3}$  edges, compared with the XMCD of Mn intentionally alloyed with Fe (yellow line). The negative sign of the XMCD  $L_3$  peak (at 635 eV) indicates antiparallel alignment of the Mn magnetization with respect to the external magnetic field. (left) Magnetic hysteresis acquired with the XMCD signal at the Fe (red) and Mn (green)  $L_3$  edges.

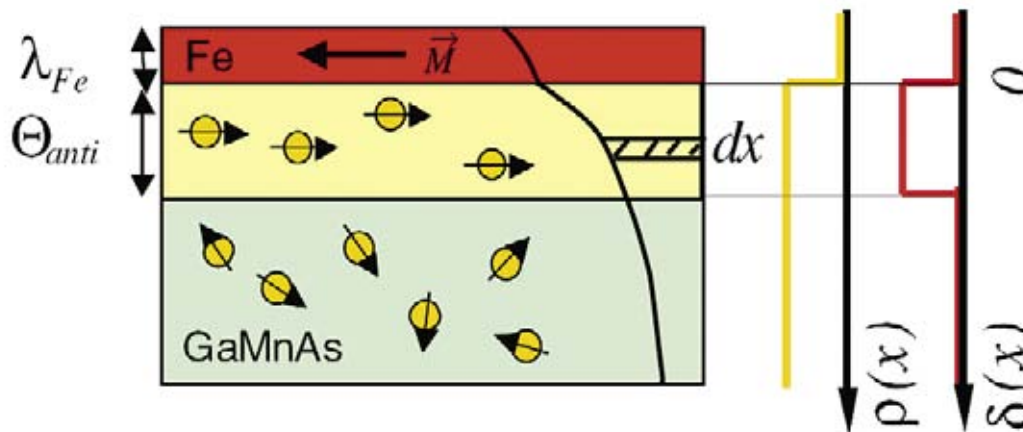


**Figure 2.** Sketch of the vertical sample structure and magnetization profile. The thickness of the (Ga,Mn)As layer that feels the magnetic proximity effect with the Fe is estimated to be at least 2 nm.

minimum depth of the Mn magnetized layer of 2 nm, corresponding to about 7 ML of GaAs. In Figure 2 it is reported a sketch of the vertical sample structure. The Fe-Mn magnetic coupling is thus unlikely to be due to alloying/interdiffusion of Mn across the interface, but in order to fully support the sharp interface picture we compared the Mn XAS/XMCD line shapes with control samples where the Mn is intentionally alloyed with the Fe. We found spectroscopic fingerprints of the Mn alloyed with the Fe (in GaAs/Mn/Fe and GaAs/Mn<sub>0.03</sub>Fe<sub>0.97</sub> multilayer) that are not present when the Mn is embedded in the GaAs crystal. In the left panel of Figure 1 the Mn XMCD of Fe/(Ga,Mn)As is compared with the Mn XMCD of Fe<sub>0.9</sub>Mn<sub>0.05</sub>/GaAs, where the

Mn is intentionally alloyed with the Fe; the latter spectrum shows a more structured shape and is shifted towards lower energies. We can thus clearly distinguish between the Mn coordinated with the GaAs crystal and the Mn diffused in the Fe layer. This confirms the picture where the magnetic proximity effect with the Fe layer extends within the GaAs crystal. The direct exchange between Fe and Mn as magnetic coupling mechanism is excluded.

#### References

- [1] L. Giovannelli *et al.*, *Phys. Rev. B* **72**, 45221 (2005)
- [2] F. Maccherozzi *et al.*, *Phys. Rev. Lett.* **101**, 267201 (2008); selected as viewpoint in *Physics-PRL, Physics* **1**, 43 (2008).

# IN A CORRELATED METAL, QUASIPARTICLES ARE NOT SUPERFICIAL AT ALL

F. Rodolakis<sup>1,2</sup>, B. Mansart<sup>1</sup>, E. Papalazarou<sup>1,3</sup>, S. Gorovikov<sup>4</sup>, P. Vilmercati<sup>4</sup>, L. Petaccia<sup>4</sup>, A. Goldoni<sup>4</sup>, J.-P. Rueff<sup>2</sup>, S. Lupi<sup>5</sup>, P. Metcalf<sup>6</sup>, M. Marsi<sup>1</sup>

<sup>1</sup>Laboratoire de Physique des Solides, Université Paris-Sud, Orsay, France

<sup>2</sup>Synchrotron SOLEIL, Saint Aubin, France

<sup>3</sup>Laboratoire d'Optique Appliquée, Ecole Polytechnique, Palaiseau, France

<sup>4</sup>Sincrotrone Trieste S.C.p.A., Trieste, Italy

<sup>5</sup>Department of Physics, Università "La Sapienza", Roma, Italy

<sup>6</sup>Department of Chemistry, Purdue University, West Lafayette, USA

E-mail: marsi@lps.u-psud.fr



BADELPH

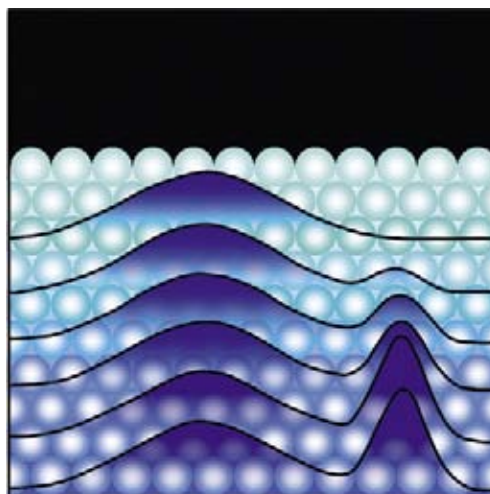
In conventional materials, electronic and transport properties such as conductivity can be well understood by applying the concepts of band theory. In more complex materials, simple band dispersion cannot account for the details of their electronic structure and electron-electron correlations are to be taken into account: these materials are called strongly correlated materials. For example, one of the best known classes of such materials - Mott-Hubbard compounds - presents remarkable macroscopic properties, such as transitions from a metallic to an insulating state, even though band theory predicts that they should simply be metallic. Notable examples of Mott-Hubbard compounds are high critical temperature superconductors, or giant magnetoresistance oxides.

The most advanced theoretical models describing Mott transitions predict that the transition from an insulating to a metallic phase is determined by the appearance of collective elec-

tronic excitations at the Fermi level, which are constituted of a coherent quasiparticle peak and incoherent Hubbard bands. A detailed study of these low energy electronic excitations is the key to understand the fascinating phenomenology of strongly correlated materials and of their phase transitions. Distressingly, the observation of these features with angle resolved photoemission (ARPES), one of the main techniques for the study of the fermiology of strongly correlated materials, often encounters puzzling difficulties in their detection and quantitative analysis, due to the intrinsic surface sensitivity of photoelectron spectroscopy. In a model compound for the study of Mott-Hubbard transition,  $V_2O_3$ , angle integrated photoemission at high photon energy [1] showed that bulk sensitivity is necessary to detect the theoretically expected line-shapes for the quasiparticles at the Fermi energy, as depicted in Figure 1.

**Figure 1.**

Pictorial view of the electronic density of states close to the Fermi energy of a Mott-Hubbard compound like  $V_2O_3$ . In the bulk, a prominent quasiparticle peak (on the right side in the figure) is found along with the incoherent Hubbard band (left side). At the surface of the material, the coherent spectral weight of the quasiparticle is strongly reduced.



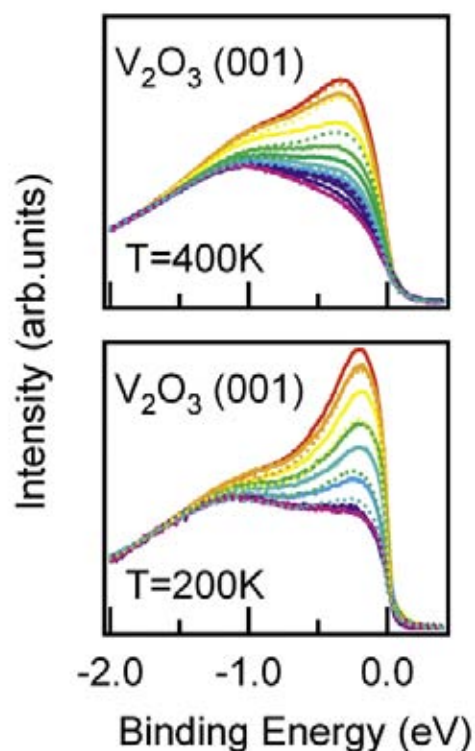


**Figure 2.** ARPES spectra at 9 eV photon energy on  $V_2O_3$  for different detection angles, from bulk sensitive normal emission (red) to more surface sensitive grazing emission (violet). The comparison of the quasiparticle attenuation at different temperatures (between 200 and 400 K) makes it possible to study the evolution of the surface dead layer with respect to the parametric distance from the Mott transition in the thermodynamic phase diagram.

Performing angle resolved photoemission at very low photon energy on the Bad EIPh beamline at ELETTRA, we were able to observe for the first time the wavevector dependence of the quasiparticle peak in the metallic phase of  $V_2O_3$ , and to follow its attenuation at the surface [2]. Detecting photoelectrons of few eV kinetic energy makes it possible to increase the bulk sensitivity of the signal, and by exploring its angular dependence we were able to see that the coherent quasiparticle states react to the presence of the surface over a characteristic length scale of the order of 10 nm. By comparing the attenuating behaviour of the quasiparticle at different temperatures (Figure 2), we were able to verify that this critical length increases when approaching a Mott instability. These results are in agreement with a parallel interpretation by theorists from the International School for Advanced Studies of Trieste [3], who predicted a surface dead layer for quasiparticles in a correlated metal, whose thickness depends only on the bulk property of the material and not on the details of its surface. The existence

of this characteristic length scale for coherent collective excitations appears to be a general property of correlated systems [4], and can play a very important role in many phenomena taking place at the surfaces and interfaces of this class of materials.

These results show that ARPES experiments at very low photon energy represent at the same time a very promising approach to further explore this issue, and a sufficiently bulk sensitive probe to investigate the genuine details of the fermiology of strongly correlated materials.

#### References

- [1] S.-K. Mo *et al.*, *Phys. Rev. Lett.* **90**, 186403 (2003).
- [2] F. Rodolakis, B. Mansart, E. Papalazarou *et al.*, *Phys. Rev. Lett.* **102**, 066805 (2009).
- [3] G. Borghi, M. Fabrizio and E. Tosatti, *Phys. Rev. Lett.* **102**, 066806 (2009).
- [4] “Insulating behaviour is only skin deep”, *Physics, Synopsis* February 17, (2009), <http://physics.aps.org/synopsis-for/10.1103/PhysRevLett.102.066805>

# EVIDENCE FOR STRONG ITINERANT FLUCTUATIONS IN THE NORMAL STATE OF $\text{CeFeAsO}_{0.89}\text{F}_{0.11}$ IRON-OXYPNICTIDES

F. Bondino<sup>1</sup>, E. Magnano<sup>1</sup>, M. Malvestuto<sup>2</sup>, F. Parmigiani<sup>1,3</sup>, N.A. McGuire<sup>4</sup>, A.S. Sefat<sup>4</sup>, B.C. Sales<sup>4</sup>, R. Jin<sup>4,5</sup>, D. Mandrus<sup>4</sup>, E.W. Plummer<sup>5</sup>, D.J. Singh<sup>4</sup>, N. Mannella<sup>5</sup>

<sup>1</sup>Laboratorio Nazionale TASC INFN-CNR, Trieste, Italy

<sup>2</sup>Sincrotrone Trieste S.C.p.A., Trieste, Italy

<sup>3</sup>Department of Physics, University of Trieste, Trieste, Italy

<sup>4</sup>Materials Science and Technology Division, Oak Ridge National Laboratory, Oak Ridge, USA

<sup>5</sup>Department of Physics and Astronomy, The University of Tennessee, Knoxville, USA

E-mail: bondino@tasc.infn.it, nmannel@utk.edu



BACH

Cuprate High-Temperature Superconductors (HTSC) and the newly discovered Fe-based superconductors (FeSC) [1] are the only families of compounds exhibiting high-temperature superconductivity with critical temperature exceeding 55 K.

A hallmark of cuprate HTSC, which sets them apart from conventional BCS-like superconductors, is the occurrence of unusual normal state properties, which are outside the framework of Fermi-liquid theory. Most of these properties appear to be related to the effects of electron correlations induced through strong on-site Coulomb repulsions—among electrons in the narrow Cu 3d bands, related to the Mott-Hubbard insulating undoped phases. A description of the normal state electronic structure of FeSC is expected to elucidate the role of electron correlations, thus providing firm grounds of comparison for establishing commonalities and differences with the cuprate HTSC and the most appropriate starting point for describing the physics of this new class of materials.

We have obtained information about the electronic structure of  $\text{CeFeAsO}_{0.89}\text{F}_{0.11}$  from photoemission spectroscopy (PES) and x-ray absorption spectroscopy (XAS) measurements performed at the BACH beamline [2].

A comparison between the Fe 2p and Cu 2p core-level spectra, shown in Figure 1(a), reveals marked differences between the normal state electronic structure in FeSC and HTSC. While the Cu 2p spectrum in HTSC is characterized by satellite structures appearing as a result of the localized character of the Cu 3d electrons, the Fe 2p spectrum in  $\text{CeFeAsO}_{0.89}\text{F}_{0.11}$  exhibits a main  $2p_{3/2}$  peak markedly different from that of Fe ionic compounds, but more akin to that of Fe metal and

intermetallic compounds. Similar conclusions are reached from inspection of the Fe  $L_{2,3}$  XAS spectrum (Figure 1(b)). This result is further confirmed by the observation of a high density of states (DOS) at  $E_F$  in the valence band (VB) (Figure 2(a)) in marked contrast to equivalent spectra from HTSC. The high DOS at  $E_F$ , which can be identified as Fe 3d DOS [2], is very effective in completely screening the Fe 2p core-hole excitation, leading to an absence of satellite structures in the core-level spectra.

The spectroscopic signatures of Fe d-electron itinerancy in  $\text{CeFeAsO}_{0.89}\text{F}_{0.11}$  are indicative of marked differences with the electronic structure of cuprate HTSC. On the other hand, much like in HTSC, superconductivity emerges in close proximity to a long-range-ordered antiferromagnetic ground state, leading credence to the central relevance of the interplay between superconductivity and spin-density-wave instability. However, the nature of the interplay between fluctuations associated with the apparent proximity to magnetism and the superconducting phase remains to be established. Due to extremely fast time scales involved, the detection of magnetic fluctuations by means of magnetic probes has so far remained elusive. A strong and unique test case for the detection of possible itinerant magnetic fluctuations can be made possible by the extremely fast time scales proper of the PES process.

In transition metals, the 3s PES spectra can exhibit a multiplet splitting arising from the exchange coupling of the core 3s electron with the net spin  $S_v$  in the unfilled 3d shell of the emitter atom. The multiplet energy separation  $\Delta E_{3s}$  permits estimating the net spin of the

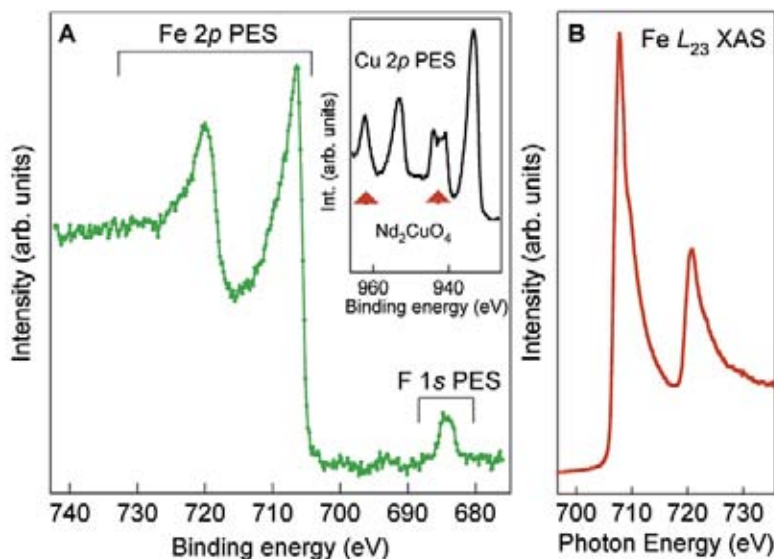


**Figure 1.** (a) PES Fe 2p spectrum collected from CeFeAsO<sub>0.89</sub>F<sub>0.11</sub> and equivalent Cu 2p in HTSC (inset, from P.G. Steeneken *et al.*, *Phys. Rev. Lett.* **90**, 247005 (2003)) (b) Fe L<sub>23</sub> XAS spectrum.

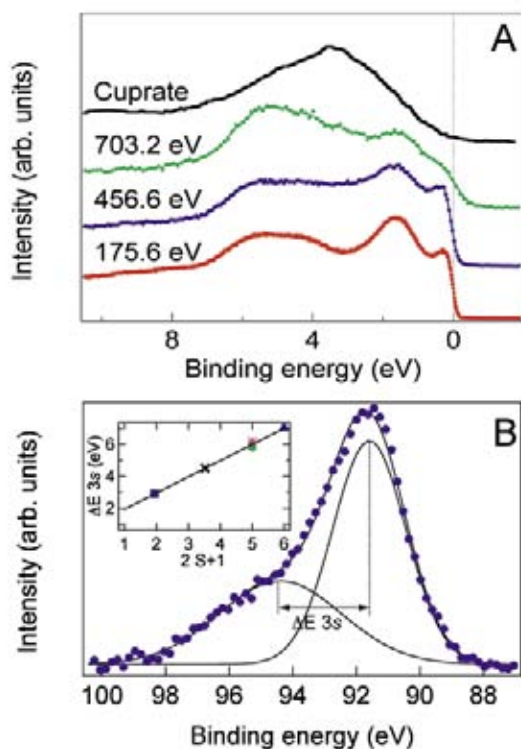


**Figure 2.** (a) VB spectra of CeFeAsO<sub>0.89</sub>F<sub>0.11</sub> measured with  $h\nu=175.5, 456.4,$  and  $703.2$  eV and VB of a cuprate HTSC (YBa<sub>2</sub>Cu<sub>3</sub>O<sub>7-y</sub>) from A. Fujimori *et al.*, *Phys. Rev. B* **35**, 8814 (1987). (b) Fe 3s core level PES spectrum of CeFeAsO<sub>0.89</sub>F<sub>0.11</sub> and a two-component fit providing a value of 2.9 eV for  $\Delta E_{3s}$ . Inset: linear extrapolation of the  $\Delta E_{3s}$  vs  $(2S_v+1)$  for several Fe compounds. The points denote the  $\Delta E_{3s}$  values for FeF<sub>3</sub> (▲), FeF<sub>2</sub> (●), FeO (\*), Fe metal (×) and CeFeAsO<sub>0.89</sub>F<sub>0.11</sub> (■) [2].

emitter atom, i.e., the local spin moment, via a formula relating  $S_v$  to  $\Delta E_{3s}$  [2]. We measured the Fe 3s spectrum of CeFeAsF<sub>0.11</sub>O<sub>0.89</sub> and we found that it exhibits a two-peak structure with a splitting  $\Delta E_{3s}=2.9$  eV seen in Figure 2(b), which would correspond to  $S_v=1 \mu_B$ . However, this result is at odds with other measurements such as Mössbauer spectroscopy, NMR, and magnetic susceptibility, according to which in CeFeAsO<sub>0.89</sub>F<sub>0.11</sub> Fe is nonmagnetic and Ce alone contributes to effective moment derived from the Curie-Weiss susceptibility. Since the

extremely short time scale involved in the PES process ( $10^{-17} - 10^{-16}$  s) can account for the disagreement with much slower ( $10^{-7}$  s) Mössbauer and NMR measurements, the splitting of the Fe 3s level can be interpreted as evidence of Fe-based spin fluctuations.

#### References

- [1] Y. Kamihara *et al.*, *J. Am. Chem. Soc.* **130**, 3296 (2008).
- [2] F. Bondino *et al.*, *Phys. Rev. Lett.* **101**, 267001 (2008) and ref. therein.

# PRESSURE AND ALLOYING EFFECTS ON THE METAL TO INSULATOR-TRANSITION IN $\text{NiS}_{2-x}\text{Se}_x$ STUDIED BY INFRARED SPECTROSCOPY

A. Perucchi<sup>1,2</sup>, C. Marini<sup>2</sup>, M. Valentini<sup>2</sup>, P. Postorino<sup>2</sup>, R. Sopracase<sup>2</sup>, P. Dore<sup>2</sup>, P. Hansmann<sup>3,4</sup>, O. Jepsen<sup>3</sup>, G. Sangiovanni<sup>3,4</sup>, A. Toschi<sup>3,4</sup>, K. Held<sup>4</sup>, D. Topwal<sup>5</sup>, D.D. Sarma<sup>6</sup>, S. Lupi<sup>2</sup>

<sup>1</sup>Sincrotrone Trieste S.C.p.A., Trieste, Italy

<sup>2</sup>CNR-INFM-COHERENTIA and Physics Department, University of Rome "La Sapienza", Roma, Italy

<sup>3</sup>Max-Planck Institut für Festkörperforschung, Stuttgart, Germany

<sup>4</sup>Institute for Solid State Physics, Vienna University of Technology, Vienna, Austria

<sup>5</sup>International Centre for Theoretical Physics, Trieste, Italy

<sup>6</sup>Centre for Advanced Materials and Solid State and Structural Chemistry Unit, India

E-mail: andrea.perucchi@elettra.trieste.it



SISSI

Understanding the physics of strongly correlated systems is one of the most challenging tasks of condensed matter research [1]. Besides displaying extremely interesting physical behaviour, their sensitivity to small changes in external parameters makes them highly appealing for future technological applications. That sensitivity is attributed to the small value of the electron bandwidth,  $W$ , in comparison with other relevant energy scales as the electron correlation,  $U$ , or the charge transfer (CT) energy gap,  $\Delta$ . The independent electron approximation breaks down and materials at half filling can be insulators, contrary to the prediction of band theory.

The CT insulator  $\text{NiS}_2$  is considered, together with vanadium sesquioxide  $\text{V}_2\text{O}_3$ , a text-book example of strongly correlated materials.  $\text{NiS}_2$  attracts particular interest as it easily forms a solid solution with  $\text{NiSe}_2$  ( $\text{NiS}_{2-x}\text{Se}_x$ ), which, while being iso-electronic and iso-structural to  $\text{NiS}_2$ , is nevertheless a good metal. A metal to insulator transition (MIT), induced by Se alloying, is observed at room temperature ( $T$ ) for  $x \sim 0.6$ . An alternative way to induce a metallic state in  $\text{NiS}_2$  is applying a hydrostatic pressure ( $P$ ). Following Mott's original idea, this technically challenging procedure offers the unique opportunity to continuously tune  $W$ , without introducing impurities or disorder. High- $P$  techniques have indeed been used in the past few years to investigate the dc transport properties of  $\text{NiS}_{2-x}\text{Se}_x$ , and a  $P$  induced MIT has been observed in pure  $\text{NiS}_2$  for  $P > 4$  GPa. We use here synchrotron infrared spectroscopy [2] in order to address and compare the  $P$ - and alloying-induced MITs [3].

From a conventional Drude-Lorentz fit of both our  $P$ - and  $x$ -dependent data sets, we were able to identify a remarkable transfer of spectral weight (SW) from high to low frequencies when either  $P$  or  $x$  is increased. Our data show that such low-energy contribution is made up of two well distinct terms: one broad mid-infrared band peaked around  $2000 \text{ cm}^{-1}$ , and a sharp contribution below  $500 \text{ cm}^{-1}$ . The narrow peak is attributed to quasi-particle (QP) coherent excitations around the Fermi energy ( $E_F$ ), while the mid-infrared term is associated to optical transitions from the QP peak to the upper and lower Hubbard bands (incoherent term).

The microscopic mechanisms inducing the  $P$ - and Se-MITs are further investigated by studying the quasi-particle SW (defined as the sum of the coherent and incoherent contributions) as a function of the cubic lattice parameter  $a$ . The lattice is expanded by Se-alloying, whereas it is compressed by  $P$ . The quasi-particle SW reveals a striking non-monotonic behaviour as a function of  $a$ . Its slow continuous increase for  $a < 5.57 \text{ \AA}$  (i.e. at the highest values of  $P$ ) reflects the progressive enhancement of the kinetic energy due to the applied  $P$  and corresponds to a nearly complete metallization of  $\text{NiS}_2$ . For  $a > 5.57 \text{ \AA}$  up to  $a_{eq} \sim 5.68 \text{ \AA}$  (namely the lattice parameter corresponding to  $\text{NiS}_2$  at ambient conditions), correlation effects get larger and the SW drops rapidly to zero as a consequence of the Mott transition. On further increasing  $a$  above  $a_{eq}$  due to the Se-alloying, the SW restarts to increase, owing to the onset of the Se-induced MIT.

Despite the opposite behaviour of the lattice parameter vs Se-alloying and  $P$ , a linear scal-

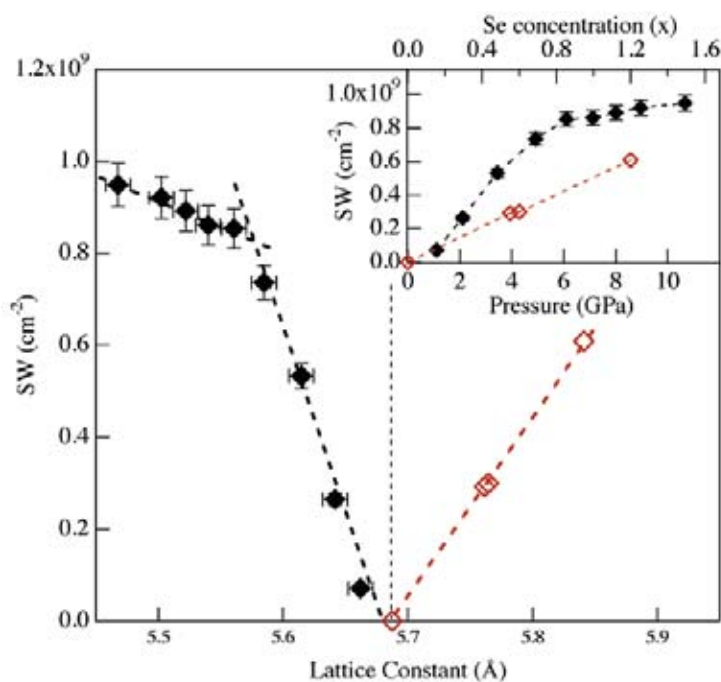


**Figure 1.** Quasi-particle SW vs lattice constant  $a$  for  $\text{NiS}_2$  and  $\text{NiS}_{2-x}\text{Se}_x$ . The light dashed vertical line marks the  $a$  value for  $\text{NiS}_2$  at ambient conditions. Inset: QP SW vs  $P$  (bottom) and  $x$  (top); top and bottom scales are chosen consistently with a scaling factor  $f \sim 0.14$  /GPa.

ing factor  $f \sim 0.14/\text{GPa}$  between  $x$  and  $P$  has been formerly established from low- $T$  dc-resistivity data, thus suggesting an equivalency between the two MITs. However, the same  $f$  does not apply comparing the optical SW dependence on  $P$  and  $x$ . The breakdown at finite frequencies of the dc linear scaling relation between  $x$  and  $P$  suggests that, while a metallic state can be obtained from  $\text{NiS}_2$ , both by applying  $P$  and by alloying Se, this state takes place through substantially different microscopic mechanisms, involving different redistributions in the electronic density of states.

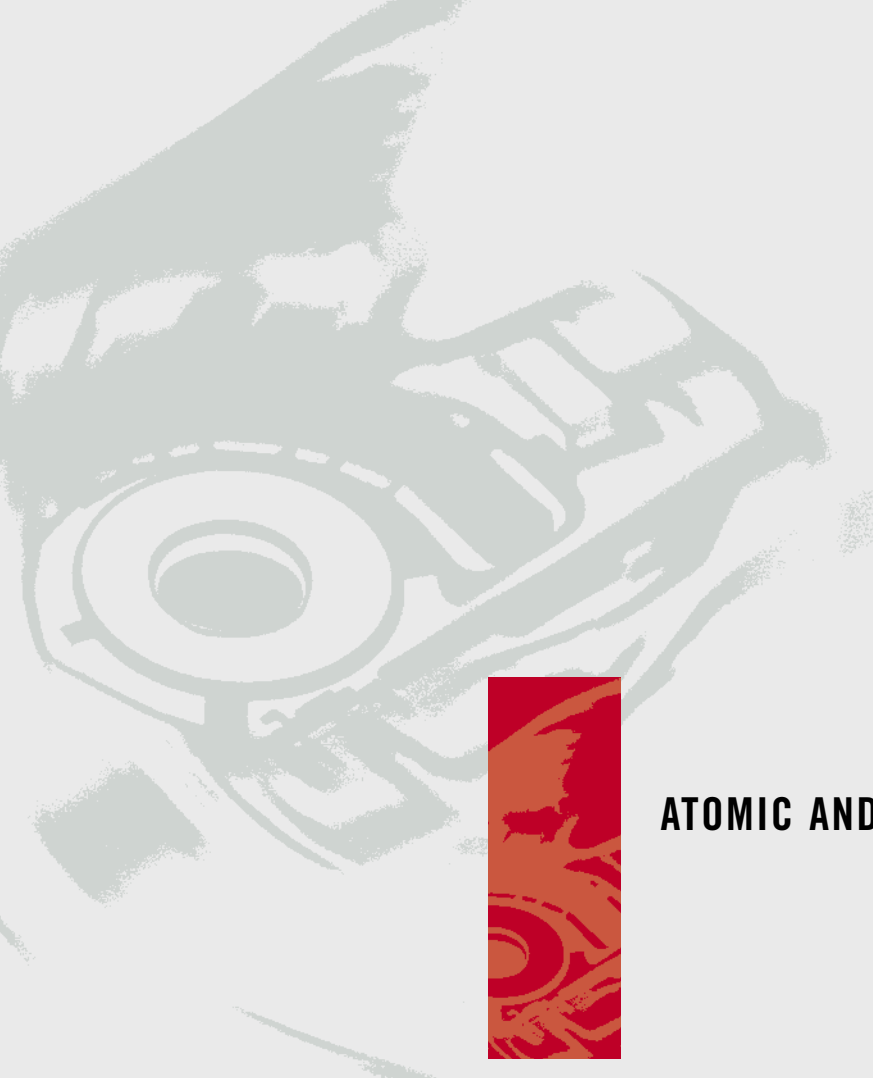
A qualitative understanding of the two different MITs can be obtained through LDA (Local Density Approximation) calculations. These demonstrate that under pressure  $W/U$  increases by a factor of 1.13, while  $U$  can be assumed to be constant, thus triggering a bandwidth-controlled MIT (BC-MIT). On the other hand, in the case of Se-substitution, the lattice expands (instead of shrinking) due to the larger atomic radius of Se ions. This leads to a very complementary scenario: while the changes of  $W$  are negligible, the CT gap  $\Delta$  shrinks. If  $U$  is assumed to be constant, the

driving force for the MIT is now the reduction of the CT gap ( $W/\Delta$  increases, as  $W$  remains unaffected).

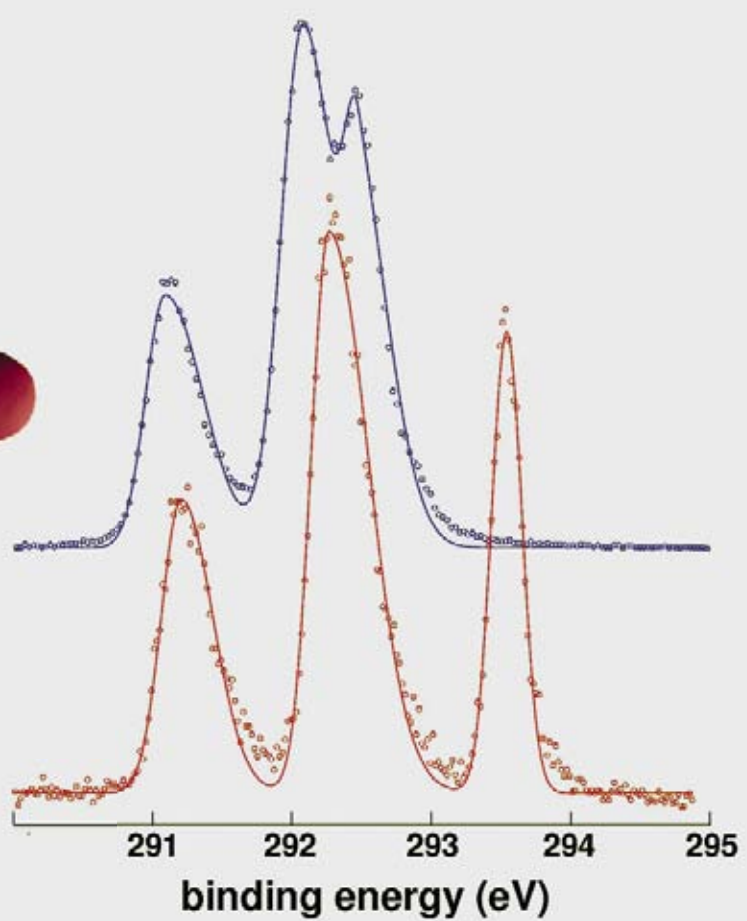
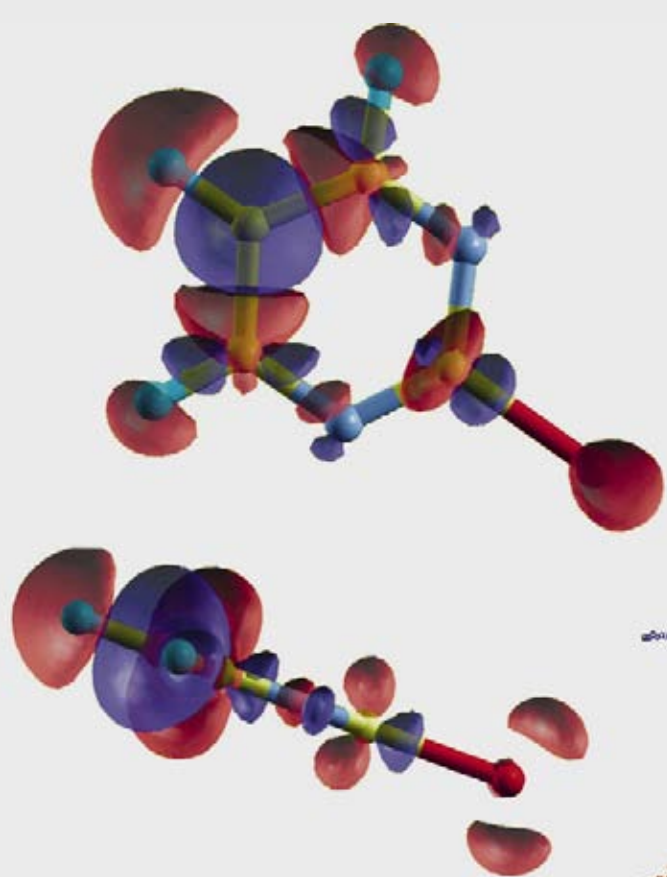
Besides important similarities between the  $P$ - and Se-dependent phase diagrams, the present optical study reveals that a simple linear scaling between  $P$  and  $x$ , as that indicated by transport, does not hold at finite frequencies. This suggests that the two MITs rely on distinct microscopic mechanisms. These mechanisms can be understood theoretically in terms of the two fundamental parameters for the MIT in a CT insulator: under pressure  $W/\Delta = \text{const.}$  and  $W/U$  increases, triggering the MIT; in contrast upon alloying, the increase of  $W/\Delta$  is responsible for the MIT, whereas  $W/U$  even decreases. This makes  $\text{NiS}_{2-x}\text{Se}_x$  under pressure an ideal system for the study of the MIT in a CT strongly correlated system.

### References

- [1] M. Imada *et al.*, *Rev. Mod. Phys.* **70**, 1039 (1998).
- [2] S. Lupi *et al.*, *J. Opt. Soc. Am. B* **24**, 959 (2007).
- [3] A. Perucchi *et al.*, *Phys. Rev. B* **80**, 073101 (2009).



# ATOMIC AND MOLECULAR PHYSICS







# EXCITATION OF $1S$ AND $3S$ METASTABLE HELIUM ATOMS TO DOUBLY EXCITED STATES

M. Alagia<sup>1,2</sup>, M. Coreno<sup>3</sup>, H. Farrokhpour<sup>4</sup>, P. Franceschi<sup>5</sup>, A. Mihelić<sup>6</sup>, A. Moise<sup>7</sup>, R. Omidyan<sup>4</sup>, K.C. Prince<sup>7</sup>, R. Richter<sup>7</sup>, J. Söderström<sup>8,9</sup>, S. Stranges<sup>10,2</sup>, M. Tabrizchi<sup>4</sup>, M. Žitnik<sup>6</sup>

<sup>1</sup>CNR-ISMN, Roma, Italy

<sup>2</sup>Laboratorio Nazionale TASC INFN-CNR, Trieste, Italy

<sup>3</sup>CNR-IMIP, Roma, Italy

<sup>4</sup>Chemistry Department, Isfahan University of Technology, Isfahan, Iran

<sup>5</sup>Physics Department, University of Trento, Povo, Italy

<sup>6</sup>Jožef Stefan Institute, Ljubljana, Slovenia

<sup>7</sup>Sincrotrone Trieste S.C.p.A., Trieste, Italy

<sup>8</sup>Physics Department, University of Uppsala, Uppsala, Sweden

<sup>9</sup>Synchrotron SOLEIL, Gif-sur-Yvette Cedex, France

<sup>10</sup>Chemistry Department, University of Roma "La Sapienza", Roma, Italy

E-mail: robert.richter@elettra.trieste.it



GASPHASE

Helium is the simplest system where electron correlation can be studied, since it has two electrons. In particular, since their discovery by Madden and Codling [1], doubly excited states below the  $N=2$  ionization threshold have become a prototype system to study electron correlation in atoms. While initially only the photoionization decay channel of the states was considered, more recently it has been shown that the inclusion of the radiative decay is needed to satisfactorily describe the full excitation-decay process [2]. At higher energies above the  $N=2$  threshold several studies have also been performed, including the observation of quantum chaos – a regime where the classical quantum numbers “lose their meaning”, close to the double-ionization potential. To this day, aspects of the helium spectrum are of interest, as a test for very accurate theory.

While in all of the experimental photoionization work to date doubly excited states were investigated using one photon excitation from the ground state, theoretical studies have also investigated the ionization and excitation of metastable helium atoms. These atoms have one electron in each of the  $1s$  and  $2s$  orbitals, and have very long lifetimes because they cannot relax to the ground state by fast processes such as fluorescence. They have been extensively studied, for instance in Bose-Einstein condensates. Transitions from metastable  $1s2s$   $1^3S$  states to the doubly excited states are much closer to one-electron transitions as each of the

doubly excited states can be described as a combination of  $2snp$ ,  $2pns$  and  $2pnd$  configurations. The calculated cross sections for some transitions are orders of magnitude higher than for the corresponding ground state excitations; the relative intensities of the series are also drastically different [3].

We have measured spectra of triplet and singlet metastable helium atoms resonantly photo-excited to doubly excited states [4]. The experiment was carried out at the Gas Phase beamline. Metastable helium atoms were prepared in a skimmed, continuous molecular beam using an electrical discharge. The yield of metastable helium production in our experiments has not been determined, but in similar sources yields of  $10^{-4}$ - $10^{-6}$  have been reported. The extreme dilution of the target, with a gas jet in which between one and a hundred parts per million of the gas constitute the sample of interest, makes the experiment very challenging. Electrons were detected using a commercial hemispherical photoelectron analyzer mounted perpendicular to both the photon and atomic beams, in the direction of the light polarization vector. The first members of three dipole-allowed  $1^3P^o$  series have been observed and their relative photoionization cross sections determined, both in the triplet (from  $1s2s$   $3S^e$ ) and singlet (from  $1s2s$   $1S^e$ ) manifolds. Our results show that, as predicted by theory, intensity ratios are drastically different with respect to transitions from the ground state. For the sin-

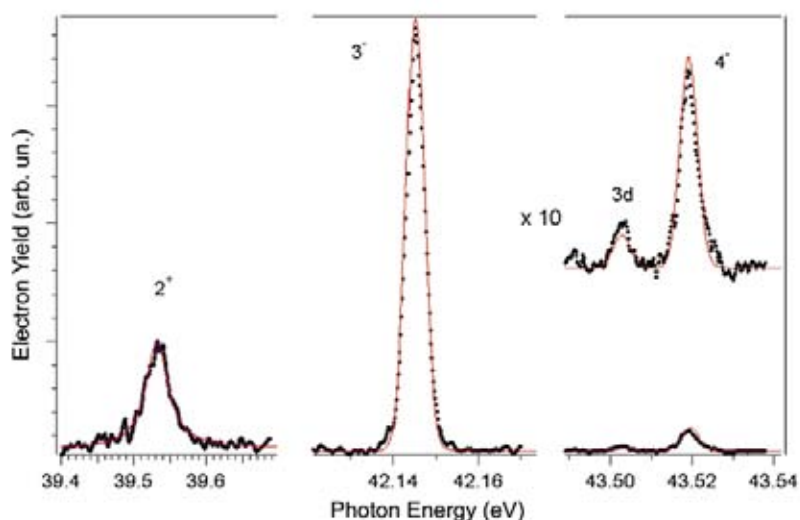


**Figure 1.** Resonant photoionization spectra of  $1S^e$  metastable helium in the region of low-lying  $1P^o$  resonances. Points: experimental data. Full line (red): calculated PI with radiation damping correction. Theory is scaled to the measurement at the  $2^+$  peak.

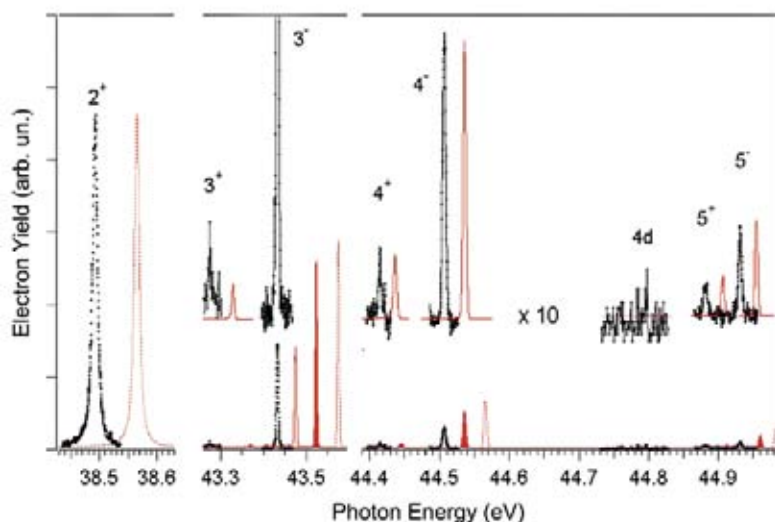


**Figure 2.** Resonant photoionization (PI) spectra of metastable  $3S^e$  helium in the region of low-lying  $3P^o$  resonances. (Points: experimental data; Dashed lines (red): calculated PI without radiation damping. Filled peaks (red): PI with radiation damping correction. Full lines (red): PI with radiation damping and angular correction. Theory is offset in energy for clarity and scaled to experiment at the  $2^+$  peak where both corrections are negligible.

glet states, they are in close agreement with the predictions, when radiation damping is included in the calculations.

In contrast, for the triplet states we find that in addition to the radiation damping also the effect of the spin-orbit interaction on the photoelectron angular distribution (PAD) must be included for a satisfactory description of the ionization process. This has been achieved by replacing the PAD asymmetry parameter with a corrected effective parameter taking into account spin-orbit splitting [4].

## References

- [1] R.P. Madden, K. Codling, *Phys. Rev. Lett.* **10**, 516 (1963).
- [2] E. Sokell *et al.*, *J. Phys. B: Atm. Opt. Mol. Phys.* **29**, L863 (1996); J.-E. Rubensson *et al.*, *Phys. Rev. Lett.* **83**, 947 (1999).
- [3] T.N. Chang, M. Zhen, *Phys. Rev. A* **47** 4849 (1993); B. Zhou *et al.*, *J. Phys. B: At. Mol. Opt. Phys.* **26**, L337 (1993); T.K. Fang, T.N. Chang, *Phys. Rev. A* **56**, 1650 (1997); L. Argenti, R. Moccia, *J. Phys. B: At. Mol. Opt. Phys.* **41**, 035002 (2008).
- [4] M. Alagia *et al.*, *Phys. Rev. Lett.* **102**, 153001 (2009).

# A MYSTERY SOLVED? PHOTOELECTRON SPECTROSCOPIC AND QUANTUM CHEMICAL STUDIES OF THE ION STATES OF $\text{CeCp}_3^+$

R. Coates<sup>1</sup>, M. Coreno<sup>2,3</sup>, M. DeSimone<sup>3</sup>, J.C. Green<sup>4</sup>, N. Kaltsoyannis<sup>1</sup>, A. Kerridge<sup>1</sup>, N. Narband<sup>1</sup>, A. Sella<sup>1</sup>

<sup>1</sup>Chemistry Department, University College London, London, United Kingdom

<sup>2</sup>CNR-IMIP, Roma, Italy

<sup>3</sup>Laboratorio Nazionale TASC INFN-CNR, Trieste, Italy

<sup>4</sup>Chemistry Department, Oxford University, Oxford, United Kingdom

E-mail: n.kaltsoyannis@ucl.ac.uk



GASPHASE

Gas-phase photoelectron spectroscopy (PES) is one of the most direct experimental techniques for obtaining information on the electronic structure of molecules, especially when synchrotron radiation is used for ionization. The technique is particularly valuable in the study of trivalent lanthanide (Ln) compounds, for which the observation of 4f ionization bands requires incident photon energies which maximize the 4f cross section and minimize that of the ligands, e.g. by using photon energies in the region of the delayed maximum in 4f cross sections, or by exciting 4d→4f giant resonances, experiments that are only feasible using synchrotron radiation.

We have recently begun to study a series of volatile organometallic Ln(III) compounds,  $\text{Ln}(\eta^5\text{-C}_5\text{H}_5)_3$  ( $\text{LnCp}_3$ ) and initially focused on  $\text{CeCp}_3$ . Being a 4f<sup>1</sup> system, it was expected to yield a simple photoelectron (PE) spectrum which could be used as a benchmark for the interpretation of more complicated spectra arising from f<sup>n</sup> systems (n>1). Rather surprisingly, our PES data (acquired on the undulator-based gas phase photoemission beamline at Elettra, using the ARPES chamber) showed unequivocally that ionization of the single 4f electron yields not to one but to *two* ion states, separated by a large energy gap (3.2 eV, see bands A and D on Figure 1).

In order to better understand this striking result, we turned to computation in the form of the CASPT2 quantum chemical method, as implemented in the MOLCAS code [1]. This approach is particularly well suited to the study of molecules with electronic structures that are not well represented by a single electronic configuration. We have recently used it to study the iconic Ce organometallic,  $\text{Ce}(\eta^8\text{-C}_8\text{H}_8)_2$  ( $\text{CeCOT}_2$ ), and concluded that

the ground state of this molecule is strongly multiconfigurational, on the basis of the occupations of the state-specific natural orbitals (NOs). NOs are derived from the molecular electron density, and can be used to quantify the multiconfigurational character of electronic states. States with NOs whose occupations differ by more than 0.1 electrons from 0, 1 or 2 are generally considered to be strongly multiconfigurational, and we found that two key NOs of  $\text{CeCOT}_2$  have such occupations [2, 3].

Our calculations on  $\text{CeCp}_3^+$ , the species probed by the PES experiment, reveal that the states responsible for bands A–D in the PE spectrum can be divided into three types. The ground state (which is assigned to band A) is strongly multiconfigurational, with two NOs whose occupations differ from integer by as much as 0.5 electrons. Furthermore, as would be expected for a state giving rise to a PE band whose cross section behaviour is typical of f ionization, this state does not possess a Ce-localized f electron. Then there follows a series of essentially single configurational excited states (assigned to bands B and C) which have a hole in the highest occupied Cp orbitals, and a Ce-localised f electron. Finally, we calculate two excited states of very similar energy, which again do not possess a metal-localised 4f electron and are strongly multiconfigurational, like the ground state. These we assign to band D in the PE spectrum.

What causes the states, giving rise to band D, to be so much higher in energy than the ground state (band A)? Analysis of the excited state NOs indicates significant Ce 5d character, by contrast to the ground state where only minor Ce 5d contributions are found. Thus the excited states responsible for band D are best char-

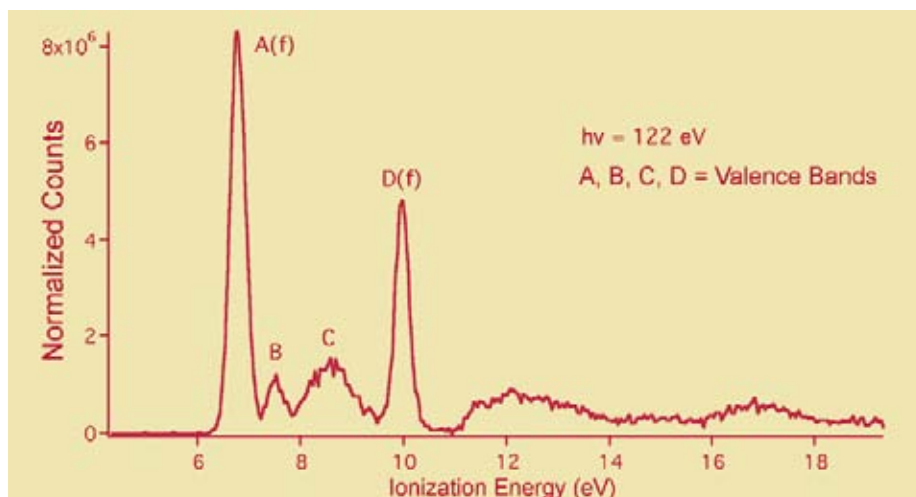


**Figure 1.** The valence photoelectron spectrum  $\text{CeCp}_3$  measured with an incident photon energy ( $h\nu$ ) of 122 eV (in the region anticipated for  $4d \rightarrow 4f$  giant resonances). Taken from reference [4], and reproduced by permission of The Royal Society of Chemistry.

acterised as resulting from ionization of the  $\text{CeCp}_3$  4f-based electron, with simultaneous  $\text{Cp} \rightarrow \text{Ce}$  5d transfer. It is this latter process which is responsible for the energetic separation of the 4f ionization bands in the PE spectrum.

In addition to rationalizing elegantly the PES data, our calculations on  $\text{CeCp}_3$  and  $\text{CeCp}_3^+$  are of wider significance in extending our understanding of the electronic structure of formally Ce(IV) organometallic molecules. We have previously calculated the ground state of  $\text{CeCOT}_2$  to have  $n_f$  close to 1 ( $n_f$  is the number of 4f electrons in the molecule), arising not from f-localised NOs, but rather from the combined f contribution to metal–ring bonding levels and their correlating orbitals [2]. Similarly, the ground state of  $\text{CeCp}_3^+$ , also formally a Ce(IV) state, has  $n_f$  close to 1, even in the absence of a 4f-localised NO. The evidence from  $\text{CeCOT}_2$  and  $\text{CeCp}_3^+$  is somewhat contrary to chemical intuition, suggesting that while both systems are formally Ce(IV), they

retain significant 4f density, a situation consistent with substantial covalency. We are currently extending our study to other formally Ce(IV) molecules, to assess the general applicability of our current conclusions.

This work has been recently published in a themed issue of *Dalton Transactions*, dedicated to the synergy between theory and experiment [4].

#### References

- [1] G. Karlström, R. Lindh, P.-Å. Malmqvist, B.O. Roos, U. Ryde, V. Veryazov, P.O. Widmark, M. Cossi, B. Schimmelpfennig, P. Neogrady, L. Seijo, *Comp. Mat. Sci.* **28**, 222 (2003).
- [2] A. Kerridge, R. Coates, N. Kaltsoyannis, *J. Chem. Phys.* **113**, 2896 (2009).
- [3] A. Kerridge, N. Kaltsoyannis, *J. Chem. Phys.* **113**, 8737 (2009).
- [4] R. Coates, M. Coreno, M. DeSimone, J.C. Green, N. Kaltsoyannis, A. Kerridge, N. Narband, A. Sella, *Dalton Trans.* 5943 (2009).

# DISSOCIATIVE DOUBLE PHOTOIONIZATION OF CO<sub>2</sub> MOLECULES IN THE 34-50 eV ENERGY RANGE

M. Alagia<sup>1</sup>, P. Candori<sup>2</sup>, S. Falcinelli<sup>2</sup>, M. Lavollée<sup>3</sup>, F. Pirani<sup>4</sup>, R. Richter<sup>5</sup>, S. Stranges<sup>6</sup>, F. Vecchiocattivi<sup>2</sup>

<sup>1</sup>CNR-ISMN, Roma, Italy

<sup>2</sup>Civil and Environmental Engineering Department, University of Perugia, Perugia, Italy

<sup>3</sup>CNRS, Université Paris-Sud, Orsay, France

<sup>4</sup>Dipartimento di Chimica, University of Perugia, Perugia, Italy

<sup>5</sup>Sincrotrone Trieste S.C.p.A., Trieste, Italy

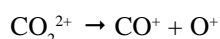
<sup>6</sup>Chemistry Department, University of Rome "La Sapienza", Roma, Italy

E-mail: vecchio@dyn.unipg.it



GASPHASE

The large interest for the double ionization of CO<sub>2</sub> is mainly due to the importance of CO<sub>2</sub> in several atmospheric phenomena of the Earth and of other planets. As an example, the role of the CO<sub>2</sub><sup>2+</sup> dication and its dissociation in the atmosphere of Mars has been recently shown [1]. Like most of molecular dications, CO<sub>2</sub><sup>2+</sup> is partially unstable and, when it is formed just above the double ionization threshold energy, can dissociate to give CO<sup>+</sup> and O<sup>+</sup>. This dissociation reaction has been studied employing a variety of techniques: electron ionization mass spectrometry, photoionization mass spectrometry, and double charge exchange. In some cases, detection coincidence techniques have been also applied [2]. Such studies have shown that the dissociation reaction



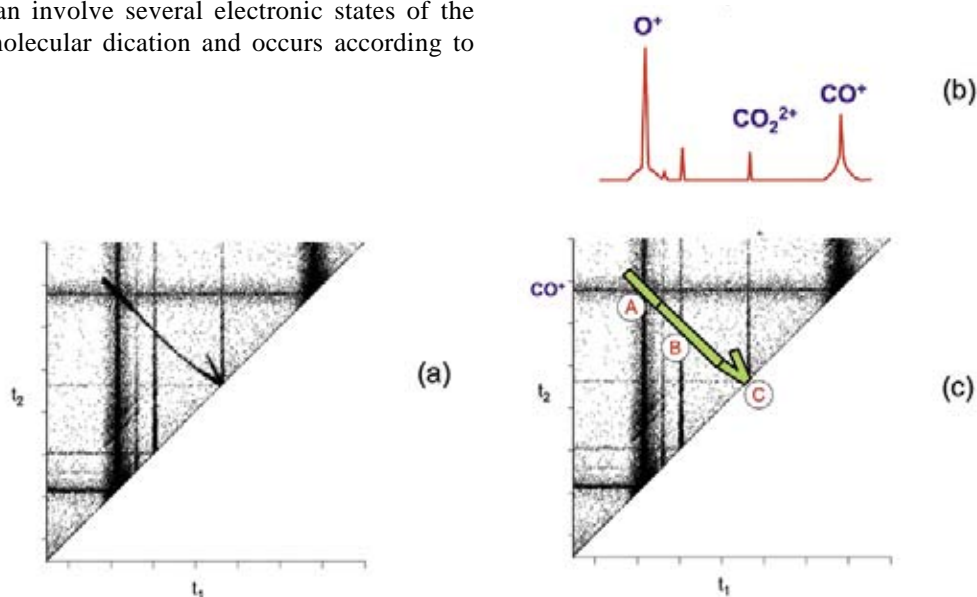
different kinetic schemes: the threshold energy for double ionization of CO<sub>2</sub> is 37.3 eV, very fast dissociations, with lifetime shorter than ~0.05 μs, occur predominantly when the ionization energy is larger than about 41 eV, while between 37.3 and 41 eV also dissociations through possible metastable (CO<sub>2</sub><sup>2+</sup>)<sup>\*</sup> states are involved [2].

We have studied the double photoionization of CO<sub>2</sub>, in the 34-50 eV photon energy range, by synchrotron radiation at Elettra-ARPES end station of the Gasphase beamline. The synchrotron light source, provides the possibility of a continuous energy selection of photons, keeping a high intensity of the signal. The experiment has been performed by detecting electron-ion and electron-ion-ion coincidences. Details of the experimental apparatus and of the used conditions have been reported in a

**Figure 1.**

An example of the spectrum of coincidences for the double photoionization of CO<sub>2</sub> at a photon energy of 44 eV: (a) plot of the delay times  $t_1$  and  $t_2$  of the two dissociation products, CO<sup>+</sup> and O<sup>+</sup>; (b) mass spectrum of the product ions at the same photon energy; (c) plot reported above, where the different areas analysed for obtaining the lifetime of metastable (CO<sub>2</sub><sup>2+</sup>)<sup>\*</sup> dication are indicated.

can involve several electronic states of the molecular dication and occurs according to



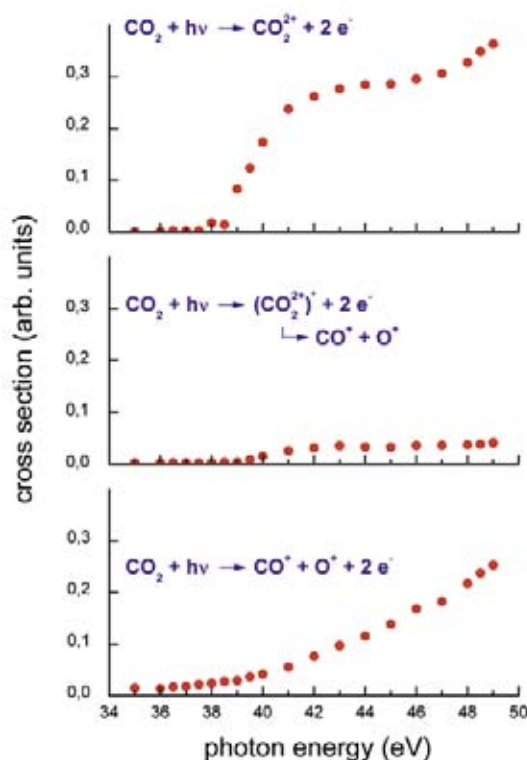


**Figure 2.** Photon energy dependence of the cross section for the three photoionization processes observed in the 34-50 eV energy range.

recent paper [3]. The results obtained allow us to assess the photon energy dependence of the cross sections for the three processes possible in the investigated energy range: i) the molecular dication  $\text{CO}_2^{2+}$  formation, ii) the fast dissociation, and iii) the dissociation through the formation of a metastable  $(\text{CO}_2^{2+})^*$  state. An analysis of the coincidence plots led also to the determination of the lifetimes for the metastable state.

Figure 1 shows a typical coincidence plot, obtained with photons of 44 eV, where the delay times,  $t_1$  and  $t_2$ , of product ions are reported, showing the characteristic features for a dissociative double photoionization [2,3]. The analysis of such spectra gives the cross section energy dependence reported in Figure 2.

Combining the results of the present experiment with those reported previously by other authors [2] it is possible to better assess some of the characteristics of the double photoionization of  $\text{CO}_2$ .

- The present results confirm that the molecular dication,  $\text{CO}_2^{2+}$ , is produced with a threshold energy of 37.3 eV, in good agreement with a previous determination [2].

- The dissociative double photoionization, namely those events leading to  $\text{CO}^+$  and  $\text{O}^+$  in a time shorter than  $\sim 0.05 \mu\text{s}$ , exhibits a cross section that increases with the photon energy,

becoming, at about 50 eV, comparable with that for  $\text{CO}_2^{2+}$  formation.

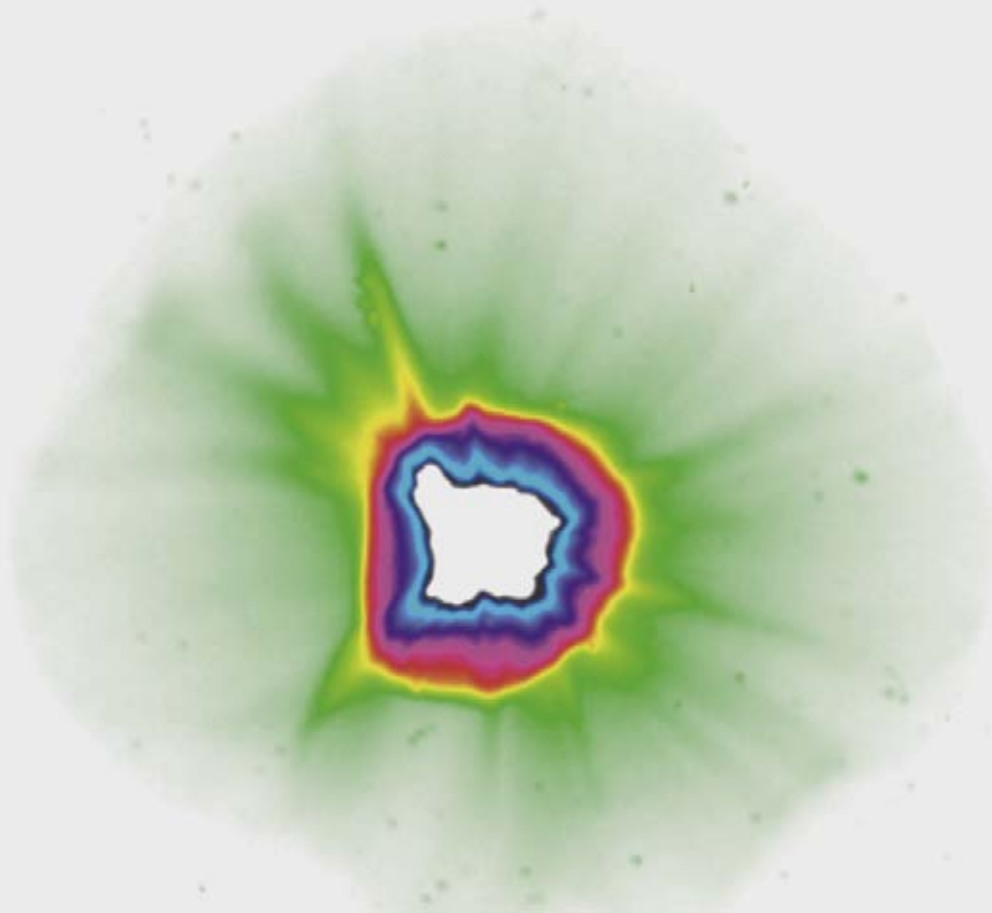
- This process appears with an energy threshold lower than that exhibited by the molecular dication formation, confirming recent results [2]. This observation could be an indication of the presence, below the threshold, of a possible indirect ionization process, where an excited molecular monocation  $(\text{CO}_2^+)^*$  is formed and then dissociates with the formation of an autoionizing oxygen atom. Finally, the cross section for the dissociation through the  $(\text{CO}_2^+)^*$  metastable dication show a very low cross section in all the investigated energy range.

## References

- [1] C. Nicolas, C. Alcaraz, R. Thissen, J. Zabka, O. Dutuit, *Planetary and Space Science* **50**, 877 (2001); O. Witasse, O. Dutuit, J. Liliensten, R. Thissen, J. Zabka, C. Alcaraz, P.L. Blelly, S.W. Bougher, S. Engel, L.H. Andersen, K. Seiersen, *Geophys. Res. Lett.*, **29**, 1263 (2001).
- [2] A.E. Slattery, T.A. Field, M. Ahmad, R.I. Hall, J. Lambourne, F. Penent, P. Lablanquie, J.H.D. Eland, *J. Chem. Phys.* **122**, 084317 (2005).
- [3] M. Alagia, P. Candori, S. Falcinelli, M. Lavollée, F. Pirani, R. Richter, S. Stranges, F. Vecchiocattivi, *J. Phys. Chem A* to be published, DOI: 10.1021/jp9048988.



**FREE ELECTRON LASER AND OTHER  
COHERENT LIGHT SOURCES**





# RECENT UPGRADES OF ELETTRA AND PERSPECTIVES FOR FERMI@ELETTRA

## New performances of the accelerator facilities at the Elettra laboratory, from synchrotron radiation to free electron laser

*An interview with Emanuel Karantzoulis and Stephen Milton*

We have asked Emanuel Karantzoulis and Stephen Milton to illustrate how the accelerator facilities of Elettra have been evolving in the last year. In the following you will find their views on the Elettra synchrotron full energy injection, the machine experiments of top-up injection, the construction and the early commissioning phase of FERMI@Elettra.

Emanuel Karantzoulis has worked in various branches of physics (high-energy, non-linear and accelerator physics). He has mainly worked at DESY, Hamburg, Germany and with the HERA project on proton machines. He then moved to Sincrotrone Trieste in Italy and was involved in the design, realisation and commissioning of the synchrotron. He is the head of the Elettra storage ring complex and Coordinator of the Elettra Cluster.

At the same time he is also involved in the FERMI@Elettra project.

Stephen Val Milton is the Director of the FERMI@Elettra. From 1998 until 2002 he led the APS free-electron laser project, LEUTL. This project was the first to achieve full saturation of a self-amplified spontaneous emission free-electron laser in the visible to ultraviolet wavelength range. Following the completion of the LEUTL project he took over as Director of the ANL component of the Linac Coherent Light Source (LCLS) where he was responsible for the delivery of the 130-m long undulator system of the LCLS at the Stanford Linear Accelerator Center.

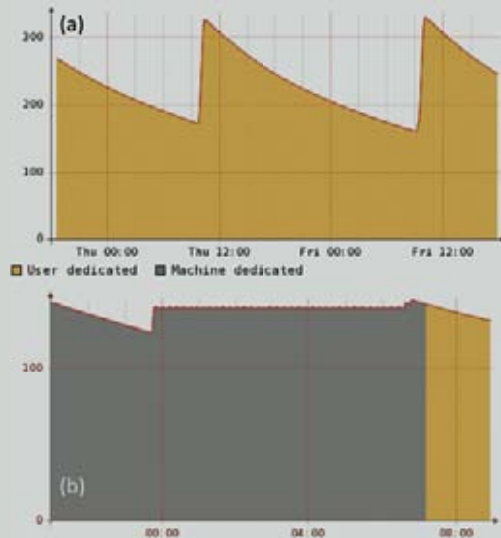


**Emanuel, in 2008 the Elettra synchrotron light source was upgraded with the so-called “full energy injection system” that allows the electron beam to be injected in the storage ring directly at any user required energy, with great advantages for the facility performance. Can you please give us an update about the degree of availability of the Elettra synchrotron light source at the present time?**

The present availability of Elettra has increased with respect to the past. Before the upgrade the daily injection was about 45 minutes long. Currently, the operation of the full energy injector takes about 15 minutes to refill the electron current in the storage ring. This improvement is even more important for beam loss events. In the past, after a beam loss, about an hour and a half was needed to refill the storage ring and get back to operation while now only 15 minutes are sufficient to return to a fully operational status.

The commissioning of the booster power supplies and the pre-injector, started in 2008 as the final part of the full commissioning, is now finished and in 2009 the machine is already showing further improvements in terms of stability and functionality. The final goal for 2009 is to reach a total availability of more than 95%.

**The top-up operational mode is one of the main goals of Elettra for the near future. Can you briefly describe how it works? What machine physics studies have already been carried on and what is next to come? Last but not least, which are the expected main advantages for the user community?**



As I mentioned, the injection procedure at the moment takes about 15 minutes every day to fully restore the electron current in the storage ring, thus interrupting the experimental activities of every beamline in this period. Moreover, after the injection the increase in the electron current can affect the beam stability and reproducibility.

Top-up (or fill-up) is an operating mode whereby the stored beam intensity is kept constant to about 0.5% or even better. To achieve this, electrons are injected in predefined time periods that correspond to the decay time of the beam. The operation lasts only 5-10 s and after topping up the injection system is switched off. It is important to underline that the procedure is carried on during the normal experimental activities with

beamline shutters open and insertion devices closed. Since the shutters remain open the users have practically stable beam intensity, meaning also stable thermal load on the beamline optics. The disturbance from the injection system when optimized does not seem to give any problem, but in any case a gate signal will be provided to the beamlines signaling the start and end of the injection. Of course many interlock/radiation protection systems are involved in order to guarantee the safety standards.

All the necessary machine physics studies have been performed including dynamic aperture measurements with all insertion devices closed, injection system optimization settings and injection efficiency measurements. We have achieved top-up at both Elettra operating energies (2.0 and 2.4 GeV), and top-up runs for a maximum of 12 hours were performed. During the tests the machine was set in the top-up mode with all the beamline shutters closed. The graphs show the intensity during “normal” runs for users (Figure 1(a)) and during top-up (Figure 1(b)) tests. Though plotted on different time scales, the comparison of the two graphs shows how in the top-up mode the electron beam current can be kept constant over several hours.

**The full energy injection and the top-up operation are establishing Elettra as a renewed, updated synchrotron in the European scenario of 3<sup>rd</sup> generation light sources. Are there further upgrades in the future plans?**

We are thinking about several upgrades, especially to exploit the higher stability and virtually infinite lifetime of the beam. Already two beamlines (FEL/Nanospectroscopy and SuperEsca/Esca Microscopy) have asked for new low-gap undulator chambers in order to increase the photon flux at higher energies (e.g. around 1 keV for SuperEsca beamline) preserving the same total energy range. I expect a gradual reduction of the undulator gap of almost all the beamlines in the future. At the same time we are trying to air-cool the hot points of the storage ring in order to increase the intensity, especially at 2.4 GeV where we aim to operate at 180 mA. To reach current values above 180 mA a new RF-upgrade will be necessary. We are also thinking to activate the third harmonic cavity so that its effects will be valid at any current. There are also several studies targeting a possible decrease of the machine coupling to 0.5%. This quantity is simply the ratio between the vertical and horizontal emittance of the electron beam. The current

value is 1%, and lowering it to 0.5% would increase the brilliance, and consequently the total photon flux delivered to the beamlines. Finally we are working on a way to fit an 8<sup>th</sup> corrector in the achromat in order to let the bending magnet beamlines control both the position and the angle of the source, thus decoupling them from undulator beamlines.

**FERMI@Elettra FEL is the new ultra-coherent light source of the Elettra laboratory. Stephen, Could you please give us an overview of the project?**

The FERMI@Elettra project was conceived as a user facility designed to deliver laser-like, ultrashort pulses to a variety of user end stations for a wide array of experimental programs. The project consists of completely renovating and upgrading the previous linac so that it can supply the necessary high-brightness electron bunches at the correct energy to the long undulator chains. There it interacts with a seed pulse that converts the electron bunch into a number of microbunches that subsequently radiate at the defined resonant wavelength and undergo further microbunching. The resultant output is an intense laser-like pulse of light at wavelengths ranging from 100 nm to 4 nm with harmonics extending down to the 1 nm range. This light is then guided via the photon transport and beamline system to the experimental stations.

**Which are the unique features of FERMI@Elettra, as a user facility light source? What will be the new experimental possibilities with such a source?**

FERMI's operating range spans the vacuum ultraviolet to soft x-rays (100 nm to 3 nm), and the seeded operation promises to provide both transverse and longitudinally coherent pulses with durations less than 100 femtoseconds. The use of APPLE II-type undulators will allow for variable polarization, from completely linear both horizontal and vertical to circular with either helicity. The seeded nature and full polarization control will set FERMI aside as a truly unique light source in this photon energy range.



These features enable many experimental programs otherwise not possible via other sources. What excites people most is the combination of the extremely short pulses, in the range from 10 to 100 femtoseconds, the ultrahigh peak brightness of the pulses, and the relatively high photon energy. This combination allows one to not only look at a process in a static manner, but permits the measurement of the dynamics, and it's that additional dimension of time that makes things very interesting. People are also excited about the high intensity of the pulses that allows single shot measurements at a brightness sufficient to observe the specimen under study. This ability to do single shot experiments opens up another branch of studies. And finally the combination of transverse and longitudinal coherence enables other experiments, some of which are quite novel such as the ability to form transient gratings for spectroscopic experiments.

**Could you please tell us about the status of the project? Which are the main deadlines that have been achieved to date? And what are the main goals for the next year?**

Presently we have entered the initial stages of commissioning the linac system, a major milestone, while simultaneously installing the remaining parts of the linac. Civil construction also continues. The new undulator hall and experimental hall are quickly being formed and the building that houses the new mechanical and electrical services is quickly being constructed. By the end of next year all buildings will be complete, the linac and undulator system for the first FEL chain will be complete, the initial beamline system leading to the first experimental station will be operational, and the first experimental station will be installed and ready for beam. The major goal is to send the high quality electron beam through the undulator chain and generate high intensity FEL light for the first measurements in the first experimental station.

# SELF-INDUCED HARMONIC GENERATION IN A STORAGE-RING FREE ELECTRON LASER

G. De Ninno<sup>1,2</sup>, E. Allaria<sup>1</sup>, M. Coreno<sup>1,3</sup>, F. Curbis<sup>4</sup>, M.B. Danailov<sup>1</sup>, M. Ferianis<sup>1</sup>, E. Karantzoulis<sup>1</sup>, V.N. Litvinenko<sup>5</sup>, C. Spezzani<sup>1</sup>, M. Trovò<sup>1</sup>

<sup>1</sup>Sincrotrone Trieste S.C.p.A., Trieste, Italy

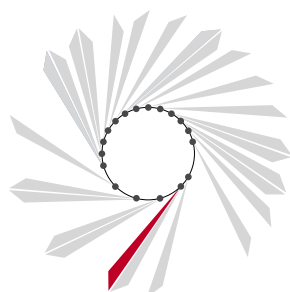
<sup>2</sup>Physics Department, University of Nova Gorica, Slovenia

<sup>3</sup>CNR-IMIP, Roma, Italy

<sup>4</sup>Experimental Physics Institute, University of Hamburg, Hamburg, Germany

<sup>5</sup>Brookhaven National Laboratory, Upton, USA

E-mail: giovanni.deninno@elettra.trieste.it



SR FEL

Coherent harmonic generation (CHG) using a “seeded” relativistic electron beam represents a valuable alternative to self-amplified spontaneous emission (SASE) for obtaining intense, tunable, short-pulse radiation in the wavelength region from the deep ultraviolet down to x-rays. The process leading to CHG is based on the frequency up-conversion of a high power laser (the seed) through interaction with a relativistic electron beam within an optical klystron, i.e. two undulators separated by a dispersive section, the first undulator being referred to as the modulator and the second as the radiator.

We have shown [1] that efficient CHG can be obtained from an optical klystron installed in a storage ring (SR), and used as the interaction region for an oscillator free electron laser (FEL). In this configuration, schematically shown in Figure 1, the light emitted by the electrons when passing through the undulators is stored in an optical cavity and amplified during successive interactions with the particle beam until lasing is achieved. This intra-cavity laser signal can provide the seed necessary to initiate CHG.

In fact, CHG relies on the production of significant electron bunching at the radiator entrance. In a SR FEL, bunching is produced in the modulator and in the dispersive section by the interaction of the electron beam with the fundamental field component, which is stored and amplified in the optical cavity.

Coherent emission in the wavelength range between 260 and 36.5 nm has been observed at the Duke and Elettra SR FEL's [1]. Results indicate that the temporal structure of the harmonic radiation is naturally characterized by very short spikes (hundreds of femtoseconds), in which the majority of the emitted energy is concentrated.

The energy of the fundamental and harmonic light pulses was measured both at Duke and at Elettra. In the Duke case, using holed cavity mirrors at 260 nm, and pulse energy of 3 mJ in the fundamental, produced several nJ extracted energy at 86.1 nm (third harmonic) and a fraction of nJ at 51.5 nm (fifth harmonic) and 36.5 nm (seventh harmonic). Experiments at Elettra utilized mirrors at 660 and 450 nm, partially transmitting at 220 and 150 nm (respectively), producing measured micro-

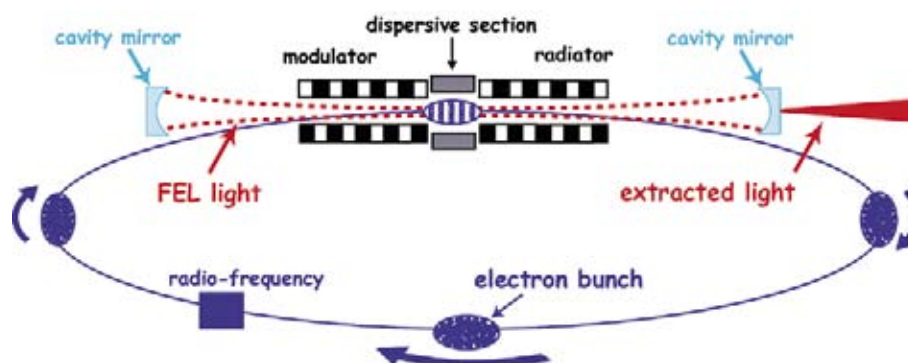


**Figure 1.** Schematic layout of storage ring FEL. The radio-frequency cavity is used to provide electrons with the energy they lose during one turn of the ring.

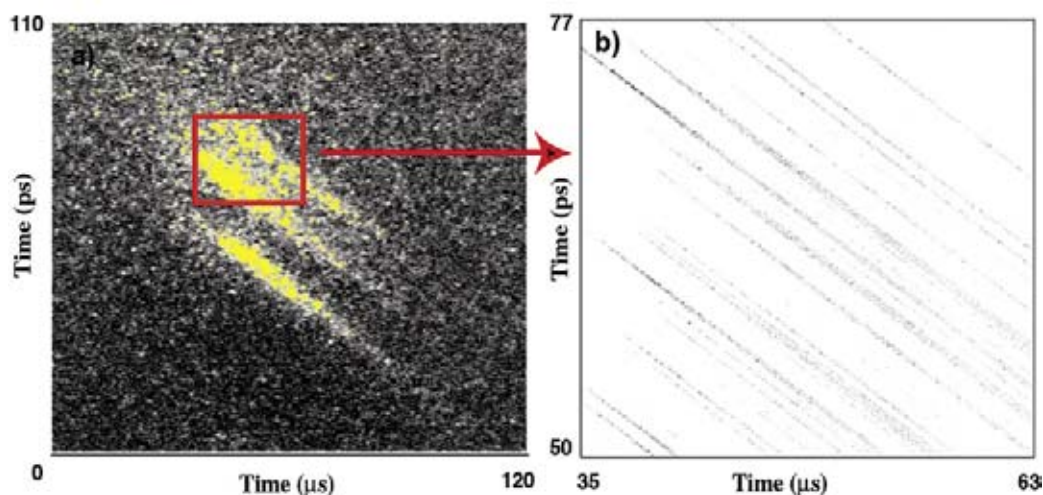


**Figure 2.** (a) Streak camera image (from Duke) of the third harmonic at 233 nm showing micropulses. The slope in the pulse evolution is due to a small detuning of the electron and radiation round-trip times. (b) Numerical streak image produced using GINGER, with the same temporal ranges as in (a). Both experimental and numerical results have been obtained using the set of parameters reported in [1].

pulse energies of the same order of those generated at Duke, i.e. a few mJ (intra-cavity) at the fundamental wavelength and few nJ at the third harmonic. FEL radiation arises from spontaneous emission by the electrons. Because particle density inside the bunch is inhomogeneous, the emitted micropulse is composed of spikes having various peak powers. The typical duration of a single spike is approximately equal to the “slippage” distance along the optical klystron, due to a process analogous to a SASE system. Spiky micropulses at the fundamental wavelength are stored in the optical cavity and amplified during successive interactions with the electron beam. As a consequence, the majority of the power at the fundamental wavelength is concentrated in a few intense isolated spikes, which will be reflected in the temporal struc-

ture of the harmonic micro-pulses. This prediction is confirmed by experiments, see Figure 2. The picture gives a clear indication of the predicted spiky structure in harmonic pulses, in this case with a measured duration of about 2 ps (RMS). However, this is close to the instrument resolution and underlying finer structure could not be resolved. Simulations at higher temporal resolution, performed using the numerical code GINGER [2], confirm the existence of a much finer structure seen in Figure 2(b), i.e. spikes on the order of a few hundreds of fs.

### References

- [1] G. De Ninno *et al.*, *Phys. Rev. Lett.* **100**, 104801 (2008).
- [2] W. Fawley, *Report No. LBNL-49625*, LBL, 2002.

# EXPERIMENTS FOR CHARACTERIZING THE HARMONIC EMISSION IN A FREE ELECTRON LASER

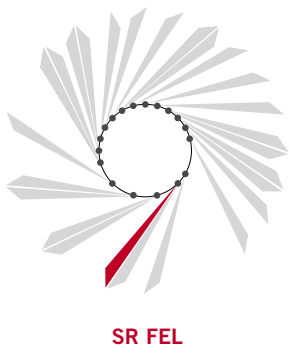
E. Allaria<sup>1</sup>, F. Curbis<sup>1,3</sup>, M. Danailov<sup>1</sup>, G. De Ninno<sup>1,2</sup>, C. Spezzani<sup>1</sup>, M. Trovò<sup>1</sup>

<sup>1</sup>Sincrotrone Trieste S.C.p.A., Trieste, Italy

<sup>2</sup>Physics Department, University of Nova Gorica, Slovenia

<sup>3</sup>Experimental Physics Institute, University of Hamburg, Hamburg, Germany

E-mail: [enrico.allaria@elettra.trieste.it](mailto:enrico.allaria@elettra.trieste.it)



Free Electron Lasers (FELs) are widely considered as the possible light source that may allow a big step forward in the investigation of the matter due to their capability of producing short and tunable pulses of very high peak brightness in a wide spectral range, ranging from the far infrared to x-rays [1]. FELs are also able to generate pulses with extremely large average power. A problem that has been recently investigated, both theoretically and numerically, is the harmonic emission. The capability of FELs to produce strong and coherent harmonic emission is considered both a desired and undesired phenomenon, depending on the experiment for which the FEL is designed.

A major attention has been recently dedicated to the possibility for high gain FELs to produce coherent harmonic emission with helical undulators. The discussion within the FEL community has been stimulated by a work [2] that, in disagreement with the standard theory for undulator emission, predicted a large amount of emission on harmonics of the resonant FEL wavelength (both odd and even). More recently, theoretical results

showed instead that for helical undulators the harmonic emission is concentrated out of axis.

In the present study [3], we provide an experimental characterization of the harmonic emission in FELs, both in planar and helical undulators.

The experiment [3] has been performed on the FEL beamline of the Elettra storage ring, whose layout is reported in Figure 1. The beamline relies on an optical klystron, made of two independent APPLEII undulators with a variable dispersive section in-between. The experimental conditions required for investigating the FEL behaviour in the high gain regime has been obtained by initializing the FEL process with an external powerful laser (seeding).

The setup is optimized in order to ensure the best spatial and temporal overlap between consecutive laser pulses and electron bunches inside the first undulator, which is tuned to be in resonance with the seed laser. The high power of the used laser (~5 GW) induces an energy modulation on electrons with the period of the laser wave-

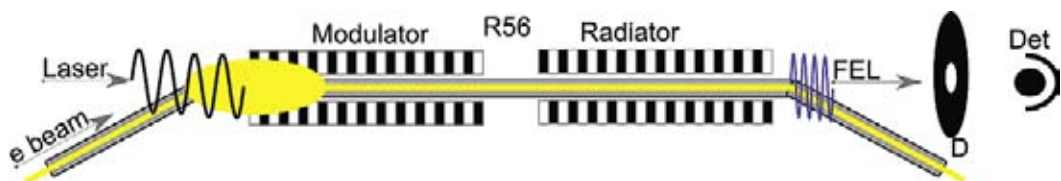


**Figure 1.** Experimental setup. A powerful laser interacts with the electron bunch (e) within the first undulator (modulator) and induces an energy modulation which is then converted into bunching by a dispersive section (R56). The bunched electrons emit coherently in the second undulator (radiator) at the resonant wavelength and at the harmonics of the latter. The emitted light passes through a diaphragm (D) and is transported into a diagnostic area, where temporal (PMT) and spectral (CCD) analyses are performed.

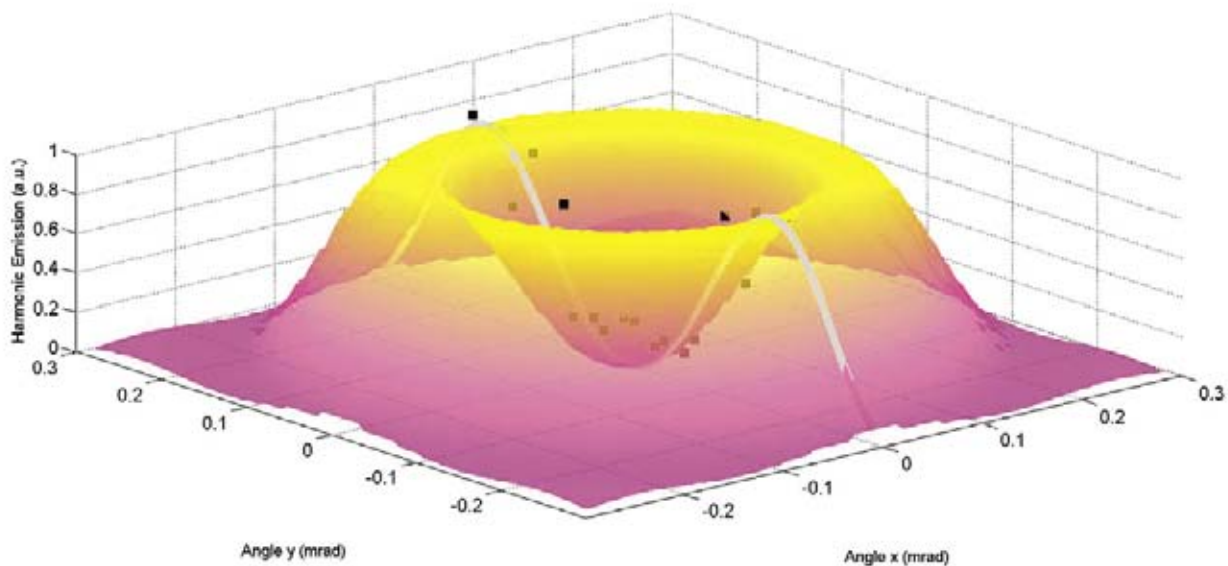


**Figure 2.** Angular distribution of second harmonic emission in a single-pass FEL with helical undulators, as predicted by theory [4]. The experimental data (black squares) agree well with theory.

length. Such a modulation is typically a factor five larger than the initial uncorrelated energy spread. At the exit of the dispersive section, the energy modulation is converted into density modulation. The imposed density modulation is responsible of the coherent emission on the second undulator, both at the resonant and at the harmonics wavelengths.

Our measurements [3] showed that for a FEL, similarly to synchrotron radiation, the second harmonic in planar undulators is virtually zero on axis, and only a very small signal can be detected, which is originated by the contamination coming from out-of-axis radiation. The same behaviour has been observed for both the second and the third harmonic emission from FEL with helical undulator, providing an experimental validation of recent theoretical results [3,4]. The case of the second harmonic in helical

undulator configuration is shown in Figure 2. The radiation angular distribution has been measured by moving the diaphragm placed at the exit of the second undulator. The Elettra storage ring FEL has been used for a detailed experimental characterization of the process of coherent harmonic generation in single-pass free electron lasers providing a useful experimental confirmation of some recent theoretical results about the harmonic emission process in FELs.

#### References

- [1] P. Emma, *Proceedings PAC09*, (2009) *in press*.
- [2] H. Freund *et al.*, *Phys. Rev. Lett.* **94**, 074802 (2005).
- [3] E. Allaria *et al.*, *Phys. Rev. Lett.* **100**, 174801 (2008).
- [4] G. Geloni *et al.*, *Nucl. Instrum. Meth. A* **581**, 856 (2007).

# GENERATION OF ULTRA-SHORT PHOTON PULSES USING ELECTRON STORAGE RINGS: A NEW BRIGHT SOURCE OF COHERENT VUV LIGHT

G. De Ninno<sup>1,2</sup>, E. Allaria<sup>1</sup>, M. Coreno<sup>1,3</sup>, F. Curbis<sup>4</sup>, M.B. Danailov<sup>1</sup>, E. Karantzoulis<sup>1</sup>, A. Locatelli<sup>1</sup>, C. Spezzani<sup>1</sup>, M. Trovò<sup>1</sup>

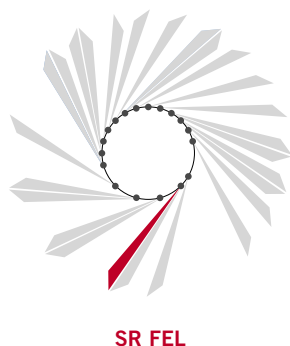
<sup>1</sup>Sincrotrone Trieste S.C.p.A., Trieste, Italy

<sup>2</sup>Physics University, University of Nova Gorica, Slovenia

<sup>3</sup>CNR-IMIP, Roma, Italy

<sup>4</sup>Experimental Physics Institute, University of Hamburg, Hamburg, Germany

E-mail: giovanni.deninno@elettra.trieste.it



Over the last few years, a strong demand has emerged for a source of radiation in the VUV spectral range with high brilliance, close-to-full coherence, variable polarization, bandwidth approaching the transform limit, and stable temporal structure in the femtosecond time scale [1]. Nowadays, the possibility to realize a source with all the above mentioned characteristics relies principally on single-pass free electron lasers (FELs). FELs can be operated in several different schemes. The most promising ones are based on the self-amplification of the electron beam spontaneous emission, and on the generation of coherent harmonics from an input signal provided, e.g. by a conventional laser (seeding). In the standard seeded scheme, generation of coherent harmonics (CHG) is obtained by coupling the input signal with the electron bunches extracted from a linear accelerator (linac). As an alternative to single-pass linac-based devices, electrons can be provided by a storage ring (SR), as shown in Figure 1. We have

recently demonstrated [2] the possibility of using SR CHG to produce powerful and stable VUV radiation. Taking advantage of the FEL undulator system installed on the Elettra SR [3], we have generated ultrashort (close to 100 fs FWHM) coherent UV pulses at 132 nm (sixth harmonic of a Ti:Sapphire laser), with fully adjustable polarization, relatively high repetition rate (1 kHz) and bandwidth close to the transform limit. The pulse train is very stable and the peak power is orders of magnitude above that of standard synchrotron radiation. The source layout is shown in Figure 1. The region of seed-electron interaction is composed of two APPLEII identical undulators (10 cm-period, 2 m-long), separated by a magnetic chicane. APPLEII undulators allow to freely determine the polarization of the emitted light. The seed laser is a Ti:Sapphire, having a fundamental wavelength of 794 nm, a maximum repetition rate of 1 kHz and a maximum energy per pulse of 2.5 mJ. A nonlinear optical

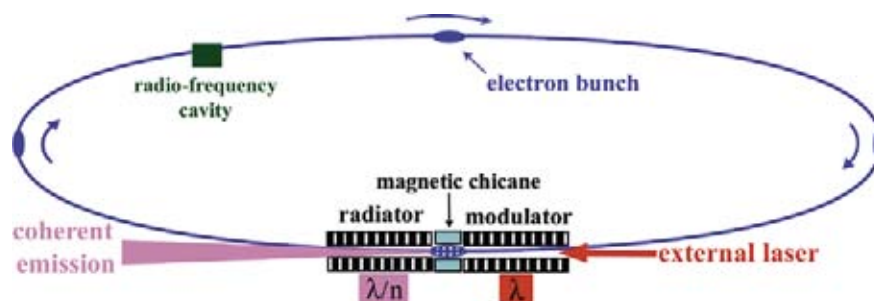


**Figure 1.** Schematic layout of the CHG setup implemented on the Elettra SR. The SR is filled with a relativistic electron bunch, which interacts in the modulator with an external (Ti:Sapphire) laser of wavelength  $\lambda$ . In the magnetic chicane, electrons are subdivided in micro-bunches separated by  $\lambda$ . Finally, in the radiator, they emit coherently at  $\lambda/n$ ,  $n$  being an integer number. The radio-frequency cavity is used to provide electrons with the energy they lose during one turn of the ring.



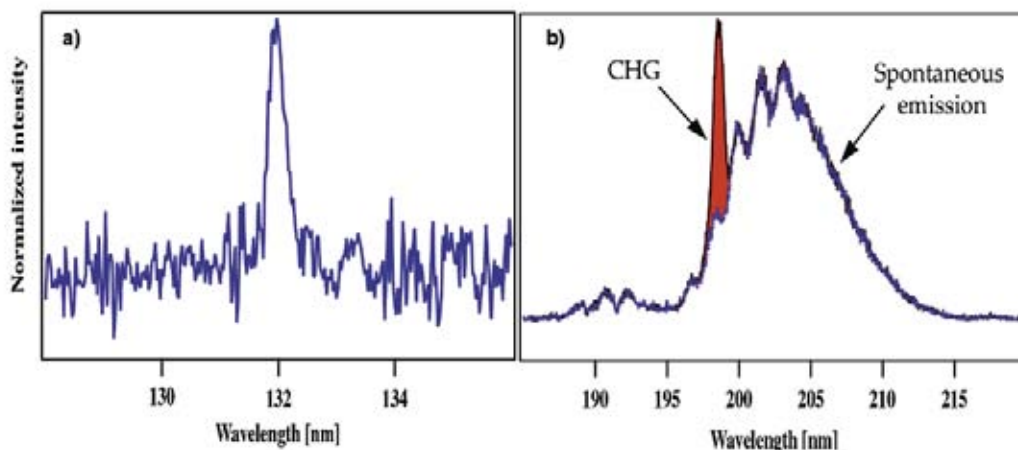


**Figure 2.** (a) Spectrum of the coherent emission at 132 nm (linear polarization). The integration time is 1 ms; the spectrum is obtained after subtraction of the background due to spontaneous emission. (b) Spectrum of spontaneous and coherent emission for the case in which the radiator is tuned at 203 nm, i.e. slightly mismatched with respect to the second harmonic of the seed laser (198.5 nm).

crystal was used to generate second harmonic pulses with energy of up to 800  $\mu\text{J}$  and duration of 120 fs FWHM, so that CHG was seeded at 397 nm. The process leading to CHG using the Elettra SR is described in [2] and references therein. The spectrum of the coherent signal at 132 nm (radiator for linear polarization) is shown in Figure 2(a), after subtraction of the radiator spontaneous emission. A direct measurement of the spectral width gives a bandwidth,  $\Delta\lambda$ , of about 0.33 nm FWHM. Assuming Gaussian temporal and spectral profiles, at the transform limit one would get  $\Delta t = 0.44 \cdot \lambda^2 / (c \cdot \Delta\lambda) \approx 77$  fs FWHM, which is close to the expected value for the harmonic pulse duration. Data shown in Figure 2(b) demonstrate the good spectral stability of the source. In this case, the radiator is tuned at  $\lambda_0 = 203$  nm, i.e. is slightly mismatched with respect to  $\lambda_2 = 198.5$  nm, which is the second harmonic of the seed laser. As

it can be seen, while the part of the spectrum generated by spontaneous emission is centered around the “detuned” wavelength (i.e. 203 nm), the position of the coherent signal is “locked” to the second harmonic of the seed laser. Potential applications of the source we have developed range from atomic and molecular physics to the study of electronic excitations on surfaces, interfaces and nanostructures.

### References

- [1] R. Neutze *et al.*, *Nature* **406**, 757 (2000); W.A. Barletta, H. Winck, *Nucl. Instr. and Meth. A* **500**, 1 (2003); N. Gedik *et al.*, *Science* **316**, 425 (2007); A. Cavalieri, *Nature* **448**, 651 (2007).
- [2] G. De Ninno *et al.*, *Phys. Rev. Lett.* **101**, 053902 (2008).
- [3] G. De Ninno *et al.*, *Nucl. Instr. and Meth. A* **507**, 274 (2003).

# IMPACT OF AN INITIAL ENERGY CHIRP AND AN INITIAL ENERGY CURVATURE ON A SEEDED FREE ELECTRON LASER

A.A. Lutman<sup>1</sup>, G.Penco<sup>2</sup>, P.Craievich<sup>2</sup>, J.Wu<sup>3</sup>

<sup>1</sup>Electrotechnic and Electronic Engineering Department, University of Trieste, Trieste, Italy

<sup>2</sup>Sincrotrone Trieste S.C.p.A., Trieste, Italy

<sup>3</sup>Stanford Linear Accelerator Center, Stanford University, Stanford, USA

E-mail: [alberto.lutman@elettra.trieste.it](mailto:alberto.lutman@elettra.trieste.it)

An x-ray Free Electron Laser (FEL) calls for a high quality electron bunch with a low emittance, a high peak current and a high energy. During the acceleration, bunch compression and transportation, the electron bunch is subjected to the radio frequency curvature and wakefield effects. Thus, the energy profile of the electron bunch coming into the undulator can have a temporal structure. This structure can impact the FEL process in the undulator. The effects of the electron bunch initial energy chirp on the FEL performance and the possible short-pulse generation have been studied for self-amplified spontaneous emission (SASE) FEL [1], and a seeded FEL as well [2]. In the latter case, the situation is complicated by the interplay of the electron energy chirp and a possible frequency chirp in the seed. In our work, we included the effect from a possible energy curvature in the electron bunch when it enters the undulator. To this aim, we derived an analytical form for the seeded FEL Green's function in the case of both linear energy chirp and curvature [3], then considering a seed laser with a Gaussian envelope profile we derived a closed form for the electric field envelope of the radiation [4]. This analytical form, besides describing the envelope as function of the longitudinal coordinate, can also be used to evaluate properties of the FEL light such as the central frequency shift and the frequency chirp. Finally we proposed a condition on the frequency shift and chirp on the seed laser to achieve short FEL pulses for a given electron bunch initial condition.

The Green function in [3] is derived within the one dimensional Vlasov-Maxwell framework, considering a negligible uncorrelated energy spread and characterizing the linear energy chirp with  $\alpha$  and the quadratic curvature with  $\beta$ . Moreover the function depends on the longitudinal coordinate  $z$ , and on two

phase coordinates  $\xi$  and  $s$  separately, being the amplifier system time variant. Expressions for rms time length  $\sigma t$  and bandwidth  $\sigma\omega$  of the Green function are given explicitly. The electric field envelope of the radiation can be evaluated performing a convolution with the seed laser expression at the undulator entrance. As long as the convolution is done numerically, any expression for the seed can be chosen. If the seed laser is a fundamental Gaussian mode with a linear frequency chirp on it, the expression of the FEL can be determined analytically and is given explicitly in [4]. A time jitter can be put on the seed, in order have it interacting with different parts of the electron bunch. The impact of the chirp and curvature on the FEL radiation strongly depends on the ratio between the length of the Green function and the length of the seed laser. To this aim the parameter  $K$  has been introduced to distinguish between three different regimes. For seeds much longer than the Green function, the main effect of the linear chirp on the electrons is a shift of the central frequency of the FEL pulse and it gives only a small quadratic contribution to the frequency chirp. The effect of the curvature on the energies is a strong frequency chirp on the FEL pulse. In this case the intrinsic chirp of the pulse is almost negligible. Decreasing the length of the seed, the linear chirp shifts the central frequency of the pulse, but also has an asymmetric effect on the frequency chirp of the pulse as shown in Figure 1, the curvature is translated into frequency chirp. In the case of the shortest seeds, the FEL pulse is more similar to the Green function itself, and the curvature on the electrons has a very small effect. In this case we have a strong intrinsic chirp and the linear chirp on the electrons gives a strong frequency chirp on the pulse which is linear with the  $\alpha$  parameter. The

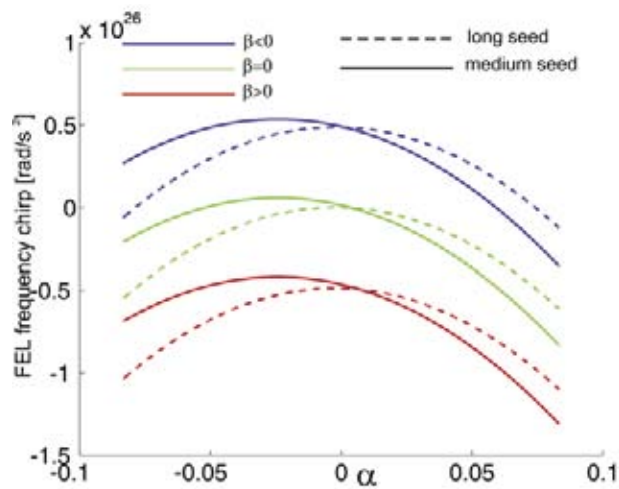


**Figure 1.** Frequency chirp of the FEL pulse as function of the adimensional chirp parameter  $\alpha$ . Curves are  $\beta$  parameterized,  $\beta < 0$  (blue),  $\beta = 0$  (green),  $\beta > 0$  (red). Long seed (dashed lines), medium seed (solid lines).

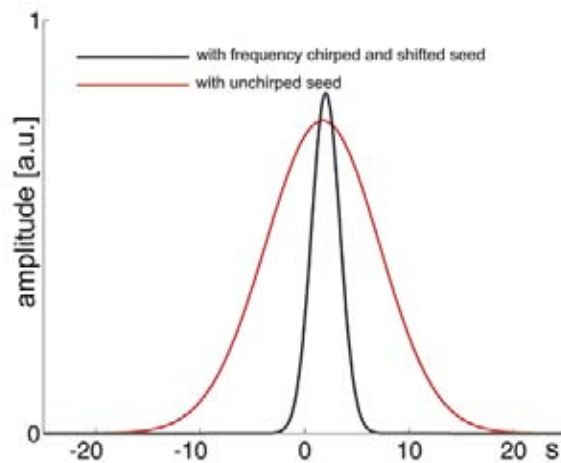


**Figure 2.** Comparison between the FEL amplitude with an unchirped seed laser (black) and the FEL amplitude with an opportune shift and chirp on the initial condition to achieve short pulses (red). Amplitude of envelopes are plotted in respect to the adimensional normalized phases.

effect of a initial seed with a frequency chirp and shift has also been investigated. We also proposed a way to manipulate the seed in order to have the phase of the seed opposite to the one of the Green function on a particular phase coordinate. In this way, very short and chirped FEL pulses can be achieved as shown in Figure 2. Explicit expressions for the initial conditions for the seed are given as function of the  $\alpha$  and  $\beta$  parameters.

## References

- [1] S. Krinsky, Z. Huang, *Phys. Rev. ST Accel. Beams* **6**, 050702, (2003)
- [2] J. Wu, J.B. Murphy, P.J. Emma, X. Wang., T. Watanabe, X. Zhong, *J. Opt. Soc. Am. B* **24**, 484 (2007).
- [3] A.A. Lutman, G. Penco, P. Craievich, J. Wu, *J. Phys. A: Math Theor.* **42**, 045202 (2009).
- [4] A.A. Lutman, G. Penco, P. Craievich, J. Wu, *J. Phys. A: Math Theor.* **42**, 085405 (2009).

# PHYSICS AND SIMULATION CHALLENGES OF FERMI@ELETTRA

S. Di Mitri<sup>1</sup>, E. Allaria<sup>1</sup>, M. Cornacchia<sup>1</sup>, P. Craievich<sup>1</sup>, G. De Ninno<sup>1</sup>, G. Penco<sup>1</sup>, S. Spampinati<sup>1</sup>, M. Trovò<sup>1</sup>, W. Fawley<sup>2</sup>, S. Lidia<sup>2</sup>, J. Qiang<sup>2</sup>, K. Sonnad<sup>2</sup>, M. Venturini<sup>2</sup>, R. Warnock<sup>2</sup>, A.A. Zholents<sup>2</sup>, M. Borland<sup>3</sup>, R. Fiorito<sup>4</sup>, A. Shkvarunets<sup>4</sup>, J.C. Tobin<sup>4</sup>

<sup>1</sup>Sincrotrone Trieste S.C.p.A., Trieste, Italy

<sup>2</sup>Lawrence Berkeley National Laboratory, Berkeley, USA

<sup>3</sup>Argonne National Laboratory, Argonne, USA

<sup>4</sup>University of Maryland, College Park, USA

E-mail: [simone.dimitri@elettra.trieste.it](mailto:simone.dimitri@elettra.trieste.it)

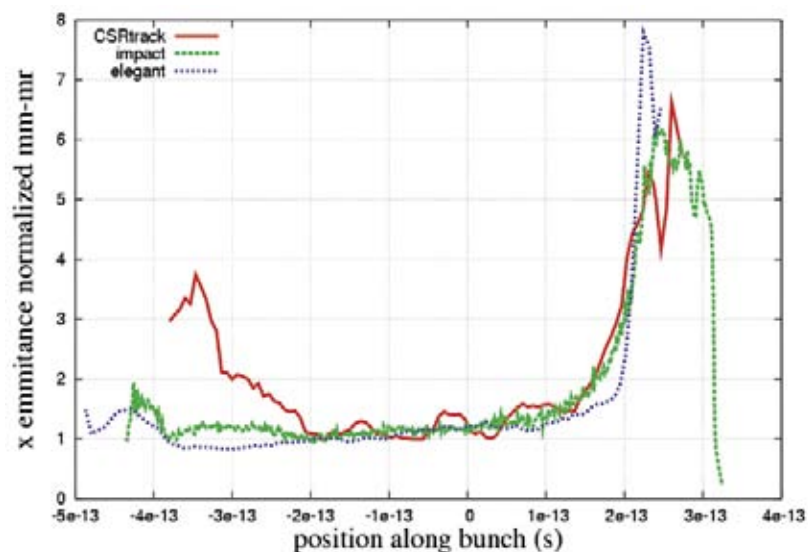
The physics of FERMI@Elettra user facility [1] relies on a high charge, monochromatic electron bunch that will drive external-seeded, high power Free Electron Laser (FEL) output radiation, in the fundamental wavelength range 100-4 nm. To provide more than  $10^{12}$  photons per pulse in 1 meV bandwidth even at the shorter wavelengths, a high electron density in the 6-dimensional spatial and velocity space is required. Unfortunately, many single particle and collective phenomena in the linac can degrade the electron beam transverse density (emittance) and energy distribution (energy spread). Such a large variety of physics processes implied challenging design strategies to control those parameters that translated into a large simulation and advanced computing effort. This activity led the Elettra laboratory to establish collaborations with laboratories world-wide, to start up a Workshop on Microbunching Instability and to pursue the

development and modification of codes according to new computing needs. This article presents some highlights of the physics and simulation challenges that characterized the FERMI@Elettra design study (please see Ref. [2] for a detailed discussion).

The FERMI@Elettra electron bunch is characterised by a very small transverse emittance; its minimum value of 8 nm rad is provided out of the injector (100 MeV) and its preservation is mainly affected by emission of Coherent Synchrotron Radiation (CSR) during the bunch length compression (this is performed in dedicated magnetic chicanes to increase the peak current) and by transverse wake field (image charge field in the accelerating structures). Both CSR and wake field impart a kick along the bunch that laterally displaces its longitudinal slices, so diluting the transverse particle density. The CSR effect was evaluated with three different codes, as

**Figure 1.**

Predicted slice horizontal normalised emittance of a 0.8 nC, 1 mm long bunch compressed by a factor 10. The emittance value before compression is 1mm-mrad in the core. The result from *elegant* code agrees well with that from IMPACT, while CSRTrack3D predicts some emittance bumps in the core of a shorter bunch. Several millions of macroparticles were tracked by the codes to improve their phase space resolution.



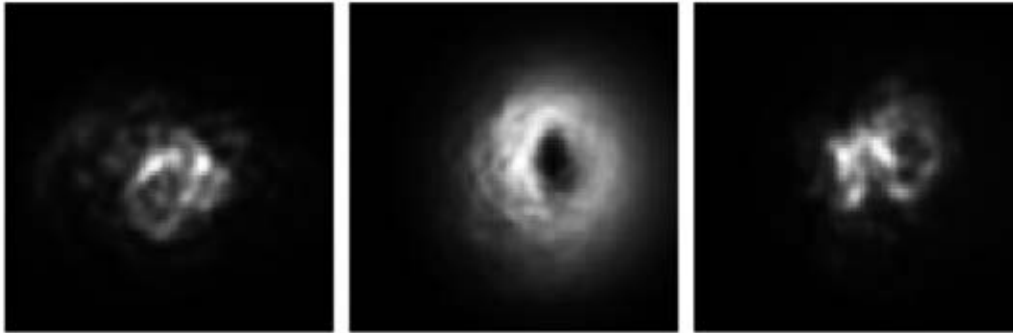


**Figure 2.** Predicted transverse intensity pattern of CTR observed in the near field region. The  $(x,y)$  coordinates are in arbitrary units, proportional to the real transverse coordinates at the virtual screen. The simulation of CTR emission is based on 5 million particles simulation that represents, respectively: left, uncompressed beam transported up to 230 MeV; centre, compressed beam transported up to the linac end, at 1.2 GeV; right, compressed beam transported up to the linac end with additional  $\delta_{\text{uncorr}}$  of 10 keV rms at 100 MeV. The emission at  $(30\mu\text{m})$   $3\mu\text{m}$  was simulated for the (un)compressed beam.

shown in Figure 1. Only one code was taking care of the real horizontal particle distribution that implies some emittance bumps in the bunch core. As for the transverse wake fields, since its effect depends on the transverse offset of the bunch with respect to the linac axis, all expected perturbations to the beam trajectory in the linac were simulated. A special trajectory correction scheme was also simulated to demonstrate the feasibility of the suppression of the emittance growth.

In the longitudinal plane of the particle motion, the energy spread was minimized by treating separately the correlation of the energy vs. the longitudinal particle position inside the bunch ( $\delta_{\text{corr}}$ ) and the slice energy spread ( $\delta_{\text{uncorr}}$ , here also called uncorrelated for practical purposes).  $\delta_{\text{corr}}$  is determined by the linac radio-frequency accelerating voltages and phases and by the longitudinal wake field; this depends in turn by the particle distribution. Thus, back-tracking from the linac end to the gun was implemented to predict the initial particle distribution that, at the end, minimizes  $\delta_{\text{corr}}$  to the 0.1% level for a given linac setting. The main sources of  $\delta_{\text{uncorr}}$  in the gun were recognized; nevertheless, new theory developments imply that modifications to existing codes are needed. At the same time, not current experimental set up is able to resolve the predicted  $\sim 1$  keV energy spread level as of yet. This area therefore requires additional computational and experimental efforts. The major uncertainty, however, concerns the final  $\delta_{\text{uncorr}}$  in the presence of CSR and space charge forces (intra-bunch Coulomb interactions). Owing to their combined action, FERMI@Elettra acts like a huge amplifier of small density and energy modulations; this dynamics is called microbunching instability. Four codes were benchmarked and adopted to simulate different regimes of the instability. The codes' reliability in pre-

dicting the final particle energy distribution is limited to  $\sim 10$ 's keV by intrinsic numerical noise of tracking codes and by nonlinear growth of the instability strength. Unfortunately, the FEL radiation output is still sensitive at this level. A deeper look into it was nevertheless made possible by an additional code calculating the detailed Coherent Transition Radiation emission of the electron bunch. As demonstrated by the recent LCLS FEL commissioning at SLAC, this can be used to detect the presence of longitudinal bunching, as shown in Figure 2. Analytical calculations supported by simulations demonstrated that the microbunching instability can be suppressed by increasing  $\delta_{\text{uncorr}}$  on purpose to a level that is still acceptable for the FEL process. This will be done in FERMI through the interaction of the electron beam with a seeding laser in a short planar undulator located at very low energy.

Once the FERMI set up was fixed, the global machine behavior was studied with start-to-end simulations from the gun to the undulator end. Static and dynamics imperfections were included in the global jitter study assuring a good level of confidence in the FERMI@Elettra performance. Eighty-four 6-dimensional particle distributions were tracked and passed through four chained tracking codes to simulate the electron beam generation, manipulation and transport, to simulate the external seeding process and the FEL generation over a wide range of wavelengths. The electron beam and FEL output stability was predicted in accordance with the Users' requirements.

## References

- [1] C.J. Bocchetta *et al.*, *FERMI@elettra Conceptual Design Report*, <http://www.elettra.trieste.it/> (2007).
- [2] S. Di Mitri *et al.*, *Nucl. Instr. and Meth. A* **608**, 19 (2009).

# DAMPING OF THE TUNNELING MECHANISM IN HIGH-ORDER HARMONIC GENERATION PROCESSES INDUCED BY fs VISIBLE LASER PULSES

A. Simoncig<sup>1,2</sup>, A. Caretta<sup>1</sup>, B. Ressel<sup>2</sup>, L. Poletto<sup>3</sup>, F. Parmigiani<sup>1,2</sup>

<sup>1</sup>Physics Department, University of Trieste, Trieste, Italy

<sup>2</sup>Sincrotrone Trieste S.C.p.A., Trieste, Italy

<sup>3</sup>Laboratorio LUXOR INFN-CNR, Padova, Italy

E-mail: fulvio.parmigiani@elettra.trieste.it

Nowadays, most of the coherent high-order harmonic generation (HHG) sources are based on near infrared (near-IR) ultrashort laser field [1,2]. Nonetheless, it is important to note that the power density threshold needed for HHG can be lowered at shorter wavelength, i.e. the second harmonic (SH) of the fundamental laser beam. This effect can be rationalized by considering that an increase of the EUV photon generation is expected by reducing the optical period of the driving pulse, which in turn will decrease the diffusion process influencing the dynamics of the involved electron wave function. These arguments brought us to study the generation of HH pulses farther on the non-perturbative conditions choosing different values of the Keldysh parameter ( $\gamma_K$ ) [1]. Of course, different  $\gamma_K$  will result into different ionization mechanisms. In particular, for  $\gamma_K \ll 1$  the radiation-matter interaction takes place as a non-perturbative process and the ionization is described by a tunneling model [1,2], whereas for  $\gamma_K \gg 1$  the radiation-matter interaction is perturbative and the ionization mechanism is multi-photonic (multi-photon ionization or MPI).

It is then interesting to consider  $\gamma_K \geq 1$  where a hybrid regime is expected, but never properly described. In fact, for the hybrid regime the dominant ionization mechanism, characterizing the first step of the HHG interaction, is neither MPI nor tunneling.

Here we report the experimental evidence that when the Keldysh parameter is varied from 1 to 3 the HH photons number exponentially decays [3]. This behavior clearly shows the existing competition between the tunneling ionization and the MPI processes, providing an unambiguous evidence of a hybrid dynamical region, where a full-tunneling approximation model cannot account for HHG processes.

Starting from the Ammosov-Delone-Keoinov (ADK) model and properly modifying the Yudin-Ivanov (Y-I) rate equation we obtain a novel phenomenological model that adequately describes the transition from the tunneling ionization region to the MPI region [4].

The light source is based on an amplified Ti:Sapphire laser that generates near-IR ( $\lambda_0 \approx 800$  nm) linearly polarized pulses with a time structure of 50 fs at 1 kHz repetition rate (r.r.) and 2.5 mJ/pulse. After collimating the beam the laser pulses are split into two orthogonally polarized beams, by a continuously variable attenuator (CVA). The CVA is designed to vary the splitting ratio with continuity, while preserving the temporal structure, allowing to modify  $\gamma_K$  continuously, therefore controlling the ionization dynamics. The p-polarized beam is frequency doubled by a Beta Barium Borate, type-I, (BBO) non-linear crystal (thickness 0.35 mm), with conversion efficiency up to  $\approx 35\%$ . The SH beam is then separated from the residual near-IR beam by 3 dichroic high reflectivity band-pass mirrors set at  $\lambda_{SH} \approx 400$  nm. After these mirrors the SH beam is separated from the residual near-IR beam. The SH pulse is then focused into a suitable gas-cell filled up to  $10^{-3}$  mbar with Xe, while the entire apparatus operates at a background pressure of  $10^{-8}$  mbar. After generation the HH spectral components are dispersed and analyzed by a grating monochromator and a suitable detector system.

Figure 1 reports the number of photons per pulse of the 10<sup>th</sup> harmonic (15.6 eV, i.e. 79.6 nm) generated in Xe by varying  $\gamma_K$  from 1 to 3.2.

From these data, the three different regimes can be clearly recognized. The most interesting behavior of these data is represented by the transition from the non-perturbative regime ( $\gamma_K < 1$ , tunnelling ionization) to the perturba-

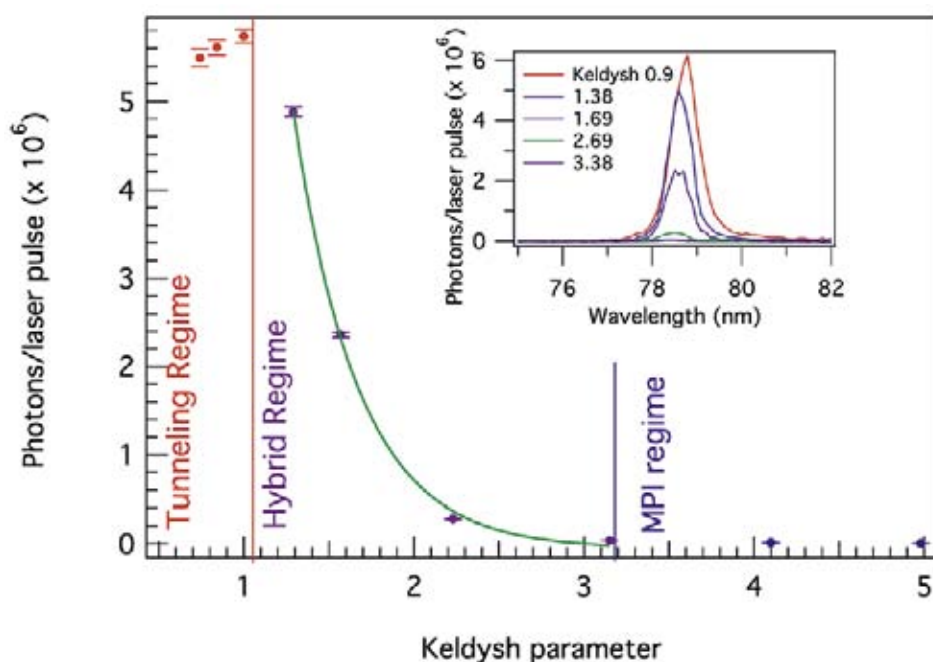


**Figure 1.** Experimental evidence for the damping of the HHG photons/pulse as a function of  $\gamma_K$ . From these data different regimes can be recognized. The red and blue dots refer to the tunneling and MPI regimes, respectively, while the violet ones to the hybrid regime. The green line is the exponential fit function in the hybrid dynamical region.

tive regime ( $\gamma_K > 3$ , MPI). A quite phenomenological picture of this process can be gained by considering that the recombination of the excited electron with the ion, during the radiation-atom interaction, depends on the phase at which the atom has been ionized [1]. However, the Y-I model predicts that in the MPI regime the role of the phase into the ionization rate equation is almost negligible [4]. This implies a drop of the efficiency of the HHG process for  $\gamma_K \geq 1$ . This effect is clearly observed in our experiment.

These experimental results help also to give more insight about the meaning of  $\gamma_K$ , which, for the hybrid regime, can be viewed as the contribution of the tunneling mechanism to the whole HHG process, or as a parameter related to the damping of the tunnelling regime. Instead,  $\tau$  (that can be considered as a Keldysh time) contains all the information concerning the threshold condition for generating high-order harmonics.

In conclusion, our experiment reports the clear evidence that the HHG in Xe using 400 nm, 60 fs laser pulses, undergoes an exponential decay

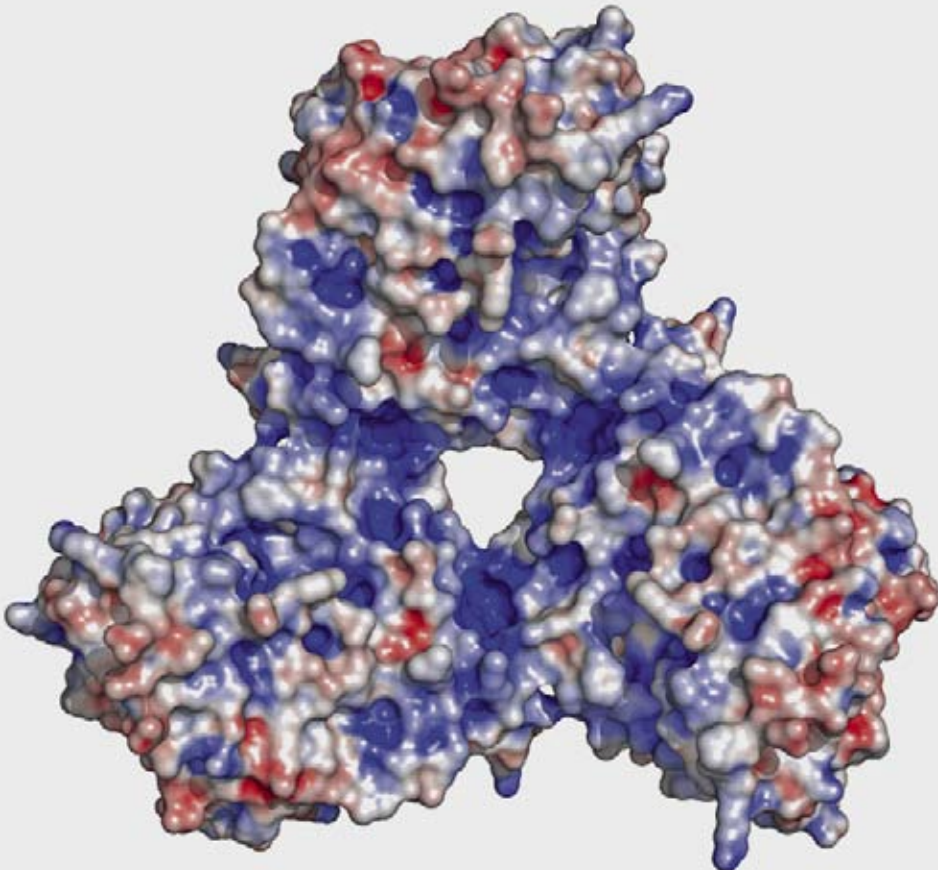
for  $\gamma_K > 1$ , reaching the MPI regime for  $\gamma_K > 3$ . This behavior provides the unambiguous evidence for hybrid dynamical region, where a full-tunneling approximation model cannot account for HHG processes. Starting from the ADK model and properly modifying the Yudin-Ivanov rate equation we obtain a phenomenological model that properly describes the HHG hybrid dynamical regime. In addition the present letter underlines the possibility of generating, efficiently, HH using the SH of a Ti:Sapphire laser and operating in the hybrid regime [4].

#### References

- [1] T. Pfeifer, C. Spielman, G. Gerber, *Rep. Prog. Phys.* **69**, 443 (2006).
- [2] M. Lewenstein, Ph. Balcou, M.Y. Ivanov, Anne L'Huillier, P.B. Corkum, *Phys. Rev. A* **49**, 2117 (1994).
- [3] A. Simoncig, A. Caretta, B. Ressel, L. Poletto, F. Parmigiani, *Appl. Phys. Lett.* **95**, 041107 (2009).
- [4] G.L. Yudin, M.Y. Ivanov, *Phys. Rev. A* **64**, 013409 (2001).



**LIFE SCIENCES**





# STRUCTURAL BIOLOGY AT ELETTRA: RECENT ADVANCES AND NEW PERSPECTIVES

## Major changes in the infrastructure for biocrystallography

*An interview with Dorian Lamba*

Macromolecular crystallography is a rapidly growing field and synchrotron facilities are constantly under pressure from the increasing demands of a fast increasing user community. Elettra is currently modernising and expanding the infrastructure for structural biology, with a major upgrade of the existing beamline, the building of a second beamline, and the set-up of an automated crystallisation facility.

Doriano Lamba is a Senior Scientist at the Istituto di Cristallografia, C.N.R., Trieste Outstation. He received his Diploma in Chemistry and his Ph.D. in Biophysics, in 1980 and 1988, respectively, from the Università "La Sapienza" - Roma, and from the University of Leeds. From 1993-1996 he was a Postdoctoral Research Associate at the Max Planck Institut für Biochemie, Martinsried (München) advisors R. Huber (Nobel Laureate) and W. Bode. He is the Italian delegate to the International Network Protein Engineering Centres and member of the management committee of the Integrated Structural Biology Infrastructure for Europe.



### What is new regarding the facilities for structural biology at Elettra?

Over the last couple of years Elettra has heavily invested in modernising and expanding the infrastructure for structural biology. A tunable beamline primarily designed for macromolecular crystallography (XRD1) has been recently upgraded and automatised, whereas a second beamline (XRD2) is currently being developed.

In a parallel effort, a state-of-the-art laboratory for structural biology has been set-up with facilities for gene cloning, PCR and protein over expression in a variety of systems, in both bacterial and baculovirus-infected insect cell systems. Several low and high-pressure chromatography systems are available for protein purification and a range of biophysical techniques (such as dynamic light scattering, circular dichroism, microcalorimetry and surface plasmon resonance) can be used for biophysical characterisation. The primary goal of the laboratory is to provide a regular supply of pure, homogenous, functional proteins for crystallization experiments. A dedicated crystallization suite, consisting of a nanolitre-drop

dispensing Mosquito and a Hydra II eDrop robots will be soon complemented by a liquid handler and an automated crystal imaging system, currently being purchased. Plans for the automation of the cloning and protein expression pipelines are currently being evaluated.

### How does the updated XRD-1 beamline compare with the previous setup?

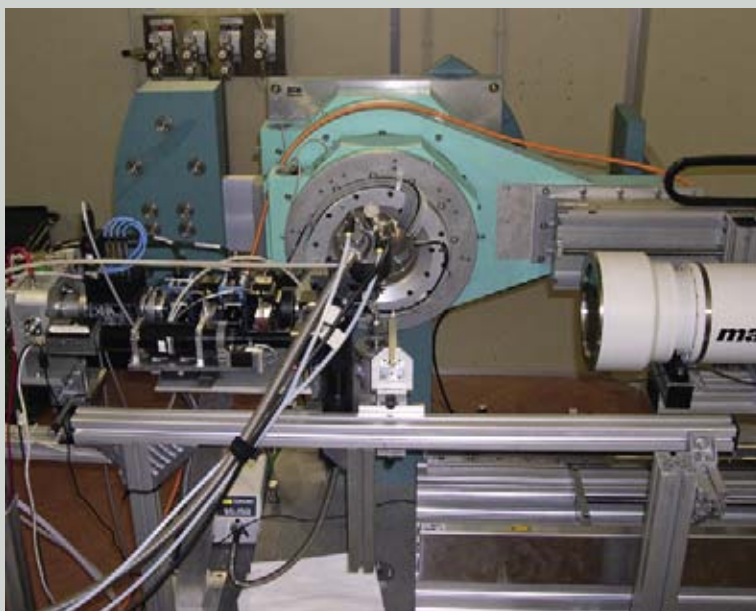
The XRD1 beamline was among the first to become operational at Elettra and the upgrade, after more than 10 years of function, was absolutely mandatory.

The optics has been largely rebuilt, with the addition of a vertical collimating mirror and the replacement of the previous three-section toroidal Pt-coated focusing mirror with a 1-section bendable one. A new monochromator crystal with a highly effective internal cooling channel system, mounted on a piezo element for the fine adjustment of the Bragg angle and controlled by a digital feedback system, has improved the brilliance by at least a factor of ten as well as the positional stability of the beam. A  $\kappa$ -goniometer mounted on a kinematic table, for fast alignment under the X-ray beam, has recently replaced the single axis goniostat system. A marC-CD165 detector is mounted on the  $2\theta$  arm while on the base of the instrument is placed a mar345 Imaging Plate that can be moved back and forward on motorized tracks. A PILATUS 2M single photon counting hybrid pixel detector will be available to the XRD1 users' community by the end of the year. An innovative, *in-house* designed and built integrating ionization chamber as well as monochromatic attenuators (aluminum foils of varying thicknesses) independently and remotely controlled have been implemented too. A semi-automatic two-click crystal centering procedure has been introduced and a substantial progress has been achieved in the beam line control system towards *user-friendly* automated strategies.

The new upgraded XRD1 beam line hutch is fully compliant with a white beam experimental setup. The tunability of the wavelength provides the opportunity to use the Multiwavelength Anomalous Diffraction (MAD) technique for solving the phase problem over a broad range of wavelengths, covering the absorption edges of all the heavy atoms commonly used in macromolecular biocrystallography. In addition, the multipole wiggler spectrum provides high photon flux at low energies, allowing optimization of the anomalous signal at the sulphur, xenon and calcium edges. Helium purged beam path and helium based cryo-cooling at 100 K are available for data collection experiments with longer wavelengths.

#### Illustration 1.

XRD-1 Crystallography beamline. The experimental station is equipped with a  $\kappa$ -diffractometer with motorized xyz stage for sample alignment, CCD detector (soon to be replaced a Pilatus 2M detector), collimating slits / ionization chambers stage and a cryostream for 100 K data collection.



### What are the advantages of the new detector?

The PILATUS 2M detector, with more than 2 million pixels covering a large active area, operates in “single-photon counting” mode and is based on the newly developed hybrid-pixel technology. The main difference to existing detectors is that the photons are directly transformed into electric charge and processed in the CMOS readout chips. This absolutely new design shows no dark

current or readout noise, excellent quantum efficiency and leads to a high dynamic range, short readout times (less than 4 ms), high framing rate and an excellent point-spread function of one pixel. The quantum efficiency is optimal for experiments in the energy range from 3 to 15 keV, however the detector can be used for energies of up to 40 keV. The counting rate per pixel is above  $2 \times 10^6$  photons/s to handle the high flux of modern synchrotron light sources. Other important features are an electronic shutter and the possibility to suppress fluorescent background from the sample.

The detector is an order of magnitude faster than comparable CCDs and it is expected to produce data of unprecedented quality. With its high quantum efficiency, the exposure times can be minimized, which significantly reduces the radiation damage to the crystal. In addition the large detector area with a high number of pixels and small point-spread function allows resolving many orders of reflections. The wide dynamic range permits the precise detection of weak and strong signals. The high frame rate combined with the short readout time reduces the measurement times dramatically.

The PILATUS 2M detector is especially tailored to collect fine phi sliced crystallographic data at high speed in the continuous sample rotation mode. In this mode, the crystal is rotated by a fraction of its mosaic spread ( $0.02$ - $0.2^\circ$ ) during each frame, leading to thousands of images for a  $180^\circ$  rotation. Such an experiment would be very time-consuming with a CCD detector, due to the long readout times. With the PILATUS 2 M detector the crystal can be rotated continuously in the beam without opening and closing the shutter for each frame.

#### Are we getting closer to “FedEx-crystallography”?

Macromolecular crystallography is fast evolving and automated sample handling, alignment and data management protocols will be required to work efficiently with the expected increase in demand. An *in-house* designed sample-mounting system is currently being tested to allow for automatic evaluation and data collection from multiple crystals without physical intervention from the user. A secure remote data collection capability and the implementation of a mail-in crystallography program/service in order to provide users with high quality data and to maximize data collection efficiency, are included in the to-do list. Since shipping costs are considerably less than food, lodging, and travel expenses for personnel, FedEx-crystallography saves users' money as well as time. The expertise of Elettra and IC-CNR beamline scientists, and remote consultation with users when necessary, should insure the highest possible quality of data collected using this mode, establishing a new paradigm for macromolecular crystallography experimentation.

#### Can you briefly comment on other applications of synchrotron radiation to the life sciences?

For example, the application of phase sensitive X-ray imaging techniques to radiology and biomedical imaging (at the SYMREP beamline) has led the first protocol for clinical mammography, carried out on patients recruited from the local hospital among those with doubtful diagnosis. X-ray microtomography (mCT) is a powerful and non-destructive technique extensively used to visualize the inner structure of thick biological specimens. In the two image modalities (phase contrast and absorption), it is applied to studies on bone regeneration and to evaluate the change in bones morphology and density in osteoporosis or other pathologies. It is also used for research on teeth and implants and to characterize atherosclerotic plaques in the arterial wall, for modelling purposes. Very demanding are the mCT applications for cell tracking purposes in small animals: as an example, the migration of tumor cells marked by gold nano-particles inside the body of mice has been followed with high sensitivity.

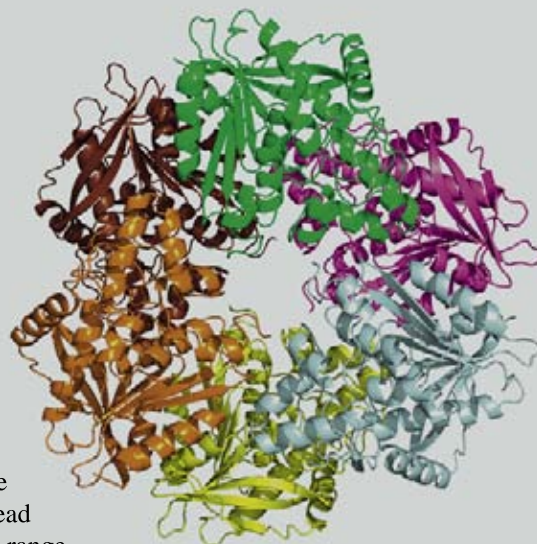


**Illustration 2.** Quaternary structure of *Bacillus pumilus* Acetyl Xylan Esterase (AXE). A cartoon of the hexameric molecular architecture of AXE with each monomer in a different colour.

# RADIATION-DRIVEN REACTIVATION OF HUMAN CARBONIC ANHYDRASE: A MOVIE OF BINDING AND PROCESSING OF THE CO<sub>2</sub> AT THE ATOMIC LEVEL

B. Sjöblom<sup>1</sup>, M. Polentarutti<sup>2</sup>, K. Djinović-Carugo<sup>1,3</sup>

<sup>1</sup>Department for Structural and Computational Biology, University of Vienna, Vienna, Austria

<sup>2</sup>Sincrotrone Trieste S.C.p.A., Trieste, Italy

<sup>3</sup>Department of Biochemistry, University of Ljubljana, Ljubljana, Slovenia

E-mail: maurizio.polentarutti@elettra.trieste.it



XRD1

Carbonic anhydrase, a zinc metalloenzyme, catalyzes the reversible hydration of carbon dioxide (CO<sub>2</sub>) to bicarbonate (HCO<sub>3</sub><sup>-</sup>). It is involved in processes connected with acid–base homeostasis, respiration, photosynthesis, gluconeogenesis, lipogenesis, ureagenesis, tumorigenicity as well as the growth and virulence of various pathogens. Its importance is witnessed by a large volume of publications and more than 100 distinct human carbonic anhydrase II (HCAII) 3D structures. Despite the interest, a structure of an HCAII in complex with its substrate or product remained elusive.

The generally accepted catalytic mechanism of HCAII is described by a 3-step kinetic scheme: (i) a Zn–OH<sup>-</sup> moiety (present at the bottom of a 15 Å cone-shaped cavity) catalyzes the interconversion of CO<sub>2</sub> to HCO<sub>3</sub><sup>-</sup>, leaving a water molecule as the fourth zinc ligand; (ii) a proton is transferred from the zinc-bound water to the imidazole ring of His-64; and (iii) this proton then leaves His-64 for the surrounding solvent.

Despite the high dissociation constant for CO<sub>2</sub> and the very high enzyme turnover rate, we generate a stable HCAII:CO<sub>2</sub> complex pressurizing the HCAII crystals under CO<sub>2</sub> gas (10 bars), with the dual effect of (i) inhibiting the enzyme by decreasing the pH in the crystal *via* the spontaneous reaction of CO<sub>2</sub> with water, and (ii) supplying substrate to the enzyme at a high concentration.

The structure obtained from diffraction data collected from the CO<sub>2</sub>-loaded HCAII crystal was refined to 1.56 Å resolution and showed the CO<sub>2</sub> located in the active site of the enzyme, in a position totally in line with the previous conjectures based on indirect results. Surprisingly, a map calculated from a second dataset – collected after two months on the same sample – showed the CO<sub>2</sub> partially converted

to HCO<sub>3</sub><sup>-</sup> and a third map from subsequent third dataset exhibited only bicarbonate in the active site (whereas the enzyme was supposed to be inhibited due to the low pH). A series of control experiments confirmed the independence of the enzyme activation from thermal/temporal processes and indicated that the substrate is gradually transformed into bicarbonate as a function of the absorbed X-ray dose. This led to the design of a X-ray diffraction experiment to monitor and quantify the structural changes associated with substrate-product interconversion and determine the X-ray dose needed for enzyme “reactivation”. The generation of a series of molecular models as a function of the applied dose led to a movie of the enzymatic reaction which can be seen as supplementary material in the original publication [1]. The movie starts in a state corresponding to the HCAII:CO<sub>2</sub> complex, proceeds through decreasing substrate to product ratios and ends in a state with 65% CO<sub>2</sub> and 35% HCO<sub>3</sub><sup>-</sup>.

The unexpected recovery of enzyme activity during X-ray exposure may be caused by diverse radiation-induced events. For the reaction to proceed in the enzyme (initially inactive because of low pH in the crystal due to pressurisation by CO<sub>2</sub>), the zinc-bound water molecule must release a proton. This results in an active enzyme, in which a hydroxide ion reacts with the CO<sub>2</sub> to create bicarbonate.

We considered different, mutually nonexclusive mechanisms caused by the photoelectric effect, which is responsible for 84% of the photons absorbed by the matter at these X-ray energies: (i) a macroscopic increase in pH *via* radiolysis of water molecules in the bulk solvent triggered or produced by the primary and secondary electrons generated during X-ray-sample interaction; and/or (ii) a shielding/

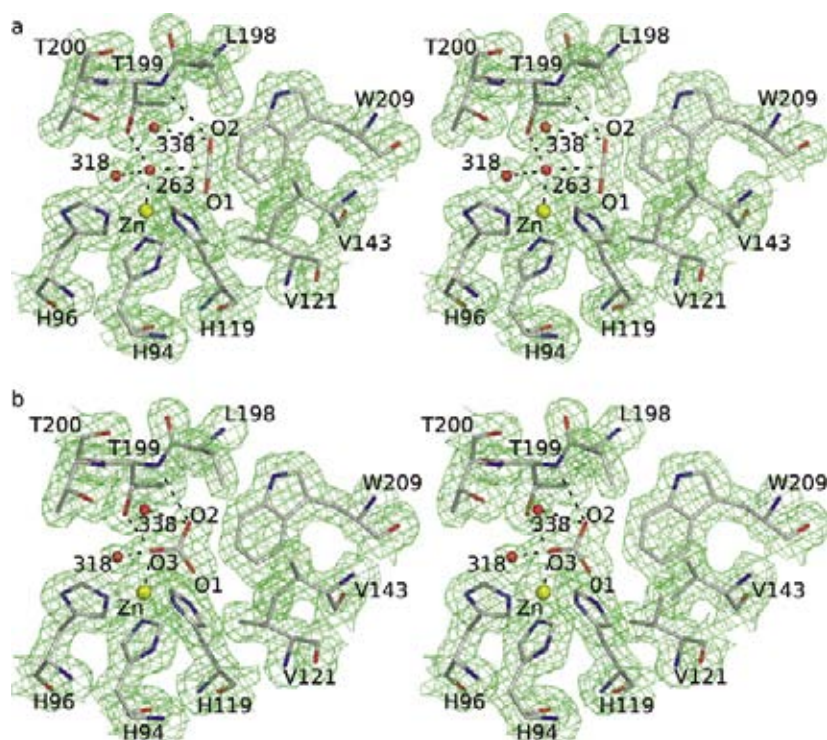


**Figure 1.** Stereoview of the electron density map and corresponding models of HCAII active site in complex with (a)  $\text{CO}_2$  at 1.56 Å resolution and (b)  $\text{HCO}_3^-$  at 1.66 Å resolution. The bicarbonate has van der Waals contacts with the same residues as  $\text{CO}_2$ .

masking effect by the produced electrons on the positively charged  $\text{H}^+$  species in the bulk, mimicking a pH increase; and/or (iii) a local event involving photoionization or electronic ionization of the zinc-bound water molecule, creating a hydroxyl radical that either recombines with an electron to yield the required hydroxyl ion or reacts with  $\text{CO}_2$  to create a bicarbonate radical that would, in turn, recombine with an electron or hydrogen radical from the neighbourhood. The local photoionization or electronic ionization of water molecules has a higher probability close to the zinc ion, which would result in generation of primary and secondary electrons in the vicinity of the metal ion because of its larger photoelectric cross-section.

To distinguish among the possible mechanisms of HCAII activation by X-rays, we performed the data collection at a 0.94 Å wavelength, far from the zinc-absorption edge. At the same absorbed dose, we found no significant difference in the substrate to product ratio with respect to the dataset collected at the

zinc-absorption edge, using 1.278 Å wavelength. We additionally observe that the process does not depend on the dose rate: the two experiments were conducted by using beams that differed by more than one order of magnitude in flux. The finding that the photon energy (at the zinc absorption edge in the first case and far away from it in the second) does not influence the substrate to product ratios leads to the conclusion that the zinc ion and its interaction with X-rays do not play a pivotal role in the process. This result does not clearly indicate the mechanism of the enzyme activation, but it does exclude a *local* effect influencing only the active-site zinc ion and bound water molecule, therefore promoting the hypothesis based on *bulk* effects resulting in a macroscopic increase of pH in the crystal.

## References

- [1] B. Sjöblom, M. Polentarutti, K. Djinovic-Carugo, *PNAS* **106**, 10609 (2009); <http://www.pnas.org/content/106/26/10609/suppl/DCSupplemental>

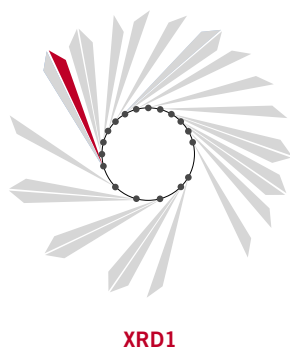
# CRYSTAL STRUCTURE OF MYCOBACTERIUM TUBERCULOSIS YEFM ANTITOXIN REVEALS THAT IT IS NOT AN INTRINSICALLY UNSTRUCTURED PROTEIN

P. Kumar<sup>1</sup>, B. Issac<sup>1</sup>, E.J. Dodson<sup>2</sup>, J.P. Turkenburg<sup>2</sup>, S.C. Mande<sup>1</sup>

<sup>1</sup>Laboratory of Structural Biology, Centre for DNA Fingerprinting and Diagnostics, Hyderabad, India

<sup>2</sup>Department of Chemistry, University of York, York, United Kingdom

E-mail: shekhar@cdfd.org.in



Toxin-antitoxin (TA) genes are found ubiquitously on chromosomes of all free-living prokaryotes, as well as encoded on plasmids in many bacteria and archaea. When present on plasmids, they act as plasmid stabilizing machinery, a phenomenon known as post-segregational killing (PSK). However, the function of chromosomally encoded TA systems is still debated. Two different theories have been proposed for the roles of TA modules. The first one attributes TA systems for programmed cell death, while the other suggests their role as stress managers.

YefM-YoeB TA module comprises the antitoxin YefM and its cognate toxin, YoeB. YefM is a dimeric protein with three distinct structural domains. The N-terminal region is responsible for dimerization and binding to the operator sequence of the *yefM-yoeB* operon. The central region is a long helix, whose

hydrophobic zipper-like interactions drive dimerization. The highly pliable C-terminal region forms a non-covalent trimeric complex with YoeB (2:1) and neutralizes its toxic activity. YoeB is a ribonuclease, which cleaves mRNA, both translated as well as that undergoing translation on the ribosomes.

Crystal structure of the YefM<sub>2</sub>-YoeB complex of *E. coli* was already known and suggested that YefM is unstructured in the absence of YoeB. However, we have been able to crystallize YefM of *M. tuberculosis* in its apo-form. The structure of apo-YefM antitoxin reveals that it is not an intrinsically unstructured protein, but forms a well defined 3D-structure.

*M. tuberculosis* YefM was crystallised in two different conditions. Both crystals however belong to the same space group, P2<sub>1</sub>2<sub>1</sub>2<sub>1</sub> with similar cell dimensions, whereas Se-Met crys-

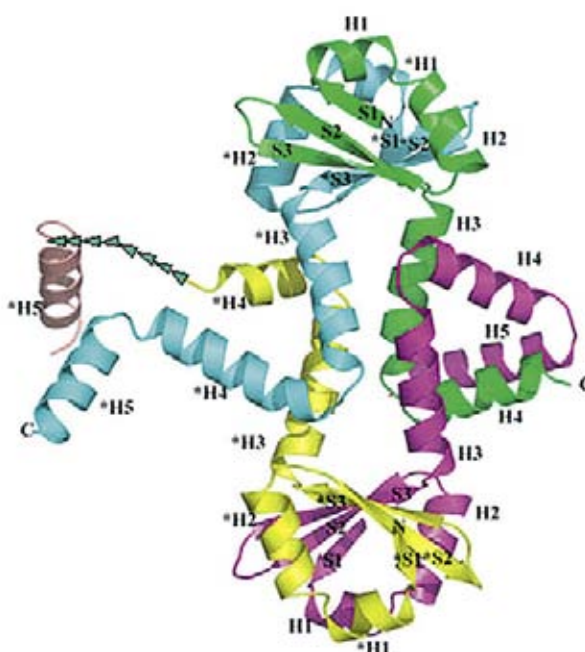


**Figure 1.**

Cartoon representation of the tetrameric antitoxin. Chain A (Green), chain B (Cyan), chain C (Magenta), chain D (yellow) and chain E (wheat colour). Chain E is probably an extended part of the D chain, which is not connected to chain D because of the missing density of a few residues.

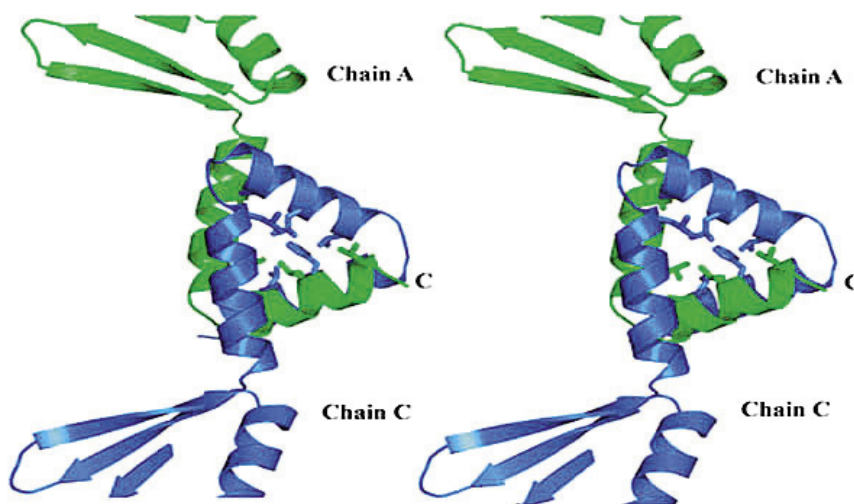


**Figure 2.** Stereo representation of the C-terminal domain of the antitoxin shows the residues involved in the interaction with the toxin as well as the inter-dimer hydrophobic core cluster formation.

tals grown under similar conditions belong to the space group,  $P4_32_12$ . The 3D-structure of the apo YefM was determined by combination of Single wavelength Anomalous Dispersion (SAD) and molecular replacement using Se-Met derivative of YefM. Initial SAD phases were determined with MLPHARE and improved by PIRATE. Density modification with DM yielded very good electron density map. An initial model was fitted into the electron density with BUCCANEER. The model was further refined with REFMAC5 to generate a partial model that was used for molecular replacement (using AMORE) on the native orthorhombic datasets. One of the native crystal datasets was twinned, and was detwinned with SFCHECK before molecular replacement. The final  $R_{\text{cryst}}$  and  $R_{\text{free}}$  were 20.7 and 25.4 % for Crystal I and 17.9 and 21.6 % for Crystal II respectively.

The native crystals contained four molecules of YefM in the asymmetric unit. Se-Met crystals contained two molecules in ASU, with the symmetry arrangement creating identical packing as in the native isoform (crystal I). The N-terminal was rich in hydrophobic residues, which are responsible for the dimerization of YefM. The central helix of each mono-

mer forms a hydrophobic zipper-like structure, which contributes to the dimeric interactions of each monomer. The C-terminal region forms a hydrophobic cluster stabilised by interdimeric interactions in the tetramer. Most of the residues which are involved in the interactions are conserved across many bacterial species. The dimer of YefM of *M. tuberculosis* superposes well with that of *E.coli* with RMSD value of 1.03 Å over 93 C $^{\alpha}$  atoms. Although the overall structure of the *M. tuberculosis* YefM dimer is similar to the *E. coli* YefM dimer in the YefM<sub>2</sub>-YoeB complex, the central helices and the C-terminal helices by virtue of their pliability adopt very different conformation. Interestingly, the residues which are responsible for the tetrameric structure formation are involved in the formation of the YefM<sub>2</sub>-YoeB complex of the *E.coli*.

#### References

- [1] I. Cherny, E. Gazit, *J. Biol. Chem.* **279**, 8252 (2004).
- [2] K. Kamada, F. Hanaoka, *Mol. Cell.* **19**, 497 (2005).
- [3] P. Kumar, B. Issac, E.J. Dodson, J.P. Turkenburg, S.C. Mande, *J. Mol. Biol.* **383**, 482 (2008).

# INSIGHTS INTO THE MOLECULAR BASIS OF TRANSCRIPTIONAL ACTIVATION IN ARCHAEA: STRUCTURAL ANALYSIS OF BldR FROM *SULFOLOBUS SOLFATARICUS*

A. Di Fiore<sup>1</sup>, G. Fiorentino<sup>2</sup>, R.M. Vitale<sup>3</sup>, R. Ronca<sup>2</sup>, P. Amodio<sup>3</sup>, C. Pedone<sup>1</sup>, S. Bartolucci<sup>2</sup>, G. De Simone<sup>1</sup>

<sup>1</sup>Istituto di Biostrutture e Bioimmagini-CNR, Naples, Italy

<sup>2</sup>Università degli Studi di Napoli Federico II, Naples, Italy

<sup>3</sup>Istituto di Chimica e Biomolecolare-CNR, Pozzuoli, Italy

E-mail: gdesimon@unina.it



XRD1

The multiple antibiotic resistance regulator (MarR) family is a significant class of transcriptional regulators, since its members control a variety of important biological functions, such as regulation of response to environmental stress, control of virulence factor production, resistance to antimicrobial agents and regulation of aromatic catabolic pathways [1]. Although the majority of the MarR family members have been characterized as transcriptional repressors, examples of transcriptional activators have also been reported. BldR is a newly identified member of the MarR family, which has been demonstrated to act as a transcriptional activator in the stress response to aromatic compounds in *S. solfataricus* [2]. In particular, by binding to its own promoter BldR is able to induce autoactivation, while by binding to the *Sso2536* promoter stimulates gene transcription, accumulation of the alcohol dehydrogenase (ADH) enzyme and, hence, the enzyme-catalyzed conversion of aldehydes to less toxic alcohols [2]. Recently, great inter-

est has been dedicated to defining the structural properties of the MarR family. However, even though significant progress has recently been made, little is known about the DNA-binding mechanism of these proteins. The sole structural information available to date on this topic was provided by the crystal structure of the transcriptional regulator OhrR from *Bacillus subtilis* (*BsOhrR*) complexed with the *ohrA* operator [3]. BldR differs from *BsOhrR* since it activates rather than represses gene expression. Thus, to provide the first structural information on the DNA-binding mechanism of an activator of the MarR family, we solved the crystallographic structure of BldR at 1.90 Å resolution. This structure was used as starting point to build a molecular model of BldR in complex with its DNA target by using homology modeling techniques and molecular dynamic simulations. Analysis of the X-ray structure revealed that, as already observed for other MarR family members, BldR is a dimer and adopts the typical MarR fold (Fig-

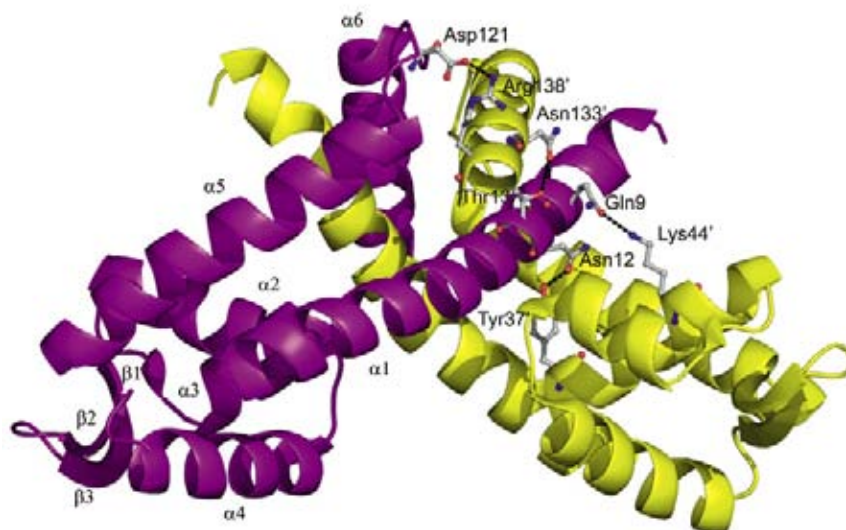


**Figure 1.** Dimer structure of BldR with one monomer colored in violet, the other in yellow. Residues involved in the polar interactions at the dimer interface are also shown.





**Figure 2.** Solvent accessible surface of BldR dimer bound to DNA. The BldR dimer is colored in pink while in cyan and violet are reported the recognition helix  $\alpha 4$  and the wing of both subunits, respectively. DNA is shown as a stick model.

ure 1), while MD simulation studies allowed us to clarify the molecular determinants responsible for BldR affinity and specificity toward its associated DNA sequence. In particular, the BldR dimer contacts DNA by using the recognition helices  $\alpha 4$ , which are positioned within two consecutive DNA major grooves, and the winged  $\beta$ -strands, which interact with minor grooves (Figure 2). Two residues responsible for binding specificity, namely Ser65 and Arg90, were also identified. Interestingly, structural comparison of the BldR-DNA complex with its *BsOhrR* counterpart showed that these transcriptional regulators adopt a very similar DNA-binding mode. The observation of a strong similarity in the DNA-binding mechanism of BldR with respect to *BsOhrR* is quite surprising not only due to the different kingdom of origin of the two proteins but especially for the different regulatory function that they perform. Thus, this finding, together with recently reported studies which demonstrated that BldR specific binding sites on its own and *Sso2536* promoter sequences are located immediately upstream of the TATA-box, seem to indicate that the ability of MarR family members to act as activators or repressors is not related to a particular DNA-binding mechanism but is essentially due to the position of the specific binding site

on the target DNA. Our results imply that, despite the high structural homology, differences in the sequences of the MarR proteins may support one action rather than another. Since, in these proteins, residues responsible for specific protein-DNA contacts are generally limited in number, it is conceivable that single protein mutations could lead to a change in the specificity of the binding site and/or a switch from positive to negative regulation. Given that genes encoding MarR homologues control transcription of operons, which generally encode for multisubstrate efflux pumps contributing to the microorganism's multidrug resistance, these findings could have interesting pharmacological and biotechnological applications. Indeed, in-depth knowledge of multidrug efflux system gene regulation could help identify new tools to overcome such threatening resistance.

#### References

- [1] S.P. Wilkinson, A. Grove, *Curr. Issues Mol. Biol.* **8**, 51 (2006).
- [2] A. Di Fiore, G. Fiorentino, R.M. Vitale, R. Ronca, P. Amodeo, C. Pedone, S. Bartolucci, G. De Simone, *J. Mol. Biol.* **388**, 559 (2009).
- [3] M. Hong, M. Fuangthong, J.D. Helmann, R.G. Brennan, *Mol. Cell.* **20**, 131 (2005).

# FTIR MICROSCOPY CHARACTERIZATION OF SYNBEADS, A POROUS SUPPORT FOR SOLID PHASE PEPTIDE SYNTHESIS

L. Sinigo<sup>1</sup>, P. Bravin<sup>1</sup>, C. Ebert<sup>1</sup>, N. D'Amelio<sup>2,3</sup>, L. Vaccari<sup>4</sup>, L. Ciccarelli<sup>5</sup>, S. Cantone<sup>6</sup>, A. Basso<sup>1,6</sup>, L. Gardossi<sup>1</sup>

<sup>1</sup>Laboratory of Applied and Computational Biocatalysis, University of Trieste, Trieste, Italy

<sup>2</sup>Bracco Imaging S.p.A., CRB Trieste, Trieste, Italy

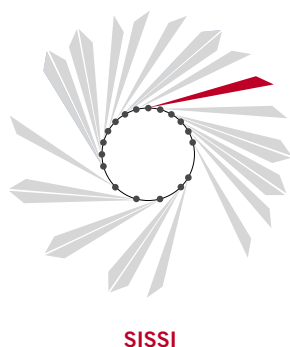
<sup>3</sup>CBM Srl, Consorzio per il Centro di Biomedicina Molecolare, Trieste, Italy

<sup>4</sup>Sincrotrone Trieste S.C.p.A., Trieste, Italy

<sup>5</sup>Resindion S.r.l., Mitsubishi Chemical Corporation, Milan, Italy

<sup>6</sup>SPRIN s.r.l., c/o University of Trieste, Trieste, Italy

E-mail: basso@sprinttechnologies.com



Nowadays, the most common method for peptide synthesis is on solid supports (Solid Phase Peptide Synthesis-SPPS). This approach, sketched in Figure 1 (top line), offers several advantages if compared with conventional chemical synthesis in liquid phase, such as the easier removal of reactant excess and by-products that make the technique suitable for the production of a wide array of compounds needed both for screening and large scale production, a crucial aspect considering the increasing demand of peptidic drugs [1].

For synthesis automation on large scale, solids supports are required to be mechanically stable, chemically inert and to ensure good diffusion of reagents, the latter generally achieved by using insoluble matrices endowed with swelling capacity. Non swelling supports, such as silica and derivatives, find limited applications in SPPS due to their low porosity and consequent limited accessibility even if their use would allow reducing the reaction volumes and solvent consumption, a key point for industrial applicability [2].

Synbeads are a new class of promising rigid macro porous methacrylic supports developed by SPRIN s.r.l. (Trieste) in collaboration with Resindion Mitsubishi Chem. Corp. (Milan, Italy) [3], whose chemical accessibility and degree of functionalization were improved by using a multidisciplinary approach based on HPLC, NMR and ES-MS analysis. In particular, FTIR microscopy was employed for the analysis of functional groups distributions and diffusion phenomena in Synbeads, revealing bead properties never disclosed before.

Figure 1 shows the chemical distribution of carbonyl ester group, the most characteristic of methacrylic matrix, for the un-functionalized Synbeads A310 that highlight a quite uniform functional-group distribution at bead *core* level, without the presence of clusters and aggregations, reflecting the optimized homogeneous polymerization mechanism.

For studying the kinetic of reagent diffusion inside the bead, the amidation reaction of amino-terminated A310 Synbeads with 3-nitropropionic acid (see Figure 2(a)) was followed at different reaction time (10 to 60 minutes), monitoring the nitro-group absorption band centered at 1555  $\text{cm}^{-1}$ . The advancement profile of the reaction, shown in Figure 2(b), suggest that the reactants fast reach the bead core efficiently saturating the matrix functional groups, as also suggested by NMR and ninhydrin test. To verify this hypothesis, thin bead slices at different reaction times were mapped along their diagonal by means of SR FTIR microscopy. Only SR brightness guaranteed to achieve the spatial resolution and S/N spectra ratio needed for such a kind of analysis. It was possible to verify for the first time that in the first reaction minutes the bead core was preferentially functionalized with respect to the external shell (see Figure 2(c)). Moreover, while the degree of functionalization of the core did not change significantly in time, the degree of functionalization of external regions increased, reaching an almost homogenous distribution of products at reaction completion.

The proposed approach is non-damaging and label-free, based on the vibrational pattern of molecules, and has the potentialities to be extended to any type of solid support.

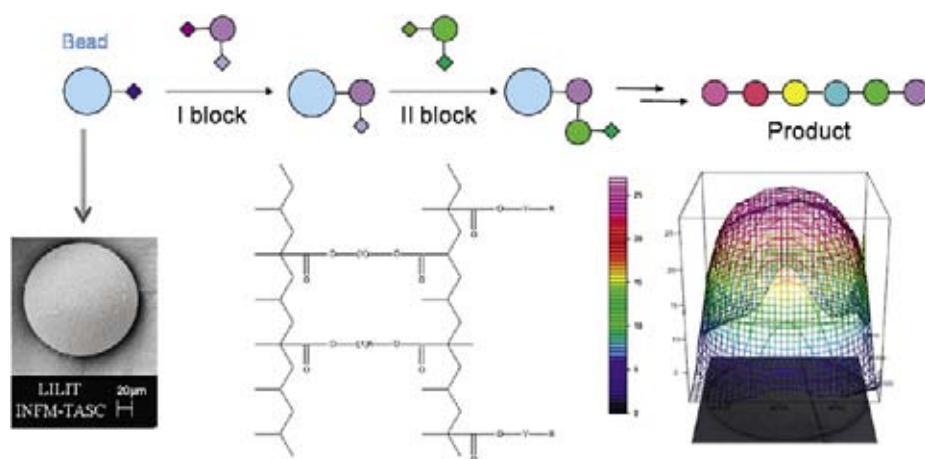


**Figure 1.** (Top) Sketched of the general synthetic approach common to reaction supported on solid beads. (Bottom) From the left to the right (a) SEM image of a single bead Synbead A310 matrix (b) Chemical design of Synbeads. For the specific case of Synbead A310,  $R = NH_2$  (c) 3D chemical image of the carbonyl ester group distribution (integration interval  $1764-1681\text{ cm}^{-1}$ ) in un-functionalized Synbead A310. The colour scale represents the integral values in arbitrary units (a.u.). The optical image of the bead section is also shown at the bottom of 3D chemical image. Data have been collected with conventional source and bidimensional FPA detector, 64 accumulation scans and  $4\text{ cm}^{-1}$  spectral resolution. The spatial resolution is  $5.3\text{ }\mu\text{m}$ .

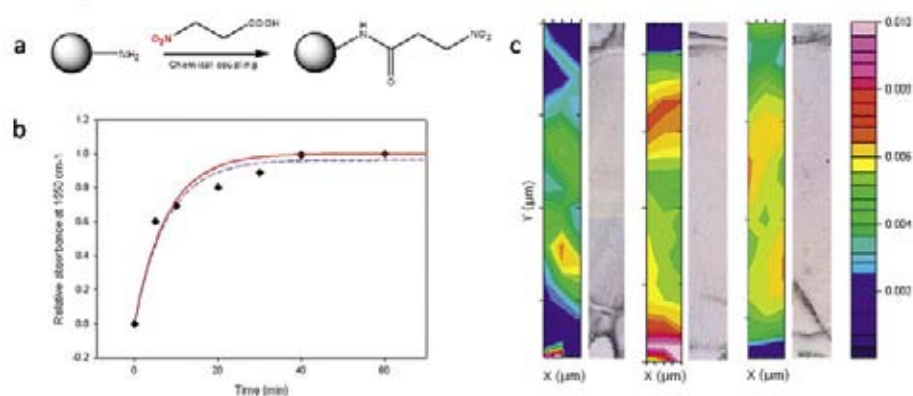


**Figure 2.** (a) Scheme of the amidation reaction of Synbead A310 with nitropropionic acid; (b) Kinetic of the reaction of functionalization of Synbead A310 with nitropropionic acid, evaluated by FTIR-ATR spectroscopy. The concentration of nitrogroup normalized on carbonyl ester matrix is reported as a function of reaction time; (c) Nitro-group distribution normalized on carbonyl group for 10, 40 and 60 minutes of reaction. Data have been collected with SR source and MCT detector, 512 accumulation scans,  $4\text{ cm}^{-1}$  spectral resolution and  $10\text{ }\mu\text{m}$  spatial resolution.

## References

- [1] T. Bruckdorfer, O. Marder, F. Albericio, *Curr. Pharm. Biotechnol.* **5**, 29 (2004).
- [2] A. Basso, P. Braiuca, C. Ebert, L. Gardossi, P. Linda, *J. Chem. Technol. Biotechnol.* **81**, 1626 (2006).
- [3] Patent n. MI2007A000782 of 17/04/2007 “Prodotti di supporto per la sintesi in fase solida e processo per la loro preparazione”.
- [4] L. Sinigoi, P. Bravin, C. Ebert, N. D’Amelio, L. Vaccari, L. Ciccarelli, S. Cantone, A. Basso, L. Gardossi, *J. Comb. Chem.* **11**, 835 (2009).

# NUCLEATION AND GROWTH OF DEOXYGUANOSINE 5'-MONOPHOSPHATE QUADRUPLEXES IN DILUTE SOLUTION STUDIED BY SAXS

P. Mariani<sup>1</sup>, F. Spinozzi<sup>1</sup>, F. Federiconi<sup>1</sup>, H. Amenitsch<sup>2</sup>, L. Spindler<sup>3</sup>, I. Drevensek-Olenik<sup>4</sup>

<sup>1</sup>Dipartimento SAIFET, Università Politecnica delle Marche, Ancona, Italy

<sup>2</sup>Institute of Biophysics and Nanosystems Research, Graz, Austria

<sup>3</sup>J. Stefan Institute, Ljubljana, and University of Maribor, Maribor, Slovenia

<sup>4</sup>J. Stefan Institute, and University of Ljubljana, Ljubljana, Slovenia

E-mail: mariani@univpm.it



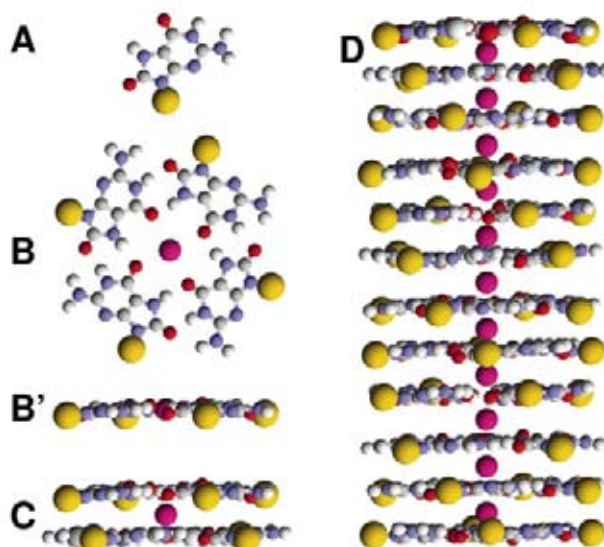
SAXS

Since the early studies [1], nucleic acids have revealed themselves to be far more polymorphic than originally assumed. Interestingly, even the non-Watson-Crick structures have been demonstrated to be implicated in biological events, thereby making them more than laboratory curiosities. G-quadruplexes are 4-fold helical structures spontaneously formed in solution by guanine-rich sequences in the presence of alkaline ions [2]. They are built by the vertical stacking of G-quartets, which are planar arrangements of four guanines, stabilized by hydrogen bonding. G-quadruplexes received broad attention in the last decades: indeed, quadruplex forming sequences were identified both in eukaryotic telomeres (*i.e.*, the region of repetitive DNA at the ends of chromosomes, where the enzyme telomerase, responsible for maintaining the length of telomeres and involved in around 85% of all

cancers, explicates its activity), as well as in a number of non-telomeric genomic DNA [1]. Besides this, G-quadruplexes have drawn attention in nanoelectronics, as G-quartets have been proposed as building blocks for molecular nanowires [2,3]. Compared to DNA, the G-quartet stacking is expected to provide better conditions for  $\pi$ -overlap and better stability under various external conditions, increasing the probability of charge transport through the wires.

Thermodynamic as well as structural information are required to develop a complete understanding of the critical interrelationships among structure, energetic, and biological function of G-quadruplexes. In this frame, the 2-deoxyguanosine-5'-monophosphate, d(pG), can be regarded as a useful model [2-4]: despite the absence of sugar-phosphate backbone, d(pG) in aqueous solutions and in the

**Figure 1.** Representation of the different d(pG) assembled forms observed in solution: (A) guanine; (B and B') G-quartet, top and lateral views; (C) G-octamer, lateral view. The  $K^+$  is located between the two stacked quartets; (D) G-quadruplex, lateral view. The yellow spheres represent the sugar and phosphate groups.



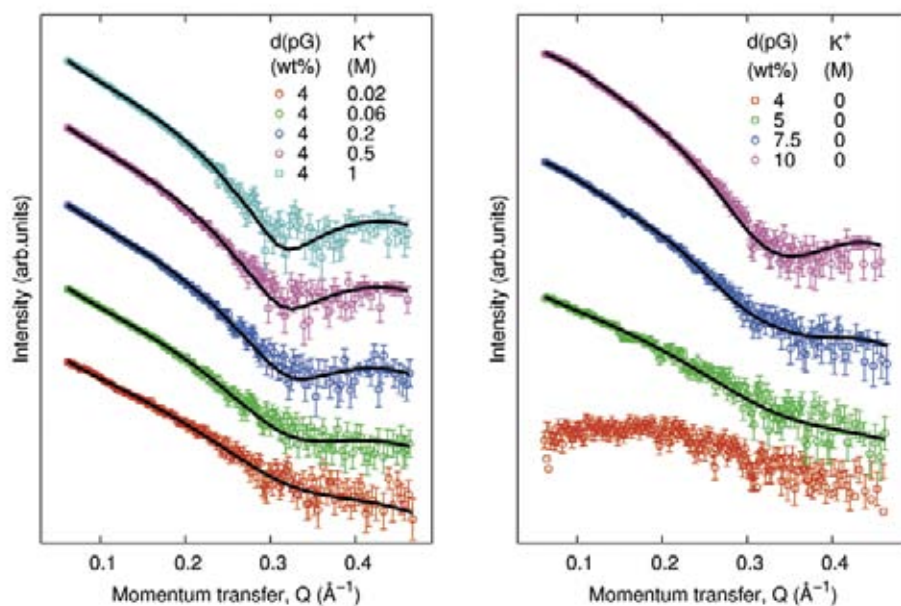


**Figure 2.** SAXS profiles observed in different experimental conditions, reported in the legend. Best fitting curves are shown in solid. Data are scaled by a proper factor.

presence of alkaline ions forms quadruplexes, as shown in Figure 1. The cation, located between two G-quartets, stabilizes the quartets by coordination of the oxygen atoms in the tetramer cavity, enhancing base-stacking interactions.

To detail the d(pG) quadruplex formation in dilute conditions, small angle X-ray scattering (SAXS) experiments have been performed at the Elettra SAXS beamline, as a function of d(pG) concentration (from 4 to 10 wt%) and at a fixed d(pG) concentration (4 wt%) but in the presence of KCl, from 0.01 to 1 M [4]. A few results are shown in Figure 2. A global fit analysis showed that only a few aggregate species (free d(pG), G-quartets, G-octamers, and monodisperse G-quadruplexes) are present in solution. Moreover, the self-assembling process resulted strongly dependent on excess  $K^+$ , which induces aggregation and quadruplex growth.

The thermodynamics of the self-assembling was then analyzed in the framework of a nucleation-elongation model, in which an unfavorable nucleation step, leading to quartets and octamers, is followed by a favorable spontaneous elongation. To account for the monodisperse length of quadruplexes, an additional process, based on a balance between annealing, which favours longer assemblies, and fragmentation, which favours shorter ones, was considered. The analysis showed that the nucleation step is strongly affected by excess  $K^+$ , resulting in a decrease of the criti-

cal concentration at which assembling starts to occur and confirming that G-quartet formation is definitely controlled by cations. As G-quartet and G-octamer formation still remains the disfavoured step, the  $K^+$ -induced elongation was recognized to play the major role in determining the final composition of the different assembled species. Indeed, the assessed annealing and fragmentation rate constants confirmed that the stabilization of the stacking process induced by  $K^+$  is the main reason for the formation of longer quadruplexes in salted water.

The discovered  $K^+$  effect is very important in telomere biology, as it has been reported that cations determine the type of quadruplex formed (*e.g.*, parallel *vs.* antiparallel) and a higher selectivity for  $K^+$  against  $Na^+$  ions has been found [1]. Moreover, the exceptional stability of G-quadruplexes *in vitro* in the presence of  $K^+$  and the topology of their 3D structure have inspired models for a special functionality of telomere and suggested that it can be targeted for anticancer drug design [1,4].

## References

- [1] S. Burge *et al.*, *Nucleic Acids Res.* **34**, 5402 (2006).
- [2] J.T. Davis, *Angew. Chem. Int. Ed.* **43**, 668 (2004).
- [3] K. Kunstelj *et al.*, *Coll. Surf. B: Biointerfaces* **59**, 120 (2007).
- [4] P. Mariani *et al.*, *J. Phys. Chem. B* **113**, 7934 (2009).

# TAUTOMERISM IN DNA/RNA BASES: AN EXPERIMENTAL AND THEORETICAL CORE LEVEL SPECTROSCOPIC STUDY

O. Plekan<sup>1,2</sup>, V. Feyer<sup>1</sup>, R. Richter<sup>1</sup>, M. Coreno<sup>3</sup>, G. Vall-Ilosera<sup>4</sup>, K.C. Prince<sup>1,5</sup>, A.B. Trofimov<sup>6,7</sup>, I.L. Zaytseva<sup>6</sup>, T.E. Moskovskaya<sup>6</sup>, E.V. Gromov<sup>6,8</sup>, J. Schirmer<sup>8</sup>

<sup>1</sup>Sincrotrone Trieste S.C.p.A., Trieste, Italy

<sup>2</sup>Permanent address: Institute of Electron Physics, Uzhgorod, Ukraine

<sup>3</sup>CNR-IMIP, Montelibretti, Rome, Italy

<sup>4</sup>Department of Physics, Royal Institute of Technology, Stockholm, Sweden

<sup>5</sup>Laboratorio Nazionale TASC, INFN-CNR, Trieste, Italy

<sup>6</sup>Laboratory of Quantum Chemistry, Irkutsk State University, Irkutsk, Russia

<sup>7</sup>Favorsky Institute of Chemistry, Irkutsk, Russia

<sup>8</sup>Physikalisch-Chemisches Institut, Universität Heidelberg, Heidelberg, Germany

E-mail: prince@elettra.trieste.it



GASPHASE

Tautomerism is a form of isomerism which occurs in some nucleic acid bases (NABs) and may have some relevance to genetic mutations, when rare tautomers are incorporated into genetic material. Of the five NABs of DNA and RNA, guanine and cytosine have significant populations of two or more tautomers in the gas phase, whereas uracil, adenine and thymine exist only as single isomers [1-3]. The most important types of tautomerism in this class of compounds are amino-oxo, amino-hydroxy and amine-imine forms. Further conformers (rotamers) exist, based on rotation of hydroxyl and imine groups to give *cis* and *trans* isomers.

Nowadays most of our knowledge about geometrical structure (tautomers, conformers) of DNA/RNA bases and their derivatives comes from microwave, infrared and matrix isolation studies. However laser ablation and jet cooling are thermally non-equilibrium processes, therefore the measured tautomer populations are not necessarily related to equilibrium thermodynamic parameters, while the matrix experiment does not give absolute values for the absorption intensities, but only relative values because the precise concentration and optical path length are not known. Thus the population and thermodynamic parameters, such as Gibbs free energies, enthalpy and entropy, of molecular tautomers extracted from the above methods must be supported by detailed calculation. Due to these difficulties some controversy existed about the number of tautomers of NABs in the gas phase. The advantage of X-ray photoemission spectroscopy

of thermally evaporated compounds is that the sample is in thermal equilibrium, and the core level photoemission intensities well above threshold are directly proportional to the population of the corresponding chemical state.

Figure 1 shows the oxygen 1s photoemission spectra of four NABs. The spectra of cytosine and guanine manifest two peaks, while a single peak is observed in the spectra of uracil and thymine. Cytosine and guanine molecules contain only one oxygen atom, so the presence of different features directly indicates the presence of more than one chemical species (see Figure 1).

In Figure 1, the theoretical data are also shown as bars. The vertical ionization transitions were computed using the fourth-order algebraic-diagrammatic construction approximation scheme for the one-particle Green's function adapted for the case of *K*-shell ionization by means of an additional core-valence separation approximation. The calculations reproduce the experimental XPS energies and intensities very well (see Figure 1).

Our results clearly demonstrate that the features at lower binding energy in O 1s photoelectron spectra of cytosine and guanine originate from the ionization of oxo tautomers. The lowest energy O 1s band of cytosine spectrum shows a maximum and shoulder associated with the ionization of amino-oxo and imino-oxo tautomers, respectively. The maxima at higher binding energy are assigned to the two closely spaced ionization lines belonging to the hydroxy type tautomers. In this pair of

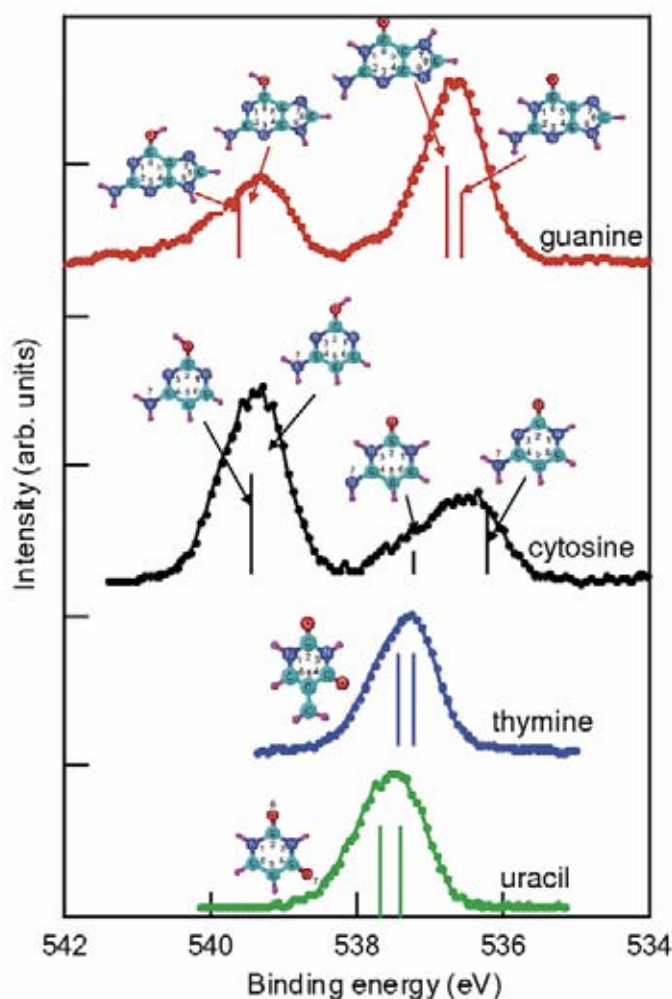


**Figure 1.** O 1s photoelectron spectra of nucleic acid bases; bars indicate calculated binding energies.

rotamers, the electronic structure is only slightly different, and so the ionization energies differ by very little, as expected.

Our calculations predict various two-hole-one-particle (2h-1p) photoelectron satellites, most of which have very small spectral intensities. Thus the satellites are not observed in the experimental spectrum of cytosine. However, we associated the weak maximum at 540.7 eV in the O 1s photoionization spectrum of guanine with two oxo tautomers. These 2h-1p satellites can be viewed as ionization of the O 1s orbitals plus  $\pi$ - $\pi^*$  excitations from the highest occupied to the lowest unoccupied molecular orbitals.

Based on the above-mentioned advantages of core level photoemission spectroscopy, the area of the fitted Gaussian peaks, with the widths and energies as free parameters, directly correspond to the population of different cytosine and guanine tautomers in the gas

phase. The small deviations expected (of the order 10%) can be corrected by theoretical calculations, which also provide an assignment of the spectral features [2,3].

For uracil and thymine, Figure 1, our calculations predict that the two non-equivalent oxygen core levels give rise to two closely spaced lines, resulting (after convolution) in one broad peak. This is in agreement with experiment where also only single maxima are observed. These results confirm the absence of oxo-hydroxy tautomerism for uracil and thymine at the present experimental condition [1].

#### References

- [1] O. Plekan *et al.*, *Chem. Phys.* **347**, 360 (2008).
- [2] V. Feyer *et al.*, *J. Phys. Chem. A* **133**, 5736 (2009).
- [3] O. Plekan *et al.*, *J. Phys. Chem. A* **133**, 9376 (2009).

# LEADING NEURONS WITH CARBON NANOTUBES

G. Cellot<sup>1</sup>, D. Scaini<sup>2</sup>, L. Casalis<sup>2</sup>, M. Prato<sup>3</sup>, Michele Giugliano<sup>4</sup>, L. Ballerini<sup>1</sup>

<sup>1</sup>Life Science Department, University of Trieste, Trieste, Italy

<sup>2</sup>Sincrotrone Trieste S.C.p.A., Trieste, Italy

<sup>3</sup>Department of Pharmaceutical Science, University of Trieste, Trieste, Italy

<sup>4</sup>Laboratory of Neural Microcircuitry, EPFL, Switzerland

E-mail: denis.scaini@elettra.trieste.it, loredana.casalis@elettra.trieste.it

Recent advances in nanotechnology have stimulated a renewed interest in the development of novel biomaterials that could potentially be used for promoting brain recovery and for improving neuronal signaling after injury. Carbon nanotubes (CNTs), in particular, with their intriguing chemical and physical properties, are promising materials for developing neural prosthesis [1,2]. It has been shown that, when carefully functionalized and purified, CNTs are not poisoning for neurons, which can grow and form networks on top of them, and propagate electrical signals stimulated by them. As a result, CNTs are the top candidates for restoring sensory and motor functions, and represent potential new tools for monitoring and/or modifying neural activity.

In spite of the extreme relevance of these systems, details about the interaction between nanotubes and neurons are still lacking. Towards this end, Laura Ballerini and Maurizio Prato, from University of Trieste, set up an international team composed of several groups to gather the expertise needed to address this complex issue.

The most rapid and complex signaling in eukaryotes is mediated by nerve impulses. Nerve cells, or neurons, interact with other cells and receive information from them in form of nerve impulses. The cell body (soma) assimilates the information derived from a number of dendritic contacts, and transmits the information in form of another nerve impulse down to the large axon. The axon ends at the synapse where it makes contact with the post-synaptic target cell. Upon stimulation, the neuron plasma membrane depolarizes, i.e. the membrane potential rises rapidly from the resting potential ( $\approx -60$  mV) to approximately +40 mV: an action potential is then generated and propagated along the axon towards the next

neuron. In neurons with extensive dendrites near the soma, such as some neurons found in the hippocampus, the action potentials can sometimes travel in the opposite direction. The backpropagating current induces a voltage change that increases the concentration of  $\text{Ca}^{2+}$  in the dendrites—an event known as calcium electrogenesis—and can be measured through the presence of a slow membrane depolarization following repetitive action potentials.

The team lead by Laura Ballerini provides a new mechanistic insight into how nanotubes favour the backpropagation of the action potential and target the integrative properties of neurons (*Nature Nanotechnology* **4**, 126 (2009)). Whole-cell patch clamp experiments were performed on hippocampal neurons cultured on planar CNT substrates (Figure 1). To study the contribution of CNTs to neuronal electrical regenerative properties, the whole-cell current-clamped single neurons were stimulated to discharge a train of six action potentials (APs). The integrated membrane potential changes occurring after the last AP of the train were analyzed and categorized as: a) after depolarization potential (ADP), b) neutral response (NR), or c) after hyperpolarization potential (AHP). Interestingly, hippocampal neurons, which intrinsically show a high degree of dendritic branching, displayed a distribution of post-train responses biased towards ADP when grown on CNT, in contrast to the distribution obtained from neurons cultured on plain glass coverslips.

Nanotubes substrates are electrically conductive and feature a nanoscale meshwork. In order to clarify whether both these physical properties are linked to ADP generation, hippocampal neurons were also cultured on two other substrate types: indium tin oxide (ITO), a perfectly flat conductive substrate and a non-



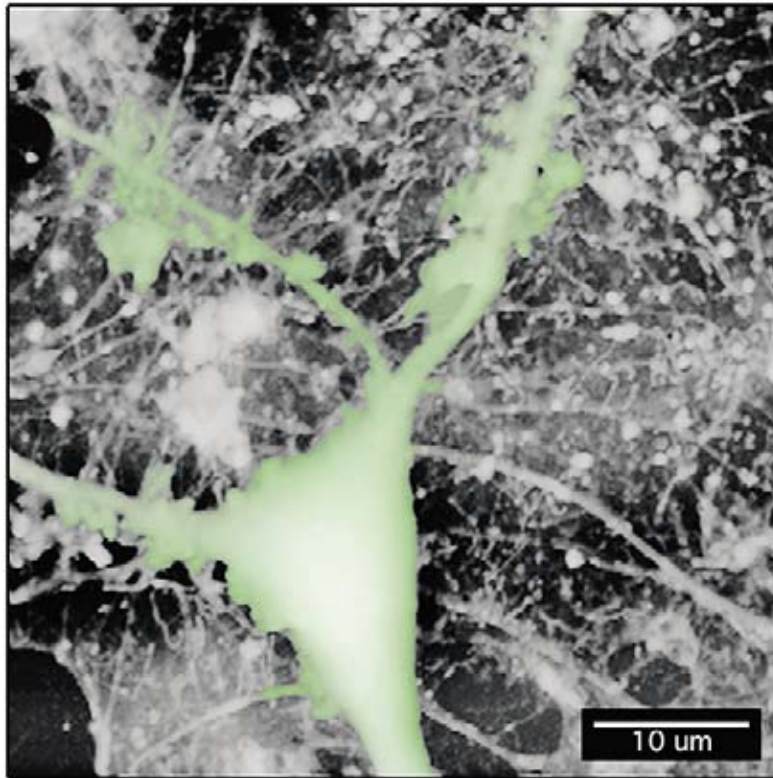


**Figure 1.** AFM topographic image of a neuron (pseudo-coloured in green) growing on a carbon nanotube carpet.

conductive substrate containing instead nanoscale features similar to carbon nanotubes (RADA16 peptides). In both cases neurons did not show significantly enhanced after-depolarization, demonstrating that this effect is specific to CNTs.

The precise mechanism at the base of nanotube-induced potentiation of neuronal activity is still not completely understood. Atomic force microscopy (AFM) images taken at the laboratory SENIL (SISSA/Elettra NanoInnovation Laboratory) @Elettra, and transmission electron micrographs (TEM) of neurons grown on CNTs suggest that one mechanism might rely on the detected discontinuous and tight contact between nanotubes and membranes. Nanotubes may be effectively short-circuiting the dendrites and soma — that is, diverting the electrical activity through the nanotubes — and this may be sufficient to account for the enhanced after-depolarization of neurons grown on nanotubes. Alternatively, such hybrid areas might be characterized by a nanotubes induced clustering of calcium channels. However, morphological modifications induced by the nanotubes substrates might cer-

tainly have an impact on “backpropagation” of action potentials, although significant changes in the passive neuronal membrane properties could be ruled out.

As already emphasized by G. A. Silva in the “news and views” that accompanies our paper [3], “understanding the mechanisms that underlie the effect of carbon nanotubes on neural cells will be critical for designing functional neural devices based on empirical data and engineering principles, rather than qualitative trial-and-error approaches. The engineering challenges involved demand this, but the potential impacts of successfully interfacing carbon nanotube devices with neural cells will be well worth it”.

#### References

- [1] G. Massobrio, P. Massobrio, S. Martinoia, *Nano Lett.* **8**, 4433 (2008).
- [2] A. Kepecs, Lisman, *Net. Comp. Neural. Sys.* **14**, 103 (2003).
- [3] G.A. Silva, *Nature Nanotech.* **4**, 82 (2009).
- [4] S. Chen, Y. Yaari, *J. Physiol.* 586, 1351 (2008).



THEORY@ELETTRA

$G(E)$   
 perturbation series (Fig. 15a)

diagrams in conventional "propagator" theory  
 diagrams in "locator" theory

$$G(E) = \sum_{\nu} \frac{V_{\nu} V_{\nu} V_{\nu}}{(E - E_{\nu})^2} + \dots \quad (13)$$

since  $E_{\nu}$  is a continuum, has a finite imaginary part as  $E$  approaches

$$\frac{1}{E - E_{\nu}} \rightarrow \frac{1}{E - E_{\nu} - i\eta} + \pi \delta(E - E_{\nu}) + \dots \quad (14)$$

comes from the width  $\eta$  (not  $V_{\nu}$ )  
 has a finite width in energy, and  $\text{Im}G$ , the  
 cross function of  $E$  (Fig. 16)

$$\frac{1}{\sum_{\nu} \delta(E - E_{\nu})} \quad (15)$$

of energy state



# SURFACE CORE LEVEL SHIFT: HIGHLY SENSITIVE PROBE TO OXYGEN-INDUCED RECONSTRUCTION

L. Bianchettin<sup>1</sup>, A. Baraldi<sup>1,2</sup>, S. de Gironcoli<sup>3,4</sup>, E. Vesselli<sup>1,2</sup>, S. Lizzit<sup>5</sup>, G. Comelli<sup>1,2</sup>, R. Rosei<sup>1,2</sup>

<sup>1</sup>Physics Department, University of Trieste, Italy

<sup>2</sup>Laboratorio Nazionale TASC INFN-CNR, Trieste, Italy

<sup>3</sup>International School for Advanced Studies of Trieste, Trieste, Italy

<sup>4</sup>CNR-INFN DEMOCRITOS, Theory@Elettra Group, Trieste, Italy

<sup>5</sup>Sincrotrone Trieste S.C.p.A., Trieste, Italy

E-mail: degironc@sissa.it, baraldi@elettra.trieste.it



The measurement of Surface Core Level Shifts (SCLS) by means of synchrotron radiation, high-resolution x-ray photoelectron spectroscopy represents a powerful tool, extremely sensitive to the atom- or molecule-surface interactions and capable of providing, for specific systems, direct information about the trends in chemical reactivity of transition metal surfaces [1]. Because of their localized nature, core electrons are influenced by the electronic charge redistribution (charge transfer, polarization, hybridization, etc.) resulting from the creation of adsorbate-substrate bonds. This property has been exploited in a large variety of surface structures, such as oxide thin films, surface defects, and hydrogen chemisorbed phases. It is therefore expected that also the strain/stress induced on surfaces by atomic and molecular adsorption should induce changes in the core electron binding energies of similar magnitude as that observed in the case of under-coordinated transition metal atoms, where a strong interplay between the coordination number and the local bond strain was found.

A peculiar class of surface structures where the potential of the surface core level shift approach can be employed is represented by the reconstructed surfaces with a reduced symmetry, where chemisorption determines a large distortion of lattice parameters. Here, the local character of the information derived from SCLS measurements and calculations can be used to unveil how the combined changes in surface- and electronic-structure affect the local chemical reactivity of transition metal surfaces.

A specific case belonging to this class is the clock reconstruction of Rh(100). The latter structure, induced by 0.5 ML of adsorbed

oxygen, is described as a  $(2 \times 2)pg$  with the oxygen atoms sitting in threefold sites, along the main diagonal of the rhombus created by the substrate rotation [2,3]. The local atomic arrangement is peculiar, with a remarkable 11% distortion of the nominal (100) terminated bulk lattice, which can be considered as the onset of oxygen subsurface penetration in the surface oxide formation process.

We have investigated the oxygen-induced reconstruction of Rh(100) by combining first-principles Density Functional Theory simulations with synchrotron radiation high-energy resolution x-ray photoelectron spectroscopy [4].

*Ab initio* calculations made it possible to identify the origin of the different components contributing to the Rh $3d_{5/2}$  core level spectra (reported in Figure 1(a)) measured at the SuperESCA beamline during the oxygen adsorption up to the reconstructed phase. In the  $(2 \times 2)pg$  structure, shown in Figure 1(b), oxygen adsorbs off the rhombus centre thus generating two non equivalent surface atoms (Figure 1(c)), which are characterized by considerably different core level shifts, dominated by initial state effects. In this asymmetrically reconstructed phase, the computed SCLS values for the two non equivalent surface atoms Rh $_{10}$  and Rh $_{20}$  are -185 and +140 meV, respectively, in very good agreement with the measured shifts of -195 and +115 meV.

In addition, the theoretical approach allowed us to unravel the existing correlation between the surface core level shifts and the electronic structure properties, in particular the d-band average energy displacement  $\Delta B_d$ . Indeed the Hammer-Nørskov model proposes to use the d-band centre  $B_d$  as an indicator of

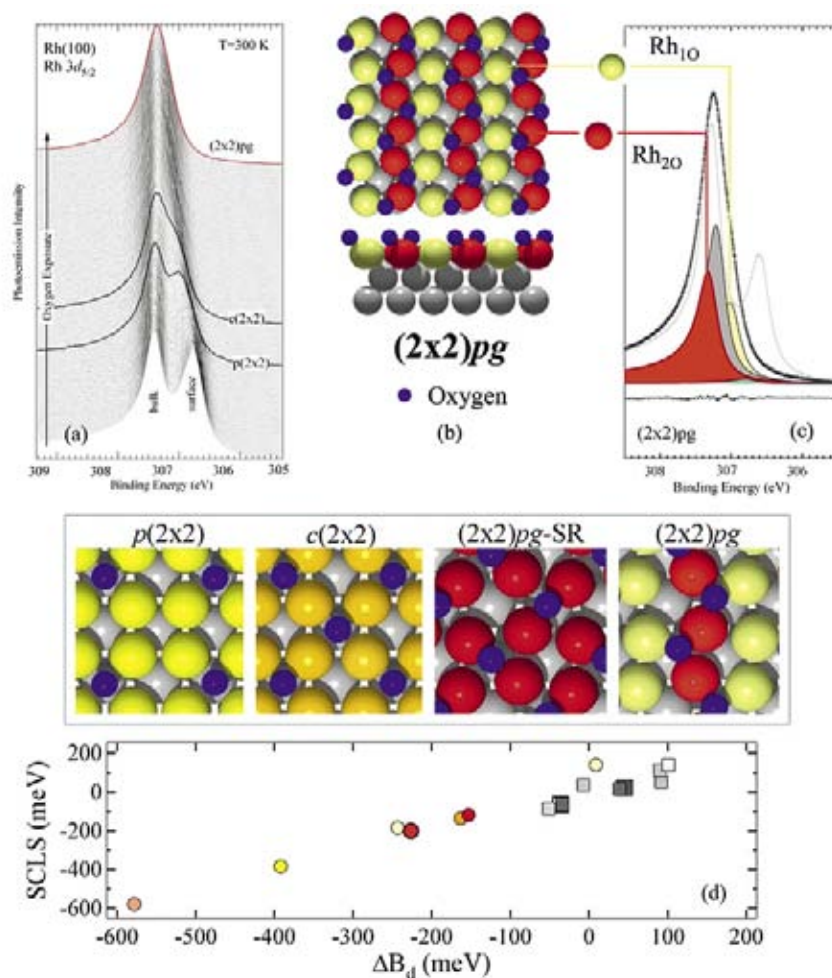


**Figure 1.** (a) Series of Rh $3d_{5/2}$  core level spectra acquired during oxygen uptake at T=300 K. (b) Top and side views of the structural model for the (2×2)pg. (c) High-energy resolution Rh $3d_{5/2}$  core level spectrum from the (2×2)pg-O structure. Thin grey curve is the spectra from the clean Rh(100) surface. (d) Calculated SCLS plotted as a function of the d-band centre displacement  $\Delta B_d$  for all the non equivalent first (circles) and second layers (square) atoms of the four adsorptions structures reported in the top panel. Different colours correspond to non equivalent atoms.

the local surface chemical reactivity. Our study shows that the SCLS versus  $\Delta B_d$  linear relationship holds for the oxygen-induced reconstruction of Rh(100), as shown in Figure 1(d), confirming that SCLS can be used to evaluate the surface chemical reactivity changes when calculated final state effects contributions are small.

## References

- [1] A. Baraldi, S. Lizzit, G. Comelli, M. Kiskinova, R. Rosei, K. Honkala, J.K. Nørskov, *Phys. Rev. Lett.* **93**, 046101 (2004).
- [2] D. Alfè, S. de Gironcoli, S. Baroni, *Surf. Sci.* **437**, 18 (1999).
- [3] A. Baraldi, J. Cerda, J.A. Martin-Gago, G. Comelli, S. Lizzit, G. Paolucci, R. Rosei, *Phys. Rev. Lett.* **82**, 4874 (1999).
- [4] L. Bianchettin, A. Baraldi, S. de Gironcoli, E. Vesselli, S. Lizzit, G. Comelli, R. Rosei, *J. Phys. Chem. C* **113**, 13192 (2009).

# OPTIMAL REPRESENTATION OF THE POLARIZATION PROPAGATOR FOR LARGE-SCALE GW CALCULATIONS

P. Umari<sup>1</sup>, G. Stenuit<sup>1</sup>, S. Baroni<sup>1,2</sup>

<sup>1</sup>INFM-CNR Democritos, Trieste, Italy

<sup>2</sup>International School for Advanced Studies of Trieste, Trieste, Italy

E-mail: pumari@sissa.it



The Density-Functional Theory (DFT) has grown into a powerful tool for the numerical simulation of matter at the nanoscale, allowing one to study the structure and dynamics of realistic models of materials consisting of up to a few thousands atoms, these days. The scope of standard DFT, however, is limited to those dynamical processes that do not involve electronic excitations. The most elementary of such excitations is the removal/addition of an electron from a system originally in its ground state. These processes are accessible to direct/inverse photoemission spectroscopies and can be described in terms of quasi-particle (QP) spectra [1]. In insulators, the energy difference between the lowest-lying quasi-electron state and the highest-lying quasi-hole state is the QP band gap, a quantity that is severely (and to some extent erratically) underestimated by DFT. Many-body perturbation theory (MBPT), in turn, provides a general, though unwieldy, framework for QP and other excitation such as optical spectra. A numerically viable approach to QP energy levels (known as the GW approximation, GWA) was introduced

in the 60's [2], but it took two decades for a realistic application of it to appear [3], and even today the numerical effort required by MBPT is such that its scope is limited to systems of a few handfuls of atoms. Even so, and in spite of the success met by MBPT in real materials, the approximations made for the most demanding of its applications are such as to shed some legitimate doubts on their general applicability. We have introduced [4] a strategy to substantially reduce the computational cost of MBPT calculations. This is based on the adoption of Wannier-like orbitals to represent the response functions whose calculation is the main size-limiting factor of MBPT. Indeed, we introduced a scheme for constructing an optimal basis set for representing with controllable accuracy the polarizability operators. Although we focused on QP spectra within the GWA, this strategy easily generalizes to optical spectra. Our scheme has been implemented in the Quantum-Espresso density functional package, for norm-conserving as well as ultra-soft pseudopotentials. We have benchmarked our method

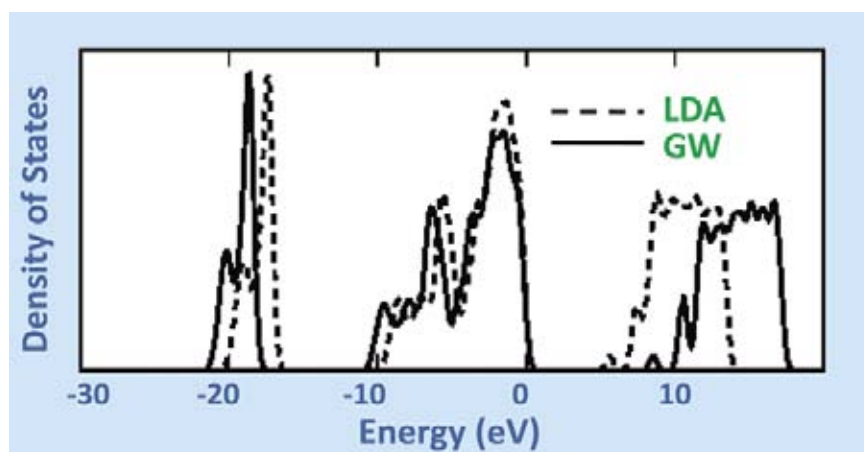


**Figure 1.** Electronic density of states for a model of vitreous silica: LDA (dashed line) and GW (solid line). A Gaussian broadening of 0.25 eV has been used.

calculating the vertical ionization potentials of the benzene molecule and the band structure of crystalline silicon, and then we demonstrated its potentialities by case calculations on vitreous silica and on the free-base tetraphenylporphyrin molecule. We think that this study will open the path to a widespread use of many-body perturbation theory approaches not only for the calculation of quasi-particle energies but also for the calculation of neutral excitations and of optical spectra. Similar ideas could also be used to implement efficient schemes for an accurate determination of the total energy of a system accounting also for dispersion terms, permitting therefore to calculate van der Waals forces. The idea of optimal basis sets could also be extended to other fields of computational physics. Now, we think that the most limiting factor of many-body per-

turbation theory approaches is the formalism which requires sums over empty states. Indeed, these sums converge very slow and at the moment results can be obtained only upon extrapolation. Therefore, we are working now on an extension of our method in order to reformulate the formalism for the calculation of the quasi particle energies in a way where explicit sums over empty states do not appear.

#### References

- [1] L. Hedin, S. Lundqvist, *Solid State Phys.* **23**, 1 (1969).
- [2] L. Hedin, *Phys. Rev.* **139**, A796 (1965).
- [3] M.S. Hybertsen, S.G. Louie, *Phys. Rev. Lett.* **55**, 1418 (1985).
- [4] P. Umari, G. Stenuit, S. Baroni, *Phys. Rev. B* **79**, 201104 (2009).

# BONDING AT THE ORGANIC/METAL INTERFACE: ADENINE ON Cu(110)

V. Feyer<sup>1</sup>, O. Plekan<sup>1</sup>, K.C. Prince<sup>1</sup>, F. Šutara<sup>2</sup>, T. Skála<sup>1</sup>, V.Cháb<sup>3</sup>, V. Matolín<sup>2</sup>, G. Stenuit<sup>4</sup>, P. Umari<sup>4</sup>

<sup>1</sup>Sincrotrone Trieste S.C.p.A., Trieste, Italy

<sup>2</sup>Faculty of Mathematics and Physics, Charles University, Prague, Czech Republic

<sup>3</sup>Institute of Physics, Academy of Science of the Czech Republic, Prague, Czech Republic

<sup>4</sup>INFN-CNR Democritos, Trieste, Italy

E-mail: pumari@sissa.it



The interaction of organic molecules with surfaces is of great current interest, both from applied (organic electronics, sensors, biocompatibility) and fundamental points of view. Nucleobases represent an important class of biomolecules, and in studies of their adsorption, adenine on Cu has drawn much attention as a prototypical case. On the Cu(111) surface, this molecule self-organizes into chains and networks, a phenomenon which may give insight into the origins of life and have applications in organic device technology [1]. Adenine also forms chains on Cu(110) which are chiral due to the low symmetry of this surface, and enantio-selective in their interactions with amino acids [2,3]. We studied the adsorption system adenine/Cu(110) by core level photoemission, x-ray absorption and ab initio cal-

culations. The experiments were performed at the Materials Science Beamline. The calculations were performed within the density-functional framework using the Quantum-Espresso package. We found [4] that the theory predicts the appearance of two phases: a parallel geometry at low concentration and a perpendicular one at high concentration. The predicted saturation coverage is 0.33 ML and this value was found in agreement with the measured saturation coverage, which is  $0.3 \pm 0.05$  ML. At low coverage, the molecule adsorbs nearly parallel to the surface and bonds by interaction of one amino and one imino nitrogen atom (see Figure 1). At high coverage adenine/Cu(110) undergoes a phase transition driven by the gain in the adsorption energy density and the bonding changes significantly. Now, the

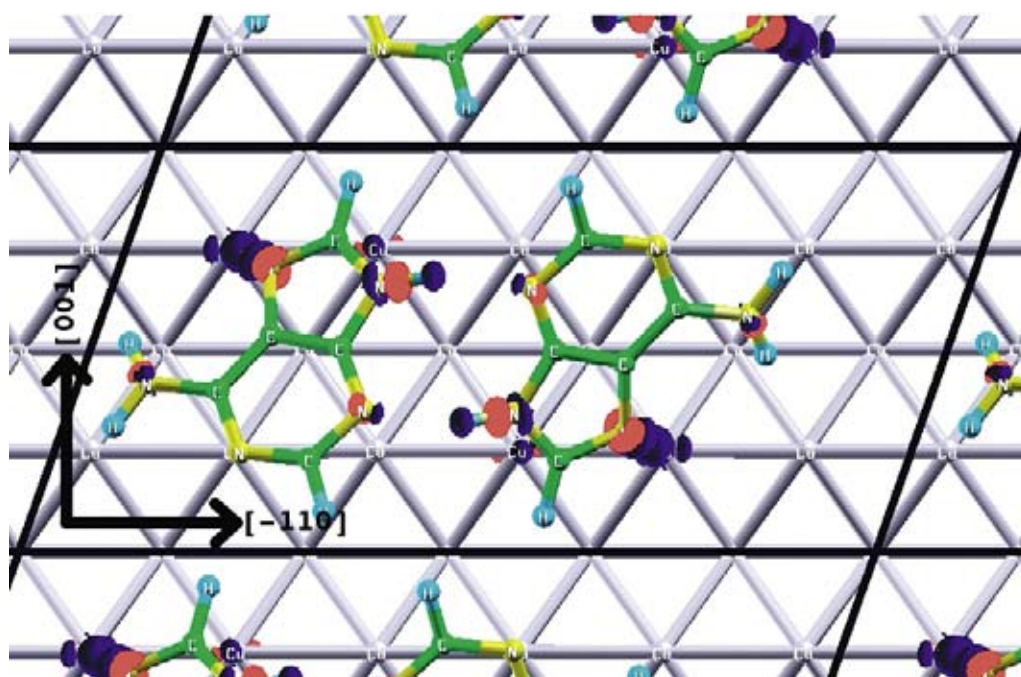


**Figure 1.** Total charge-density difference for adenine adsorbed in the parallel geometry. Regions of electron accumulation/depletion are in blue/pink; isosurface value:  $\pm 0.008 e/\text{Bohr}^3$ .



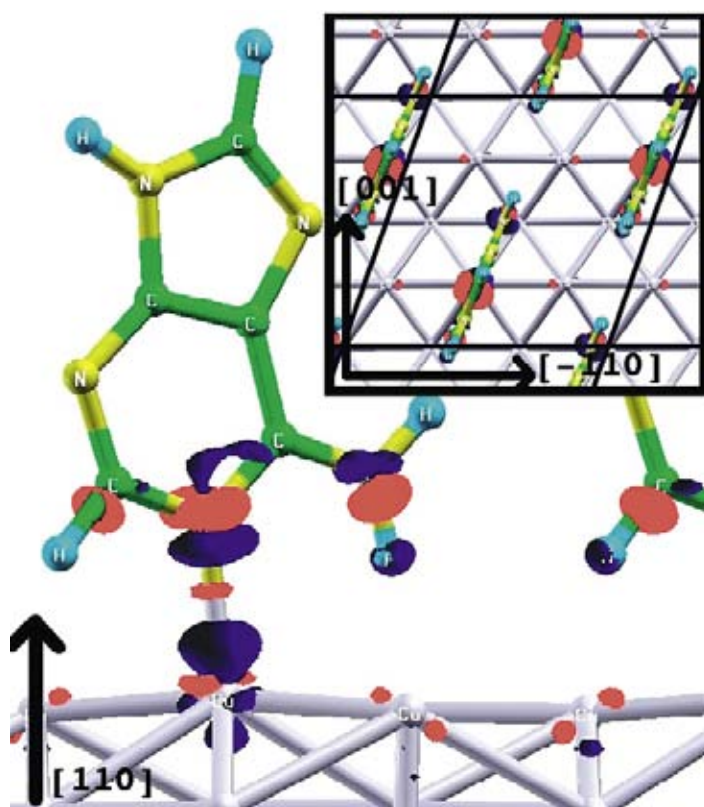


**Figure 2.** Total charge-density difference for adenine adsorbed in the tilted geometry. Regions of electron accumulation/depletion are in blue/pink; isosurface value:  $\pm 0.005$  e/Bohr<sup>3</sup>.

molecular plane is strongly tilted, and the bonding is markedly different (see Figure 2). For the calculated geometries we simulated the NEXFAS and the N 1s core level XPS spectra which were found to agree well with the experimental measurements. The angular dependence of the NEXAFS spectrum, as well as the N 1s core level spectrum, changes to reflect this re-orientation. These findings permitted to solve long-standing contradictions between calculated adsorbate geometries and published vibrational spectra. Compared to adenine adsorption on the less corrugated Au(111) surface, the bonding is markedly different. On Au, two phases are observed, but in both of them the molecules are nearly parallel to the surface, and physisorbed. On Cu(110) chemisorption bonds form and this appears to be the reason for the perpendicular geometry which is not observed on Au. Indeed, there is a general tendency for large, flat molecules to adsorb parallel to the surface at low coverage, particularly if the molecule contains unsaturated ring structures. How the adsorption geometry evolves is then determined by the nature of other functional groups, which are amine and imine groups for adenine, and the

relative strength of the interactions. The present study indicates the difficulty of understanding a system which had apparently been well-studied by STM, vibrational spectroscopy and theoretical calculations. The apparent contradictions between these studies have been finally resolved by this study. The results of this study will be useful for analyzing the adsorption of other nucleobases such as guanine, thymine, cytosine and uracil on metallic surfaces. However, in some cases the adsorption could result more complicated because of tautomerization processes. Our study also highlights the need for affordable first-principles schemes which would permit an accurate description on van der Waals forces.

#### References

- [1] M. Furukawa, H. Tanaka, K. Sugiura, Y. Sakata, T. Kawai, *Surf. Sci.* **445**, L58 (2000).
- [2] Q. Chen, D.J. Frankel, N. V. Richardson, *Langmuir* **18**, 3219 (2002).
- [3] Q. Chen, N.V. Richardson, *Nat. Mat.* **2**, 324 (2003).
- [4] V. Feyer, O. Plekan, K.C. Prince, F. Šutara, T. Skála, V. Cháb, V. Matolín, G. Stenuit, P. Umari, *Phys. Rev. B* **79**, 155432 (2009).

# INSIGHT INTO THE INITIAL STAGES OF OXIDATION ON GRAPHITIC SURFACES FROM PHOTOEMISSION SPECTROSCOPY AND DENSITY FUNCTIONAL THEORY CALCULATIONS

O. Barış Malcioğlu<sup>1,2</sup>, T. Sun<sup>1,2</sup>, S. Fabris<sup>1,2</sup>, A. Barinov<sup>3</sup>, L. Gregoratti<sup>3</sup>, M. Dalmiglio<sup>3</sup>, M. Kiskinova<sup>3</sup>

<sup>1</sup>INFM-CNR Democritos, Trieste, Italy

<sup>2</sup>International School for Advanced Studies of Trieste, Trieste, Italy

<sup>3</sup>Sincrotrone Trieste S.C.p.A., Trieste, Italy

E-mail: fabris@democritos.it



Many technological applications aim at tailoring the physical, chemical and electronic properties of Carbon-based materials by reshaping their honeycomb structure. Oxidation is considered to be the most promising and effective approach for selectively functionalizing the surface of these materials. As an example, functionalized graphene sheets can be produced by oxidation of graphite to graphite oxide. Identifying the oxygenated functional groups introduced in the C network during oxidation is a real challenge and there is a lot of controversy in this respect even for the simplest case of graphite oxide. There is no consensus in the literature regarding the type and relative abundance of the great variety of possible O-functional groups (epoxide, carbonyl, quinone, carboxylic, ether, ketonic, and others) that can form on the surfaces during the oxidation process. This work [1] identifies and characterizes the oxygenated functional groups resulting from the interaction of oxygen with the surface of 'perfect' and defective highly-ordered pyrolytic graphite (HOPG), during the initial oxidation stages.

The formation of C-O bonds on perfect and defective graphite was investigated under well-controlled oxidation conditions for HOPG surfaces with various concentrations of defects using high-resolution photoemission spectroscopy in combination with density functional theory calculations (DFT). We show that C-O-C epoxy groups are the dominant species formed on the perfect graphene surfaces, whereas on defective surfaces, the O atoms are trapped by the single and di-vacancies leading to the formation of both C=O semiquinone and C-O-C ether groups.

The experiments were performed on three sets of samples, differing in the density of surface defects: 'perfect' HOPG, defective HOPG

having density of vacancies of  $\sim 0.015$  and  $\sim 0.06$  ML. The following oxidation process was carried out by exposing these samples to a flux of atomic oxygen. The numerical DFT simulation modeled these systems as periodic graphite and graphene surfaces interacting with O atoms.

The O 1s spectra measured on the perfect and defective samples after exposure to O provide evidence that there are only three relevant surface species involving O atoms bonded on the HOPG surfaces (Figure 1(b)). The binding of the first oxygen atoms to the perfect graphene cage is characterized by a single O 1s component at 532.3 eV. Our DFT calculations, in agreement with previous studies [2], predict that in the initial oxidation stage the O atoms bind by bridging two C atoms of the non-defective graphite surface and form surface epoxy groups that are strongly bound to the hexagonal network of the surface (inset in Figure 1(a)). The O 1s component at 532.3 eV is attributed to the epoxy groups that are present on both 'perfect' and defective samples. The calculations allow for characterizing the two additional components measured on defective samples, one at higher BE, 533.5 eV, and the other at lower BE, 531.4 eV. These simulations allow us to conclude that the initial oxidation of the defective HOPG surfaces involves binding of pairs of O atoms at single and double C vacancies, yielding C-O-C ether and C=O ketonic functional groups. The calculations predict that the O 1s components of the two surface groups are shifted in opposite directions with respect to the epoxy O 1s BE, the ether towards higher and the ketonic towards lower BE.

The adsorption of O on perfect HOPG leads to the appearance of two new features in the C 1s BE spectrum (Figure 1(b)), one at larger

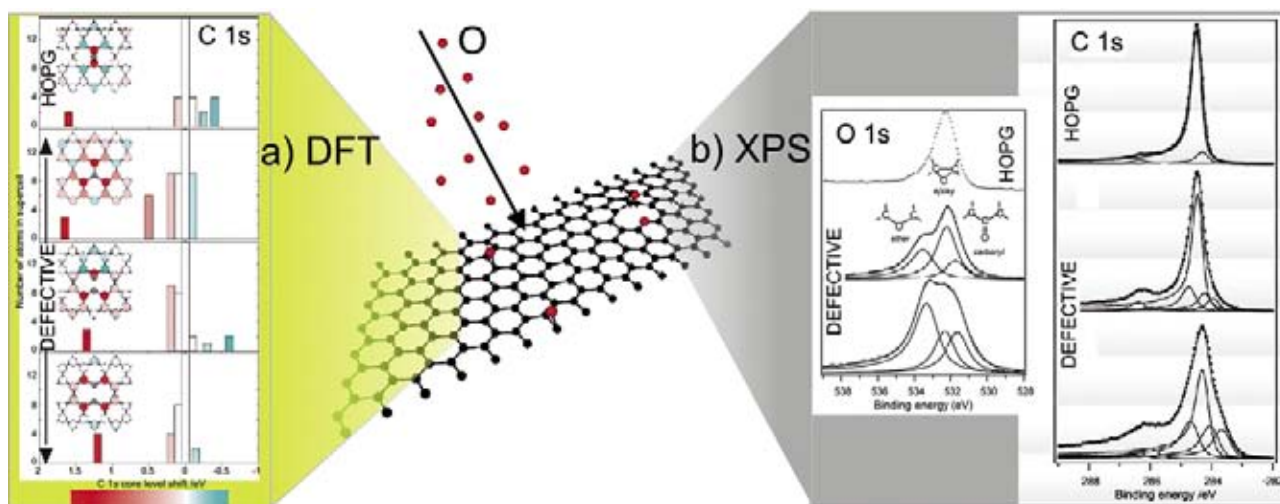


**Figure 1.** Numerical DFT simulations (a) and photoemission core-level XPS spectra (b) of the surface species resulting from the initial oxidation of defect free (HOPG) and defective graphite.

BE (+1.8 eV), and one at smaller BE (-0.3 eV). The C 1s BEs calculated for an epoxy group with respect to a C atom in undefective graphite (Figure 1(a)) are in good agreement with the photoemission spectra yielding a large positive chemical shift of +1.6 eV and a negative shift of -0.4 eV.

The oxidation of defective HOPG samples yields more structured C 1s photoemission spectra, shown in Figure 1 (right panel). Overall, the experimental C 1s spectra of the oxidized defective HOPG samples show the appearance of new features at large positive BE and clear shoulders at small negative and positive BE with respect to the main component of perfect graphite taken as 0 eV in the Figure 1(b). These components are rationalized on the basis of the simulated C 1s BE for the C atoms in the supercells modeling the different O binding configurations (Figure 1(a)). A large positive chemical shift is predicted for 1s levels of the C atoms neighboring the O atoms in the single vacancy (+1.4 eV shift for both the ether and ketonic groups) and in the divacancy (+1.2 eV shift for the ether group). The surface C atoms second neighbors to the O atom in the ketonic group display instead a negative core-level shift of -0.6 eV, thus larger than the negative component present in the epoxy group (-0.4 eV), while the C 1s level of the atoms second neighbor to the ether O atoms shift to small positive (+0.2 eV) BE. According to these

calculations, the presence of O atoms in single and double C vacancies of defective HOPG result into an overall broadening of the reference C 1s peak, in a new component with BE shifts of  $\sim -0.6$  eV, and in new components at large positive BE close to the epoxy feature but with smaller positive shifts (1.2-1.4 eV). This agreement with the experimental data allows us to associate the majority of the O atoms oxidizing the defective HOPG surfaces to the formation of ketonic and ether functional groups, in agreement with another study appeared in the literature concurrently to our work [3].

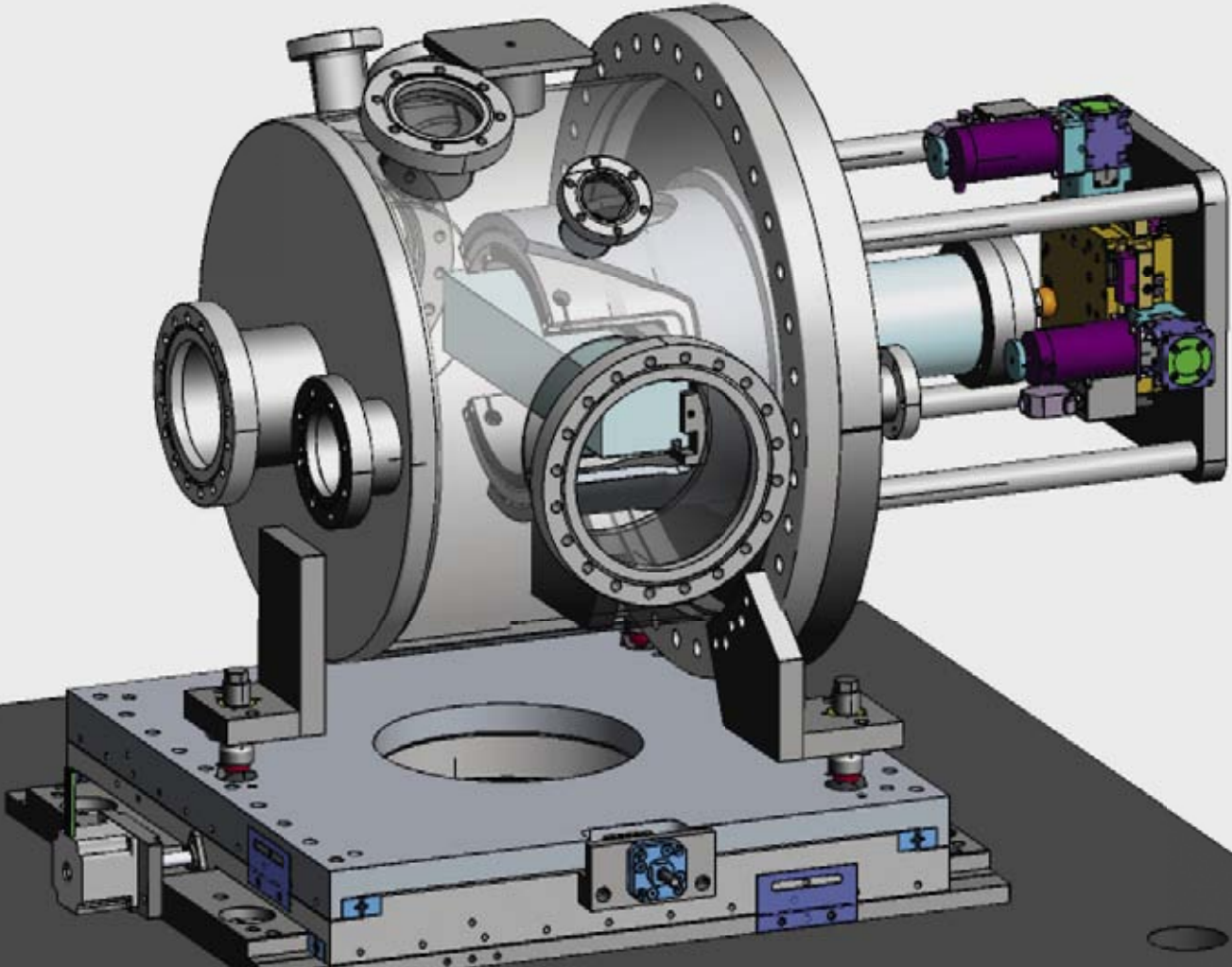
The presented results are the starting point of an ambitious program to unravel complex mechanisms of oxidation occurring in the advanced stages and/or at high temperature, when the formation of oxygen functional groups yields also gasification reactions with volatile CO and CO<sub>2</sub> products.

## References

- [1] A. Barinov, O.B. Malcioglu, S. Fabris, T. Sun, L. Gregoratti, M. Dalmiglio, M. Kiskinova, *J. Phys. Chem. C* **113**, 9009 (2009).
- [2] J.-L. Li, K.N. Kudin, M. J. McAllister, R. K. Prudhomme, I. A. Aksay, R. Car, *Phys. Rev. Lett.* **96**, 96, 176101 (2006).
- [3] K.A. Mkhoyan, A.W. Contryman, A. Silcox, D.A. Stewart, C. Mattevi, S. Miller, M. Chhowalla, *Nano Lett.* **9**, 1058 (2009).



# INSTRUMENTATION DEVELOPMENTS





# FREE JET MICROMIXER TO STUDY FAST CHEMICAL AND BIOLOGICAL REACTIONS BY SMALL ANGLE X-RAY SCATTERING

B. Marmiroli<sup>1</sup>, G. Greci<sup>2</sup>, F. Cacho-Nerin<sup>1</sup>, B. Sartori<sup>1</sup>, E. Ferrari<sup>2</sup>, P. Laggner<sup>1</sup>, L. Businaro<sup>2</sup>, H. Amenitsch<sup>1</sup>

<sup>1</sup>Institute for Biophysics and Nanosystem Research, Graz, Austria

<sup>2</sup>Laboratorio Nazionale TASC INFN-CNR, Trieste, Italy

E-mail: heinz.amenitsch@elettra.trieste.it, luca.businaro@elettra.trieste.it



DXRL and SAXS

Micro and nano fabrication techniques permit the design and fabrication of new devices and systems relying on different physical principles than at the macroscale, enabling to precisely manipulate and control biological and chemical entities. By creating a strong synergy between state-of-the-art microtechnology and advanced measurement techniques it is thus possible to access new fields of investigation. In the present case, we used microfabrication with synchrotron radiation to enhance the capabilities of state of the art synchrotron SAXS by means of a custom made microfluidic device. This allowed us to push the limits of time resolved measurements of fast chemical reactions.

SAXS is a powerful technique to determine the structure of samples with characteristic size between ten and few thousand Ångströms. Over the last decades SAXS measurements have been conducted with ever shorter time-scales, increased resolution range and smaller beam sizes. Short time-scales are of particular interest for revealing the nucleation and growth of nanoparticles or the conformational changes of proteins like un- or re-folding. Time-resolved SAXS techniques using stopped-flow or continuous-flow mixers have been successfully applied to several chemical and biological studies in the millisecond and sub-millisecond time domain. Knight and co-workers [1] first proposed rapid mixers based on hydrodynamic focusing, which have later been used in combination with SAXS for biological studies reaching a mixing time of a few hundreds of microseconds [2,3]. However, the time resolution can still be improved by using microfluidic devices.

We designed, fabricated and tested a micromixer based on hydrodynamic focusing which generates a free liquid jet in air. In this kind of device, reagent A is inserted in the

central channel and reagent B in two lateral ones. Therefore, the side flows squeeze the central one into a thin stream (less than 1 μm wide), where mixing occurs by diffusion only. Due to the small dimensions of the central stream, mixing occurs very rapidly. After the mixing, which occurs inside the device, the time evolution of the reaction is separated spatially in the steady state flow along the liquid jet ejected from the device (Figure 1(a)). The geometry and dimensions of the channels, optimized by means of finite element analysis, are stringent: smallest features with radius <1 μm, and a channel depth of 60 μm, leading to an aspect ratio (ratio between the minimum lateral feature and the height of the structure) over 60. Therefore we fabricated the device in Polymethylmetacrylate at the Deep X-ray Lithography (DXRL) beamline at Elettra, as DXRL is a unique technique to obtain high-aspect-ratio microstructures with vertical sidewalls. We defined the process steps to guarantee high quality of the channel profiles. To achieve a high-resolution DXRL mask, the fabrication process was composed of two steps: Electron Beam Lithography (EBL) to have an intermediate mask, and Soft X-Ray Lithography at the Lilit beamline at Elettra to obtain the final mask.

We selected the flow parameters so that the mixing is completed inside the device before the nozzle and the exit velocity of the jet is 13 m/s, resulting in a time resolution of 77 ns/μm. By moving up the device with respect to the x-ray beam, the free liquid jet was scanned at increasing distance from the exit of the device, equivalent to recording the scattering curve at increasing times from the beginning of the reaction. Using this method we achieved a mixing time <40 μs, and we were able to detect the evolution of the chemical reaction of formation of CaCO<sub>3</sub> from

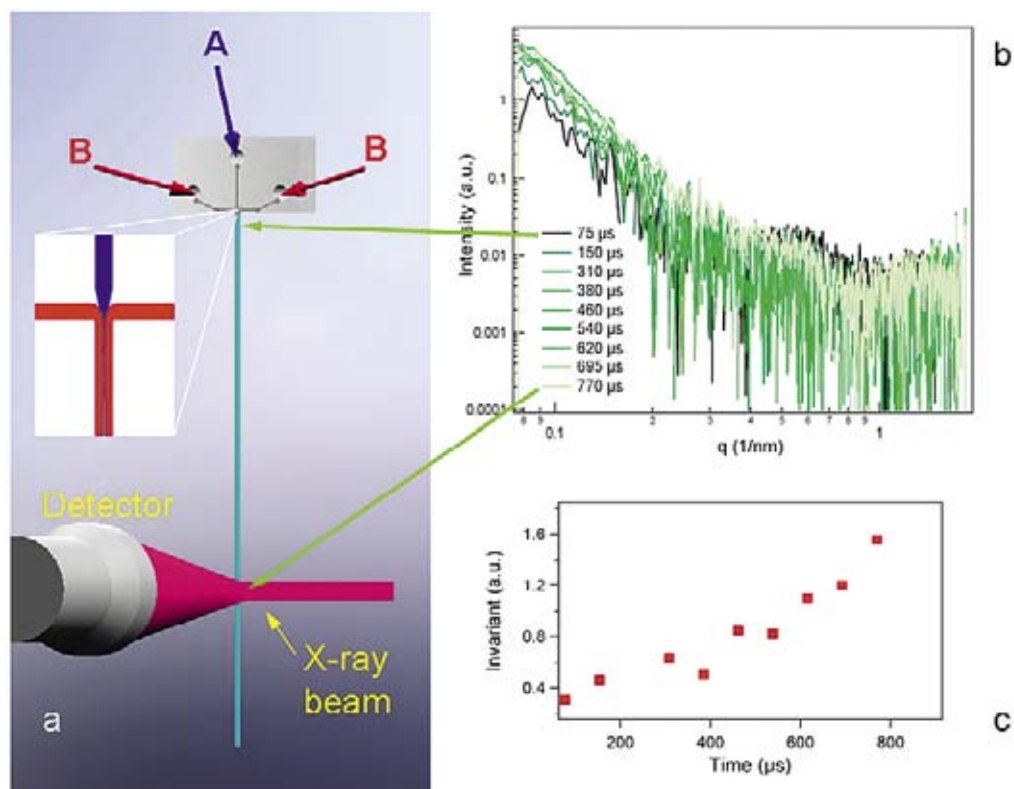


**Figure 1.** (a) Sketch of the micromixer mounted on a stainless steel sample holder and connected by high pressure tubes to syringe pumps. The micro free liquid jet in air exits from the mixer with a speed of 13 m/s. The inset shows a simulation of the hydrodynamic focusing. (b) Scattering curves of the  $\text{CaCO}_3$  formation in the time range 75–700  $\mu\text{s}$  after the beginning of the mixing. (c) Invariant versus time. The increase of the invariant is due to the increment of the volume fraction of the particles, demonstrating the evolution of the chemical reaction.

$\text{Na}_2\text{CO}_3$  and  $\text{CaCl}_2$  at the Austrian SAXS beamline at Elettra. The time of first accessible measurement was 75  $\mu\text{s}$ , and the liquid jet could be measured up to a length corresponding to 5 ms. In Figure 1(b) the scattering data of the reaction are shown in the time interval 75–700  $\mu\text{s}$  where nucleation and growth occur. To visualize the temporal behaviour of the studied system, we calculated the invariant (shown in Figure 1(c)) which is proportional to the volume fraction of the particles. It can be seen that during the first period of the reaction, the strong increase of the invariant is due to the accumulating volume fraction of the particles during the growth phase. To our knowledge these are the fastest data obtained for SAXS measurements

following up mixing processes. This experiment demonstrates that the microfabricated rapid mixer with a free jet has great potential for studying fast chemical and biological reactions in general (i.e. using spectroscopy, Time Resolved FTIR Spectroscopy) and in particular with SAXS [4].

#### References

- [1] J.B. Knight *et al.*, *Phys. Rev. Lett.* **80**, 3863 (1998).
- [2] L. Pollack *et al.*, *Phys. Rev. Lett.* **86**, 4962 (2001).
- [3] S. Akiyama *et al.*, S. Takahashi, *Proc. Natl. Acad. Sci.* **99**, 1329 (2002).
- [4] B. Marmioli *et al.*, *Lab Chip* **9**, 2063 (2009).

# RECENT UPGRADES OF THE BADELPH BEAMLINE

L. Petaccia<sup>1</sup>, P. Vilmercati<sup>1,2</sup>, S. Gorovikov<sup>1</sup>, M. Barnaba<sup>1</sup>, A. Bianco<sup>1</sup>, D. Cocco<sup>1</sup>, C. Masciovecchio<sup>1,3</sup>, A. Goldoni<sup>1</sup>

<sup>1</sup>Sincrotrone Trieste S.C.p.A., Trieste, Italy

<sup>2</sup>Physics Department, University of Trieste, Italy

<sup>3</sup>CRS SOFT-INFN-CNR, University of Rome "La Sapienza", Roma, Italy

E-mail: luca.petaccia@elettra.trieste.it



BADELPH

The BaD EIPh beamline has been opened for users since 2006. The beamline, based on a normal incidence monochromator (NIM), is primarily dedicated to high-resolution angle-resolved photoemission spectroscopy (ARPES) from solids in the low photon energy regime. The facility is proved to be efficient and user-friendly; moreover it is among the few in the world where the experiments exploiting low photon energy high-resolution ARPES can be performed. To date the available photon energy range, covered by two interchangeable gratings (Al/MgF<sub>2</sub> and SiC), has been 4.6-23 eV and the end station has been equipped with a commercial 50 mm mean-radius hemispherical electron analyzer mounted on a two-axis goniometer (Scienta SES 50, courtesy of Prof. R. Claessen, Wuerzburg University). Nevertheless, in order to fully exploit the capabilities of the monochromator, the extension of the photon energy range up to the limiting value, i.e. ~40 eV, and an increase of the efficiency of the data acquisition are necessary. To this end, the installation of the third spherical grating and replacement of SES 50 analyzer were proposed. The above proposals have been realized during the shutdown periods of the synchrotron and the extended capabilities of the beamline and the end station has been evaluated [1].

The radiation source of the BaD EIPh beamline is a Figure-8 undulator providing linearly polarized light in the horizontal plane (integer harmonics) or in the vertical plane (half-integer harmonics). The beamline consists of a Si plane-switching mirror to transfer the photon beam in the BaD EIPh branch, a spherical pre-focusing mirror which focuses the beam into an entrance slit, a 4 m NIM with a moveable exit slit, and an Au-coated toroidal mirror which refocuses the beam onto the sample in the analysis chamber. The monochromator is

now equipped with three spherical gratings with efficiencies that are optimized for the photon energy ranges of about 4.6-13 eV (1500 lines/mm, laminar profile, Al/MgF<sub>2</sub> coated), 13-19 eV (3000 lines/mm, laminar profile, SiC), and 19-40 eV (3000 lines/mm, blazed profile, Pt coated). While the groove profiles of the first two laminar gratings were designed to suppress the higher-order diffraction efficiency, the new Pt-coated grating was designed to maximize the photon flux in first-order diffraction.

The photon flux measured at the sample position is shown in Figure 1(a). The flux is within the expectations, especially for the low-energy and newly installed high-energy gratings. The energy resolution of the beamline was evaluated by means of gas-phase ion-yield measurements of different gases (Ne, Ar, and NO). In Figure 1(b) a selected Ne<sup>+</sup> autoionization spectrum is presented. These Rydberg states are long-living with a very narrow natural linewidth. As a result, the energy resolution of the beamline can be estimated directly from the full-width at half-maximum (FWHM) of the Rydberg resonances. The measured energy resolution compares well or even surpasses the theoretical prediction.

The end station of BaD EIPh consists of two preparation chambers, one analysis chamber, and a simple load-lock. The main part of the analysis chamber is the electron analyzer. Now a large SPECS Phoibos 150 spectrometer, mounted in a fixed geometry, has replaced the small SES 50. The use of a 2D-CCD detector offers the possibility of simultaneous acquisition of the energy as well as the angular distributions of the photoelectrons. With the new analyzer the maximum angular acceptance is up to ±13° while for SES 50 is ±3°. The performance of the new analyzer was evaluated measuring both the energy and



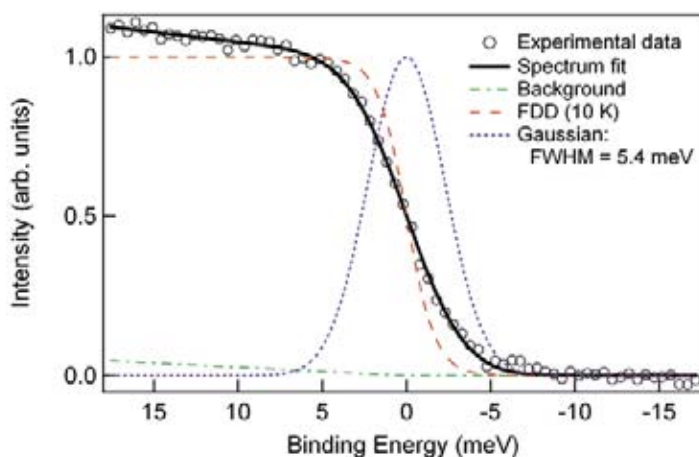
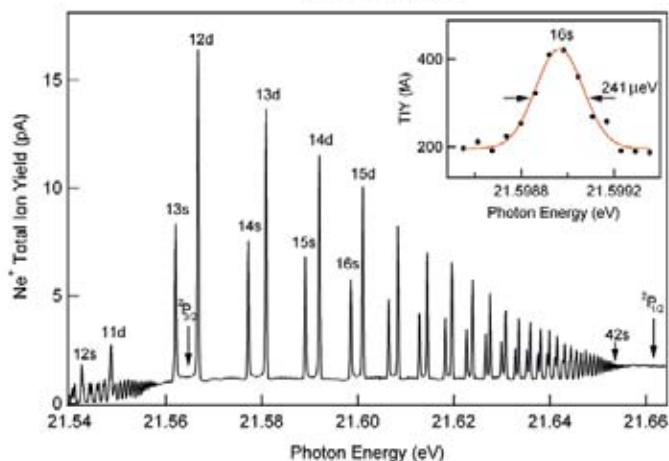
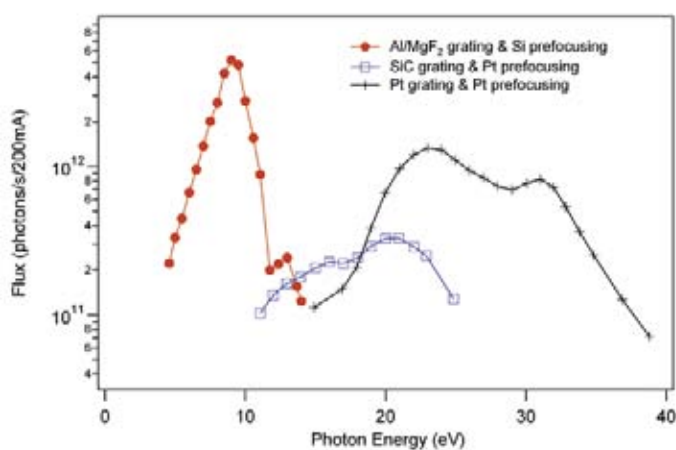


**Figure 1.** Top: First-harmonic photon flux through the beamline measured with slits of 300  $\mu\text{m}$  and with 200 mA of electron current accumulated in the storage ring. Bottom: Energy resolution of the beamline evaluated by gas-phase ion-yield measurements of Ne. The autoionization spectrum, recorded with the SiC grating operating in second-order diffraction and with 20  $\mu\text{m}$  exit slit, shows an energy resolution of 310  $\mu\text{eV}$  (resolving power  $E/\Delta E=69000$ ). Inset: 16 s resonance measured with 10  $\mu\text{m}$  exit slit showing a FWHM of 241  $\mu\text{eV}$  ( $E/\Delta E=89000$ ).

**Figure 2.** Fermi edge spectrum from polycrystalline Ag at 10 K (circles), fit of the data (solid line), and fitting function components. Photon energy 7.8 eV, beamline slits 300  $\mu\text{m}$ , entrance slit and pass energy of the analyzer 0.5 mm and 1 eV, respectively.

angular resolution. An ultimate angular resolution of about  $0.15^\circ$  was demonstrated, while an energy resolution of 4.8 meV at 7.8 eV photon energy can be estimated from the Fermi edge spectrum of polycrystalline silver at 10 K shown in Figure 2. For this spectrum the calculated energy resolution of the NIM is 2.4 meV. To conclude, the upgrade of the BaD EIPh beamline is successfully accomplished. Both the capabilities and the efficiency of the

facility are significantly improved. The BaD EIPh beamline with its end station can now be used as a state-of-the-art low-energy ARPES system.

### References

- [1] L. Petaccia, P. Vilmercati, S. Gorovikov, M. Barnaba, A. Bianco, D. Cocco, C. Masciociechio, A. Goldoni, *Nucl. Instr. Meth. A* **606**, 780 (2009).

# TRANSIENT GRATING SPECTROSCOPY TO INVESTIGATE NANOSCALE DYNAMICS

F. Bencivenga<sup>1</sup>, R. Cucini<sup>1</sup>, C. Masciovecchio<sup>1</sup>

<sup>1</sup>Sincrotrone Trieste S.C.p.A., Trieste, Italy

E-mail: [filippo.bencivenga@elettra.trieste.it](mailto:filippo.bencivenga@elettra.trieste.it)



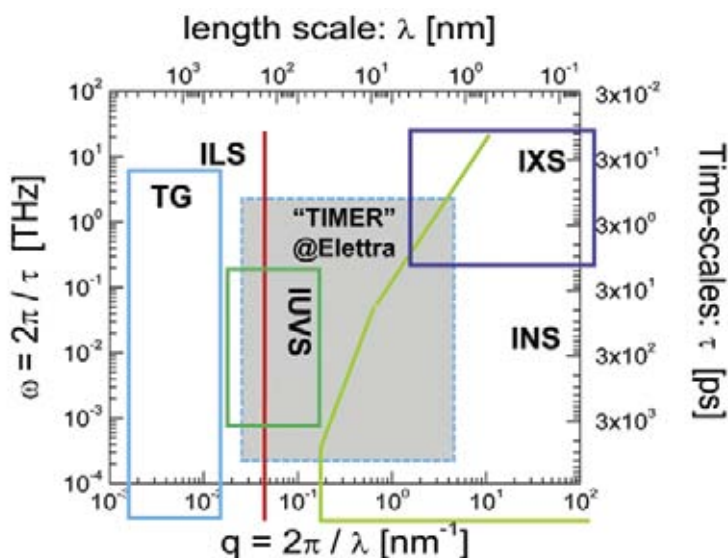
IUVS

The understanding of dynamics in disordered systems still represents a challenge for modern scientists and is motivating several experimental and theoretical studies. On the experimental side, the main limitation is represented by the lack of an experimental method able to probe collective dynamics over “mesoscopic” length-scales (i.e., in the 10-100 nm range). These scales are of the highest relevance, since they can be related to the topological disorder inherent to the amorphous phases. Our aim is to develop a Free Electron Laser (FEL)-based time-resolved technique able to extend the conventional Transient Grating (TG) method in the VUV spectral range [1]. The unique properties in terms of coherence, stability, time and frequency band-width provided by the FERMI@Elettra source will make possible the realization of this technique at Elettra. The instrument we intend to build (TIMER) will open up the possibility to study collective dynamics at the nanoscale that, nowadays, cannot be investigated by existing laser or synchrotron based instruments. Moreover, the

proposed experimental method will also be a sensitive probe for dynamics, heat transport and electron correlations in nanostructured materials.

In a naïve picture disordered systems are those characterized by the lack of translational invariance. This greatly complicates the understanding of their physical properties, which is even more complicated when other degrees of freedom come into play. These introduce different time- ( $\tau$ ) and length-scales ( $\lambda$ ) affecting the dynamical behaviour differently, depending on their values as compared to the average period of molecular vibrations ( $t_v$ ) and the average interparticle distance ( $\alpha$ ). Inelastic scattering methods can experimentally probe dynamics by measuring the spectrum of density fluctuations, naturally occurring over a broad range of frequencies ( $\omega=2\pi/\tau$ ) and wave vectors ( $q=2\pi/\lambda$ ). However, available techniques cannot explore all the ( $\lambda,\tau$ )-range of interest (see Figure 1). Particularly, the mesoscopic  $\lambda$ -range is still inaccessible mainly because of severe constraints concerning the

**Figure 1.** ( $q,\omega$ )- and ( $\lambda,\tau$ )-ranges accessible by the transient grating technique with conventional laser source (TG) and by inelastic scattering techniques: inelastic light (ILS), ultraviolet (IUVS), neutron (INS) and x-ray (IXS) scattering. The shaded area is the range that will be accessible by TIMER.



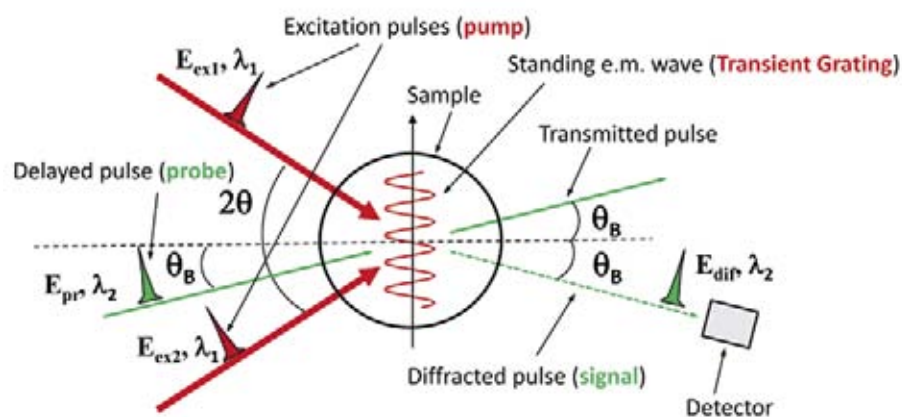


**Figure 2.** Rationale of the transient grating method.

frequency resolution. This hurdle can be circumvented by using time resolved spectroscopies, such as the TG [2]. The rationale of TG experiments is sketched in Figure 2: two photon pulses (pump) of wavelength  $\lambda_1$  interfere into the sample creating a standing electromagnetic wave (i.e., the transient grating) with period:  $\Lambda = (\lambda_1/2) \cdot \sin(\theta)$ , where  $2\theta$  is the angle between the pulses. This standing wave interacts with the sample generating a modulation of sample properties, such as density. The pump-induced density modulation can be probed by diffraction of a third pulse (probe) of wavelength  $\lambda_2$  impinging into the sample at the Bragg angle:  $\theta_B = \text{asin}(\lambda_1 \sin(\theta) / \lambda_2)$ . Finally, the TG signal is represented by the time evolution of diffracted intensity, which can be monitored by properly delaying the probe pulse with respect to the pump ones. As a result, the TG signal is related to the back time-Fourier transform of density fluctuations [3], and therefore embeds the same information as an inelastic scattering experiment.

However, the  $\lambda$ -range exploitable by TG method is presently limited by the rather large wavelength ( $>400$  nm) of available sources of coherent photon pulses. FERMI@Elettra will make available a coherent photon pulses of short

wavelength radiation (1-100 nm). The outstanding capability of this FEL source will allow the extension of TG technique in the VUV spectral range with sub-ps time resolution. Such a FEL-based TG instrument will be developed in a dedicated experimental end-station (TIMER) of FERMI@Elettra, which will enable probing dynamics in the “mesoscopic” ( $\lambda, \tau$ )-range (see Figure 2). Furthermore, TG experiments at the nanoscale would potentially be of great impact in other fields of research, since they can potentially measure correlations, electronic excitation lifetimes, heat transport, intra-molecular dynamics and non-linear material responses and, moreover, TG has recently proven to be a reliable probe for surfaces, interfaces and nanostructured materials.

### References

- [1] F. Bencivenga, C. Masciovecchio, *Nucl. Instr. Meth. Phys. Res. A* **606**, 785 (2009).
- [2] H.J. Eichler, P. Gunter, D.W. Pohl, *Laser-Induced Dynamic Gratings*, Berlin: Springer (1986).
- [3] P. Bartolini, A. Taschin, R. Eramo, R. Torre, in “*Time resolved spectroscopy in complex liquids: an experimental perspective*”, edited by R. Torre, Springer (2008).

# SYNCHROTRON RADIATION MEETS LASER ABLATION: PHOTOIONIZATION MASS SPECTROMETRY OF CLUSTERS IN A LASER PLUME

M. Coreno<sup>1</sup>, S. Orlando<sup>1</sup>, A.M. Juarez-Reyes<sup>2</sup>, L.M. Hoyos Campo<sup>2</sup>, J. Alvarez Ruiz<sup>3</sup>, M. Sanz<sup>3</sup>, M. de Simone<sup>4</sup>, A. Kivimäki<sup>4</sup>, A. Casu<sup>4,5</sup>, C. Spezzani<sup>6</sup>, M. Stankiewicz<sup>7</sup>, D.M. Trucchi<sup>8</sup>

<sup>1</sup>CNR-IMIP, Roma, Italy

<sup>2</sup>Physical Sciences Institute, Universidad Nacional Autónoma de México, México

<sup>3</sup>Chemistry-Physics Institute, SIC, Madrid, Spain

<sup>4</sup>Laboratorio Nazionale TASC INFN-CNR, Trieste, Italy

<sup>5</sup>University of Cagliari, Cagliari, Italy

<sup>6</sup>Sincrotrone Trieste S.C.p.A., Trieste, Italy

<sup>7</sup>Physics Institute, Jagiellonian University, Kraków, Poland

<sup>8</sup>CNR-ISC, Roma, Italy

E-mail: marcello.coreno@elettra.trieste.it



## GAS PHASE

Atomic or molecular clusters bear an intermediate complexity between single atoms, or molecules, and condensed matter. For this reason, systematic studies of clusters provide a unique tool to understand size-dependent physical properties of mesoscopic systems such as those employed in practical applications in nanotechnology.

The study of clusters using VUV and soft X-ray radiation has allowed, in this context, to extract a good deal of information on the photoionization and structural properties of atomic and molecular clusters [1]. However, synchrotron radiation (SR) studies have mainly dealt with clusters that are created through adiabatic expansion of samples that are already in the gas phase at ambient pressure and temperature (rare gases, N<sub>2</sub>, CO, ...) [2], whereas only few examples exist of studies of more complex systems produced using plasma cluster sources or laser ablation methods.

Here, we present preliminary results of SR photoionization spectroscopy studies on clusters produced in an expanding plume produced by laser ablation. We believe that this approach will greatly expand the choice of samples. For this, we have constructed an experimentally simple apparatus which combines the production of clusters with their simultaneous interaction in gas phase with SR. To demonstrate the feasibility of this new approach, the apparatus has been employed to investigate the valence and inner shell photoionization spectra of laser ablation plumes from carbon, sulphur, and cadmium sulphide (not shown here).

The experiment was carried out at the Gas Phase Photoemission beamline [3]. The experimental apparatus consists on a conventional Time of Flight Mass Spectrometer (TOF-MS) and a manipulator, which holds the sample pellet for laser ablation, both enclosed in an ultrahigh vacuum chamber. A 10 Hz train of 10 ns laser pulses at 532 nm, with an energy of 6.7 mJ per pulse was sent to produce ablation normal to the surface of the pellet. The plume of the ablated sample was crossed perpendicularly by the light coming from the spherical grating monochromator of the Gas Phase beamline. The ionic species resulting from the photoionization of the neutral clusters produced from the sample were mass analysed with the TOF-MS by using a multi-hit time-to-digital converter. Parent ions arising from the ablation process itself were deliberately discriminated by a convenient scheme of pulsed voltages. In this fashion, the mass spectra of the produced ions can be recorded at any photon energy of interest. Moreover, one may obtain a collection of these TOF spectra in order to assess their dependence on photon energy.

Figure 1 shows the mass spectrum of laser-ablated neutral carbon clusters following photoionization with SR at 21.2 eV (the high number of native ions in the plume could not be fully removed and this makes the intensity of C<sub>2</sub><sup>+</sup> unreliable). Figure 2 shows the spectrum of neutral S clusters ionized at photon energies of 21.2 eV and 172 eV.

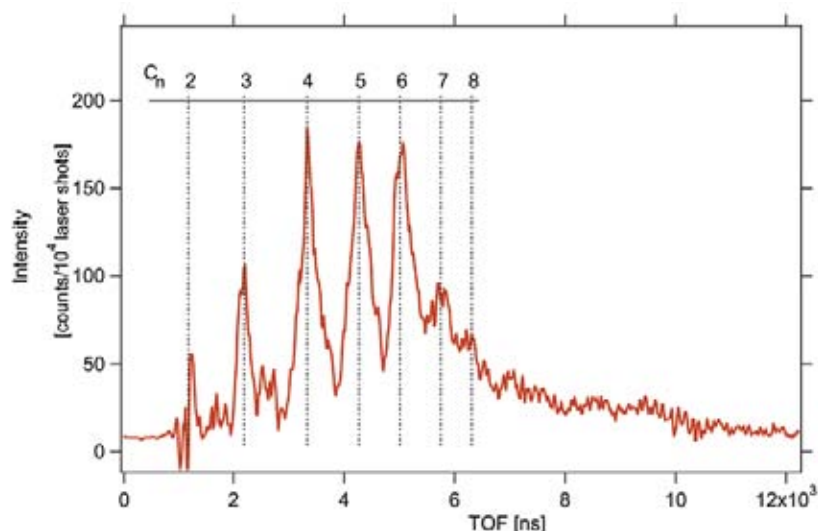


**Figure 1.** Mass spectrum of carbon clusters collected from laser ablated graphite ionized with synchrotron radiation at 21.2eV photon energy.

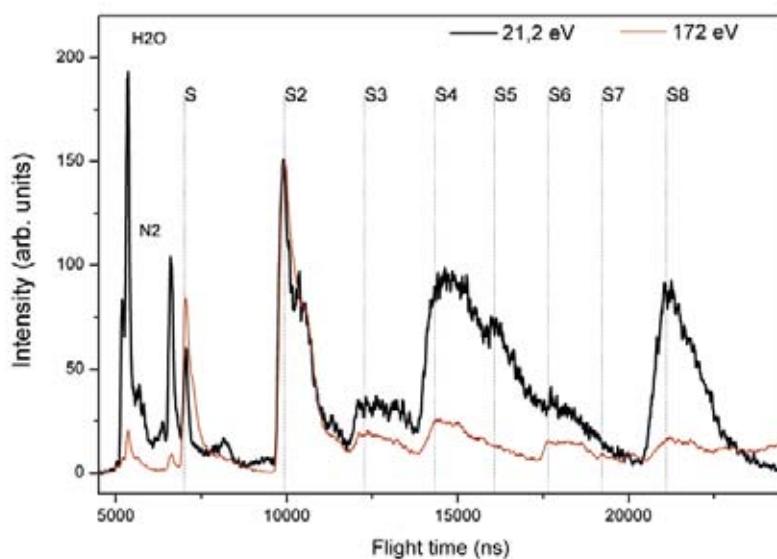


**Figure 2.** Mass spectra of sulphur clusters resulting from ionization of laser ablated sulphur pellets with synchrotron radiation at photon energies of 21.2 eV (black curve) and 172 eV (red curve).

A more thorough account of our recent results will be published shortly [4]. For the purposes of the present communication, we would like to emphasize the value of the spectra presented here: these results witness the ability of our experimental arrangement to produce clusters with laser ablation and analyse them using synchrotron radiation photoionization. We believe that this laser plume approach can have a significant impact on cluster research, broadening the range of samples to very reactive, short lived and metastable clusters as well as to clusters of materials with high evaporation temperatures.

#### References

- [1] E. Rühl, *Int. J. Mass Spectrom.* **229**, 117 (2003).
- [2] M. Tchapyguine *et al.*, *J. Electron Spectrosc. Relat. Phenom.* **166-167**, 38 (2008).
- [3] K.C. Prince *et al.*, *J. Synchrotron Radiat.* **5**, 565 (1998).
- [4] J. Alvarez-Ruiz *et al.*, *Nucl. Instrum. Meth. Phys. Res. B* (2009) in press.





## FACTS & FIGURES

# THE COMPANY

**S**incrotrone Trieste S.C.p.A. began operations in 1987: it is a **non-profit Share Company** (Società Consortile per Azioni) recognised as being of national interest by a State Law, which manages the **Elettra Laboratory**. Elettra continues to update itself and grow. In addition to significant modernisation projects relating to beamline sources and other components, a new fourth generation light source, **FERMI@Elettra**, is under construction alongside the original one.

Elettra is an Associate Laboratory of the International **Atomic Energy Agency (IAEA)** of Vienna, and forms a key node in the science and technology network of the **Central European Initiative (CEI)**.

It participates in more than twenty projects within the EU Framework Programme for Research and Development, and is the coordinator of the **Integrated Infrastructure Initiative (I3) "ELISA"**, bringing together 17 research infrastructures around Europe. This corresponds to the world's largest network of synchrotrons and FELs facilities, acting as a consortium.

On its site Elettra hosts the **National Laboratory TASC** (INFN-CNR), a facility for micromanufacturing and nanoscience. It has also established enduring working relationships with important Italian and foreign institutions, including various **CNR** (National Research Council) bodies, the **Academies of Science of Austria** and the **Czech Republic**, UNESCO's International Centre of Theoretical Physics (**ICTP**), the International School of Advanced Studies (**SISSA**), and the **Universities** of Milano, Trento, Trieste and Udine. These partners are actively contributing to the construction and operation of beamlines and support laboratories.

Elettra's scientific and technical quality and developments are constantly monitored by board-appointed international Committees which advise on all relevant aspects of the general and development policy, scientific programs, accelerator development, technology transfer and industrial applications.

## SHAREHOLDERS

- > AREA Science Park Consortium (51%)
- > Autonomous Region of Friuli Venezia Giulia (40%)
- > INFN-CNR (National Institute of Material Physics of the Italian National Research Council) (5%)
- > The national Agency for inward investment promotion and enterprise development (4%)

## ALLIANCES AND PARTNERSHIPS

- > IAEA (International Atomic Energy Agency)
- > CEI (Central European Initiative)
- > IRUVX (European Consortium for FELs up to the UV/softXray)
- > Austrian Academy of Sciences
- > Academy of Sciences of the Czech Republic
- > CNR (Consiglio Nazionale delle Ricerche – Italian National Research Council)
- > CNRS (Centre National de la Recherche Scientifique – French National Research Council)
- > ICTP - UNESCO (International Centre for Theoretical Physics)
- > INSTM (Consorzio Interuniversitario Nazionale per la Scienza e Tecnologia dei Materiali – National Inter-University Consortium for Materials Science and Technology)
- > INFN (Istituto Nazionale di Fisica Nucleare National Institute of Nuclear Physics)
- > ISAS (International School of Advanced Studies)
- > Charles University, Prague
- > University of Nova Gorica
- > University of Milano – Bicocca
- > University of Trento
- > University of Trieste
- > University of Udine



Sincrotrone Trieste S.C.p.A. is managed by a **Board of Directors**, assisted by a shareholder-appointed **Board of Auditors**, and advised by board-appointed international committees such as the **Council of Partners** for general and development policy, the **Scientific Advisory Council** for scientific programs, the **Machine Advisory Committee** for accelerator development, and the **Industrial Advisory Panel** as far as technology transfer and industrial applications are concerned.

**Machine Advisory Committee (MAC)**

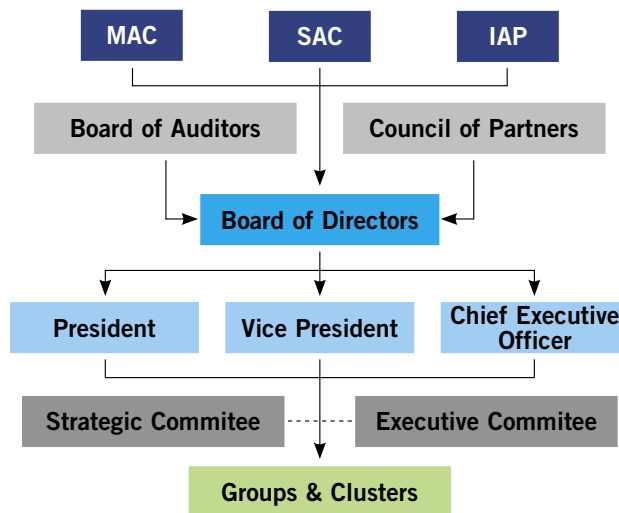
**Chairman: Richard P. Walker**  
 Paul J. Emma  
 Mikael Eriksson  
 Jerome Hastings  
 Carlo Pagani  
 Claudio Pellegrini  
 Mike Poole  
 Robert W. Schoenlein  
 Hans Weise

**Scientific Advisory Council (SAC)**

**Chairman: Ingolf Lindau**  
 David Attwood  
 Gordon Brown  
 Charles S. Fadley  
 Robert Huber  
 Sine Larsen  
 Dietrich Menzel  
 Charles V. Shank  
 Friso van der Veen

**Industrial Advisory Panel (IAP)**

**Chairman: Alberto Sangiovanni-Vincentelli**  
 Carlo Castellano  
 Enrico Albizzati  
 Maurizio Arienzo  
 Mauro Ferrari



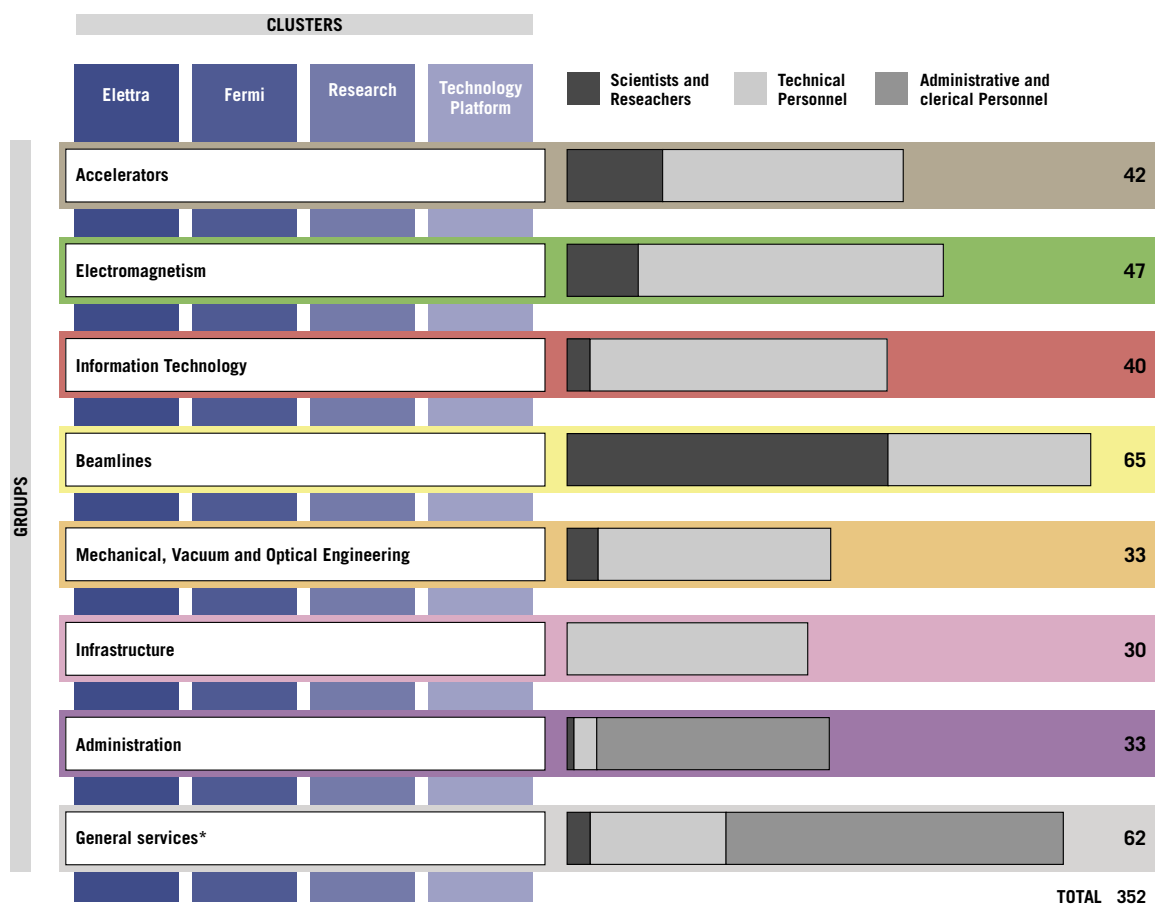
**Board of Auditors**  
**Chairman: Fabio Matarazzo**  
 Nicola Archidiacono  
 Claudio Sambri  
 Paolo Marchesi  
 Ugo Braico

**Board of Directors**  
**President: Carlo Rizzuto**  
**Vice President: Giovanni Comelli**  
**Chief Executive Officer: Alfonso Franciosi**  
 Roberto Della Marina  
 Marcello Fontanesi  
 Gemma Ravizza  
 Giorgio Rossi  
 Giorgio Sulligoi  
 Alessandro Trovarelli

**Council of Partners**  
**President: Carlo Rizzuto**  
 Fabio Barbone  
 Stefano Fantoni  
 Alain Fontaine  
 Marcello Fontanesi  
 Dante Gatteschi  
 Peter Laggner  
 Vladimir Matolin  
 Claudio Tuniz

# STAFF

**S**incrotrone Trieste has adopted a matrix-type of organization. The four Strategic Initiatives correspond to and are implemented through four **Clusters** of different **Projects**, grouped together based on the complementarity of the different project goals. The human and instrumental resources required by the different projects are managed within eight **Groups** of staff members with similar or related expertise.



\* including personnel, legal, industrial liaison, users offices, etc.

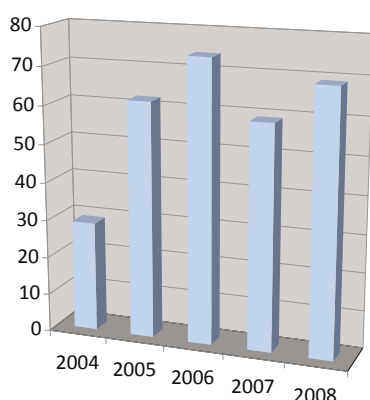
# TRAINING AND EDUCATION

The Sincrotrone Trieste company is deeply involved in the training and education of students from national and international high schools, universities and research institutions. The company is actively involved in the promotion of research activity and scientific knowledge through a series of organized schools and conferences. Among these it is worth highlighting the “Tenth school on Synchrotron Radiation: Fundamentals Methods and Applications” organized in Duino-Trieste in collaboration with the Italian Society of Synchrotron Radiation.

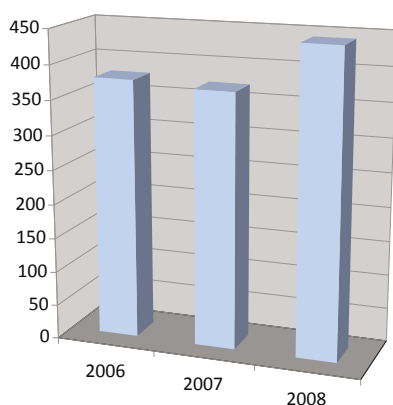
The company hosts students for training directly in Elettra’s laboratories. During the last five years, about 300 students from 41 countries have been involved in study terms or in the preparation of master’s and PhD theses. The doctorate students are involved in scientific projects related to many diverse fields, including physics, biology, engineering, nanotechnology, chemistry and medicine.

The international character of the training activities are further underscored by the presence of under- and post-graduate students’ active participation in experiments during the allocated beamtime. Indeed, in the period from 2006 to 2008, 58% of the more than 400 students came from abroad.

A collaboration with the International Centre of Theoretical Physics has been established, with the aim of giving opportunities to junior representatives of scientific institutes in developing countries for participating in Elettra’s projects.

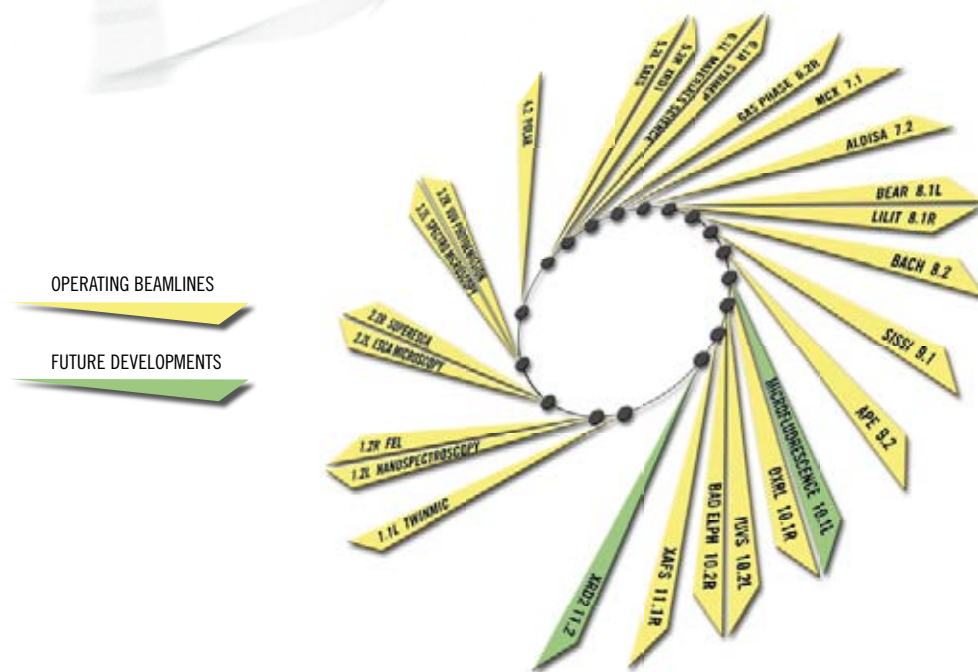


Scholarship holders and students involved in training and preparation of Laurea and PhD thesis with the Elettra’s research groups.



Under- and post-graduate students from international research groups involved in experiments at the Elettra’s beamlines.

# BEAMLINES AND USERS



BEAMLINES			source *	energy range (eV)	partner institutions
1.1L	TWINMIC	A multipurpose twin X-ray microscopy beamline for improving life conditions and human health	short id	250 - 2000	
1.2L	Nanospectroscopy	SPELEEM and LEEM-PEEM end-station	id	50-1000	Soleil (F)
1.2R	FEL	European Free-Electron Laser project	id	1,8 - 9,5	
2.2L	ESCA Microscopy	Scanning PhotoElectron Microscopy (SPEM)	id	200-1400	
2.2R	SuperESCA	Fast and High Energy Resolution Photoemission and Absorption Spectroscopy	id	85 - 1500	
3.2L	Spectro Microscopy	Angle-Resolved Photoemission microscope	id	27 - 95	
3.2R	VUV Photoemission	Angle-Resolved PhotoElectron Spectroscopy (ARPES) in the VUV range	id	16 - 1000	ISM-CNR
4.2	Circular Polarization	Dichroic measurements on chiral systems	id	5 - 1000	ISM-CNR
5.2L	SAXS	Small Angle X-Ray Scattering	id	8000 - 16000	IBM-ÖAW (A)
5.2R	XRD1	X-ray Diffraction	id	4000 - 22000	IC-CNR
6.1L	Materials science	Photoemission and X-ray absorption	bm	40 - 800	ASCR, Charles University of Prague (CZ)
6.1R	SYRMEP	SYnchrotron Radiation for MEDical Physics	bm	8000 - 35000	UNITS
6.2R	Gas Phase	Research on gaseous systems	id	14 - 1000	IMIP-CNR, INFN-CNR
7.1	MCX	Powder Diffraction Beamline	bm	2100 - 23000	UNITN, INSTM
7.2	ALOISA	Advanced Line for Overlayer, Interface and Surface Analysis	id	120 - 8000	INFN-CNR
8.1L	BEAR	Bending magnet for Emission Absorption and Reflectivity	bm	4 - 1400	INFN-CNR
8.1R	LILIT	Laboratory for Interdisciplinary LITHography	bm	1000 - 5000	INFN-CNR, INFN-CNR
8.2	BACH	Beamline for Advanced DiChroism	id	35 - 1600	INFN-CNR
9.1	SISSI	Source for Imaging and Spectroscopic Studies in the Infrared	bm	0,001 - 3	
9.2	APE	Advanced Photoelectric Effect experiments	id	10-2000	INFN-CNR
10.1L	X-ray microfluorescence	X-ray microfluorescence	bm	4000 - 20000	
10.1R	DXRL	Deep-etch Lithography	bm	2000 - 20000	
10.2L	IUVS	Inelastic Ultra Violet Scattering	id	11-2008	
10.2R	BAD Elph	Low-energy Angle-Resolved PhotoEmission Spectroscopy (ARPES)	id	4 - 25	
11.1R	XAFS	X-ray Absorption Fine Structure	bm	2300 - 25000	ICTP
11.2	XRD2	X-ray Diffraction	id		

source\* id = Insertion Device (wiggler or undulator)  
bm = bending magnet

The **Proposal Review Panel** is a panel composed of senior scientists active in different scientific fields and appointed by the Elettra laboratory management with the aim of evaluating the general User's proposals. The panel is divided into seven subcommittees.

The Proposal Review Panel meets twice a year, gives a written report for each proposal submitted for the ongoing semester and gives suggestions for **beamtime** allocation at the beamlines open to the users.

#### **Atoms, Molecules & Plasmas**

Svante Svensson (Chairman)  
Vincenzo Aquilanti  
Uwe Becker  
John M. Dyke

#### **Scattering**

Paolo Mariani (Chairman)  
Stephanie Finet  
Daniele Fioretto  
Hermann Franz  
Giulio Monaco

#### **Catalytic Material/Surface Science**

Carlo Mariani (Chairman)  
Maria Carmen Asensio  
Karol Hricovini  
Falko P. Netzer  
Michèle Rose Sauvage-Simkin  
Robertino Zanoni

#### **Hard condensed matter - Structures**

Maurizio Benfatto (Chairman)  
Robert Joseph Cernik  
Paola D'Angelo  
Marco Milanese

### **Proposal Review Panel**

Dipankar Das Sarma  
(Chairman)

#### **Condensed matter Electronic & Magnetic Structure**

Dipankar Das Sarma (Chairman)  
Hermann Dürr  
Mark Golden  
Giorgio Margaritondo  
Maurizio Sacchi

#### **Protein & Macromolecular Crystallography**

Giuseppe Zanotti (Chairman)  
Peter Brick  
Dusan Turk  
Luigi Vitagliano

#### **Instrumentation & Technological materials Life and Medical Sciences (excluding Crystallography) Polymers and Soft Matter**

Graeme Morrison (Chairman)  
Alberto Bravin  
Gianfelice Cinque  
Paul Dumas  
Christopher Hall  
Lisa Miller  
Günther Schmahl  
Andrew Smith  
Stephen William Wilkins

**USERS AT ELETTRA: TOTAL = 1108 (July 2008 - June 2009)**

Switzerland 14

Canada 4

USA 19

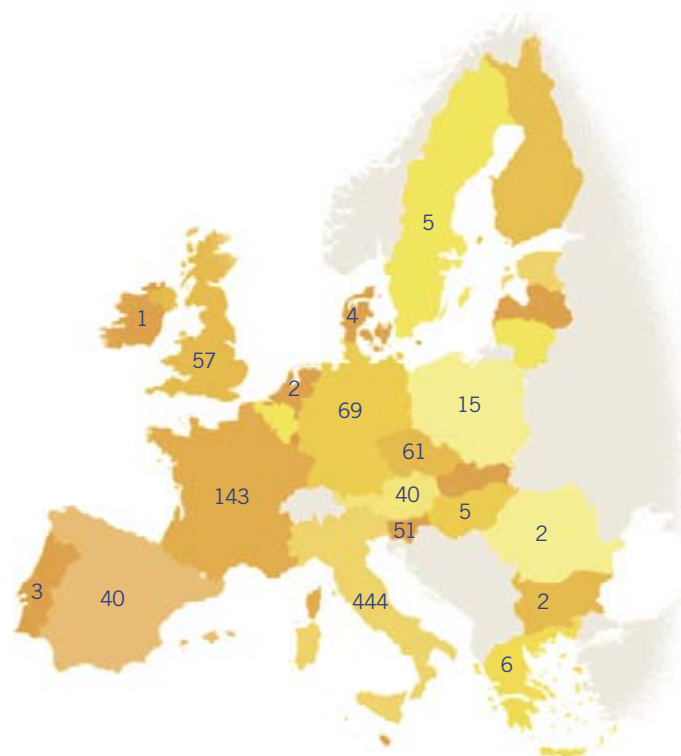
Mexico 1

Brazil 5

Argentina 2

Croatia 37

Russian Fed. 1



Japan 8

China 3

Singapore 2

Sri Lanka 1

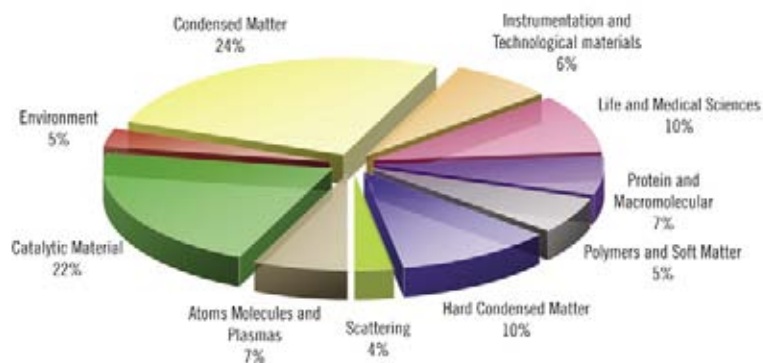
Australia 9

India 50

Iran 2

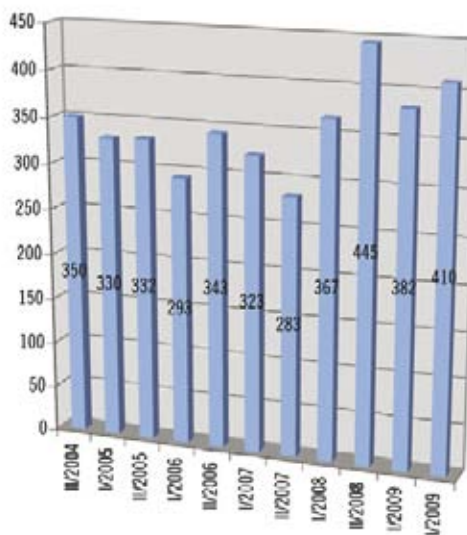
Pakistan 2

**ALLOCATED PROPOSALS BY RESEARCH AREA: TOTAL = 450 (July 2008 - June 2009)**



**2004 - 2009 PROPOSALS SUBMITTED BY SEMESTER**

From October 1st, 2007 to March 2nd, 2008 the Elettra light source was closed due to the booster installation.



# FINANCIAL FIGURES

## BUDGET ALLOCATION FOR 2009

<b>Running costs</b>	
General costs	€ 7.094.344
Personnel	€ 14.101.938
Utilities	€ 5.504.115
Accelerator group	€ 89.953
Administration group	€ 256.536
Beamlines group	€ 766.151
Coordination group	€ 1.029.596
Electromagnetism group	€ 138.285
IT group	€ 239.051
Infrastructure group	€ 885.814
Mechanical, Vacuum and Optical engineering	€ 235.982
Industrial Liason Office operation	€ 557.602
Scientific partnerships	€ 350.000
OPAC	€ 780.000
<b>Development projects</b>	<b>€ 3.185.338</b>
<b>Total Ordinary operation</b>	<b>€ 35.214.705</b>
<b>Special projects</b>	
Fermi	€ 31.155.320
<b>Total special projects</b>	<b>€ 31.155.320</b>
<b>GENERAL TOTAL</b>	<b>€ 66.370.025</b>

## PROJECTS / SPONSORED RESEARCH

The last two calendar years, 2008 and 2009 (not yet concluded), were extremely successful in attracting resources from external funding institutions: the contributions acquired through research contracts amount to 3.2 million Euro in 2008 and 2.1 million Euro in the first half of 2009. It is important to note that these research contracts deal, among others, with projects of strategic importance for Elettra's industrial development plan such as the environmental monitoring and the anti-counterfeiting technologies.

At the time of this writing, the submitted applications for external funding presently under evaluation are in excess of 10 million Euro. It is noteworthy to mention that two of these applications have been submitted within the Italian-Slovenian cross-border cooperation programme: this dimension of territorial cooperation is of highest importance in the European Union agenda as well as in Elettra's plan for the consolidation of international partnerships.

An important acknowledgement of Elettra's international profile has been obtained within the I3 project IA-SFS (Integrating Activity on Synchrotron and Free Electron Laser Science). Elettra has been the coordinator of IA-SFS (March 2004 – February 2009): this is the most significant FP6 (Sixth European Union Framework Programme) project in the field of synchrotron radiation and free electron lasers (see <http://www.elettra.trieste.it/i3/>). The European Commission selected IA-SFS as one of the 40 success stories of FP6 portrayed in the publication "Research for Europe — A selection of EU success stories" that can be ordered free of charge as hardcopy or downloaded as pdf at <http://bookshop.europa.eu/eubookshop/publicationDetails.action?pubuid=628043>.

This booklet has been translated in four languages and largely distributed to the general public, National and Regional authorities, European Parliament, Delegations and Representation of the European Union all over the world.

During the last 12 months, Elettra participated in 30 research contracts (see table) funded by the following external agencies: European Commission, Italian Ministry of Research, Italian Ministry of Foreign Affairs, Region Friuli-Venezia Giulia, International Centre for Theoretical Physics, Indian Department of Science and Technology.



**EUROPEAN/INTERNATIONAL RESEARCH CONTRACTS**

Name	Short name	Coordinator
Integrating Activity on Synchrotron and Free Electron Laser Science	IA-SFS	Elettra
European Design Study Towards a Global TeV Linear Collider	EUROTeV	DESY, Germany
Light Source Theory Network	LighTnet	STFC, United Kingdom
ICTP-Elettra Users Programme		Elettra
Transnational access of the Indian scientists to the Elettra beamlines		Elettra
Conservation materials for stained glass windows-assessment of treatments, studies on reversibility, and performance of innovative restoration strategies and products	CONSTGLASS	Fraunhofer-Institut für Silicatforschung, Germany
Deployment of Remote Instrumentation Infrastructure	DORII	PSNC, Poland
Preparatory Phase of the IRUVX-FEL Consortium	IRUVX-PP	DESY, Germany
TIME-Resolved Spectroscopy of Nanoscale Dynamics in Condensed Matter Physics	TIMER	Elettra
Realising and Managing International Research Infrastructures	RAMIRI	Imperial College of Science, UK
Research Infrastructures: Foresight and Impact	RIFI	UEFISCSU, Romania
European Light Sources Activities – Synchrotrons and Free Electron Lasers	ELISA	Elettra
Maximizing Synergies for Central European Biotech Research Infrastructures	SynBIOsis	JIC, z.s.p.o., Czech Republic
CEI Reaserch Fellowship Programme	CERES	INCE - Central European Initiative, Italy
Notte dei ricercatori 2009	PROSIT	University of Trieste, Italy

**NATIONAL RESEARCH CONTRACTS**

Name	Short name	Coordinator
BOOSTER-Elettra	BOOSTER	Elettra
Post-Genomic Structural Biology: Developing Infrastructures for Protein Crystallography	Structural biology	Elettra
FERMI@Elettra - Phase I		Elettra
High efficiency innovative light sources for solid state illumination devices with civil and automotive applications	LUCI	CNR
FERMI@Elettra - Phase II		Elettra

**REGIONAL RESEARCH CONTRACTS**

Name	Short name	Coordinator
Realization of a technological platform for the crystallographic analysis of biological macromolecules of biomedical interest for the industrial research	DAGEAS	Elettra
Study of hybrid organic/inorganic interfaces for strategic applications in the field of flexible displays and biochips	Nano-BioSOLEd	Elettra
Study and realization of prototype platforms for plane and helical undulators		Elettra
Development and realization of solid state ultrafast laser amplifiers optimized for FEL applications	FEMTOREG	Elettra
Distributed environment monitoring based on Grid	MADBAG	Elettra
Anti Counterfeiting Tags	ACT	Elettra
Development of chemical sensors for environmental and biological diagnosis based on nanowires and nanotubes	AMBIosen	Elettra
New conjugated polymers for plastic photovoltaic cells	PLASTIC PHOTOVOLTAIC CELL (SISTER II)	Area Science Park
Studies on the decay mechanisms of nanomaterials and their potential dangers in biological systems	NANOTOX	Elettra
Studies and characterization of high power X-band (12 GHz) radiofrequency devices	X-BAND	Elettra

# TECHNOLOGY TRANSFER AT ELETTRA

**T**he Industrial Liaison Office (ILO) was set-up in 2004 to promote the exceptional body of skills and technical expertise resulting from the experience accumulated in the construction and run up of the Elettra facilities over time. This know-how is of particular interest for other synchrotron facilities, suppliers of advanced instrumentation and private industrial companies operating in different fields, such as mechanics, optics, pharmacy, microelectronics, energy, chemistry etc.

Products and services are sold throughout the world. The turnover in 2008, reported on the next page, shows an increase in instrumentation business.

Scientific instrumentation sold to other synchrotron facilities and research laboratories worldwide includes: photons or charged particle detectors based on centroid finding techniques – like cross-delay anode detectors – or based on multi-channel acquisition, employed in several Elettra's beamlines, high voltage bipolar power supply systems especially suited for benders of x-ray bimorph mirrors, picoammeters with high sampling frequency, ionization chambers, beam position monitors used to characterise photon and electron beams and other devices such as charge pulse amplifiers, high voltage pulse generators and RF resonant cavities.

During the last year two new models of bipolar digital controlled current power supplies have specifically been developed: these new devices have been designed to drive some hundreds of magnets present on the FERMI FEL requiring up to 20 A ultrastable DC currents. These instruments have a very good dynamic performance and are used for beam trajectory correction: for small current adjustments (less than 5% of the maximum output current) the bandwidth is about 100 Hz. These power supplies are available upon request (see the technical description on page 140).

Another new product available is a versatile high voltage bipolar power supply system (coded MAS-TER) especially suited for applications in experimental physics (i.e. adaptive piezoelectric mirrors and electron spectroscopy lenses). In 2008 and 2009 several MAS-TER systems have already been installed at synchrotron laboratories, such as Diamond Light Source (UK), Advanced Photon Source (US-Chicago), Brookhaven National Laboratory (US-New York) (see the technical description on page 140).

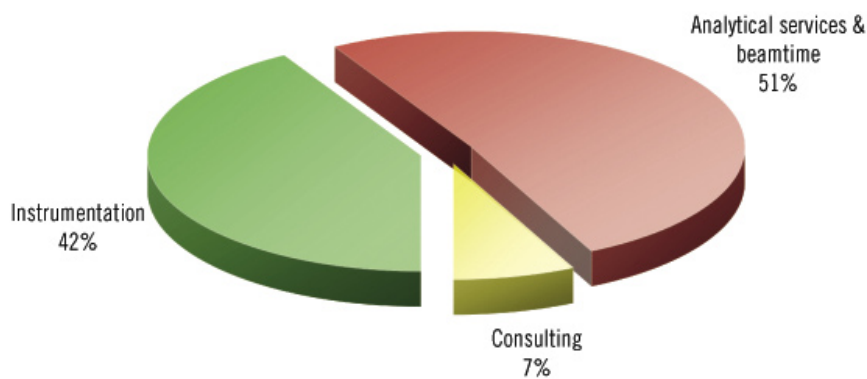
#### **How to contact us:**

Industrial Liaison Office  
Elettra Laboratory, Sincrotrone Trieste S.C.p.A.  
S.S. 14 - km. 163.5 in Area Science Park  
34012 Basovizza - Trieste, Italy  
Tel. +39 040 3758303 - Fax +39 040 3758623  
ilo@elettra.trieste.it  
<http://www.elettra.trieste.it/ILO/>

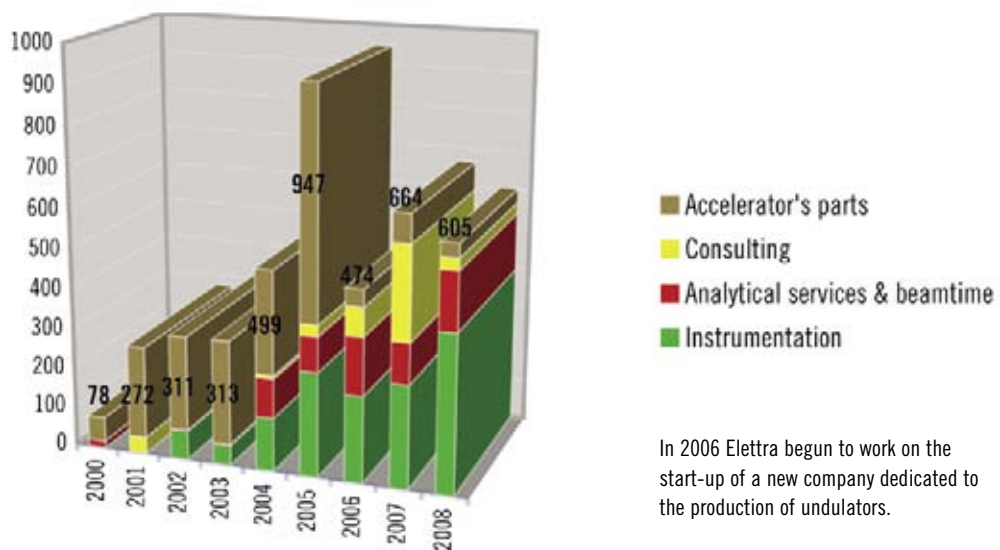
## 2008 ORDERS AMOUNT BY CUSTOMER COUNTRY

COUNTRY	NUMBER OF ORDERS	TURNOVER (Thousands of Euro)
United Kingdom	1	1,75
Germany	1	41,61
United States	2	13,57
Canada	1	12,00
Netherland	1	15,00
France	2	1,41
Italy	9	83,46
<b>TOTAL</b>	<b>17</b>	<b>168,80</b>

## 2008 ORDERS AMOUNT BY COMMERCIAL ACTIVITY



## 2008 TREND IN TURN OVER OF COMMERCIAL ACTIVITY (Thousands of Euro)



## LOW VOLTAGE BIPOLAR CURRENT POWER SUPPLIES

The A2605BS and A2620BS are bipolar DC/DC current-controlled digital power supplies.

Moderate cost, high stability, versatility, ease to install and to control are some of the most important features connected to their use in synchrotron light source research facilities.

Each DC/DC module is controlled by two DSP units supervising all processes including the remote control of the power supply over an Ethernet device. A stand-alone software driver has been developed to control the power converters from a PC. This device is also compatible and easily controllable via Epics and Tango global control systems. Up to four modules can be housed in a single 3U-rack. The power supplies implement a digital PID control that makes them adaptable in many different ways.

### A2605BS Specifications

Input Voltage Range	5/24 VDC
Max Input Current	7 ADC
Output Current Range	-5/+5 ADC
Output Voltage Range	-15/+15 VDC
Output Current Resolution	16 bit
Efficiency	90 %
Accuracy	30 ppm
Long Term Stability	50 ppm
Max Ripple	30 ppm

### A2620BS Specifications

Input Voltage Range	5/28 VDC
Max Input Current	20 ADC
Output Current Range	-20/+20 ADC
Output Voltage Range	-20/+20 VDC
Output Current Resolution	16 bit
Efficiency	95 %
Accuracy	30 ppm
Long Term Stability	50 ppm
Max Ripple	30 ppm



## MULTI CHANNEL, DIGITALLY CONTROLLED BIPOLAR POWER SUPPLY SYSTEM

MAS-TER is the new powerful and versatile power supply system especially suited for applications in experimental physics (i.e. electron spectroscopy, adaptive piezoelectric mirrors, etc). A main general purpose control unit (industrial PC) supervises all connected power supplies modules and runs proprietary software allowing complete control of the system and assuring the communication with any host computer via Ethernet connection.

The rack system has an internal bus where the individual modules are connected through multi-polar connectors for both power supply and data transfer. It can host up to 4 modules; each module is a 4 channels linear bipolar zero crossing power supply delivering +2kV/-2kV @ 0.5mA.

As the instrumentation is designed for experimental set-ups of large scientific facilities, Epics and Tango integration tools will also be provided to users.

Modular communication also satisfies users' requests: RS232, USB and Ethernet (TCP/IP and UDP) interfaces are available.

The MAS-TER system makes available proprietary know-how that allows safely control - precisely and with the highest accuracy - repeatability, resolution and stability piezoelectric bimorph mirrors based on piezoelectric ceramic actuators. Thus, it is the most reliable, efficient and powerful tool for controlling bimorph mirrors in order to easily and reliably obtain their best performances.

Each industrial PC controller is released with a preloaded Windows XP OS kernel and with a customized software application which handles the communications with all connected modules.

### MAS-TER Specifications

Up to 16 channels (4 channels/module)
500 uA effective output current
+/- 2000V zero crossing output voltage – referred to ground
16 resolution bits
Up to 1Mbit/s data transfer
Configurable communication (RS-232, USB, Ethernet TCP/IP and UDP)
Channel to channel DV hardware protection (for piezoelectric bimorph mirrors application)
< 2 bits 48hours stability
Tango, Epics, TCP/IP interfaces



# UNDULATOR DESIGN AND MANUFACTURING @ KYMA S.R.L.

Kyma S.r.l. was established in 2007 as a joint venture between Sincrotrone Trieste S.C.p.A. and the industrial companies Cosylab d.d. (Ljubljana) and Euromisure S.r.l. (Cremona).

Kyma activities focus on accelerator technology, with specific regard to the development and realization of insertion devices. More than twenty years of experience in design, assembling, characterization and operation of insertion devices at Sincrotrone Trieste, has met the manufacturing capabilities of the industrial partners, to build up a world-class company for undulator realization and application. Since 2008 a daughter company, Kyma Tehnologija d.o.o. has been established in Sežana, just 10 km from the Elettra site. Core activity of Kyma Tehnologija is assembling and characterization of undulator magnets. To this purpose a temperature-controlled chamber is available, ensuring an excellent environment for serial production of insertion devices. At present Kyma is engaged in the design and realization of all the undulators for the FERMI@Elettra Project, the new free-electron laser at present being commissioned at the Elettra Laboratory. The expertise offered by Kyma to the synchrotron and free-electron laser community covers a wide spectrum of other undulator-related products and services.

In the following two examples of undulator and measurement equipment are given.

## How to contact us:

Kyma Srl

S.S. 14 - km. 163.5 in Area Science Park

IT-34149 Basovizza - Trieste, Italy

Tel. +39 040 375 8796 - Fax +39 040 375 8623

info@kyma-undulators.eu - <http://www.kyma-undulators.eu>

## LPU@FEL1 – LINEARLY POLARIZED UNDULATOR

The FERMI project is based on the principle of high gain harmonic generation, employing multiple undulators. This first undulator in the FEL-1 chain is a standard fixed polarization device, acting as a modulator. Energy modulation is induced by the interaction of the electron beam with an external laser.

LPU@FEL1 main characteristics	
Magnetic configuration	PPM Halbach array
Magnet block dimensions	50.0x25.0x25.0 mm <sup>3</sup>
Number of period and length	30 x 100.0 mm
Overall beam length	3220 mm
Operational gap width (L)	12 ÷ 31 mm
Electron beam energy	1.2 GeV
Physical dimensions	3220x1100x2445 mm <sup>3</sup>
Weight	4510 kg



## SWB – STRETCHED-WIRE BENCH

This sophisticated measurement bench is intended to accurately measure the transverse distribution of the field integrals in groups of magnetic blocks assembled into “modules”. The data obtained give information relevant to the effects of magnetization errors, including inhomogeneities.

SWB main characteristics	
Wire length and number of wire turns	1120 / 20
Overall dimensions	360 x 210 x 130 cm <sup>3</sup>
Weight	~ 500 kg
Length of translation table	1500 mm
Software environment	LabVIEW 7.2







# VISITS

## Minister Frattini

(May 15<sup>th</sup> 2009)

The Minister of Foreign Affairs, Franco Frattini, welcomed by Carlo Rizzuto, President of the Company and chairman of the European Strategy Forum on Research Infrastructures (ESFRI), is accompanied to the experimental hall of the Elettra laboratory to visit some of the research stations, especially the Syrmep, the Materials Science and SAXS beamlines, the latter two created with the cooperation of two foreign partners, the Czech and Austrian Academies of Science.

ph. Filippo Cianciosi



## Former Italian Prime Minister Amato

(January 12<sup>th</sup> 2009)

Lawyer and Professor Emeritus of Constitutional Law, the former Italian Prime Minister, Giuliano Amato, was accompanied on a tour of the Elettra laboratory and the FERMI construction site by Alfonso Franciosi, CEO, and Giovanni Comelli, Vice President of ST.

ph. Filippo Cianciosi



**Regional Councillor  
Alessia Rosolen**

*(January 12<sup>th</sup>, 2009)*

The Regional councillor for labour, university and research with responsibility for equal opportunities and youth policies visits Elettra accompanied by senior management. A moment during the visit at the Syrmep beamline.

*ph. Filippo Cianciosi*



**The high level officials  
of the Carabinieri**

*(January 29<sup>th</sup>, 2009)*

Elettra welcomed the high level officials of the Carabinieri of Friuli Venezia Giulia, including their Commander in the Region, Brigadier General Nedo Lavagi. The visit to the main centres of AREA Science Park was aimed at obtaining a deeper understanding of the cultural realities of the Region and improving the technical and professional training of the high ranks of the Carabinieri.

*ph. Michele Pasqualetto*



## European Youth Parliament

(April 4<sup>th</sup>, 2009)

The EYP is a non-governmental organization and represents an educational project providing training for young Europeans between 16 and 18 years of age. Trieste hosted the XV National Selection, organized by the Liceo classico "Petrarca" and the Liceo Scientifico "Galilei". The picture illustrates a moment of the visit to Elettra by a group of students.

ph. Cecilia Blasetti



## International Astronomy Olympics

(October 16<sup>th</sup>, 2008)

120 youngsters, between 14 and 17 years of age, from Armenia, Bulgaria, China, Korea, Croatia, Czech Republic, Estonia, India, Indonesia, Italy, Kazakhstan, Lithuania, Romania, Russia, Serbia, Sweden and Thailand, visiting Elettra. They participated in the XIII International Astronomy Olympics, which took place in Trieste.

# WORKSHOPS, CONFERENCES, MEETINGS AND SCHOOLS

## ACTOP08 - 2<sup>nd</sup> Workshop on X-ray and XUV Active Optics

(Trieste, October 8<sup>th</sup>-11<sup>th</sup>, 2008)

The workshop, organized by ST at the Adriatico Guesthouse of the ICTP, saw the participation of more than 60 researchers from around the world.

ph. Filippo Cianciosi



## XVI Users' Meeting

(Trieste, November 24<sup>th</sup>-26<sup>th</sup>, 2008)

During the plenary session of the annual meeting of Elettra users, the prize in memory of Professors Luciano Fonda and Paolo Fasella was awarded; this prize is for young scientists who have achieved innovative results in the laboratory.

In 2008 it was awarded to Dr. Paolo Falcaro from *Coordinamento Interuniversitario Veneto per le Nanotecnologie* (CIVEN), for the growth of thin mesostructured silicon films, research that promises a range of applications in the engineered production of nano-devices.

ph. Michele Pasqualetto

## RADSYNCH

(Trieste, May 21<sup>st</sup>-23<sup>rd</sup>, 2009)

The 5<sup>th</sup> International Workshop on "RADiation safety at SYNCHrotron radiation sources", gave the opportunity to radiation physicists, radiation safety professionals and concerned parties to share experiences and exchange information about radiological issues. The event was organized by Sincrotrone Trieste.

ph. Filippo Cianciosi



## 1<sup>st</sup> IRUVX-PP Annual Meeting

(Trieste, March 9<sup>th</sup>-13<sup>th</sup>, 2009)

Over a hundred experts from across Europe - scientists and technologists, business managers, human resource managers and lawyers - met in Trieste to work on the foundation of the EuroFEL Consortium (the former IRUVX-FEL), which will bring together the free-electron laser sources within Europe in a sort of single broad laboratory. The event was organized by Sincrotrone Trieste. The project, which formally begun in April 2008 with a financial support of 5.7 million euros from the European Union, is one of 44 projects included in the ESFRI (European Strategy Forum on Research Infrastructures) Roadmap that aims to connect up the network of research laboratories by streamlining funding commitments and an agreed strategy for development.

ph. Filippo Cianciosi



## II Timing and Synchronization workshop

(Trieste, March 9<sup>th</sup>, 2009)

The Satellite workshop of IRUVX-PP. The event was organized and sponsored by INFN LNF, with the local logistical support of Sincrotrone Trieste and involved about 40 European and U.S. researchers from major laboratories active in FEL projects.



## X School on Synchrotron Radiation: Fundamentals Methods and Applications

(Trieste, September 7<sup>th</sup>-18<sup>th</sup>, 2009)

The school was organized by SILS – *Società Italiana di Luce di Sincrotrone* (Italian Society of Synchrotron Radiation) – together with Elettra, in the setting of the Castle of Duino, near Trieste. The students spent two afternoons at Elettra to practice on some beamlines employing radiation and in sessions of data analysis in the teaching classroom.

ph. Filippo Cianciosi



## “In viaggio con la luce” (Travelling with light)

(Trieste, October 27<sup>th</sup>-28<sup>th</sup>, 2009)

A training meeting on optics topics for high school teachers was held at Elettra and attended by science teachers from the scientific high schools in Bologna. The initiative was organized by Sincrotrone Trieste in cooperation with the *Istituto Nazionale di Ottica Applicata* (National Institute of Applied Optics) in Florence. The topics covered ranged from classical optics (with particular reference to its application for the observation of the sky) through to synchrotron radiation.

ph. Michele Pasqualetto (left), Giovanni Sostero (bottom)



## OTHER EVENTS

### Open Day

*(Trieste, June 6<sup>th</sup>, 2008)*

The sixth edition of the Open Day organized by AREA Science Park confirmed the great public success of previous editions. Over 4000 people visited the laboratories of the Padriciano and Basovizza sites, and nearly 800 of them chose to visit the Elettra laboratory.



## Synchrotron youngsters: at the speed of light.

A event reserved for children and meeting with great success during the Open Day. A merry-go-round of children and colourful balls to simulate the “booster” and the “ring” of Elettra, Cardboard hand-mirrors and little designs to play with images, tiny objects magnified under the microscope - just some of the activities offered that proved able to capture the imagination of the children... and keep their parents entertained.

*ph. Cecilia Blasetti, Claudio Scafuri, Roberto Visintini*



## Researchers' night - PROSIT

(Trieste, September 25<sup>th</sup>, 2008)

In the picturesque setting of Piazza Unità d'Italia and its surroundings, the scientists of the institutions in Trieste gathered for the first time in the streets to meet with the citizens. The event was a great success, held simultaneously in 39 European cities, including 7 Italian cities, and directed by the European Commission; it saw the participation of thousands of interested people who crowded until late into the night the city centre. Under the Patronage of the President of the Republic, PROSIT is an event jointly-organized by thirteen institutions in Trieste: Province, Municipality, Area Science Park, the "Abdus Salam" International Centre for Theoretical Physics (ICTP), the International Center for Genetic Engineering and Biotechnology (ICGEB), the Conservatorio Giuseppe Tartini, the National Institute of Astrophysics (INAF) - Astronomical Observatory, the National Institute of Nuclear Physics (INFN), the National Institute of Oceanography and Experimental Geophysics (OGS), the International School for Advanced Studies (SISSA), the Sincrotrone Trieste, the United World College of the Adriatic and the University of Trieste.

ph. Michele Pasqualetto







## Success for AA38 at the Barcolana

(Trieste, October 12<sup>th</sup>, 2008)

The boat, AA38, a lightweight prototype wooden sailboat built by the Cantiere Alto Adriatico of Monfalcone with the scientific and technological contributions of Elettra, was among the 191 boats out of a total of 1912 boats registered, to finish the 40<sup>th</sup> edition of the *Barcolana*, the historic European sailing regatta.

ph. Marco Peloi



## La Ville Européenne des Sciences

(Paris, November 14<sup>th</sup>-18<sup>th</sup>, 2008)

“La Ville européenne des sciences” took place at the Grand Palais in Paris, an event dedicated to the meeting of the world of science with that of society.

Elettra Laboratory featured amongst the protagonists at the event with a stand dedicated to synchrotron radiation light sources, entitled “*Le Carrefour européen de la lumière*”, developed in cooperation with three other synchrotrons: Diamond in Oxford, the European Synchrotron Radiation Facility (ESRF) in Grenoble and Soleil in Paris.

ph. Alessandra Gianoncelli

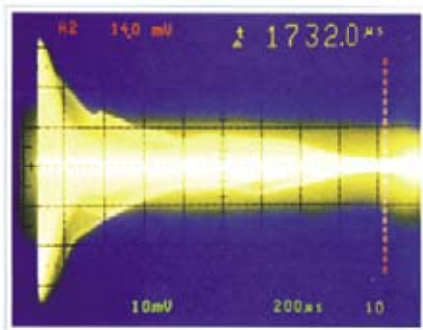


## A LOOK AT THE PAST...

(8<sup>th</sup> October 1993, 22.45)

A cry of joy and lots of slaps on the back accompany the image that shyly appears on the oscilloscope: the first electron beam had been held in the Storage Ring! A “Polaroid” photograph of the trace provides evidence of the long-awaited success.

That evening the control room was crowded as never before. The pre-conditions, in fact, were all there: a couple of days earlier, at 7:45 a.m., the electron beam had been circulated inside the vacuum ring chamber for about 1.7 ms. - the “Magic 2000”, meaning the maximum path that the electrons can do lacking an accelerating field to compensate for the energy lost as *synchrotron radiation* whilst passing through the bending magnets. A few months later - in 1994 –the first beamline, SuperESCA, was opened to users.



A souvenir picture of those present at that moment in the Control Room: R. Fabris, R.P. Walker, A. Fabris, F. Daclon, R. Visintini, E. Karantzoulis, A. Massarotti, M. Lonza, M. Mignacco (guest), R. DeMonte, C. J. Bocchetta, R. Richter and L. Barbina (who took the photograph).

## ... AND ONE TO THE FUTURE



### Start of the commissioning of the FERMI@Elettra

(15<sup>th</sup> July 2009)

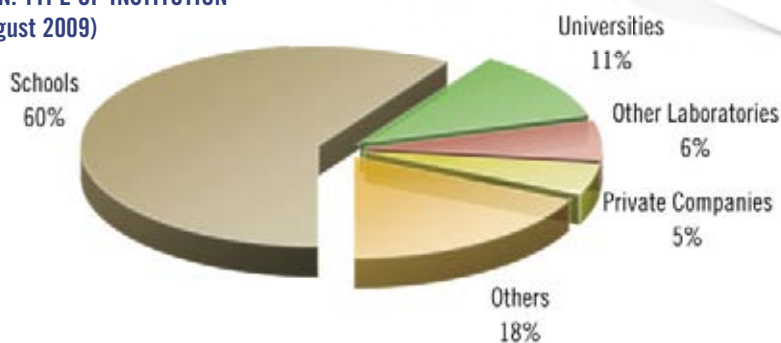
In July 2009 FERMI entered a new phase, commissioning. This important goal was celebrated with a party in the new FERMI Linac “overground and plants” building.

ph. Filippo Cianciosi

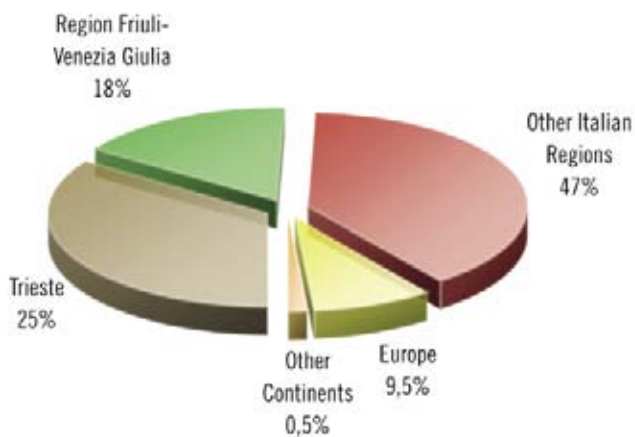
Event	Place / Date	Organisers / Collaborators
ACTOP08	Trieste 9-11/10, 2008	Sincrotrone Trieste/Soleil/Bessy/Accel
XVI Users' Meeting	Trieste 24-26/11, 2008	Sincrotrone Trieste
Time Resolved Studies with Synchrotron and FEL Radiation (satellite workshop)	Trieste 24-25/11, 2008	Sincrotrone Trieste
Emerging Applications of Synchrotron Radiation in the Life Sciences (satellite workshop)	Trieste 25-26/11, 2008	Sincrotrone Trieste
In viaggio con la luce (2nd edition)	ST 10-12/12, 2008	Sincrotrone Trieste
In viaggio con la luce (3rd edition)	ST 27-29/01, 2009	Sincrotrone Trieste
EuroFEL 1st IRUVX-PP Annual Meeting	Trieste 9-13/03,2009	Sincrotrone Trieste
Il Timing and Synchronization Workshop (satellite workshop)	Trieste 9/3, 2009	Sincrotrone Trieste/INFN-LNF
RADSYNCH RADIATION safety at SYNCHrotron radiation sources	Trieste 21-23/05, 2009	Sincrotrone Trieste
World Conference of Science Journalists	London 30/06-2/07, 2009	Diamond Light Source/Soleil/Sincrotrone Trieste
X School on Synchrotron Radiation: Fundamentals, Methods and Applications	Trieste 7-18/09, 2009	SILS/Sincrotrone Trieste
In viaggio con la luce (4th edition): incontro formativo su tematiche di ottica per insegnanti di scuola media superiore (training meeting on optics topics for high school teachers)	ST 27-29/10, 2009	Sincrotrone Trieste/Istituto Nazionale di Ottica Applicata di Firenze

# VISITS

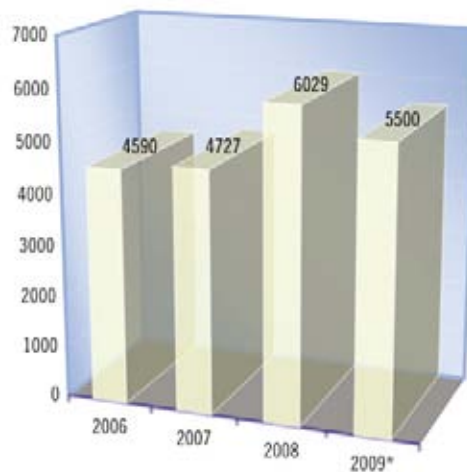
**VISITORS DISTRIBUTION: TYPE OF INSTITUTION**  
(September 2008 - August 2009)



**VISITORS DISTRIBUTION: GEOGRAPHICAL BREAKDOWN**  
(September 2008 - August 2009)



**VISITORS - PERIOD 2006-2009**



\* estimated visitors at December 2009  
(effective visitors at September 2009: 5346)



Il Consorzio per la gestione di AREA Science Park è Ente Nazionale di Ricerca che opera sul territorio regionale e nazionale per favorire la competitività delle imprese e del territorio, fornendo supporto qualificato per il trasferimento tecnologico, occupandosi di formazione imprenditoriale e internazionalizzazione.

Gestisce il primo Parco Scientifico e Tecnologico multisetoriale italiano, con 87 realtà insediate, dove si svolgono da 30 anni attività di ricerca, sviluppo e innovazione tese al raggiungimento di risultati d'eccellenza per migliorare la qualità della vita.

Ecco AREA Science Park, un luogo dove la formazione di alta qualità, la ricerca e il fare impresa si incontrano e si convertono in una fondamentale risorsa per la crescita economica e occupazionale del Paese.

*The Consortium for the management of AREA Science Park is a National Research Body which operates on a local and national level to foster territorial and business competitiveness, by supporting the technology transfer and encouraging entrepreneurial training and internationalisation.*

*It manages the first multi-sector Science and Technology Park in Italy, where the tenants, now 87, have been operating for 30 years in the field of scientific research, development and innovation, with a view to achieving excellence and improving quality of life.*

*AREA Science Park is the place where highly specialised training, research and business meet and turn into an essential resource for boosting the economic and employment growth of Italy.*

**AREA Science Park**

# Una risorsa per il territorio

*A resource for territorial competitiveness*



**AREA Science Park**  
Padriciano, 99 - 34012 Trieste - Italy  
Tel. +39.040.3755111  
Fax +39.040.226698  
info@area.trieste.it

[www.area.trieste.it](http://www.area.trieste.it)



# Sincrotrone Trieste

## Elettra Laboratory

PRODUCTS FOR RESEARCH LABS AND SYNCHROTRONS

### Power Supplies

New families of intelligent (DSP or PC embedded) power supplies, which cover many types of applications (high voltage/current, four-quadrant, etc.) and configurations are forthcoming. Epics/Tango interface are often already included and custom-built solutions are possible.

### Detectors

Photon and charged particle detectors, based on cross delay anodes, multi anodes and centroid finding techniques are continuously developed. 3D information (x, y, time) with spatial and time resolutions in the order of tens of micro- and pico-seconds are available through many custom-built solutions.

### Lab Instrumentation

Fast picoammeters, multi-point strain gauges, charge pulse amplifiers, ion chambers, pulse generators, RF filters, etc. Every tool is intelligent and in sole cases Epics/Tango interfaces are already included.

### Accelerator Components

Elettra, over the years, has acquired wide experience in developing and realizing accelerators components, such as undulators, resonant cavities, etc. For the production of Insertion Devices a specific spin-off company has been set-up.

**Sincrotrone Trieste S.C.p.A.**

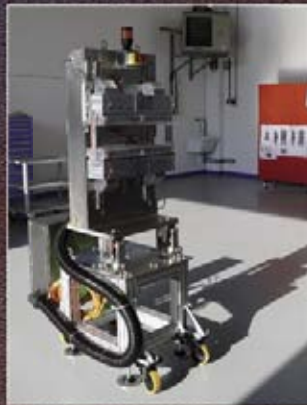
**Industrial Liaison Office**

[www.elettra.trieste.it/ilo](http://www.elettra.trieste.it/ilo)

[ilo@elettra.trieste.it](mailto:ilo@elettra.trieste.it)

Phone: +39 040 375 8303

Fax: +39 040 375 8623



**Equipment for Light Sources**

**Design development of  
Permanent Magnet  
Undulators**

**Instrumentation for Magnetic  
Measurements**

**Large Climate Chamber Test  
Services**



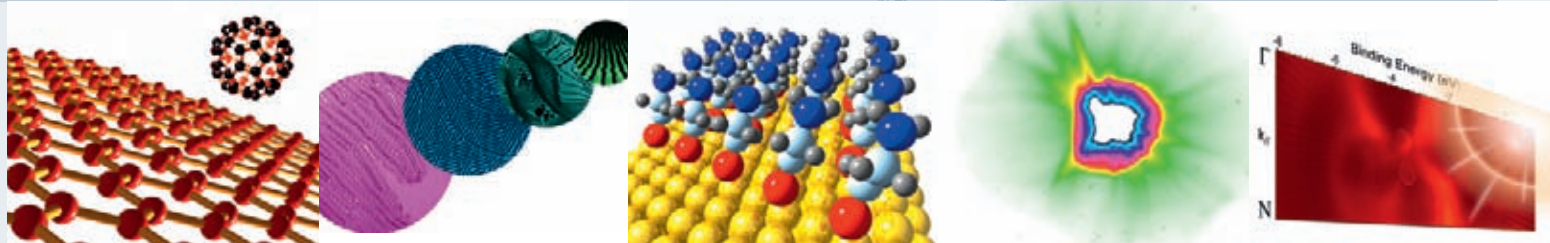
**KYMA S.R.L.**

**S.S. 14 Km 163,5 Km**

**in Area Science Park**

**IT-34149 - Trieste - Italy**

**[www.kyma-undulators.eu](http://www.kyma-undulators.eu)**



**Sincrotrone Trieste SCpA**  
S.S. 14 Km. 163,5 in AREA Science Park  
34149 Trieste ITALY  
[www.elettra.trieste.it](http://www.elettra.trieste.it) - [info@elettra.trieste.it](mailto:info@elettra.trieste.it)

